Interaction of Chemical Oxidants with Aquifer Materials

by

Xiuyuan Xu

A thesis
presented to the University of Waterloo
in fulfillment of the
thesis requirement for the degree of
Doctor of Philosophy
in
Civil Engineering

Waterloo, Ontario, Canada, 2006

Author's Declaration for Electronic Submission of a Thesis

I hereby declare that I am the sole author of this thesis. This is a true copy of the thesis, including any required final revisions, as accepted by my examiners.

I understand that my thesis may be made electronically available to the public.

Abstract

In situ chemical oxidation (ISCO) is a leading-edge technology for soil and groundwater remediation, and involves injecting a chemical oxidant (e.g., permanganate, hydrogen peroxide, or persulfate) into the subsurface to deplete contaminant mass through oxidation. Since the delivery of the chosen oxidant to the target treatment zone must occur *in situ*, the interaction between the injected oxidant and the aquifer material is a key controlling factor for a successful ISCO application. While many published ISCO studies have focused on the interaction between an oxidant and target contaminants, many questions still remain on the interaction between a potential oxidant and the aquifer material. Through a series of bench-scale experiments with aquifer materials collected from 10 sites throughout North America, the research presented in this thesis provides insight into the interaction between these aquifer materials and two widely used ISCO oxidants; permanganate and hydrogen peroxide.

The investigation into the interaction between aquifer materials and permanganate consisted of three series of bench-scale experiments: (1) long-term batch experiments which were used to investigate permanganate consumption in response to fundamental geochemical properties of the aquifer materials, (2) short-term batch experiments which were designed to yield kinetic data that describe the behavior of permanganate in the presence of various aquifer materials, and (3) column experiments which were used to investigate permanganate transport in a system that mimics the subsurface environment. The long-term experiments which involved more than 180 batch reactors monitored for ~300 days showed that the unproductive permanganate consumption by aquifer materials or natural oxidant demand (NOD) is strongly affected by the initial permanganate concentration, permanganate to solid mass ratio, and the reductive components associated with each aquifer material. This consumption cannot be represented by an instantaneous reaction process but is kinetically controlled by at least a fast and slow reactive component. Accordingly, an empirical expression for permanganate NOD in terms of aquifer material properties, and a hypothetical kinetic model consisting of two reaction components were developed. In addition, a fast and economical permanganate NOD estimation procedure based on a permanganate COD test was developed and tested. The investigation into short-term permanganate consumption (time scale of hours) was based on the theoretical derivation of the stoichiometric reaction of permanganate with bulk aquifer material reductive components, and consisted of excess permanganate mass experiments and excess aquifer material mass experiments. The results demonstrated that permanganate consumption by aquifer materials can be characterized by a very fast reaction on the order of minutes to hours, confirming the existence of the fast reaction component of the hypothetical kinetic model used to describe the long-term permanganate NOD observations. A typical experimental column trial consisted of flushing an aquifer-material packed column with the permanganate source solution until sufficient permanganate breakthrough was observed. The permanganate column results indicated the presence of a fast and slow consumption rate consistent with the long-term batch test data, and an intermediate consumption rate affecting the shape of the rising limb of the breakthrough curve. Finally, a comparison of the experimental results between batch and column systems indicated that permanganate NOD was significantly overestimated by the batch experiments; however, permanganate consumption displayed some similarity between the batch and column systems and hence an empirical expression was developed to predict permanganate consumption in physically representative column systems from batch reactor data.

The interaction between hydrogen peroxide and aquifer materials was also investigated with both batch and column experiments. A series of batch experiments consisting of a mixture of 2% hydrogen peroxide and 15 g of aquifer materials was used to capture the overall hydrogen peroxide behavior in the presence of various aquifer materials. The results indicated that the decomposition of hydrogen peroxide in the presence of various aquifer materials followed a first-order rate law, and was strongly affected by the content of amorphous transition metals (i.e., Fe and Mn). Although hydrogen peroxide decomposition is related to the total organic carbon (TOC) content of natural aquifer materials, the results from a two-week long exposure to hydrogen peroxide suggests that not all forms of natural organic matter contributed to this decomposition. A multiple linear regression analysis was used to generate predictive relationships to estimate hydrogen peroxide decomposition rate coefficients based on various aquifer material properties. The enhanced stability of hydrogen

peroxide was investigated under six scenarios with the addition of chelating reagents. The impact of a new green chelating reagent, S,S'-ethylenediaminedisuccinate (EDDS), on the stability of hydrogen peroxide in the presence of aquifer materials was experimentally examined and compared to that of the traditional and widely used chelating reagent, Ethylenediaminetetraacetic (EDTA). The results demonstrated that EDDS was able to significantly increase the stability of hydrogen peroxide, especially for aquifer materials with low TOC contents and/or high dissolvable Fe and Mn contents. Finally, to complement and expand the findings from the batch experiments, column experiments were conducted with aquifer materials from five representative sites. Each column was flushed with two types of source solutions (with or without EDDS addition) at two flow rates. The column experiments showed that the use of EDDS resulted in an earlier breakthrough and a higher stable concentration of hydrogen peroxide relative to the case without the addition of EDDS. The hydrogen peroxide decomposition rate coefficients generated from the column data were significantly higher than those generated from the batch test data and no correlation between hydrogen peroxide decomposition coefficients obtained from column and batch experiments was observed. Based on the column experimental results, a one-dimensional transport model was also calibrated to capture the hydrogen peroxide breakthrough process.

Data from bench-scale tests are routinely used to support both ISCO design and site screening, and therefore the findings from this study can be used as guidance on the utility of these tests to generate reliable and useful information. In general, the behavior of both permanganate and hydrogen peroxide in the presence of aquifer materials in batch and the column systems clearly indicates that the use of batch test data for ISCO system design is questionable since column experiments are believed to mimic *in situ* conditions better since column systems provide more realistic aquifer material contact. Thus the scaling relationships developed in this study provide meaningful tools to transfer information obtained from batch systems, which are widely employed in most bench-scale studies, to column systems.

Acknowledgements

I would like to thank a number of people who have helped me throughout the course of my Ph.D program. Firstly, I would like to express my sincere gratitude to my supervisor, Dr. Neil R. Thomson for his attention, insight, guidance, and generous support. Without his invaluable supervision, it would not be possible for me to complete this PhD program. His kindnesses made me feel very comfortable working with him. I would also like to thank the members of my committee, Dr. Eric Reardon, Dr. Peter Huck, and Dr. Susan Andrews for the valuable discussions and their comments on my research. Very special thanks to Dr. Brent Sleep for his valuable advice.

My sincere thanks go to Mark Sobon and Bruce Stickney whose advice and help with analytical equipment allowed my experimental work to move forward. I highly appreciate the lab assistance from Pam Kuipers, Heather Crone, and Maureen O'Connell. I would also like to thank Shirley Chatten and Randy Fagan in the Earth Science Organic Geochemistry Lab for their detailed work in organic carbon analysis and XRD mineral analysis, respectively.

I also thank Dr. Eric Hood from GeoSyntec Consultants, Keith Henn and Dale Mervin (Tetra Tech NUS), and Dennis Mayton (USACE) for assistance with the collection of aquifer materials.

Thanks also to professors and fellow students at in the Water Resource Group for making my time fruitful and enjoyable.

Financial support for this investigation was provided by SEDRP (CU1289) of U.S. EPA and DoD, and a Natural Sciences and Engineering Research (NSERC) of Canada Discovery Grant (N. Thomson).

I would like to thank my parents for their great support and encouragement during the long years of study. Last, and most of all, I would like to express my deepest appreciation to my wife Jing for her love, understanding, support, and patience.

Table of Contents

Author's Declaration for Electronic Submission of a Thesis ii
Abstract iii
Acknowledgements vi
Table of Contents vii
List of Tables x
List of Figures xii
Chapter 1 Introduction 1
  1.1 Research Needs 4
  1.2 Research Objectives 6
  1.3 Thesis Organization 6
Chapter 2 Characterization of Aquifer Materials 9
  2.1 Overview 9
  2.2 Aquifer Materials 9
    2.2.1 Collection and Handling 9
    2.2.2 Sample Characterization 11
  2.3 Reductive Capabilities of Aquifer Materials 13
    2.3.1 Reductive Components 13
    2.3.2 Reactivity of Reductive Components 15
    2.3.3 Theoretical Estimation of Total Reductive Capacity (TRC) 18
    2.3.4 Experimental Estimation of TRC 19
    2.3.5 Results and Discussion 21
  2.4 Impact of Air-Drying on the Reductive Properties of Aquifer Materials 22
    2.4.1 General Methodology 23
    2.4.2 Results and Discussion 23
Chapter 3 Permanganate Interaction with Aquifer Materials 34
  3.1 Overview 34
  3.2 Background 35
    3.2.1 Permanganate Properties and Reactions 35
    3.2.2 Permanganate Applications in Groundwater Remediation 37
    3.2.3 Permanganate Interaction with Aquifer Materials 38
    3.2.4 Derivation of Permanganate NOD Kinetic Expressions 40
  3.3 Long-Term Permanganate Consumption by Aquifer Materials 44
    3.3.1 Experimental Methods 44
    3.3.2 Results and Discussion 46
    3.3.3 Summary 57

3.4 Permanganate COD Tests ... 70
  3.4.1 Methods ... 71
  3.4.2 Results ... 72
  3.4.3 Summary ... 75
3.5 Short-Term Kinetic Investigations ... 79
  3.5.1 Experimental Methods ... 79
  3.5.2 Results and Analysis ... 80
  3.5.3 Summary ... 82
3.6 Column Investigations ... 88
  3.6.1 Introduction ... 88
  3.6.2 Methods ... 88
  3.6.3 Results and Discussions ... 90
  3.6.4 Summary ... 97
Chapter 4 Interactions of Hydrogen Peroxide and Aquifer Materials ... 106
4.1 Overview ... 106
4.2 Background ... 106
  4.2.1 General Properties and Reactions ... 107
  4.2.2 Fenton's Reactions ... 108
  4.2.3 Modified Fenton's Reagent ... 110
  4.2.4 Fenton-Like Approaches ... 112
  4.2.5 CHP-ISCO Use in Subsurface Remediation ... 113
  4.2.6 Mechanisms of H_2O_2 Decomposition in the Subsurface ... 115
4.3 H_2O_2 Decomposition in the Presence of Aquifer Materials in Batch Systems ... 119
  4.3.1 Methods ... 119
  4.3.2 Results and Discussion ... 120
  4.3.3 Summary ... 126
4.4 Enhanced Stability of Hydrogen Peroxide ... 132
  4.4.1 Introduction ... 132
  4.4.2 Methods ... 134
  4.4.3 Results and Discussions ... 135
  4.4.4 Summary ... 137
4.5 Column Experiments ... 144
  4.5.1 Introduction ... 144
  4.5.2 Methods ... 144
  4.5.3 Results and Discussion ... 147
  4.5.4 Summary ... 153
4.6 Modeling ... 159
Chapter 5 Conclusions and Implications, Recommendations, and Contributions ... 163

5.1 Conclusions and Implications 163
  5.1.1 Permanganate / Aquifer Material Interactions 163
  5.1.2 Hydrogen Peroxide / Aquifer Material Interactions 166
5.2 Recommendations 168
5.3 Significant Contributions 169
Appendix A Grain Size Distributions 172
Appendix B Interpretation of XRD Diffractograms 174
Appendix C Air Drying Investigation 182
Appendix D Normalization of Long-Term NOD 183
References 184

List of Tables

Table 2.1. General site information where aquifer material was collected for use in this study. 25
Table 2.2. Summary of characterization methods. 26
Table 2.3. Summary of aquifer materials characteristics. 27
Table 2.4. Trace metal concentrations (mg/kg). 28
Table 2.5. Estimation of the theoretical total reduction capacity and dichromate COD test results (units: meq/g). 29
Table 2.6. Description of aquifer material sub-samples used in the air- drying investigation. 29
Table 3.2.1. Properties and characteristics of potassium permanganate (after Siegrist et al. 2002; Hood, 2000) 42
Table 3.3.1. Experimental details of long-term permanganate NOD 59
Table 3.3.2. Estimated permanganate consumption rate (g-$KMnO_4$/kg/day). 60
Table 3.3.3. Best-fitting parameters (k_{ox} and C_{OAM} for fast reaction, k_{ox} for slow reaction, and reduction factor) and other parameters of the kinetic model parameters. 60
Table 3.4.1. Summary of the maximum permanganate consumption as estimated from theoretical considerations of the reductive capacity of various aquifer species, the dichromate and permanganate chemical oxygen demand tests, and from the long-term permanganate NOD batch tests. All values are expressed in terms of g of $KMnO_4$ per kg of dry aquifer material 76
Table 3.5.1. Experimental details for the excess aquifer material mass kinetic experiments. 83
Table 3.5.2. Experimental details for the excess permanganate mass kinetic experiments. ... 83
Table 3.5.3. Observed reaction rate coefficients and reaction order for the excess aquifer material mass kinetic experiments 83
Table 3.5.4. Observed reaction rate coefficients for excess permanganate mass kinetic experiments. 84
Table 3.5.5. Reaction rate coefficients with respect to OAM and permanganate 84
Table 3.6.1. Summary of column experiments. 98
Table 3.6.2. Characteristic BTC values for the Borden, LC34-LSU, and LC34-USU aquifer material column experiments. 98
Table 3.6.3. Characteristic BTC values for the EGDY and NFF aquifer material column experiments. 99
Table 3.6.4. Characteristic BTC values for the MAAP aquifer material column 99
Table 3.6.5. NOD (g/kg) estimated from the permanganate BTCs using Eq. (3.6.1). The NOD projected was estimated by extrapolating the rate of slow permanganate

consumption until it intersected $C/C_o = 1$. 100
Table 3.6.6. Overall permanganate consumption (NOD) rates. 100
Table 4.2.1. Physical properties of commercial hydrogen peroxide (after Strukul et al., 1992). 118
Table 4.3.1. Observed hydrogen peroxide reaction rate coefficients in the presence of autoclaved and non-autoclaved aquifer material (15 g solids, 80 mL of 2.0% H_2O_2 solution with an initial pH of 3.0). 127
Table 4.3.2. Multiple linear regression equations for the observed hydrogen peroxide reaction rate coefficient (1/hr) as a function of various aquifer material characteristics. All regression coefficients are statistically significant at the 5% LOS. 127
Table 4.4.1. First-order reaction rate coefficients (1/hour) for hydrogen peroxide decomposition in batch experiments. 139
Table 4.5.1. Summary of flow rates (mL/min) used for the hydrogen peroxide column trials. 155
Table 4.5.2. First appearance (in pore volumes) of the bromide tracer and hydrogen peroxide in the column effluent as defined by a detectable concentration in the effluent (0.05% for hydrogen peroxide, and 1.2 mg/L for Br). 155
Table 4.5.3. Observations from the MAAP column experiments with a flow rate of 0.22 mL/min. The effluent pH, dissolved total Fe, and dissolved total Mn were measured after the hydrogen peroxide concentration in the effluent reached a stable value. 156
Table 4.5.4. Observed reaction rate coefficients from selected batch and column experimental systems. (Note: the normalized decomposition rate coefficient are obtained by dividing the corresponding rate coefficients by the aquifer material mass loaded in columns and batch reactors) 156

List of Figures

Figure 1.1. Conceptual Schemes of ISCO Delivery Systems (a) passive mode using single or multiple injection(s), and (b) active mode using injection and extraction wells to hydraulically control oxidant delivery. 8
Figure 2.1. Theoretical estimation of the total reductive capacity using: (a) total organic carbon and the total Fe, Mn, and S; (b) total organic carbon, total Fe and Mn; (c) total organic carbon, amorphous Fe and Mn; and (d) total organic carbon and the ferrous Fe or total Fe. 30
Figure 2.2. Theoretical total reductive capacity (TRC) and dichromate COD test results. 31
Figure 2.3. Scatter plot of theoretical total reductive capacity (TRC), dichromate COD, and total organic carbon. The TRC value for the DNTS aquifer material is excluded. 32
Figure 2.4. Anaerobic setup for drying aquifer materials. 32
Figure 2.5. Average reductive capacity results from the air-drying investigation (a) dichromate-COD data, (b) permanganate-COD data, and (c) 7-day permanganate NOD data. 33
Figure 3.2.1. Pore-scale conceptual model for NOD showing the possibility of reaction with reduced aquifer solid species, reaction with dissolved DNAPLs, and transport of unreacted MnO_4^-. Reduced species include: (a) pyrite and organic matter coatings on grains, (b) reduced minerals such as magnetite and reduced carbonaceous matter such as charcoal, (c) dissolved and nonaqueous phase oil (DNAPL), and (d) organic matter and disseminated pyrite entrained within carbonate grains and lithic fragments. (Adapted from Mumford et al., 2005) 43
Figure 3.3.1. Long-term permanganate NOD profiles for each experimental series performed on the eight aquifer materials used in this investigation. Each data point represents the average from triplicate reactors. The legend for each profile indicates the oxidant to solids mass ratio and initial permanganate concentration used for each experimental series. Also noted on each panel is reactor spiking events. Error bars are not shown to avoid confusion 61
Figure 3.3.2. Scatter plot of the fast rate of permanganate consumption and the oxidant to solids mass ratio for each experimental series. The NOD expressed over the first 7 days was used to estimate the fast rate of permanganate consumption. 62
Figure 3.3.3. NOD_{max} and the 7-day NOD as functions of the oxidant to solids mass ratio for (a) LC34-LSU and (b) LC34-USU aquifer materials at an initial permanganate concentration of 12.7 g/L. The dashed lines are extrapolations of the linear relationship ($r^2 > 0.90$) to oxidant to solids mass ratio values representative of *in situ* conditions.... 63
Figure 3.3.4. The impact of different initial permanganate concentrations on the average observed NOD_{max} 64

Figure 3.3.5. Scatter plot of the 7-day NOD and NOD_{max} data for all experimental sites...... 64
Figure 3.3.6. Observed maximum NOD and NOD at 7 days. The number above the bar indicates the ratio of the 7-day NOD value to the maximum NOD value...................... 65
Figure 3.3.7. Reduction in COD test values after aquifer materials exposed to permanganate for Borden, DNTS, LC34-LSU, LC34-USU, MAAP, and NIROP aquifer materials compared with observed NOD_{max} for each experimental series..................................... 66
Figure 3.3.8. Best-fit logarithm functions to normalization NOD profiles for (a) DNTS and (b) LC34-USU aquifer materials... 66
Figure 3.3.9. Scatter plot of NOD_{max} and the equivalent NOD based on the bulk soil manganese concentration after exposure to permanganate for >250 days. 67
Figure 3.3.10. The observed and simulated NOD profiles for batch experiments with the Borden, DNTS, EGDY, and MAAP aquifer materials.. 68
Figure 3.3.11. The influence of the change of reduction factor k_p on the simulated permanganate NOD profile. Square symbols represent the observed NOD values for the test with 20 g Borden aquifer material exposed to a $KMnO_4$ solution with an initial concentration of 20 g/L... 69
Figure 3.4.1. Scatter plot of the dichromate and permanganate chemical oxygen demand test results (average of 5 trials), and the overall maximum permanganate NOD from the long-term batch tests for each aquifer material. All values expressed as g-$KMnO_4$ /kg. Also shown are best-fit linear relationships for each COD test as described by (1) Overall maximum NOD = 0.64±0.14 x (dichromate COD value) – 1.15±3.14 with a r^2 = 0.96 for the dichromate test; and (2) Overall maximum NOD = 1.10±0.10 x (permanganate COD value) – 0.83±1.29 with a r^2 = 0.99 for the permanganate test..... 77
Figure 3.4.2. Scatter plot of the results from the dichromate COD test, the permanganate COD test, the long-term batch test (overall maximum NOD) and the sum of the TOC and the amorphous Fe content of each aquifer material. All values expressed as g-$KMnO_4$ /kg. Also shown are best-fit linear relationships as described by (1) Overall maximum NOD = 0.81 x TRC* – 2.8 with a r^2 = 0.83 for the batch test; (2) dichromate COD = 1.3 x TRC* – 2.5 with a r^2 = 0.86 for the dichromate COD test; and (3) permanganate COD = 0.73 x TRC* – 1.7 with a r^2 = 0.82 for the permanganate COD test; where TRC* is the contribution from TOC and amorphous Fe expressed in g/kg (see Table 3.4.1). 78
Figure 3.4.3. Sensitivity of the permanganate COD test results due to changes in (a) reaction duration, (b) initial permanganate concentration, and (c) sample mass of aquifer material. All test values are expressed in terms of g of $KMnO_4$ per kg of dry aquifer material. The error bars represent ± one standard deviation. 78
Figure 3.5.1. Permanganate concentration profiles generated from the excess aquifer material mass kinetic experiments. Each data point is the average from duplicate experiments. 85

Figure 3.5.2. OAM data generated from the excess permanganate mass kinetic experiments. Each data point is the average from all aquifer material masses used. Error bars represent ±1 standard deviation. 86

Figure 3.5.3. Scatter plots (a) the reaction order vs. TOC ($r^2 = 0.68$), (b) k_{oam} vs. surface area ($r^2 = 0.63$), and (c) k_{oam} vs. Fe_T ($r^2 = 0.54$) and $k_{MnO_4^-}$ vs. Fe_T ($r^2 = 0.62$). 87

Figure 3.6.1. Typical columns used in permanganate experiments. Each column has a length of 40 cm and an inner diameter of 3.81 cm, and is equipped with four equally spaced sampling ports along its length. 101

Figure 3.6.2. Permanganate and bromide breakthrough curves for: (a) and (b) Borden aquifer material, (c) and (d) LC34-LSU aquifer material, and (e) and (f) LC34-USU aquifer material. 102

Figure 3.6.3. Permanganate and bromide breakthrough curves for: (a) and (b) EGDY aquifer material, and (c) NFF aquifer material. 103

Figure 3.6.4. Permanganate and bromide breakthrough curves for MAAP aquifer material. 104

Figure 3.6.5. Permanganate NOD from batch and column systems. The column NOD was estimated by extrapolating the rate of slow permanganate consumption until the effluent permanganate BTC intersected $C/C_o = 1$. 104

Figure 3.6.6. Scatter plot of the average 7-day NOD and the maximum 7-day NOD results from the batch tests and the NOD projected from the column experiments. Also shown are best fit linear relationships between the column NOD and the average 7-day NOD ($r^2 = 0.99$) and the maximum 7-day NOD ($r^2 = 0.99$). 105

Figure 4.2.1. Schematic diagram for Fenton [Fe(II)] and Fenton-like [Fe(III)] reactions. 118

Figure 4.3.1. Hydrogen peroxide decomposition profiles for non-autoclaved aquifer materials. 128

Figure 4.3.2. Hydrogen peroxide decomposition rate coefficients for autoclaved and non-autoclaved aquifer materials. 129

Figure 4.3.3. Total Fe and Mn dissolved concentrations in batch reactors within the first hour. 129

Figure 4.3.4. Dichromate COD test results for selected aquifer materials prior and after exposure to hydrogen peroxide for two-weeks. The error bars represented ± one standard deviation. 130

Figure 4.3.5. Results of correlation analysis of the hydrogen peroxide decomposition rate coefficients in the presence of non-autoclaved aquifer materials with an initial hydrogen peroxide concentration of 2% and a pH of 3.0. Data for the aquifer materials from NIROP, NFF, and MAAP are excluded from this analysis. 131

Figure 4.4.1. Molecular structure and acidity constants for ethylenediaminetetraacetic acid (EDTA) and ethylenediaminedisuccinic acid (EDDS) (25^0C) (adapted from

Vandevivere et al., 2001) 140
Figure 4.4.2. Hydrogen peroxide profiles in the presence of (a) DNTS aquifer materials, (b) EGDY aquifer materials, (c) LC34-USU aquifer materials, (d) MAAP aquifer materials, and (e) NIROP aquifer materials. Each data point is the average from triplicate experiments. EDDS was added at 0.5 mmol EDDS per kg of solids, EDTA was added at 1.0 mmol per kg of solids, and ferrous iron was added at a weight ratio of 0.02 (Fe^{2+}/H_2O_2). 141
Figure 4.4.3. Observed reaction rate coefficients in the presence of aquifer materials for Experimental Series 1, 4, 6 and 7. EDDS was added at 0.5 mmol EDDS per kg of solids, and ferrous iron was added at a weight ratio of 0.02 (Fe^{2+}/H_2O_2)..................... 142
Figure 4.4.4. Total Fe and Mn dissolved concentrations from Experimental Series 1 and 2. EDTA was added at 1.0 mmol EDTA per kg of solids. Samples were taken within the first hour. 143
Figure 4.5.1. Typical setup for hydrogen peroxide column experiments. 157
Figure 4.5.2. Hydrogen peroxide and bromide breakthrough curves for the column trials performed: (a) and (b) high and low flow rate for the LC34-LSU aquifer material, (c) and (d) high and low flow rate for the LC34-USU aquifer material, (e) and (f) high and low flow rate for the MAAP aquifer material. Also shown in (f) are results from the additional MAAP aquifer material column experiments where the column was first flushed with a H_2SO_4 solution (pH = 3.0) for two hours prior to a solution of hydrogen peroxide... 158
Figure 4.6.1. Calculated and observed hydrogen peroxide breakthrough curves for columns: (a) without and (b) with EDDS application for the LC34-LSU aquifer material, (c) without and (d) with EDDS application for the LC34-USU aquifer material, (e) without and (f) with EDDS application for the MAAP aquifer material. 162

Chapter 1

Introduction

Contamination of groundwater is the result of various human activities (e.g., agriculture, industry, transportation, domestic waste and resource exploitation). Of all the subsurface contamination problems, contamination by organic and energetic compounds appears to be the most widespread (US EPA, 2004a; WSTC, 2004). For example, in the United States, soil and groundwater are contaminated with chlorinated solvents at approximately 400,000 sites, and there have been more than 439,000 releases from leaking underground storage tanks (LUSTs) reported (US EPA, 2004a). Organic contaminants which are immiscible in water are referred to as non-aqueous phase liquids (NAPLs), which can form NAPL source zones (WSTC, 2004).

Remediation activities at contaminated groundwater sites include: identifying, quantifying, and controlling contaminant sources, and selecting appropriate treatment technologies. In response to the growing need to address environmental contamination, research and practice over the past 30 years have led to four categories of subsurface remediation or controlling strategies: (1) containment of contaminated zones (e.g., concrete or slurry walls), (2) ex-situ treatment (e.g., excavation), (3) natural attenuation, and (4) in situ treatment (e.g., in situ bioremediation) (Domenico and Schwartz, 1998). These technologies either have limited applicability, limited effectiveness, or are still under research and development.

In situ treatment or remediation approaches have become attractive due to favorable economics and the advantage of destroying contaminants in place. For example, projects using in situ treatment technologies have increased steadily from 31% during 1985 – 1989, to 49% during 1998- 2002 in response to the support by United States Superfund Remedial Action Program (US EPA, 2004b). An in situ remediation technology involves the reduction, extraction, removal, stabilization and/or containment of contaminants in the subsurface to an acceptable level. This objective can be accomplished by either mass transfer and recovery methods, or in-place destruction methods. A classical mass transfer and recovery technology is pump-and-treat (P&T) which has become a baseline technology for comparison of other alternative remediation methods (WSTC, 2004; Pankow and Cherry, 1996). A number of factors including subsurface heterogeneities, low solubility, sorption, and diffusion into low permeability zones have made P&T much less efficient than originally envisioned. In situ mass destruction methods are based on the knowledge that many contaminants are amenable to be fully or partially destroyed by physical, chemical, and biological processes. Examples of these methods include in situ vitrification, electrokinetics, in situ chemical oxidation (ISCO), and in situ bioremediation (Khan et al., 2004). Of all the in situ treatment methods, the most promising technologies are in situ bioremediation and ISCO (Domenico and Schwartz, 1990). Compared with in situ bioremediation which is usually limited by rates of contaminant desorption and dissolution (Ogram et al., 1985), the reactions in ISCO are near immediate, and therefore treatment is far more rapid than with biological techniques (ESTCP, 1999).

The use of chemical oxidation to destroy contaminants has been practiced for over 100 years in the water and wastewater industry (USEPA, 1999; Eillbeck and Mattock, 1987); however, the use of this technology for the destruction of contaminants in the subsurface is still relatively new. Over the past decade there has been a significant development in the application of ISCO for the remediation of organic contaminants, especially NAPLs (Watts and Teel, 2006; Hood, 2000; ESTCP, 1999; Siegrist et al, 1999). This technology involves injecting chemical oxidants (e.g., ozone, hydrogen peroxide, or permanganate) into the vadose or saturated zone to reduce the contaminant mass through oxidization. Currently, hydrogen peroxide (H_2O_2, including its derivative, Fenton's reagent), permanganate (MnO_4^-), ozone (O_3), persulfate ($S_2O_8^{2-}$), and dissolved oxygen (O_2) are widely used in ISCO (Hung et al., 2002; ITRC, 2001; Michael et al., 2000; USEPA, 1999; 1998; Masten and Davis, 1997;

Clancy et al., 1996). Although other oxidants are available, they are used less due to cost, effectiveness, difficulty in implementation, or generation of potential toxic by-products. The use of ozone and oxygen in ISCO applications is relatively less popular in groundwater remediation than in soil remediation, while the use of persulfate is relatively new for groundwater remediation although it has been employed extensively for many industrial and environmental applications (Barbash et al., 2006; Watts and Teel, 2006; Liang et al., 2004a; 2004b; Huang et al., 2002). The other two oxidants (hydrogen peroxide and its related reagents, and permanganate) have gained widespread usage in ISCO applications (Watts, 2006; Crimi et al., 2004; Forsey, 2004; Tunnicliffe and Thomson, 2004; Lee et al., 2003; Gates-Anderson et al, 2001; ITRC, 2001; 2000; Siegrist et al, 2001; USEPA, 1998; Hood, et al., 1997).

Successful application of an ISCO technology requires: 1) an effective chemical reaction (i.e., sufficient rate and extent) between the injected oxidants and target contaminants, and 2) effective delivery of the oxidants throughout the contaminated zone (Siegrist et al., 2001; Siegrist et al., 1999; Yin and Allen, 1999). Generally, ISCO technologies are applicable for source zone mass destruction, and are sensitive to variations in the subsurface permeability as well as to the distribution of contaminant mass.

A number of systems have been proposed for delivering oxidants to the target treatment zone. The passive delivery method (Figure 1.1 a) involves the injection of the oxidant solution using driven well points, and the density contrast between the oxidant solution and background groundwater induces lateral and vertical spreading to cover the targeted areas (Stewart, 2002; Nelson et al., 2001). When this mode is implemented, the problems associated with groundwater treatment and disposal of hazardous wastes is avoided; however, unreacted oxidant and contaminants may migrate down-gradient to previously uncontaminated zones. To overcome this problem and maintain a high oxidant concentration within the target zone, active oxidant delivery may be used (Figure 1.1 b). Design of either delivery system is very site specific (e.g., depth and distribution of contaminant zones, hydrogeology, operation and maintenance flexibility, and site accessibility), and involves determining the spacing, number, and layout of delivery points, and the rate and duration of oxidant delivery (Siegrist et al. 2001; Hood, 2000; Yin and Allen, 1999). Nevertheless, in either case, transport of the oxidant to target zones is achieved through hydraulic gradient driven advection, density-driven advection, or dispersive mixing.

Although extensive research studies and applications have been conducted since it was proposed, the science of ISCO treatment is still not fully understood (Watts and Teel, 2006; Lee et al, 2003; Seol et al., 2003; Huang et al., 1999; Siegrist et al., 1999; Hood and Thomson, 1997; Gates et al., 1994), and therefore, it is still facing many of obstacles to widespread acceptance and application. For example, many of existing ISCO studies have focused on the interaction between the oxidant and target contaminants (Waldemer et al., 2006; Crimi and Siegrist, 2005; 2004; Huang et al., 2002; Kang et al., 2002; Chen et al., 2001; Hood, 2000; Hood et al., 2000; Yan et al., 2000; 1999; Clancy et al., 1996), while many questions still remain on the interaction between the potential oxidants and the aquifer material. An understanding of this interaction is essential for the successful design of an efficient oxidant delivery system, and to better understand treatment expectations.

1.1 Research Needs

Clearly, the fate of oxidants used in ISCO treatment is strongly affected by the subsurface conditions (e.g., hydrodynamic and geochemical properties of aquifer materials and groundwater) in addition to the presence of contaminants. A comprehensive understanding of the interactions between aquifer materials and the injected oxidants is important not only to further the specific understanding of ISCO, but also for the successful design and application of ISCO treatment systems.

There is a myriad of factors potentially affecting the fate of injected oxidants since the subsurface environment is very complicated; however, it is impractical to account of all these factors in designing an ISCO system. Aquifer hydrodynamic properties (e.g., permeability) have been accepted as a controlling factor for oxidant transport in the subsurface (WSTC, 2004; USEPA, 2004; 1998; Seol et al., 2003; Schroth et al., 2001); however, the mobility and fate of the oxidant in the subsurface are also strongly affected by interactions (e.g., redox) with the aquifer matrix. Unfortunately, existing empirical assessment of these interactions is only at the developmental stage, while the quantification at the mathematical level is quite limited (Crimi and Siegrist, 2005). Therefore, a better understanding of the major factors controlling oxidant fate during ISCO applications is critical for this technology to gain widespread acceptance.

It has been demonstrated in numerous ISCO studies (Watts and Teel, 2006; Mumford et al., 2005; ITRC, 2001; ESTCP, 1999) that when permanganate is injected into the subsurface it will react with not only the target contaminants but also any other reduced constituents (including organics and inorganics). This unproductive consumption will increase the mass of permanganate required relative to the stoichiometric mass required to satisfy oxidation of the target contaminants (Watts and Teel, 2006; Mumford et al, 2005; 2004; Hartog, 2003; Haselow et al, 2003; Hartog et al., 2002; Siegrist et al., 2001; Hood, 2000; ESTCP, 1999; Fountain, 1998). This increase in permanganate consumption is typically referred to as natural oxidant demand (NOD) (Mumford et al., 2005). Several studies have reported NOD as a single value (Haselow et al., 2003; Hood, 2000); however, recent studies have observed that permanganate behaves kinetically in the presence of aquifer materials (Mumford et al, 2005). Therefore, there is a need to develop a comprehensive understanding of the permanganate-NOD kinetics as well as an acceptable bench-scale protocol to quantify permanganate consumption to support the design of permanganate ISCO treatment systems.

There exist natural catalysts in the subsurface (e.g., iron and manganese) that will enhance the decomposition rate of hydrogen peroxide. Many specific studies have been conducted to evaluate the impact of components such as organic matter and iron-based minerals on catalyzed hydrogen peroxide or Fenton's reagent oxidation (Crimi and Siegrist, 2005; Kwan and Voelker 2003; Petigara et al., 2002; Watts et al., 2002; Yeh et al. 2002; Watts et al. 1999; Lin and Gurol 1998; Valentine and Wang 1998; Voelker and Sulzberger 1996; Watts et al. 1994; 1993; Barcelona and Holm 1991). However, conflicting information with respect to the impact of organic matter on oxidation in peroxide systems has been documented (Watts and Teel, 2005; Petigara et al., 2002; Huling et al., 2001). While the successful application of hydrogen peroxide-based ISCO is strongly limited by the instability of hydrogen peroxide (Pignatello et al., 2006; Watts et al, 2006), an understanding of the factors that control the decomposition of hydrogen peroxide by aquifer solids and ways to improve its stability in the subsurface are required.

1.2 Research Objectives

The overall goal of this research was to investigate the interactions between two oxidants (permanganate and hydrogen peroxide) and aquifer materials. To meet this goal, the following specific objectives were defined:

- Identify and quantify the controlling factors related to oxidant consumption (for permanganate) or enhanced decomposition (for hydrogen peroxide)
- Determine appropriate kinetic relationships that capture the reaction between aquifer materials and permanganate or peroxide
- Develop bench-scale approaches to estimate oxidant consumption or enhanced decomposition by aquifer materials
- Evaluate and explore methods to enhance the stability of hydrogen peroxide in the subsurface environment
- Based on the data collected, develop predictive tools that can be used for ISCO system design

1.3 Thesis Organization

Chapter 2 describes the collection, handling, and characterization of the aquifer materials used in this research. The results of this characterization effort and subsequent quantification of total reductive capacity provide a basis for the comparison of oxidant interaction across different aquifer materials. Chapter 3 focuses on the investigation of permanganate interaction with aquifer materials through three series of carefully designed bench-scale experiments: (1) long-term batch experiments were used to investigate the permanganate consumption in response to fundamental chemical properties of aquifer materials, (2) short-term batch experiments were designed to investigate the kinetic behavior of permanganate in the presence of various aquifer materials, and (3) column experiments were used to investigate permanganate transport in a system that mimics the subsurface environment. Chapter 4 addresses research activities dealing with the interaction between hydrogen peroxide and aquifer materials. Batch experiments with a mixture of hydrogen peroxide and aquifer materials were used to capture the hydrogen peroxide behavior in the presence of various aquifer materials. Then, with the addition of chelating reagents, the enhanced stability of hydrogen peroxide was investigated under several scenarios. Finally, column experiments were performed to complement and expand the findings from the batch experiments. Chapter 5 summarizes the conclusions and significant contributions from this research.

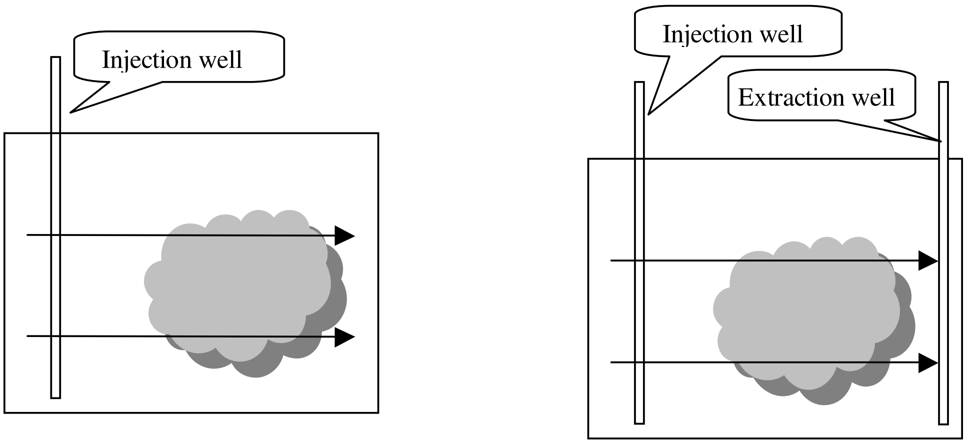

(a) **(b)**

Figure 1.1. Conceptual Schemes of ISCO Delivery Systems (a) passive mode using single or multiple injection(s), and (b) active mode using injection and extraction wells to hydraulically control oxidant delivery.

Chapter 2

Characterization of Aquifer Materials

2.1 Overview

This chapter describes the collection, handling, and characterization of the aquifer materials that were used in this research effort. Based on the physico-chemical properties of these aquifer materials, the theoretical total reductive capacity of each aquifer material was estimated and compared with the results from the dichromate chemical oxygen demand (COD) test.

2.2 Aquifer Materials

2.2.1 Collection and Handling

Wet uncontaminated aquifer material samples from nine sites were obtained for use in this investigation (see Table 2.1 for site information, soil texture, and a general description of the depositional environment). All of these sites are Department of Defense (DoD) and/or Department of Energy (DoE) sites throughout the United Sates except for Borden Canadian Forces Base (CFB) in Canada. Sites were selected based on: (1) the nature of the hydrostratigraphic units present and their suitability to the application of ISCO treatment technology if contaminated, (2) the availability of some basic geochemical information, and (3) the ability to coordinate our sample collection requirements with ongoing drilling activities at each site.

At least 50 kg of wet material was received from each site except for NAS-Dallas where around 10 kg of wet material was received in core tube liners (2-1.0 m long, 0.05 m diameter). Material was collected in the field in 2-19 L (5 US Gallon) buckets, except for the Borden aquifer material which was collected in aluminum core tubes (8-1.5 m long, 0.05 m diameter). Additional aquifer material from both DNTS (5-0.40 m long, 0.09 m diameter) and LAAP (5- 0.45 m long, 0.1 m diameter) was collected in core tube liners. The small mass of NAS-Dallas material limited its utility to those aspects of this investigation that required a minimal mass of aquifer material (i.e., the chemical oxygen demand test). All aquifer material was collected from unconsolidated deposits, with material obtained from seashore erosional deposits, alluvial deposits, fluvial deposits, a prograded beach environment, and a glacial drift deposit. The groundwater redox potential indicated that the aquifer material from LC34-USU, LC34-LSU, DNTS, and MAPP may have been anaerobic; however, only material from DNTS was collected in intact core tube liners in an effort to maintain the original redox state of the aquifer solids. All aquifer materials were stored at 4°C. In addition, where possible, a visual inspection of the aquifer material was immediately conducted after it was received at the University of Waterloo and variations in soil color, stratification details, and anomalies were noted. Based on a visual inspection and grain size data, all aquifer material collected for this investigation was predominantly sand; however, aquifer material from EGDY had large cobbles, material from NIROP contained gravel, and the LAAP material had a significant clay fraction.

The first four aquifer materials received at the University of Waterloo (LC34-USU, LC34-LSU, EGDY, and NIROP) were completely air-dried at 80°C in an incubator oven (Gallenkamp, 1H-100) to constant weight, and then allowed to cool to room temperature. Aquifer material from the remaining six sites were not immediately air-dried, but were used in a limited investigation focusing on the impact of air-drying on the reductive capacity of these aquifer materials (see Section 2.4). In response to the findings from this air-drying investigation, aquifer materials from these six remaining sites were also air-dried at 80°C in the incubator oven to constant weight. After air-drying and cooling to room temperature, each aquifer material was homogenized in large sterilized tubs by gently mixing by hand. Care was taken to avoid excess abrasion that may have led to grinding or pulverizing of soil particles. The use of a riffle box for this purpose was explored and deemed to be unsuitable. After mixing, the material was transferred to high density polyethylene (HDPE) bags (Cole-Parmer, 60104), sealed and stored at 4°C. As required during this investigation, sub-samples were selected at random from re-mixed stored material and air dried at 80°C to a constant mass again prior to use.

Due to the handling difficulty with the large size (>2mm) aquifer materials, only material passing though the No.10 U.S. Standard mesh sieve (2.00 mm) was used primarily throughout the course of this research. However, for aquifer materials with a significant large size (>2 mm) fraction (>10% by weight), separate experiments were performed to quantify permanganate consumption of these materials (see Chapter 3).

2.2.2 Sample Characterization

An overall description for the sample characterization performed and methods used is listed in Table 2.2.

The grain size distribution was determined by ASTM Method D422-63 with a 152 hydrometer (Appendix A). Specific gravity was characterized by ASTM Method D854-92. Entrapped air was removed by a vacuum system that was operated for >6 hours and pycnometers were filled with degassed water. Surface area was estimated by Porous Material Inc., Ithaca NY using a nitrogen multipoint BET analysis (Ball et al., 1990). The total organic carbon (TOC) analyses were performed at the University of Waterloo using the method developed by Churcher and Dickhout (1987). Cation Exchange Capacity (CEC) analyses were performed by the University of Guelph using Barium chloride method (Rhoades, 1982). X-ray diffraction (XRD) mineralogical analyses were performed on ground material at the University of Waterloo using an aluminum random powder mount and a Siemens D500 difractometer. Mineral phases were assigned based on comparison of spectra to standards from the International Center for Diffraction Data. This method has a quantification level of 5%.

The analyses of total carbon (TC) and total sulfur were preformed by Activation Laboratories Ltd., Ancaster, ON, Canada with LECO combustion using an infrared spectrometry method with a method detection limit (MDL) of 0.1 mg/g.

All metal analyses were also conducted by Activation Laboratories Ltd., Ancaster, ON. Fe(II), one of the most common reduced metals in aquifer solids, was expressed as FeO, which was determined through titration, using a cold acid digestion of ammonium metavanadate, sulphuric acid and hydrofluoric acid in an open system with a MDL of 78 mg/g (Wilson, 1955). In this method, ferrous ammonium sulphate was added after digestion and potassium dichromate was used as the titrating agent. Total Mn was determined by digesting a 0.25 g sample with four acids beginning with hydrofluoric, followed by a mixture of nitric and perchloric acids. This sequence uses precise heat ramping and holding cycles which takes the sample to dryness. After dryness is attained, samples are brought back into solution using hydrochloric acid. Samples are analyzed using a Perkin Elmer Optima 3000 ICP with a MDL of 1 mg/g. All other reported trace metals were determined by the Instrumental Neutron Activation Analysis (INAA) analytical technique. This technique is dependent on measuring gamma radiation induced in the sample by irradiation with neutrons. The primary source of neutrons for irradiation is usually a nuclear reactor. Each element which is activated emits a “fingerprint” of gamma radiation which can be measured and quantified. Further details are provided by Hoffman (1992).

The results of this sample characterization effort are presented in Table 2.3 and Table 2.4. The XRD mineral analyses are presented in Appendix B.

2.3 Reductive Capabilities of Aquifer Materials

2.3.1 Reductive Components

Reductive components present on the medium grain surface and in groundwater can vary more widely than those either in surface water or within aquifer solids. Of the various elements that comprise aquifer materials, those with variable oxidation states (including oxygen, iron, manganese, sulfur, and carbon) are mainly responsible for redox reactions (Hartog et al., 2003; Martin, 2003; Christensen et al., 2000; Appelo and Postma, 1996; Heron et al., 1994; Barcelona and Holm, 1991).

IRON: Iron is the most abundant transition metal in the earth's crust (about 56 ppt) (Martin, 2003). Iron occurs in two valence states (i.e., ferrous Fe(II) and ferric Fe(III)) in almost all mineral classes. In aquifer systems, the common iron minerals, which may dynamically affect groundwater constituents, include ferric-iron minerals such as hematite, goethite, magnetite, lepidocrocite, and amorphous iron oxyhydroxide, which are favored in oxidized conditions, and ferrous-iron such as amphiboles, proxenes, micas, siderite, and amorphous ferrous sulfide, which are favored in reduced conditions. Mackinawite and pyrite might be also important in reduced environments but would not survive in a typical surficial aquifer.

MANGANESE: Manganese is another important transition metal responsible for the redox environment in the subsurface. Of all the oxidation states, Mn(II), Mn(III), Mn(IV) are of greatest environmental importance in aquifer systems (Appelo and Postma, 1996; Hem, 1978; Tebo and He, 1998). The most stable form of manganese is Mn(IV), which exists in insoluble oxides such as pyrolusite, birnessite, nsutite and vernadite. Mn (II) can exist in carbonates (e.g., rhodocrosite) or can occur as an insoluble ion under acidic conditions (even for a high oxidizing situation). The thermodynamically unstable Mn(III) does not occur in the soluble form except in the presence of strong complexing agents such as humic and other organic acids (Hem, 1978; Tebo and He, 1998); however, it widely exists in the forms of oxides and oxyhydroxides such as manganite, bixbyite, and hausmannite ($Mn^{2+}Mn^{3+}{}_2O_4$ –

Mn_3O_4).

<u>SULFUR:</u> Sulfur plays an important role in the subsurface redox processes with its various oxidation states. Sulfur-containing minerals in aquifer systems mainly occur as element sulfur (S), sulfate (e.g., gypsum) and sulfide (e.g., mackinawite, pyrite, and marcasite), etc. Of all sulfur minerals, the most common sulfur-containing minerals affecting the constituent evolution in groundwater are gypsum and pyrite (Hartog, 2003; Christensen et al., 2000; Appelo and Postma, 1996; Brennan and Lindsay, 1996)

<u>CARBON:</u> Carbon in aquifer systems includes both inorganic and organic carbon. Most of the inorganic carbon in aquifers exists in carbonates, which are ubiquitous in aquifer systems (Appelo and Postma, 1996; Morse and Arvidson, 2002). Natural organic matter exists from various sources such as organic material in water recharged from the ground surface, plant debris or roots of dead vegetation and other biomass types. The importance of aquifer organic matter (AOM) as a redox contributor and sorbent has been long recognized (Appelo and Postma, 1996; Christensen et al., 2000; Hatog, 2003; Pignatello, 1998). Due to the variety of AOM sources, the composition at the molecular level is still poorly understood and unexplored (Hartog, 2003; Pignatello, 1998). It is widely accepted that the bulk organic fraction in a typical aquifer system mainly consists of humic compounds that bear little physical and chemical resemblance to their precursor biopolymers, with molecular weights ranging from 200-20,000 g/mol (Pignatello, 1998). However, this is not always true in all cases due to chemical heterogeneity. Humic substances are composed of fulvic acid (water soluble), humic acid (water soluble only at alkaline condition) and humin (water insoluble). Their major functional groups are carboxylic acids, phenolic and alcoholic hydroxyls, and ketone and quinine groups (Kappler and Haderlein, 2003). Aquifer organic matter generally co-occurs with other aquifer substrates (e.g., complex) and is even bound to mineral particles (Pigenatello, 1998; Appelo and Postma, 1996; Gu et al., 1994; Mayer, 1994; Brownawell et al., 1990). Studies at the microscopic scale indicate that AOM may be present as coatings on solids, isolated particles, and incorporated into mineral matrices (Song et al., 2002; Weber et al., 1998; Luthy et al., 1997).

2.3.2 Reactivity of Reductive Components

The introduction of a strong chemical oxidant that occurs during ISCO treatment will obviously impact the naturally-occurring multivalent elements in their reduced states (Mumford, 2002; Siegrist et al., 2001) and lead to its unproductive consumption (for permanganate) or enhanced decomposition (for hydrogen peroxide). Theoretically, the reduced constituents commonly present in aquifer systems that may contribute to the consumption or enhanced decomposition of injected oxidants are organic matter, Fe(II)-contained minerals (e.g., micas, amphiboles, pyroxenes, pyrite and siderite), Mn(II, III)-contained minerals (e.g., rhodocrosite and hausmannite), S(-I, -II)-contained minerals (e.g., pyrite and mackinawite) and other trace metals such as As- and Cr(III)-contained minerals (Appelo and Pastma, 1996). However, in practice, only substrates containing Mn(II), Fe(II), and S(-I,-II), reduced forms of nitrogen (if they exist), and AOMs are considered the predominant reductants in a natural aquifer while other reduced constituents are minimal (Hartog, 2003; Christensen et al., 2000; Korom et al., 1996; Appelo and Postma, 1996).

A number of studies have focused on the reactivity of the aquifer reductants (e.g., organic- C, Fe(II), Mn(II), and S(I, II)-containing substances) with respect to oxygen. This is especially true in the weathering of naturally occurring minerals in aquifer systems (Rivas-Perez et al., 2003; Appelo and Postma, 1996). As mentioned previously, iron is very important in the subsurface redox process, and therefore has been and remains to be a major research topic. Three types of reduced iron species, structural Fe (II), surface-complexed Fe(II), and exchangeable Fe(II), associated with clay minerals could be a highly reactive source of total reactive iron (II) in the subsurface (Hofstetter et al., 2003). Hartog et al. (2001; 2002) identified oxygen-sensitive components in a pristine aquifer in which all reductants were simultaneously oxidized in decreasing rates. Studies on the effect of different parameters on the pyrite oxidation by oxygen in the near neutral pH range show that the reaction rate was first-order with respect to the surface area of the pyrite grain (Nicholson et al., 1988). In addition to the direct dissolution of pyrite, the generation of either Fe^{2+} and sulfate or ferric hydroxide and sulfate ion, which obeys the first-order redox reaction with respect to oxygen, is also involved in the overall reactions that are responsible for the pyrite decomposition (Kamei and Ohmoto, 2000).

The complete oxidation of Mn(II), Fe(II), S(-I,-II), and As(III) (as AsO_2^-), and reduced forms of nitrogen are given by the half-reactions

$$Mn(II) + 2H_2O \rightarrow MnO_2(s) + 4H^+ + 2e^- \tag{2.1}$$

$$Fe(II) + 3H_2O \rightarrow Fe(III)(OH)_3(s) + 3H^+ + e^- \tag{2.2}$$

$$S(-II) + 4H_2O \rightarrow SO_4^{2-} + 8H^+ + 8e^- \tag{2.3}$$

$$S(-I) + 4H_2O \rightarrow SO_4^{2-} + 8H^+ + 7e^- \tag{2.4}$$

$$AsO_2^- + 2H_2O \rightarrow AsO_4^{3-} + 4H^+ + 2e^- \tag{2.5}$$

$$NH_4^+ + 3H_2O \rightarrow NO_3^- + 10H^+ + 8e^- \tag{2.6}$$

AOM has been extensively studied as a sorbent (Luthy et al., 1997; Pignatello, 1998; Weber et al., 1998). It is also well recognized that AOM serves as a reactant in various reactions in the subsurface (Appelo and Postma, 1996). For example, in Fenton's/Fenton's-like systems, the carboxylate or phenolic functional groups in natural organic substances may act as a ligand of Fe(II), a scavenger of hydroxyl radicals, and reductant of ferric oxides (Voelker and Sulzberger, 1996). Also, as a sorbent for hydrophobic substances as well as a competing reductant for hydrogen peroxide, the presence of AOM may also impact the decomposition rate of hydrogen peroxide (Yeh et al., 2002). Studies have shown that there is a relationship between the AOM availability and sorption to mineral surface in sediments (Mayer, 1994; 1999). AOMs may be chemically refractory as well as labile towards oxidation, and therefore, the AOM oxidation by an oxidant is highly dependent on the reactivity of the various organic structures that makes up the AOM. In the presence of oxygen, the most labile compounds are consumed at high rates while the degradation of the recalcitrant fraction is at a low rate. As such, a first-order reaction model is employed to describe the overall decrease of AOM reactivity with time (Hartog, 2001; 2003). However, recalcitrant organic compounds such as lignin or macromoleculars degrade much faster under aerobic than anaerobic conditions (Canfield, 1994) in the presence of oxidants (such as nitrate). Furthermore, the co-occurrence of several potentially reactive reductants on the aquifer solid surface might also complicate the reactivity of the organic matter. For example, Hartog (2002) observed that the oxidation of AOM in the fine fractions demonstrated less importance than the oxidation of pyrite and siderite while AOM oxidation was quite important in coarse fractions. This might be attributed to the decreasing reactivity of AOMs in the fine fractions as a result of sorption and complexation of AOMs by clay minerals (Mayer, 1994). Humic acid is stable and resistant to weathering in an oxidative environment (Fujikawa and Fukui, 2001); however, in the presence of alkaline permanganate, the oxidation of humic acids might release different kinds of products (e.g., benzenepolycarboxylic acids, phenolic acids, and fatty acids) with varying resistance to the attack of permanganate, depending on the reaction temperature (Almendros et al., 1989). Degradation to carbon dioxide is generally thought to be the complete mineralization of most organic compounds (Appelo and Postma, 1996; Starwart, 1964; 1965; Stumm and Morgan, 1996), but some studies have also concluded that oxalate might be the only organic product in the oxidation of humic and non-humic soils by permanganate or even hydrogen peroxide (Harada and Inoko, 1977; Farmer and Mitchell, 1963).

Although the reductive reactivity of AOMs depends on their availability and structure as well as the type of the oxidant, almost all studies presumed that the end carbon product of the oxidation of an AOM was carbon dioxide. In addition, many studies tend to consider that the presence of alkyl and O-alkyl moieties was significant in the humic materials (Hatcher et al., 1981; Almendros and Leal, 1990); therefore, regardless of its complexities, AOM is usually presented as a general organic form CH_2O (Andersen et al., 2001; Christensen et al., 2000; Hartog et al., 2001; Heron et al., 1993; Mumford, 2002). As such, the reaction can be written as

$$CH_2O + H_2O \rightarrow 4e^- + 4H^+ + CO_2 \tag{2.7}$$

If C_nH_{2m} is taken as a general form for organic matter (Verschuren, 1983), the following example half-reaction occurs

$$C_nH_{2m} + 2nH_2O \rightarrow 4ne + nCO_2 + (2m + 4n)H^+ \tag{2.8}$$

Other expressions for AOMs have been also suggested; for example, Hartog (2002; 2003) identified the main types of organic matter present in their research aquifer material and used syrinagate ($C_9H_{10}O_5$) as a representative model which produces

$$C_9H_{10}O_5 + 9O_2 \rightarrow 5H_2O + 9CO_2 \tag{2.9}$$

Other studies have also shown that quinine groups might be the main redox active moieties of humic substances (Kappler and Haderlein, 2003; Scott et al., 1998), and therefore, it might be reasonable to use phthalic acid ($C_8H_6O_4$ or $C_6H_4(COOH)_2$) to represent the AOMs (Barcelona and Holm, 1991) with a half-reaction of

$$C_8H_6O_4 + 12H_2O \rightarrow 8CO_2 + 30H^+ + 30e^- \tag{2.10}$$

2.3.3 Theoretical Estimation of Total Reductive Capacity (TRC)

The total reductive capacity (TRC) has been used as an index to quantify the reductive properties of aquifer materials or solids (Christensen et al., 2000) and theoretically, represents the sum of the reduced equivalencies of species associated with a given aquifer material that is required to convert them to their corresponding naturally occurring highest stable oxidation states.

Using the analytical data provided in Table 2.3 and Table 2.4, the reduction capacity for selected species was estimated for all the aquifer materials. In these calculations, it was assumed that phthalic acid was a reasonable model compound for the reduction capacity of humic substances (Barcelona and Holm, 1991), and Eq.(2.10) was used to estimate the TRC contribution from the AOM. Since insufficient information on the form of the inorganic species was available, the calculation of TRC from reduced iron, manganese, and sulfur was conducted with different combinations (i.e., as total or amorphous Fe or Fe(II), total or amphorous Mn, and total S) using Eqs 2.1 to 2.4. The estimated theoretical TRC values are listed in Table 2.5 and shown in Figure 2.1. Table 2.5 indicates that the estimated TRC spans from 0.28 to 1.56 meq/g based on total organic carbon (TOC), total Fe and Mn, total S, and from 0.08 to 1.23 meq/g based on TOC and amorphous Fe and Mn. As expected, the contribution of total S is <10% to the TRC (as estimated from the total species content) for all aquifer materials except for the NFF aquifer material where the contribution is ~16% of the total TRC. Figure 2.1 (b) indicates that the contribution from total Mn is insignificant relative to the contribution from total Fe and total organic carbon (TOC), while Figure 2.1(c) indicates that the contribution from amorphous Fe and Mn (in their reduced forms) is insignificant relative to the contribution from TOC. Figure 2.1(d) indicates that for Borden, DNTS, and LAAP aquifer materials the contribution of ferrous iron content to the total TRC is greater than the TOC contribution. Acknowledging that the TRC reflects the reductive capability, the maximum permanganate NOD is expected for the NFF and EGDY aquifer materials while the minimum permanganate NOD is expected for the MAAP and DNTS aquifer materials.

2.3.4 Experimental Estimation of TRC

To quantify the overall reactivity of the naturally-occurring reductants with chemical oxidants, various terminologies such as "natural oxidant demand (NOD)", "soil oxidant demand (SOD)", and "total reductive capacity (TRC)" or "natural reductive capacity (NRC)" have been developed (Mumford et al., 2005; Hartog et al., 2002; Huang et al., 2001; Christensen et al., 2000; Hood, 2000; Powell et al., 1988; Barcelona and Holm, 1991; Pedersen et al, 1991). Powell et al. (1988) and Barcelona and Holm (1991) concluded that the reductive capacity measurement could be rapidly realized using acidified dichromate chemical oxygen demand (DCOD) method, and many subsequent studies have used this method to experimentally determine the reductive capacity of aquifer solids (Lee and Batchelor, 2003; Korom, 1996; Pedersen et al., 1991).

In this work, the above mentioned dichromate COD test method proposed by Barcelona and Holm (1991) was slightly modified and used to quantify the total reductive capacity (TRC) of aquifer materials. Initially sub-samples of the air-dried aquifer material were ground to <150 μm with a mortar and pestle, and aliquots of dry ground solids (~1.5 g) were transferred to pre-cleaned reaction tubes. A volume (~20 mL) of potassium dichromate digestion solution (potassium dichromate (BDH Laboratories), sulfuric acid (EM Science), and mercury sulphate (EM Science)) and a sulfuric acid reagent solution (sulfuric acid (EM Science) and silver sulphate (Alfa Aesar)) were added to each reaction tube. The reagents (sulfuric acid/potassium dichromate/mercury sulfate) were prepared following standard methods (APHA, 1998). When gas evolution ceased, the reaction tubes were sealed, inverted carefully by hand three times, and then heated (PMC, Model 350) at 150^{o}C for 3 hours. After cooling, the reaction tubes were centrifuged for 1 hour at 4000 rpm (Beckman, Model TJ-6) to clear the supernatant solution for measurement of un-reacted Cr(VI) by spectrophotometer (Milton Roy, 20D) at 420 nm. A standard curve using potassium hydrogen phthalate (KHP) (EM Science) was developed in parallel, and was used to quantify the chemical oxygen demand (APHA, 1998). KHP has a theoretical chemical oxygen demand of 1.176 mg O_2/mg KHP and based on the developed standard curve and the mass of each sample the chemical oxygen demand (g O_2/kg of aquifer material) was determined.

The dichromate COD values for the tested aquifer materials are listed in Table 2.5. For comparison and convenience, all dichromate COD values were converted into an equivalent mole of electrons per mass of aquifer material. All dichromate COD tests were performed three to five times for each aquifer material. Statistical outliers were removed by the Barnett and Lewis (1994) outlier detection test. Because the fraction of reductive components that acidified dichromate ions can react with might vary across different solid materials (Christensen et al., 2000), it is not surprising that the tested aquifer materials exhibit a wide range of dichromate COD values (0.06 to 2.05 meq/g). The maximum dichromate COD

(2.05 meq/g) was determined for the NFF aquifer material while the MAAP aquifer material yielded the minimum value (0.06 meq/g). The results from the COD tests confirm the TRC results that suggest that the maximum permanganate NOD will be realized for the NFF and EGDY aquifer materials, while the minimum permanganate NOD will be obtained for the MAAP and DNTS aquifer materials.

2.3.5 Results and Discussion

The TRC and dichromate COD data (Table 2.5 and Figure 2.2) show that the theoretical estimation of the TRC is generally greater than the corresponding dichromate COD value except for the NFF aquifer material. As discussed in Section 2.3.3, if the bulk soil concentrations of all the reduced species that may participate in the oxidation reaction are known, then the total reductive capacity can be estimated from the appropriate half – reaction equations (i.e., Eqs.2.1-2.10); however, this TRC is only a theoretical estimate. It has been argued that not all reduced components are responsible for the reductive capacity. For example, Lee and Batchelor (2003) observed that only 16% of Fe (II) in soil minerals was able to reduce the [Cr(VI)] oxidant. Based on the long-term observations of permanganate demand of a sand aquifer material, Mumford et al. (2005) showed that not all organic carbon could be oxidized. It is most likely that part of the biopolymeric residues of natural organic substances, if encapsulated in black carbon matrices, were not fully exposed to the oxidant (Song et al., 2002), and therefore an experimentally measured reductive capacity could be less than the theoretical reductive capacity (Hartog, 2003).

The results from a correlation analysis indicate that there is a strong linear relationship (r^2 = 0.94) between the dichromate COD test results and total organic carbon (TOC) content (Figure 2.3). However, if the high dichromate COD and TOC values for NFF aquifer material are removed to eliminate the potential bias, then the linear relationship is not as strong (r^2 = 0.89). In contrast, a weak linear relationship (r^2 = 0.58) between theoretical TRC and TOC can be improved (r^2 = 0.86) if the data from DNTS are excluded, which has an extremely high TRC value, possibly being overestimated due to the use of total iron instead of reduced iron contents in the calculation (see Figures 2.1(b) and (d)). Nevertheless, the good linear relationship between both the TRC and Dichromate COD (DCOD) values and TOC content indicates that organic carbon is a major reductant in these aquifer materials. Further correlation analysis results showed that linear relationships do not exist between either TRC or DCOD and any combinations of total Fe, total Mn, amorphous Fe, and amorphous Mn ($r^2 < 0.5$).

2.4 Impact of Air-Drying on the Reductive Properties of Aquifer Materials

Implicit in the use of air-dried aquifer materials is the assumption that exposure of aquifer materials to atmospheric conditions has a negligible impact on the *in situ* total reductive capacity of these aquifer materials for the selected oxidants of interest. Certainly air drying will affect the estimation of the total reductive capacity of aquifer materials from anaerobic systems where reduced metals are present; however, we know very little related to the impact of air drying on aquifer materials from aerobic classified aquifer systems. The reported disequilibrium between the aqueous phase (groundwater) and the aquifer solids provide additional support for this concern (Sparks et al., 1998). Barcelona and Holm (1991) investigated the impact of handling and storage on aquifer material reduction capacity and concluded that neither drying, two years storage at 4°C, or grinding to less than the No. 100 US Standard mesh-sieve (<150 μm) had any impact on the measured reduction capacity relative to freshly collected samples. However, this finding is specific to material from their study site which was a sand-and-gravel aquifer with a low total organic carbon content (<0.001 g/g). Based on limited literature data and our concern with the use of air dried aquifer materials in this study, it was necessary to investigate the impact of air drying on the reduction properties of aquifer materials. Since four aquifer materials were air dried prior to the initiation of this study, only the six "wet" aquifer materials (Borden, DNTS, MAAP, NFF, NIROP, and NAS) were used.

2.4.1 General Methodology

Sub-samples of the six "wet" aquifer materials were transferred into an anaerobic glove box continuously purged with nitrogen gas (industrial grade, 99.995% pure). A representative sub-sample from material received in buckets was collected by mixing the contents in one bucket and then removing ~1.5 L from at least 0.1 m below the free water surface. For material received in core tubes or sleeves, the sub-sample was limited to a segment of a core (see Table 2.6). Inside the glove box, each sub-sample was mixed wet as much as feasible and then split into three portions. Only wet material passing through the No. 10 U.S. Standard mesh sieve was used. The first portion was removed from the glove box, air dried at 80°C, and all subsequent handling was conducted under normal atmospheric conditions. The second portion was dried under nitrogen gas at 80°C (Figure 2.4) and then removed from the glove box and exposed to atmospheric conditions for 1 month prior to testing. The third portion was dried under nitrogen gas at 80°C and all subsequent handling and testing was conducted within the nitrogen purged glove box.

To estimate the reduction capacity and discriminate any statistical differences in the various aquifer material drying methods, three tests were used; the dichromate chemical oxygen demand (COD) test, the permanganate chemical oxygen demand (COD) test, and a 7-day permanganate batch reactor test using two mass loadings (solids concentration of 0.375 and 0.75 g/mL), a 10 g-$KMnO_4$/L solution, and 40 mL reactors. The 7-day permanganate batch reactor tests were run in the same manner as the batch reactors used in the long-term permanganate demand investigation described in Chapter 3, but sampled and terminated after 7 days. Details of permanganate COD tests are described in Chapter 3. Five replicates were performed for each test.

2.4.2 Results and Discussion

The average reduction capacity results are presented in Appendix C and shown in Figure 2.5 and for convenience are expressed in terms of g of $KMnO_4$ per kg of dry aquifer material.

Statistical outliers were removed by the Barnett and Lewis (1994) outlier detection test.

In general, the reduction capacity as measured by the various tests was higher for the nitrogen dried samples relative to the nitrogen dried/air exposed and air dried samples. For reasons that are unknown, the exception to this trend is the material from Borden. There is no statistically significant difference (*t*-test, $\alpha = 5\%$) in the dichromate-COD results, the permanganate-COD results and the 7-day permanganate NOD results between any combination of drying methods expect for the aquifer material from NFF. This is likely due to the large single sub-sample variance from each test and is reflective of reduction capacity heterogeneity within each aquifer material. For the NFF material there was a statistically significant difference (*t*-test, $\alpha = 5\%$) between the air dried and nitrogen dried dichromate-COD values, and between the air dried and the 7-day permanganate NOD values. This indicates that some fraction of the reductive capacity was lost during air drying and storage. As further evidence to support the impact of air drying on the NFF aquifer materials, the total organic carbon for the air dried and the nitrogen dried material was 0.00216 g/g (1 sample/2 replicate measurements) and 0.00310 g/g (2 samples/2 replicate measurements each) respectively. The approximately 0.001 g/g decrease in the organic carbon content as a result of air drying confirms the impact of air drying on the NFF aquifer materials.

Perhaps aquifer materials with a high reductive capacity will show a significant impact from the air-drying process, while low reductive capacity aquifer materials will not show a significant impact from the air-drying process. Unfortunately the NFF aquifer material appears to have the highest reductive capacity of all the aquifer materials used in this investigation, and hence we are unable to provide guidance as to when air-drying may impact reductive capacity laboratory estimates. Although this issue remains unresolved, the impact of air dying clearly cannot be dismissed.

Table 2.1. General site information where aquifer material was collected for use in this study.

No.	Sample ID	Sample Location	Soil Texture	Depositional Environment	Depth to Water (ft bgs)	K (ft/day)	Sample Depth (ft bgs)
1	Borden	Groundwater Field Laboratory, CFB Borden, Ontario	fine/medium sand	Late Wisconsinian Period/ deposited in a prograded beach environment/ glaciolacustrine sand/ unconfined aquifer	~3	~3	10-15
2	DNTS	National Test Site, Dover AFB, DE	sandy loam	Colimbia formation from fluvial deposits; Pleistocene	~20	~2.8	30-42
3	EGDY	East Gate Disposal Yard, Fort Lewis, WA	loamy sand, gravel, cobbles	Vashon glacial drift deposit/ recessional outwash	~18	16-1141	18-25
4	LAAP	Site 16 Landfill, Longhorn Army Ammunition Plant, TX	clay loam	Wilcox Group: quaternary alluvium mantling & tertiary age formations - generally unconsolidated sediments	~18	2	13-28
5	LC34 LSU	Launch Complex 34, Cape Canaveral AFS, FL	loamy coarse /medium sand	Pleistocene and recent seashore erosional deposits	~6	1.3-6.4	32-45
6	LC34 USU	Launch Complex 34, Cape Canaveral AFS, FL	loamy coarse / medium sand	Pleistocene and recent seashore erosional deposits	~6	1.3-6.4	10-27
7	MAAP	Milan Army Ammunition Plant, TN	sand	Tertiary age sands of Clairborne group (Memphis sand) silt and clay layers in sand may be carbonaceous and lignitic	~ 1	~ 163	46 - 68
8	NIROP	NIROP, Bacchus Works Facility, Utah	gravels, loam	Harkers formation; Alluvial deposit from quaternary age	~40	2-238	170-180
9	NFF	NFF, Cecil Field, Florida	loamy fine sand	Post-Miocene, likely Pliocene to Pleistocene; long-transport fluvial deposits which have experienced extensive erosion and reworking	~	~3	24-36
10	NAS	NAS Dallas, TX	silty loam	Information Not Available	~	~	~

Table 2.2. Summary of characterization methods.

Properties	Items	Methods	Reference
Physical	Grain size analysis	ASTM method D422-63 with a 152-hydrometer	ASTM (1990)
	Specific surface area	Nitrogen multipoint BET analysis	Ball et al. (1990)
	Specific gravity	ASTM method D854-92	ASTM (1990)
Chemical	XRD Mineral analysis	Simens D500 difractometer	-
	Soil pH	ASTM method D4972-01	ASTM (1990)
	Cation exchange capacity	Performed by U. of G. using Barium chloride method	Rhoades (1982)
	Amorphous iron and manganese	Selective dissolution analysis method	Jackson et al. (1986)
	Total Fe	INAA performed by ACTlab, Ancaster, ON	www.actlabs.com
	Fe(II) as FeO	Titration with cold acid digestion performed by ACTlab, Ancaster, ON	
	Total Mn	Perkin Elmer Optima 3000 ICP by ACTlab, Ancaster, ON	
	Other trace metals	Instrumental Neutron Activation Analysis (INAA)	Hoffman (1992)
	Total S	The infrared method performed by ACTlab, Ancaster, ON	www.actlabs.com
	Total organic carbon	Complete combusion of samples performed by UofW	Churcher and Dickhout (1987)
	Total Carbon	The infrared method performed by ACTlab, Ancaster, ON	www.actlabs.com

Table 2.3. Summary of aquifer materials characteristics.

Characteristic	Borden	DNTS	EGDY	LAAP	LC34 LSU	LC34 USU	MAAP	NFF	NIROP	NAS
grain size:										
% gravel	0.2	8.3	73.62	0	4.01	0.90	0	0	52.80	-[5]
% sand	89.7	67.4	21.22	39.7	83.84	91.96	95.7	90.6	32.08	-
% clay & silt	10.1	24.3	5.16	60.3	12.16	7.15	4.3	9.4	15.12	-
% < 2 mm	99.4	89.7	18.30	100	86.55	95.25	100	100	32.50	-
d_{60} [mm]	0.2	0.54	22.75	0.075	0.49	0.25	0.35	0.2	7.85	-
d_{30} [mm]	0.15	0.18	6.30	0.0055	0.13	0.15	0.25	0.17	1.50	-
d_{10} [mm]	0.075	0.003	0.450	<0.0013	0.065	0.085	0.15	0.075	0.040	-
hydraulic conductivity [cm/s] [1]	0.00563	0.000009	0.203	<0.00000169	0.004	0.007	0.0225	0.0056	0.002	-
coefficient of uniformity [-]	2.67	180.00	50.56	>57.69	7.54	2.94	2.33	2.67	196.25	-
coefficient of gradation [-]	1.50	20.00	3.88	>0.310	0.53	1.06	1.19	1.93	7.17	-
specific gravity [g/mL]	2.71	2.67	2.67	2.6	2.71	2.69	2.65	2.66	2.64	-
pH [-]	8.4	6.1	7.2	6.9	8.6	8.8	7.0	3.7	8.9	-
bulk surface area [m^2/g]	4.155	7.431	3.121	11.208	2.160	1.919	4.333	3.024	7.598	4.191
cation exchange capacity [cmol(+)/kg]	3.5	2.6	8.4	16.1	12.8	8.3	0.9	5.7	17.6	4
% total carbon [g/g]	1.58	0.14	0.30	0.06	4.15	3.15	0.01	0.26	3.55	0.65
% total organic carbon (g/g): < 2 mm sample	-	-	0.228	-	0.184	0.0878	-	0.393	0.0315	-
% total organic carbon (g/g): bulk sample	0.024	0.028	0.170	0.046	0.074	0.039	0.077	0.216	0.030	0.059
Fe (amorphous) [mg/g]	0.297	0.356	1.189	0.260	0.504	0.407	0.037	-[5]	0.754	0.318
% total sulphur [g/g][2]	0.02	0.01	-[5]	0.01	-[5]	-[5]	0.01	0.10	-[5]	0.01
bulk mineralogy[3]	quartz	quartz[4]	quartz	quartz[4]	quartz	quartz	quartz[4]	quartz[4]	quartz	-
	plagioclase		feldspar		calcite	calcite			calcite	-
	calcite		(plagioclase)		aragonite	aragonite			dolomite	-
	trace magnetite & ilmenite				trace feldspars	trace feldspars			trace feldspars	-

Notes:

1. Estimated by the Hazen Equation.
2. MDL 0.01% [g/g]
3. No Fe or Mn minerals detected.
4. Other minor minerals may also exist
5. Data not collected.

Table 2.4. Trace metal concentrations (mg/kg).

Sample		MDL	LC34-USU		LC34-LSU		NIROP		EGDY		MAAP		BORDEN		LAAP		NFF		DNTS		NAS	
ID	Name		Avg	Std Dev	Avg	Std Dev	Avg	Std Dev	Avg	Std Dev	Avg	Std Dev	Avg	Std Dev	Avg	Std Dev	Avg	Std Dev	Avg	Std Dev	Avg	Std Dev
Au	Gold	0.002	<0.002	-	<0.002	-	<0.002	-	0.03	-	<0.002	-	<0.002	-	<0.002	-	<0.002	-	0.003	-	<0.002	-
Ag	Silver	5	<5	-	<5	-	<5	-	<5	-	<5	-	<5	-	<5	-	<5	-	<5	-	<5	-
As	Arsenic	0.5	2.6	0.1	5.6	0.14	13.7	1.33	48.9	2.70	1.3	0.20	1.0	-	4.7	0.62	2.6	0.5	9.5	0.75	4.6	0.75
Ba	Barium	50	150	27.0	200	7	360	26	507	11.5	<50	-	660	50	550	47	66	-	330	31	137	5.77
Br	Bromine	0.5	1.1	0.15	2.6	0.071	0.9	-	0.7	-	<0.5	-	0.8	-	<0.5	-	0.8	-	<0.5	-	0.6	-
Ca	Calcium	10000	100000	6000.0	160000	0.0	90000	10000	20000	6000	<10000	-	60000	6000	<10000	-	<10000	-	<10000	-	20000	6000
Ce	Cerium	3	29	4.5	36	2.1	48	3.1	44	0.58	5	2	35	3.0	96	5.9	31	3.8	79	7.0	20	0.6
Co	Cobalt	1	1	-	2	0	5	0	13	0.58	1	-	5	0	6	1	3	0.6	6	0	4	1
Cr	Chromium	5	10	2	15	0.71	85	8.5	82	4.9	7	2	26	2.5	70	6	15	3.2	89	6.5	14	3.6
Cs	Cesium	1	<1	-	<1	-	2	0	2	-	<1	-	<1	-	3	0	<1	-	5	0	<1	-
Eu	Europium	0.2	0.5	0.1	0.7	0.07	1.0	0.31	1	0.1	<0.2	-	1.2	0.058	1.7	0.15	0.3	0.1	1.5	0.12	0.4	0
Fe	Iron (total)	1000	3700	58	6100	71	12900	954	39200	1970	867	57.7	17500	833	22700	1710.0	4500	720	63800	4250	11500	1630
Fe^{2+}	Iron (ferrous)	78									700	0	11700	987	14400	1340	3890	404	8890	701	4090	661
Hf	Hafnium	1	6	0.6	7	0.7	5	0.6	4	0.6	7	0.6	8	0.6	13	0.58	11	2.1	9	0.6	3	0
Hg	Mercury	1	<1	-	<1	-	<1	-	<1	-	<1	-	<1	-	<1	-	<1	-	<1	-	<1	-
Ir	Iridium	0.005	<0.005	-	<0.005	-	<0.005	-	<0.005	-	<0.005	-	<0.005	-	<0.005	-	<0.005	-	<0.005	-	<0.005	-
La	Lanthanum	0.5	11.4	0.862	13.6	0.0707	27.8	0.874	15.7	0.100	2.3	0.26	13	0.12	37.7	1.01	14.3	0.896	39.2	2.60	10.5	0.862
Lu	Lutetium	0.05	0.18	0.029	0.22	0.028	0.3	0.01	0.42	0.021	0.09	0.03	0.42	0.055	0.55	0.025	0.14	0.0058	0.69	0.061	0.13	0.021
Mo	Molybdenum	1	2	-	2	0.7	2	-	5	-	<1	-	1	-	5	-	2	-	<1	-	3	0.6
Mn	Manganese	1	98	7.5	68	2.5	297	26.4	700	20	25	6.1	421	27.8	112	1.89	65	5.8	154	20.6	151	23.5
Na	Sodium	100	2900	58	4000	0	3700	170	22000	660.0	200	0	20800	971	3600	150	267	57.7	967	57.7	600	60
Nd	Neodymium	5	10	2.5	13	1.4	23	1.5	13	0.58	<5	-	12	1.0	34	2.0	13	1.0	33	2.0	10	0.6
Ni	Nickel	20	<21	-	<28	-	<31	-	<55	-	<20	-	<39	-	<36	-	<20	-	<46	-	<20	-
Rb	Rubidium	15	<15	-	21	2.8	28	11	33	-	<15	-	49	14	81	8.9	<15	-	82	2.1	16	-
Sb	Antimony	0.1	0.2	0	0.3	0	0.7	0.1	1.3	0.058	0.1	-	0.2	-	1.0	0.17	0.2	0.1	0.7	0.2	0.3	0.1
Sc	Scandium	0.1	1.4	0.058	2.2	0.071	3.9	0.10	15.0	0.61	0.7	1.05E-08	6.4	0.23	9	0.5	2.0	0.46	12.5	1.10	1.5	0.10
Se	Selenium	3	<3	-	<3	-	<3	-	<3	-	<3	-	<3	-	<3	-	<3	-	<3	-	<3	-
Sm	Samarium	0.1	2.1	0.20	2.6	0.071	3.6	0.058	3.7	0.12	0.4	0.1	3.3	0.26	5.8	1.19E-07	2	0.1	6.6	0.56	1.9	0.058
Sn	Tin	100	<100	-	<100	-	<100	-	<100	-	<100	-	<100	-	<100	-	<100	-	<100	-	<100	-
Sr	Strontium	500	600	-	900	0	<500	-	600	-	<500	-	567	-	<500	-	<500	-	<500	-	<500	-
Ta	Tantalum	0.5	0.6	-	<0.5	-	0.6	-	1.1	-	<0.5	-	<0.5	-	0.8	-	0.6	1.05E-08	1.5	0.12	<0.5	-
Tb	Terbium	0.5	<0.5	-	<0.5	-	0.5	-	0.5	-	<0.5	-	<0.5	-	<0.5	-	<0.5	-	0.8	-	<0.5	-
Th	Thorium	0.2	3.4	0.61	3.9	0.071	6.2	0.32	4.5	0.21	1.3	0.17	2.0	0.15	9.8	0.29	4.9	0.38	11.7	0.833	2.2	0
U	Uranium	0.5	1.9	0.058	2.7	0.49	3.3	0.10	2.3	0.25	0.5	-	0.6	-	3.9	0.78	3.1	0.36	2.9	0.35	0.6	0.1
W	Tungsten	1	<1	-	<1	-	4	0.6	<1	-	<1	-	<1	-	1	-	<1	-	<1	-	<1	-
Yb	Ytterbium	0.2	1.2	0.12	1.4	0.071	1.9	0.058	2.7	0.15	0.5	0.2	2.7	0.31	3.6	0.10	0.9	0.1	4.6	0.42	0.8	0.2
Zn	Zinc	50	<50	-	<50	-	<50	-	74	-	<50	-	<50	-	59	-	<50	-	103	21.1	<50	-

▓ 1 MDL was used in calculating the average
░ 2 MDLs were used in calculating the average

Table 2.5. Estimation of the theoretical total reduction capacity and dichromate COD test results (units: meq/g).

	TRC (meq/g)					DCOD (meq/g)	
	TOC + Fe_T+Mn_T+S_T	TOC+ Fe_T+Mn_T	TOC + Amorphous(Fe+Mn)	TOC + Fe_T or Fe(II)	TOC	Avg.	Stdev
Borden	0.45	0.40	0.08	0.28	0.08	0.19	0.01
DNTS	1.26	1.24	0.09	0.25	0.09	0.12	0.03
EGDY	1.44	1.44	0.74	1.42	0.71	1.03	0.02
LAAP	0.58	0.55	0.15	0.40	0.14	0.15	0.01
LC34-LSU	0.69	0.69	0.58	0.68	0.58	0.57	0.01
LC34-USU	0.34	0.34	0.28	0.34	0.28	0.21	0.01
MAAP	0.28	0.26	0.24	0.25	0.24	0.06	0.02
NAS	0.42	0.40	0.19	0.26	0.18	0.33	0.01
NFF	1.56	1.31	1.23	1.30	1.23	2.05	0.01
NIROP	0.34	0.34	0.11	0.33	0.10	0.14	0.01

Note:
1. Assuming all Fe_T is Fe(+II).
2. Assuming all Fe (amorphous) is Fe(+II).
3. Assuming all Mn_T is Mn(+II).
4. Assuming all Mn (amorphous) is Mn(+II).
5. Assuming all S_T is S(-II).

Table 2.6. Description of aquifer material sub-samples used in the air- drying investigation.

Site	State	Sampling Procedure
DNTS	wet	-a 0.38 m long section of a core extracted from 11.8 to 12.5 m below ground suface was used
LAAP	wet	-half of the contents from a 0.33 m core extracted from 8.8 to 9.4 m below ground surface was used
MAAP	wet	-contents of a bucket were well mixed before removing sub-sample
Borden	wet	-a 0.8 m long section of core collected from 10 to 10.8 m below ground surface was used
NFF	wet	-contents of a bucket were well mixed before removing sub-sample
NAS	wet	-a 0.6 m long section of core collected from 1.2 to 1.6 m below ground surface was used (sand material only)

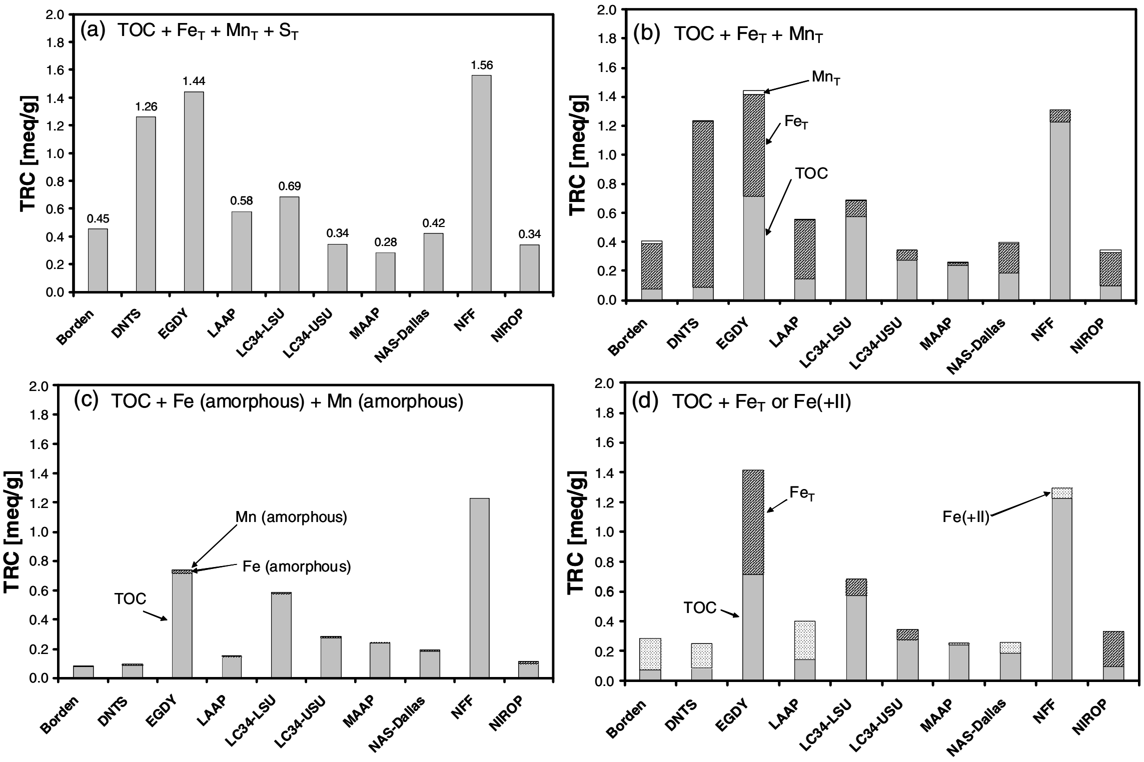

Figure 2.1. Theoretical estimation of the total reductive capacity using: (a) total organic carbon and the total Fe, Mn, and S; (b) total organic carbon, total Fe and Mn; (c) total organic carbon, amorphous Fe and Mn; and (d) total organic carbon and the ferrous Fe or total Fe.

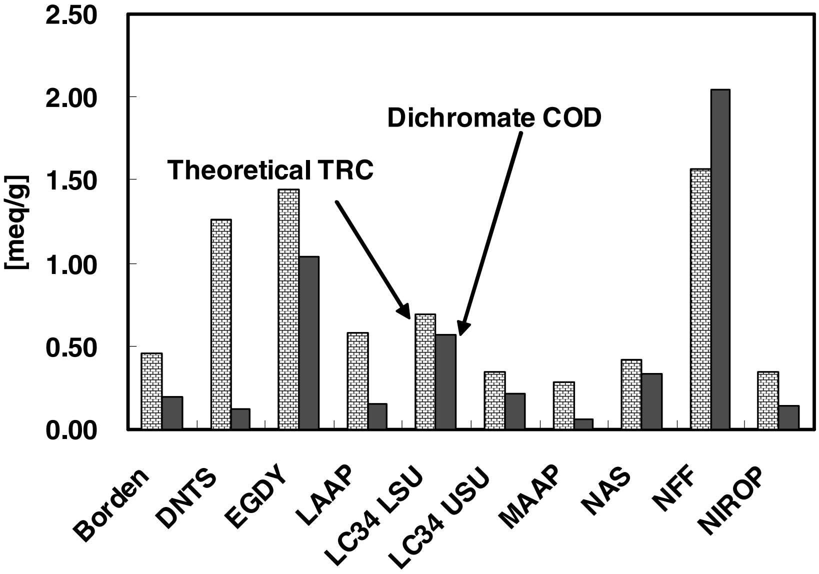

Figure 2.2. Theoretical total reductive capacity (TRC) and dichromate COD test results.

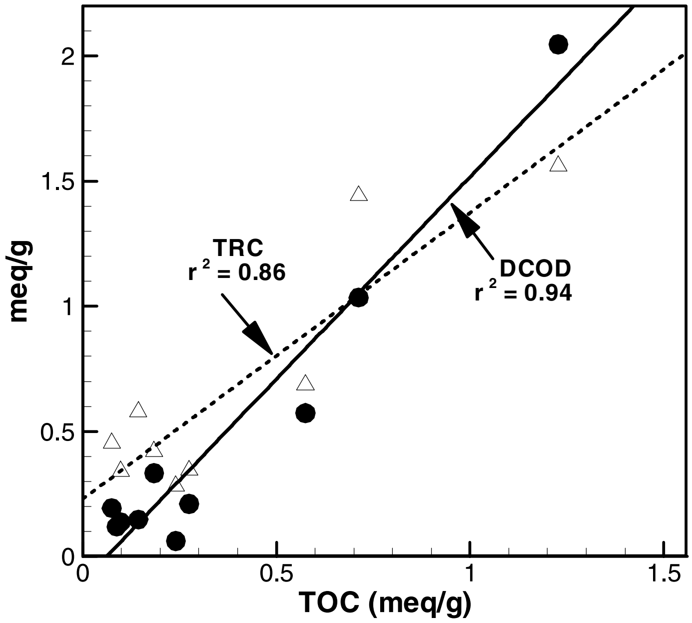

Figure 2.3. Scatter plot of theoretical total reductive capacity (TRC), dichromate COD, and total organic carbon. The TRC value for the DNTS aquifer material is excluded.

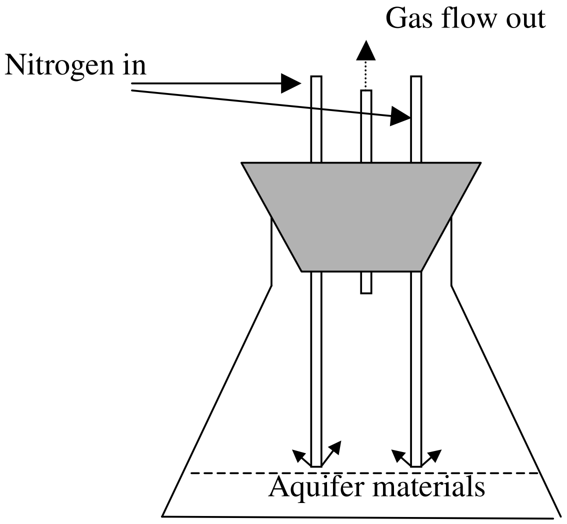

Figure 2.4. Anaerobic setup for drying aquifer materials.

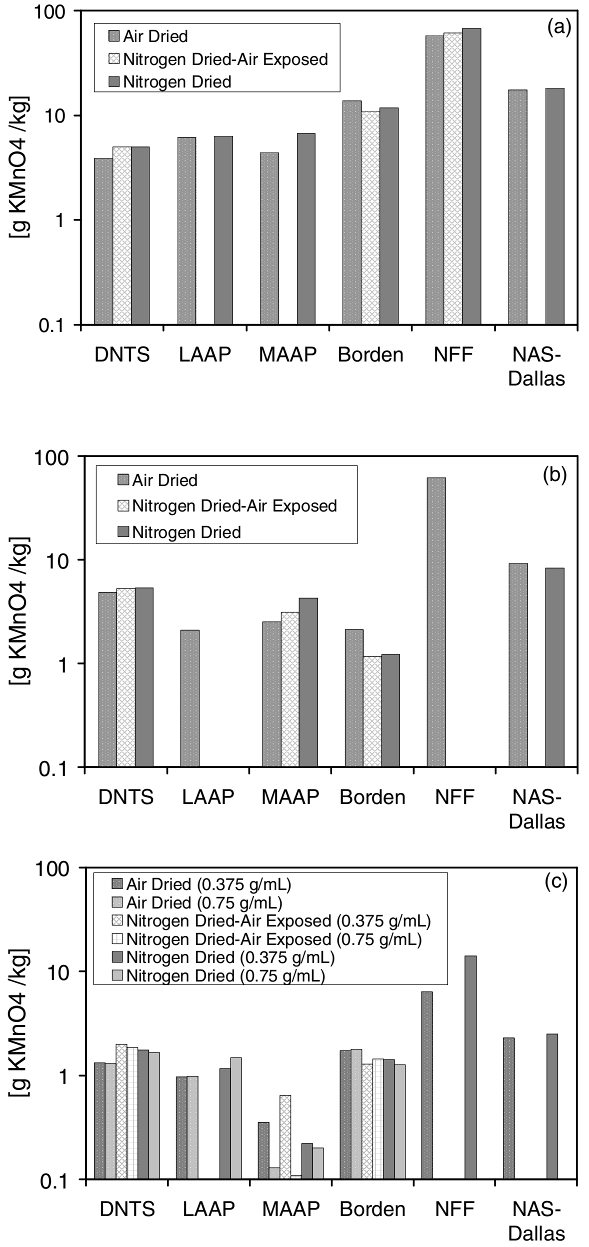

Figure 2.5. Average reductive capacity results from the air-drying investigation (a) dichromate-COD data, (b) permanganate-COD data, and (c) 7-day permanganate NOD data.

Chapter 3

Permanganate Interaction with Aquifer Materials

3.1 Overview

This chapter focuses on the interaction of permanganate with aquifer materials and begins with a background discussion of the physical and chemical properties, relevant reactions, and application in groundwater remediation. Then, the theoretical kinetic expressions accounting for the reactions between permanganate and aquifer materials are addressed, followed by details on the experimental investigation and data analyses. Three series of experiments (long-term batch tests, short-term batch tests, and column tests) were designed and performed to investigate permanganate behaviour in the presence of aquifer materials. Long-term batch experiments were conducted to focus on fundamental chemical properties affecting permanganate consumption by aquifer materials. The maximum permanganate NOD determined from long-term batch experiments were then used to examine the potential use of a permanganate COD test to quickly and economically quantify the maximum NOD of aquifer materials. Short-term batch experiments were designed to investigate the kinetic behaviour of permanganate in the presence of various aquifer materials. Column experiments, which mimic *in situ* conditions were used to investigate permanganate transport.

3.2 Background

3.2.1 Permanganate Properties and Reactions

Manganese species have the potential valence states ranging from +1 and +7, of which the +2, +4, and +7 states are the only ones that are stable over a wide range of acidity. Manganese in permanganate has the highest oxidation state. Potassium permanganate, which is the most commonly used reagent in ISCO applications, is a crystalline solid that is derived from mined potassium ores. It is relatively stable to thermal decomposition but not to photolytic decomposition (both in the solid form and in solution). Neutral permanganate solutions are relatively stable because water is the only solvent that reduces permanganate very slowly in the presence of manganese dioxide (or dust) in neutral permanganate solutions (Stewart, 1965) according to

$$2MnO_4^- + H_2O \xrightarrow{MnO_2} 2MnO_2 + 2OH^- + \tfrac{3}{2}O_2 \qquad (3.2.1)$$

Permanganate solutions in acidic condition are less stable than in neutral conditions, but unless the solutions are boiled, the decomposition is still relatively slow. Concentrated permanganate solutions in alkaline conditions can also slowly decompose to produce oxygen and manganate, which is unstable and can slowly disproportionate to permanganate and manganese dioxide (Steward, 1965). The general physical and chemical properties of permanganate are listed in Table 3.1.

The reaction stoichiometry and kinetics involving permanganate in natural systems are quite complex and are not fully understood. The most common permanganate reaction employed in environmental engineering is the complete reduction of permanganate (Mn(VII)) to manganese dioxide (MnO_2) (Mn(IV)) (Schnarr et al., 1998; Siegrist et al., 2001; Crimi and Siegrist, 2004), which is a three-equivalent reaction. This reaction proceeds differently in acidic and basic solutions as given by (Stewart, 1965):

$$MnO_4^- + 4H^+ + 3e^- \rightarrow MnO_2(s) + 2H_2O \qquad \mathrm{E^o(v) = +1.70\ V} \qquad (3.2.2)$$

in acidic solutions, and by

$$MnO_4^- + 2H_2O + 3e^- \rightarrow MnO_2(s) + 4OH^- \qquad \mathrm{E^o(v) = +0.59\ V} \qquad (3.2.3)$$

in basic solutions.

In addition to Eqs. (3.2.2) and (3.2.3), some other reactions involving permanganate participation are given by the following half-reaction equations (Stewart, 1965):

$$MnO_4^- + MnO_4^{3-} \rightarrow 2MnO_4^{-2} \qquad (3.2.4)$$

$$MnO_4^- + H_2O \rightarrow MnO_4^{-2} + OH^\bullet + H^+ \qquad (3.2.5)$$

$$2MnO_4^- + 4H^+ \rightarrow O_2(g) + 2H_2O + 2MnO_2(s) \qquad (3.2.6)$$

$$MnO_4^- + 8H^+ + 5e^- \rightarrow Mn^{+2} + 4H_2O \qquad (3.2.7)$$

$$2MnO_4^- + 3Mn^{+2} + 4OH^- \rightarrow 5MnO_2(s) + 2H_2O \qquad (3.2.8)$$

Eq.(3.2.8) is called Guyard reaction (Stewart, 1965) which describes the exchange between Mn(VII), Mn(IV), and Mn(II), and can be used for the volumetric determination of manganese. The Guyard reaction is expected to be very fast in strongly acidic solutions. Permanganate is a strong oxidant and only several oxidants (e.g., solid bismuthate in acid, ammonium persulfate, lead dioxide, potassium periodate, and ozone) are able to oxidize manganese ions to permanganate (Stewart, 1965).

Permanganate can serve as a multiple equivalent oxidant depending on the characteristics of the substrate that is attacked. For example, under basic conditions, sulfide can be oxidized to sulfate by excess permanganate while sulfur and tetrathionate might also be produced due to incomplete oxidation of sulfide in neutral or acidic solutions (Stewart, 1965). Permanganate can also easily oxidize metal ions (e.g., ferrous iron, chromium ion, and vanadium ion) from reduced states to oxidized states (Siegrist et al., 1999; Stewart, 1965). The reactions between permanganate and some organic compounds may involve different reaction pathways such as hydrogen atom abstraction and hydride ion abstraction (Stewart, 1964; Siegrist et al., 2000). Permanganate has a unique affinity for oxidizing organic compounds containing carbon-carbon double bonds, aldehyde groups or hydroxyl groups (Stewart, 1964; 1965). It was also addressed by Stewart (1965) that "permanganate oxidation for organic compounds is often, but by no means, considerably faster in alkaline than in neutral solution" because a change of the organic substrate (e.g., ionization of alcohol) might occur in a basic solution. However, a general phenomenon is that the oxidation rate is accelerated in strongly acidic conditions due to a conversion of permanganate ion to the more active oxidant, permanganate acid.

3.2.2 Permanganate Applications in Groundwater Remediation

The oxidation ability of permanganate has been widely used to characterize soil carbon fractions (Longinow et al., 1987; Moody et al., 1997) and treat contaminants in the water/wastewater industry (Carlson and Knocke, 2000; USEPA, 1999). Over the past decade, it has been applied in the subsurface remediation context and a number of bench-scale and pilot-scale studies and full-scale applications of permanganate-based ISCO have been conducted (Hood, 2000; Huang et al., 1999, 2002a, b; Li and Schwartz, 2004a, b; Mackinnon and Thomson, 2002; Schnarr et al., 1998; Seol et al., 2003; Siegrist et al., 2001; Tunniciliffe and Thomson, 2004; Urynowicz and Siegrist , 2005; Yan and Schwartz, 1999; 2000). Because permanganate is highly reactive with compounds containing C=C bonds, the most common use of permanganate-based ICSO is to remediate groundwater contaminated by tetrachloroethylene (PCE), trichloroethylene (TCE), dichloroethylene (DCE), and vinyl chloride (VC) (Siegrist et al, 2001) where the following reactions are applicable

$$\text{PCE: } 4KMnO_4 + 3C_2Cl_4 + 4H_2O \rightarrow 6CO_2 + 4MnO_2 + 4K^+ + 8H^+ + 12Cl^- \qquad (3.2.9)$$

$$\text{TCE: } 2KMnO_4 + C_2HCl_3 \rightarrow 2CO_2 + 2MnO_2 + 2K^+ + H^+ + 3Cl^- \qquad (3.2.10)$$

DCE: $8KMnO_4 + 3C_2H_2Cl_2 \rightarrow 6CO_2 + 8MnO_2 + 8K^+ + 2OH^- + 6Cl^- + 2H_2O$ (3.2.11)

VC: $10KMnO_4 + 3C_2H_3Cl \rightarrow 6CO_2 + 10MnO_2 + 10K^+ + 7OH^- + 3Cl^- + H_2O$ (3.2.12)

With the formation of a cyclic hypomanganate diester as a reaction intermediate when the carbon-carbon double bond is electrophilically attacked by MnO_4^- (Waldemer and Tratnyek, 2006), the reaction pathways, end-products, and kinetics for the reactions between permanganate and these contaminants are quite similar and have been well investigated (Siegrist et al., 2001; Yan and Schwartz, 1998; 1999; 2000).

In addition to chlorinated ethenes, recent studies have also shown that permanganate is able to oxidize various other contaminants such as hexahydro-1,3,5-trinitro-1,3,5-triazine (RDX), methyl t-butyl ether (MTBE), some polycyclic aromatic hydrocarbons (PAHs), pesticides, and phenol or various substituted phenols (Adam et al, 2004; Damm et al., 2002; Forsey, 2004; Tollefsrud and Schreier, 2002; Waldemer and Tratnyek, 2006).

Permanganate destruction of DNAPLs has been improved by the use of phase-transfer catalysts to enhance the penetration of permanganate into DNAPLs (Seol and Schwartz, 2000); however, this technology has also led to the decrease of subsurface permeability and the clogging of subsurface media (Schroth et al., 2001). Recently, encapsulation of particulate potassium permanganate has been proposed to reduce the unproductive consumption by aquifer solids (Kang et al., 2004).

3.2.3 Permanganate Interaction with Aquifer Materials

The majority of permanganate-based ISCO studies have focused on the oxidation of target contaminants (Huang et al., 2000; Urynowicz and Siegrist , 2005; Waldemer and Tratnyek, 2006), and little effort has been given to the interactions between permanganate and aquifer materials. ISCO pilot-scale experiments have demonstrated that permanganate in excess of the stoichiometric requirements by the target contaminant is usually required. This excess amount of permanganate has been attributed to the consumption of permanganate by the surrounding aquifer material, and is referred to as natural oxidant demand (NOD) and expressed as a mass of $KMnO_4$ per mass of dry aquifer materials (Hood, 2000; Mumford et al., 2004; 2005).

During an ISCO application, an aqueous solution of permanganate is injected into the treatment zone, and will react with oxidizable inorganic and organic substances in the solid phase, and dissolved reductants in the aqueous phase (Crimi and Siegrist; 2005; Mumford et al., 2005). It has been experimentally verified that in ISCO applications, the permanganate ion reacts with various reductants to form manganese dioxide between a pH of 3.5 and 12. In a strong acid condition (pH<3.5), Mn^{2+} cations are formed. Above a pH of 12, which is a very rare case in natural subsurface systems, Mn(VI) could be formed (Hood, 2000; MacKinnon and Thomson, 2002; Schnarr et al., 1998; Siegrist et al., 2001).

Most of existing studies report permanganate NOD as a single value that applies to the entire aquifer over the entire duration of the ISCO application (Hood, 2000; Dresher et al., 1998; Siegrist et al., 2001). The implication of this instantaneous sink conceptual model is that no injected permanganate can leave a region of an aquifer prior to the satisfaction of the entire NOD within that region (Mumford et al., 2005; Mumford, 2002). Therefore, the single-valued NOD in this conceptual model represents the ultimate NOD or the maximum permanganate mass that could be consumed. However, recent studies (Mumford et al., 2005; Mumford et al., 2002) have observed that the consumption of permanganate by aquifer materials in batch tests is not an instantaneous reaction process but is kinetically controlled (measurable consumption rates are present for >21 weeks). This finding suggests that, in addition to advection and dispersion, the transport of permanganate within the contaminated region will be controlled by the kinetic competition for permanganate between the target organic compound(s) and the NOD. In an alternative conceptual model for permanganate NOD proposed recently (Mumford et al., 2005) and shown in Figure 3.2.1, permanganate in a pore space can react with dissolved phase contaminant species, react with naturally-occurring oxidizable matter associated with aquifer materials, or proceed to the next pore space. Compared with the above-mentioned instantaneous sink conceptual model, the transport and consumption of permanganate is not strictly a function of maximum NOD and the contaminant demand, but is a function of transport processes and reaction rates associated with contaminant components and reduced species associated with aquifer materials. This conceptual kinetic model proposed by Mumford et al. (2005) forms the basis for this investigation as documented in the following sections of this chapter.

3.2.4 Derivation of Permanganate NOD Kinetic Expressions

The overall heterogeneous reaction between the bulk oxidizable aquifer matter (OAM) and permanganate may be written as

$$OAM + pMnO_4^- \rightarrow pMnO_2 + q\,\text{Oxidized - }OAM \tag{3.2.13}$$

where p and q are stochiometric coefficients. The term bulk oxidizable aquifer matter refers to all significant non-target reductants associated with the aquifer materials including organic carbon, and minerals containing S(-II), Mn(+II), and Fe(+II). Associated with (3.2.13) are the following general rate law expressions:

$$\frac{d(C_{OAM})}{dt} = -k_{bulk}^{OAM}(C_{OAM})^{\beta}(C_{MnO_4^-})^{\alpha} \tag{3.2.14}$$

and

$$\frac{d(C_{MnO_4^-})}{dt} = -k_{bulk}^{MnO_4^-}(C_{MnO_4^-})^{\alpha}(C_{OAM})^{\beta} \tag{3.2.15}$$

where k_{bulk}^{OAM} and $k_{bulk}^{MnO_4^-}$ is the bulk reaction rate coefficient with respect to the OAM and permanganate; α and β are the overall reaction order with respect to permanganate and the OAM; t is time, and C_{OAM} and $C_{MnO_4^-}$ are the concentrations of the bulk oxidizable aquifer material (mass/system volume) and permanganate (mass/volume of solution). In this investigation the concentration of the bulk oxidizable aquifer material (C_{OAM}) is estimated from

$$C_{OAM} = DCOD\, m_{aq} / V_{total} \tag{3.2.16}$$

where $DCOD$ is the dichromate COD test result expressed as g-KMnO$_4$/kg of dry aquifer material, m_{aq} is the mass of dry aquifer material, and V_{total} is the total system volume (solution and aquifer material); hence the units for C_{OAM} are g-KMnO$_4$/L.

Based on Eqs.(3.2.13) to (3.2.15), permanganate consumption (e.g., NOD) by aquifer materials is expected to be the function of time, reaction orders, concentrations, and reaction coefficients with respect to OAM and permanganate, as expressed as:

$$NOD_t = f(\alpha, \beta, C_{MnO4}, C_{oam}, k_{oam}, k_{MnO4}, t) \tag{3.2.17}$$

Equation (3.2.17) forms the theoretical basis for this thesis to account for permanganate consumption by aquifer materials, indicating that the influencing factors should at least include permanganate concentration, the composition of components in aquifer materials, and their chemical properties.

Table 3.2.1. Properties and characteristics of potassium permanganate (after Siegrist et al. 2002; Hood, 2000)

Property	Descriptions
Chemical formula	$KMnO_4$
Purity (% by weight)	Technical grade = 98%
Molecular weight	158.03 g/mol
Solid density	2.703 g/cm^3
Bulk density	~ 1605 kg/m^3
Form and features	Dark purple solid with metallic luster, sweetest astringent taste, odorless, granular crystalline, oxidizer
Solubility in distilled water:	
0°C	27.8 g/L
20°C	65.0 g/L
40°C	125.2 g/L
60°C	230.0 g/L
Aqueous solubility	$S = 30.55+0.796T+0.0392T^2$ (T in °C) S = 62.9 g/L at 20oC
Aqueous specific gravity	$S_g = 1.000+0.007C$ (C: the concentration of $KMnO_4$ in %w/w)
Specific conductance	Sc (mS/cm) = 0.7002C + 0.0915 (C: the concentration of $KMnO_4$ in %w/w)
Average Mn-O bond distance	1.629±0.008Å
Average O-Mn-O bond angle	109.4±0.7°
Stability	Stable indefinitely if held in cool dry area in sealed containers
Incompatibilities	Avoid contact with acids, peroxides, and all combustible organics or readily oxidizable materials
Materials compatibility	In neutral or alkaline conditions, it is not corrosive to iron, mild steel or stainless steel. However, chloride corrosion may be accelerated. Plastics such as polypropylene, PVC, epoxy resins, Lucite, Viton A, and Hypalon are suitable but Teflon FEP and fibbers are often incompatible

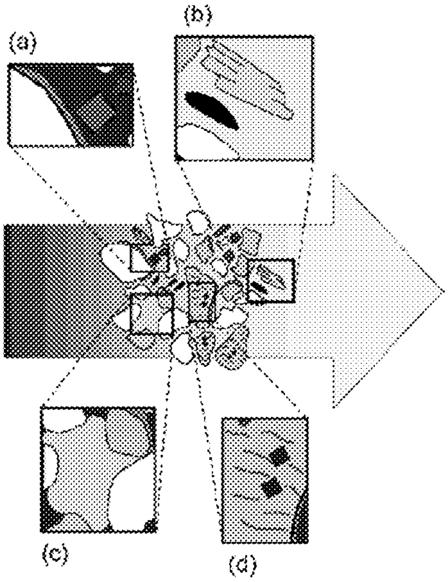

Figure 3.2.1. Pore-scale conceptual model for NOD showing the possibility of reaction with reduced aquifer solid species, reaction with dissolved DNAPLs, and transport of unreacted MnO_4^-. Reduced species include: (a) pyrite and organic matter coatings on grains, (b) reduced minerals such as magnetite and reduced carbonaceous matter such as charcoal, (c) dissolved and nonaqueous phase oil (DNAPL), and (d) organic matter and disseminated pyrite entrained within carbonate grains and lithic fragments. (Adapted from Mumford et al., 2005)

3.3 Long-Term Permanganate Consumption by Aquifer Materials

To identify factors controlling permanganate NOD, estimate the ultimate NOD for the various aquifer materials, and to investigate long-term permanganate NOD kinetic behavior, a series of long-term batch experiments were performed.

3.3.1 Experimental Methods

Table 3.3.1 lists the details for the long-term batch experiments performed in this study. In order to explore permanganate consumption due to different oxidant to aquifer material mass ratios, a range of initial permanganate concentrations (1 to 20 g $KMnO_4$/L) and mass of aquifer materials (10 to 50 g) were used. For experiments using the Borden, DNTS, LC34, MAAP and NIROP aquifer materials nominal 40 mL reactors were used, while 125 mL reactors were used for the EGDY and NFF aquifer materials due to their high NOD which necessitated a sufficient mass of permanganate to be available. In addition, due to the relatively high NOD of the LC34-USU and LC34-LSU aquifer materials (estimated from TRC and DCOD test), a 125 mL reactor was also used for the 1.0 g/L concentration to ensure that sufficient permanganate mass was present. The various masses of aquifer materials allow for the impact of different oxidant to aquifer material mass ratios to be explored. Nominal oxidant to aquifer mass ratios of 2, 10, 20, 35 g $KMnO_4$/ kg of aquifer solids were used for all aquifer materials expect for EGDY and NFF where nominal oxidant to aquifer mass ratios of 46, 83, 100, 170 g $KMnO_4$/ kg of aquifer solids were used. Experimental controls consisted of identical volume reactors filled with the potassium permanganate solution but containing no aquifer materials.

$KMnO_4$ solutions were prepared by adding analytical grade $KMnO_4$ (EM Science) to Milli-Q water and boiling for ~1 hour. The cooled solution was filtered (0.45-µm glass fibre, Pall

Corporation) and standardized by titration into a sulphuric acid and sodium oxalate solution (APHA, 1998). Each test was performed in triplicate and all reactors were shielded from light to prevent photo-catalytic oxidant decomposition (Steward, 1965) and stored in a controlled temperature environment (~20°C). At specified times each reactor was sampled by removing an aliquot (~150 μL) of the solution and the $KMnO_4$ concentration was determined by spectrophotometry (Milton Roy Company, Spectronic 20D) at 525 nm with a method detection limit of 1.3 mg/L. The spectrophotometer was calibrated prior to each sampling episode. Nitrogen gas was used to fill the head space in the reactor after sampling.

The decrease in permanganate concentration and the mass of aquifer material were used to estimate the NOD (mass $KMnO_4$ consumed / mass of dried aquifer material) after a sampling episode at time *t* by using

$$NOD_t = \sum_{t} [\, m_{ox,\ t-1}^{test} - C_{ox,t}^{test} V_{ox,t-1}^{test} - (m_{ox,t-1}^{crtl} - C_{ox,t}^{crtl}\ V_{ox,t-1}^{crtl})(V_{ox,t-1}^{test} / V_{ox,t-1}^{crtl})] / m_{aq}^{test} \tag{3.3.1}$$

where, m_{ox} is the mass of permanganate, C_{ox} is the concentration of permanganate, V_{ox} is the volume of permanganate solution in the reactor, m_{aq} is the mass of dry aquifer material added to the test reactor, the superscripts *test* and *crtl* denote the test reactor and control reactor respectively, and the subscript *t* and *t-1* denote values at the current and previous sampling episodes respectively. NOD results from reactors subjected to this sequential sampling method at least 5 times were compared to NOD results from a limited number of reactors sampled once. This comparison indicated that there was no statistical difference in the NOD values (*t*-test, $\alpha = 5\%$).

Except for the reactors containing the LAAP aquifer material, all reactors were monitored until the NOD value estimated from Eq.(3.3.1) stabilized at a maximum value (maximum NOD or NOD_{max}). The LAAP aquifer material proved to be problematic due to the high degree of fine material (~60% silt and clay; d_{30} = 5.5 μm) which clogged various filters and interfered with analytical aspects. For selected reactors we replenished (spiked) the oxidant mass in the reactors to observe if the NOD stabilization was due to oxidant limitations.

Once the maximum NOD for each experimental reactor was reached, aquifer material was removed and rinsed with Milli-Q water to remove excess permanganate. The rinsed samples from triplicate reactors for each test were mixed together, gently homogenized by hand, and dried at 80^{o}C to a constant weight. Following the modified Chao's method (Chao, 1972) proposed by Neamana et al. (2004), manganese oxides were extracted for two hours from a 0.5 g of the post-experimental sample of each long-term batch test using acidified 1.0M NH_2OH-HCl (pH = 2.0, adjusted by 2% HNO_3) solution. The manganese content was quantified using an inductively coupled plasma (ICP) emission spectroscopy (MDL 0.01 mg/L) with a Spectro Flame instrument (Spectro Analytica, Fitchburg, MA). In addition, dichromate COD tests (as illustrated in Chapter 2) were also performed to quantify the dichromate COD value for each of post-experimental samples of each long-term batch test.

3.3.2 Results and Discussion

General Observations

Temporal NOD profiles for each aquifer material are shown in Figure 3.3.1 with each data point representing the average from triplicate reactors. The general trend of the NOD temporal profiles for each aquifer material and experimental series demonstrate similar characteristics: an initial fast consumption rate followed by a much slower consumption rate that persisted until each experimental series was terminated. The maximum observed value was deemed to represent the ultimate NOD or NOD_{max}, and varied depending on the experimental conditions.

The initial fast consumption rate was more pronounced for some aquifer materials (e.g., EGDY and LC34-USU) as compared to others (e.g., Borden and MAAP) indicating that the nature and quantity of the reduced species associated with a given aquifer material affects the early time permanganate consumption. Assuming that the majority of this fast consumption was expressed within the first 7 days of exposure to permanganate, then the average observed fast consumption rate varied from a low of 0.023 g-$KMnO_4$/kg/day for the MAAP aquifer material to a high of 8.4 g-$KMnO_4$/kg/day for the NFF aquifer material (Table 3.3.2). The 7-

day exposure period to represent the fast consumption rate was chosen here for convenience since the first reactor sampling episode was conducted at 7 days and we acknowledge that the consumption rate is much higher during the first several hours of exposure (as will be discussed in Section 3.5). For a given aquifer material the fast consumption rate increased with an increase in the oxidant to solids ratio (Figure 3.3.2); for example as the oxidant to solids mass ratio was increased for the LC34-USU aquifer material from 6 to 50 g/kg at a permanganate concentration of 10 g/L, the consumption rate increased from 0.40 to 0.95 g-$KMnO_4$/kg/day, possibly due to auto decomposition of permanganate and the high possibility that permanganate ions attack reductive component associated with aquifer solids. Also for a given oxidant to solids ratio the fast consumption rate was observed to increase with an increase in permanganate concentration clearly indicating the sensitivity of the early time NOD results to experimental parameters.

In general, a slow permanganate consumption rate ranging from 0.00050 to 0.0035 g-$KMnO_4$/kg/day was observed for most of the aquifer materials used in this investigation by ~150 days of exposure to permanganate, with the exception of the EGDY and NFF aquifer materials which continued to have a relatively higher rate of 0.020 and 0.074 g-$KMnO_4$/kg/day at the conclusion of their respective experiments (Table 3.3.2). Excluding these two aquifer materials, the overall average slow consumption rate was 0.0018 g-$KMnO_4$/kg/day which is two-orders of magnitude lower then the average observed fast consumption rate.

For reactors in which permanganate was consumed prior to the termination of the experimental trial and were respiked, the consumption rate either remained consistent with the rate prior to the spiking event (Figure 3.3.1(e)) or increased presumably in response to the increase in permanganate concentration (Figure 3.3.1(b)). In cases where there was a dramatic increase in consumption due to a spiking event, the consumption rate returned quickly to the pre-spiked rate. In either case a permanganate-limiting reaction condition existed which was satisfied by the addition of permanganate.

Table 3.3.2 presents both the average NOD_{max} and the overall maximum NOD (NOD^{*}_{max}) from all the experimental series for each aquifer material. The average NOD_{max} captures the expected outcome from a range of experimental parameters and the NOD^{*}_{max} reflects the conservative NOD and most likely should be used for design considerations. The NOD^{*}_{max} varies from 2 to 98 g/kg and is within the range of values reported from other investigations (e.g., Mumford et al., 2005; Haselow et al., 2003; Siegrist et al, 2001). For a given aquifer material the average NOD_{max} represents between 40 and 90% of the NOD^{*}_{max} . Consistent with the observed tends in the fast permanganate consumption rate, a larger NOD_{max} was observed for a larger oxidant to solids mass ratio; however, variations to this general observation were apparent for experimental series with the same oxidant to solids mass ratio but different permanganate concentrations. In this case the NOD_{max} was observed to be both higher (e.g., Borden and DNTS) or lower (e.g., LC34-USU and MAAP) for a higher permanganate concentration perhaps as a result of experimental variability. Figure 3.3.3 illustrates that for a given aquifer material the NOD_{max} and the NOD at 7 days (NOD_7) was a linear function (r^2 = 0.94 - 0.97) of the oxidant to solids mass ratio for a given initial permanganate concentration and hence extrapolations from these data are possible to obtain *in situ* conditions. For example, assuming a field porosity of 0.3 and a bulk density of 1800 kg/m^3 for the LC34-USU aquifer material, an estimated *in situ* NOD_{max} is ~5 g/kg. This *in situ* estimate is 50% of the NOD based on the results from the experimental series performed with an oxidant to solids mass ratio of 49 g/kg and highlights one of the concerns of using well-mixed batch reactors to estimate *in situ* NOD values. However this issue can be overcome if a range of oxidant to solids mass ratios is employed to generate NOD data and this linear scaling between oxidant to solids mass ratio data from well-mixed batch reactors experiments is exploited to estimate potential *in situ* NOD values. Finally, the NOD_{max} for a given aquifer material is related to the initial permanganate concentration with a higher initial concentration in general yielding a higher NOD_{max} (Figure 3.3.4).

The importance of the fast consumption rate to the overall consumption of permanganate is further illustrated in Figure 3.3.5 where these data indicate an excellent linear relationship exists between the NOD_{max} and the 7-day NOD (NOD_7). The average ratio of NOD_7 to

$\mathrm{NOD_{max}}$ for all the experimental series performed was 50%, and varies from a high of 70% for the NFF aquifer material to a low of 21% of the MAAP aquifer material (Figure 3.3.6). The best-fit linear expression which can be used for prediction purposes is given by

$$\mathrm{NOD_{max}} = 1.5\,\mathrm{NOD_7} + 0.7 \quad (r^2 = 0.95) \tag{3.3.2}$$

where $\mathrm{NOD_7}$ and $\mathrm{NOD_{max}}$ are in terms of g of $KMnO_4$ per kg. This linear relationship implies that NOD profiles are scaleable over time; a concept that is supported by the approximately identical difference between the $\mathrm{NOD_7}$ and $\mathrm{NOD_{max}}$ values across a range of oxidant to solids mass ratios for the LC34-USU aquifer material (Figure 3.3.3).

The reduction in the COD test values for each experimental series varied from a low of 1% for the MAAP aquifer material to as high at 96% for the LC34-LSU and LC34-USU aquifer materials. This reduction in COD test values is related to the $\mathrm{NOD_{max}}$ (Figure 3.3.7). Since the initial COD test values can be used as a surrogate for the potentially oxidizable aquifer material as concluded from Chapter 2, the non-zero COD test values at the termination of each experimental series are consistent with the findings reported by Mumford et al. (2005) and indicate that not all of the reduction capacity that is captured by dichromate COD test is oxidizable by permanganate.

Correlation Analysis

In an attempt to relate the various NOD profile metrics (average and maximum $\mathrm{NOD_7}$, and average $\mathrm{NOD_{max}}$ and $\mathrm{NOD^{*}_{max}}$) to relevant aquifer material characteristics (including soil pH, surface area, CEC, total and amorphous Fe and Mn, and TOC) a correlation analysis was preformed excluding data for the NFF aquifer material. The results from this analysis indicated that: (i) the maximum $\mathrm{NOD_7}$ and the $\mathrm{NOD^{*}_{max}}$ are highly correlated with TOC content (r = 0.93 and 0.90 respectively), and this correlation only increases slightly with the addition of amorphous Fe (r = 0.94 and 0.91 respectively); (ii) the average $\mathrm{NOD_7}$ and average $\mathrm{NOD_{max}}$ are highly correlated with TOC content (r = 0.90 and 0.88 respectively); (iii)the average NOD expressed after the 7 days was highly correlated with TOC content (r = 0.86); and (iv) all NOD metrics showed little correlation ($r < 0.5$) with soil pH, surface area, CEC, and total Fe, and a mild correlation with total Mn ($r < 0.75$)). The high degree of correlation between the TOC content and the NOD metrics implies that organic carbon is the major reduced species contributing to permanganate consumption for the aquifer materials used in this investigation. Based on this analysis the following empirical relationships were developed and can be used to estimate average NOD_7, average $\mathrm{NOD}_{\max}$, and $\mathrm{NOD}^*_{\max}$

$$\text{Avg NOD}_7 = \begin{cases} 0.36\,(\mathrm{TOC}) - 1.5 & r^2 = 0.80 \\ 0.36\,(\mathrm{TOC} + \text{amorphous Fe}) + 1.6 & r^2 = 0.82 \end{cases} \tag{3.3.3a}$$

$$\text{Avg NOD}_{\max} = \begin{cases} 0.74(\mathrm{TOC}) - 3.4 & r^2 = 0.78 \\ 0.74(\mathrm{TOC} + \text{amorphous Fe}) + 0.7 & r^2 = 0.80 \end{cases} \tag{3.3.3b}$$

$$\mathrm{NOD}^*_{\max} = \begin{cases} 0.80\,(\mathrm{TOC}) - 2.3 & r^2 = 0.81 \\ 0.81\,(\mathrm{TOC} + \text{amorphous Fe}) + 2.8 & r^2 = 0.83 \end{cases} \tag{3.3.3c}$$

where the units for all terms are expressed in g of $\mathrm{KMnO_4}$ per kg of dry aquifer material, and assuming that phthalic acid is a reasonable model compound for the reduction capacity of the TOC content (Barcelona and Holm, 1991) (1 mg/g of TOC = 16.46 g of $\mathrm{KMnO_4}$/kg), and the amorphous Fe is in a reduced form (1 mg/g of Fe = 0.94 g of $\mathrm{KMnO_4}$/kg).

NOD Profile Normalization

As mentioned above, the NOD profiles appear to be scalable over time and following the approach used by Mumford et al (2005), each NOD profile was normalized by the their respective $\mathrm{NOD}_{\max}$ and fit to a logarithmic function of time expressed as

$$\mathrm{NOD(t)} = \mathrm{NOD}_{\max}\ \left[\, a \cdot \ln(t) + b \,\right] \qquad (t \geq 7) \tag{3.3.4}$$

where a and b are fitting parameters, and t is the time in days. Figure 3.3.8 shows examples of the excellent fits of Eq (3.3.4) to the DNTS and LC34-USU NOD data, and in general the coefficient of determination was > 0.94 for all fits. The slope parameter a represents the normalized rate of permanganate consumption and the average value for overall aquifer materials and initial concentrations was 0.14 with a 12% coefficient of variation. The normalized NOD profiles for all aquifer materials are presented in Appendix D. Attempts to correlate the *a* and *b* fitting parameters from NOD profiles with similar oxidant to solids ratio to aquifer material characteristics were unsuccessful perhaps due to experimental variability or the similarity amongst the aquifer material used in this investigation. If only the NOD profiles with an initial $KMnO_4$ concentration of 20 g/L are used, then statistically significant expressions of parameters *a* and *b* are given by:

$$a = 0.104 + 0.744(\text{amorphous Fe}) \qquad r^2 = 0.78 \tag{3.3.5}$$

$$b = 0.514 - 0.251(\text{amorphous Fe}) - 0.0158\,\text{CEC} \qquad r^2 = 0.96 \tag{3.3.6}$$

where amorphous Fe is in terms of mg/g, CEC in terms of cmol(+ev)/kg, and all regression coefficients are statistically significant at a level of significance (LOS) of 0.05.

Substituting Eqs (3.3.5) and (3.3.6) into Eq. (3.3.4), an empirical equation to estimate the temporal NOD is obtained for an initial concentration of 20g/L, as given by:

$$\text{NOD}(t) = \text{NOD}_{\text{max}} \left\{ \begin{array}{l} [0.104 + 0.744(\text{amorphous Fe})] \cdot \ln(t) \\ \qquad + [0.514 - 0.251(\text{amorphous Fe}) \text{ - } 0.0158\,\text{CEC}] \end{array} \right\} \tag{3.3.7}$$

Interestingly, the parameters *a* and *b* are not related to TOC which is generally considered to be a major reductant. One possible explanation is that TOC is related to NOD_{max} (as indicated by Eq. 3.3.3) and its primary effects have been removed as part of the normalization. The parameter *a* represents the normalized rate of permanganate consumption. Since CEC indicates the availability of reacting species which are held by negatively charged colloids that have a comparatively large surface area, the strong dependence of parameters *a* and *b* on the amorphous *Fe* content and/or CEC indicates the rate of permanganate consumption may be surface-controlled.

Unfortunately, the lack of sufficient and proper data for other initial concentration levels restricts the development of other permanganate NOD expressions. Given sufficient observations and following the similar procedure as detailed above, temporal permanganate NOD expressions corresponding to other initial permanganate concentrations can be developed.

Manganese Oxide Deposition

The theoretical reduction of permanganate will produce manganese dioxide according to the reaction given by Eq.(3.2.2) or Eq.(3.2.3). Visual inspection of the post-experimental materials revealed some level of colour change of solid grains compared to the pre-experimental materials and dark brown fine particles were present. These dark brown colloidal-like particles are believed to be manganese dioxide, which is the end-product of permanganate reduction by aquifer materials. The quantity of manganese dioxide was observed to be large in reactors containing the NFF and EGDY aquifer materials and smaller in the reactors containing the MAAP and DNTS aquifer materials. If all the permanganate consumed within the batch reactors was presumably reduced to manganese, then quantification of the bulk soil concentration of manganese would provide an indication of the magnitude of this assumed end-product of permanganate reduction, and the level of manganese oxide precipitates associated with the solids. Based on the manganese data determined from selected aquifer material samples after exposure to permanganate for more than 250 days, an equivalent NOD (NOD_{Mn}) (one mole or 159 g of potassium permanganate is equivalent to 1 mole or 55 g of manganese) was calculated and is presented in Figure 3.3.9 along with NOD_{max} data. This figure shows an excellent linear relationship between NOD_{max} and NOD_{Mn} ($r^2 = 0.94$) and indicates that approximately 97% of permanganate consumed in these batch reactors produced Mn (presumably as manganese dioxide) that was associated with the aquifer solids.

The presence of this manganese oxide coating on the grains will restrict the ability of permanganate to further oxidize reduced species either on the surface or internal to the grains. To investigate this hypothesis, we used Chao's method (Chao, 1972) to remove the manganese oxide coatings from samples of the LC34-LSU and LC34-USU aquifer material that were exposed to a ~10 g/L permanganate solution for >300 day and then initiated a series of new well-mixed batch reactor tests for these two materials. After exposure to a 20 g/L permanganate solution for 2 months, we observed an ~6% increase in the permanganate NOD values suggesting that some degree of passivation of the aquifer material occurs due to the formation of manganese oxide coating on the grains.

General Long-Term NOD Kinetic Model

As discussed above, the typical permanganate NOD profile observed from our long-term batch experiments demonstrate a characteristic fast rise followed by a lengthy period of slow increase. Based on this observation, we assumed that these profiles could be described by a kinetic expression consisting of a fast and slow reacting OAM species. We also assumed that an overall second-order rate law (first-order for each reactant in Eq.(3.2.13)) would be sufficient to capture the fast and slow reactions. The documented presence of manganese oxides may deplete permanganate according to the autocatalytic reaction given by (Steward, 1965):

$$2MnO_4^- + H_2O \xrightarrow{MnO_2} 2MnO_2 + 2OH^- + \tfrac{3}{2}O_2 \qquad (3.3.8)$$

In addition to the role that manganese oxides play in the ongoing consumption of permanganate through the auto-decomposition reaction, they also give rise to passivation due to manganese oxide coating on grains. As demonstrated in this effort and elsewhere these manganese oxide coatings limit permanganate oxidation (Li and Schwartz, 2004a, b; MacKinnon and Thomson, 2002). In this kinetic model, we assume that this passivation can be captured by a decreasing reaction rate coefficient for the slow reacting OAM which is equivalent to increasing the diffusional resistance with an increase in the manganese oxide coating thickness. For simplicity, we assumed a linear expression given by:

$$k_{OAM}^{slow} = \left(k_{OAM}^{slow}\right)^0 - k_p\left(\frac{m_{MnO_2}}{m_{aq}}\right) \qquad (3.3.9)$$

where k_{OAM}^{slow} is the reaction rate coefficient with respect to the slow reacting OAM ([$L^3M^{-1}T^{-1}$]), k_p is an empirical reduction factor ([$L^3M^{-1}T^{-1}$]), m_{MnO_2} and m_{aq} are the mass of manganese oxide produced [M] (which can be calculated based on the mass decrease of permanganate) and the mass of aquifer material [M]; and the supscript "0" denotes the manganese dioxide free situation. Therefore, the governing batch system equations are given by:

$$\frac{d(\theta C_{MnO_4^-} V_T)}{dt} = -k_{ox}^{fast} \theta C_{OAM}^{fast} C_{MnO_4^-} V_T - k_{ox}^{slow} \theta C_{OAM}^{slow} C_{MnO_4^-} V_T - k_{MnO_2} \theta C_{MnO_4^-} V_T \qquad (3.3.10a)$$

for the rate of change of permanganate,

$$\frac{dC_{OAM}^{fast} V_T}{dt} = -k_{OAM}^{fast} C_{OAM}^{fast} C_{MnO_4^-} V_T \qquad (3.3.10b)$$

for the rate of change of fast reaction OAM, and

$$\frac{dC_{OAM}^{slow} V_T}{dt} = -k_{OAM}^{slow} C_{OAM}^{slow} C_{MnO_4^-} V_T \qquad (3.3.10c)$$

for the rate of change of the slow reacting OAM, where θ is the porosity of the system ([L^3L^{-3}]), defined as volume of solution per volume of system, C_{OAM} and $C_{MnO_4^-}$ are the concentrations of the bulk OAM and permanganate ([ML^{-1}], defined by mass of OAM per volume of system and mass of $KMnO_4$ per volume of system, respectively; k_{ox} and k_{OAM} are reaction rate coefficients with respect to permanganate and OAM ([$L^3M^{-1}T^{-1}$]); the supscripts "fast" and "slow" denote the "fast reaction" and "slow reaction", respectively; k_{MnO_2} is the rate coefficient for the permanganate auto-decomposition reaction catalyzed by MnO_2 ([T^{-1}]), V_T is the total volume of the system, and t is time.

We also assumed that the concentration of OAM could be represented by dichromate chemical oxygen demand (DCOD) test values which serve as a surrogate for the aquifer material reduction capacity as discussed in Chapter 2. Finally, based on mass balance considerations, the stoichiometric mass ratio between permanganate and OAM can be expressed as:

$$\beta_{fast} = \frac{k_{ox}^{fast}\theta}{k_{OAM}^{fast}\rho_b} \tag{3.3.11a}$$

$$\beta_{slow} = \frac{k_{ox}^{slow}\theta}{\left(k_{OAM}^{slow}\right)^0 \rho_b} \tag{3.3.11b}$$

where β is permanganate mass required by per unit mass of OAM, and ρ_b is the bulk density of system ([ML^{-3}], mass of solids/volume of system).

Parameters in this kinetic model can be grouped into three categories: (1) the system parameters, θ, ρ_b, and V_T, which are set by the experimental conditions for each batch test; (2) literature parameters k_{MnO_2}, β_{fast}, and β_{slow} which can be assigned reasonable values from the literature; and (3) the fitting parameters k_p, k_{ox}^{fast}, k_{ox}^{slow}, and C_{OAM}^{fast} which must be obtained through model calibration. The first-order coefficient rate coefficient (k_{MnO_2}) for the permanganate auto-decomposition reaction catalyzed by manganese oxide was assigned to a value of 5 x 10^{-5} day^{-1} as reported by Steward (1965) for a neutral 0.02 M permanganate solution that decomposed by 0.2% over 6 months. This value of k_{MnO_2} is consistent with the range of first-order rate coefficients estimated from the tails of the long-term NOD profiles (1 x 10^{-4} to 1 x 10^{-5} day^{-1}). The stoichiometric mass ratio between permanganate and the slow OAM (β_{slow}) was assigned a value of 12 based on the observations reported by Mumford et al. (2005) while β_{fast} was assigned a value of 2.0 based on the assumption that fast reacting OAM species were low-carbon organic matter or highly oxidized forms of organic matter (e.g., organic acids) and minerals containing Fe(II), Mn(II), and S(-II) etc. Model calibration was performed using a least-squares estimator where the fitting parameters were given an initial estimate and bounds. The remaining model parameters (k_{OAM}^{fast}, k_{OAM}^{slow}, and C_{OAM}^{slow}) are related to the fitting parameters through Eq.(3.3.11) and by

$$C_{OAM}^{fast} + C_{OAM}^{slow} = DCOD^{initial} - DCOD^{final} \tag{3.3.12}$$

where $DCOD^{initial}$ and $DCOD^{final}$ are the initial and final dichromate COD test values expressed in *g*-$KMnO_4$/*kg* of dry aquifer material.

The model calibration for experiments using the Borden, DNTS, EGDY, and MAAP aquifer materials is listed in Table 3.3.3, and the simulated NOD profiles are shown in Figure 3.3.10. The portion of the fast reacting OAM for all aquifer materials is considerably less than the slow reacting OAM (85% of total OAM is slow). However, since the fast reaction rate coefficient with respect to permanganate is considerably (at least 30 times) higher than that that of the slow reaction, the fast reacting OAM is quickly consumed, generating a fast rise of each NOD profile over an very short time. The length of time over which the fast reaction is active appears to be much shorter than 7 days which is consistent with the observations from short-term experiments (detailed in Section 3.5).

The calibration exercise indicated that C_{OAM}^{fast} and k_{ox}^{fast} or k_{OAM}^{fast} are mainly controlled by the first observed NOD value (i.e., 7-day NOD), while k_{ox}^{slow} or k_{OAM}^{slow} is mainly controlled by the remaining NOD data. Figure 3.3.11 presents the response of a NOD profile for Borden to the change of the reduction factor k_p, and clearly shows that a small reduction factor will result in an overestimate of NOD while a large reduction factor will lead to a underestimate of NOD. This indicates that passivation due to manganese dioxide affects the long-term behavior of permanganate consumption. The reduction factor for each aquifer material shows some level of variation with the lowest coefficient of variation (1.3%) for Borden, and the highest value (114%) for MAAP. The reason for this variation of the reduction factor is unknown but might be related to the varying reaction environment (i.e., pH and reactant concentrations) in each batch reactor.

Nevertheless, the results shown in Figure 3.3.10 suggest that the proposed two-component kinetic model is able to capture the long-term permanganate consumption by aquifer materials.

3.3.3 Summary

This investigation indicates that the rate of permanganate consumption (i.e., the overall reaction rate) is strongly affected by the oxidant to solids mass loading ratio, and the initial permanganate concentration. An higher initial permanganate concentration or higher oxidant to solids mass ratio produced relatively faster NOD reaction rates and generated corresponding higher values of NOD_{max}. In addition, it appears that TOC content determines the maximum NOD value while amorphous Fe content, along with CEC, determines the permanganate consumption rate by aquifer materials.

The first principles and experimental data suggest that the permanganate consumption by aquifer materials is at least consisted of a fast and a slow reaction, accordingly, a conceptual kinetic model accounting of these two reactions was developed to kinetically capture the permanganate NOD profiles observed from long-term experiments. Meanwhile, empirical expression of long-term permanganate NOD (at an initial $KMnO_4$ concentration of 20 g/L) in terms of aquifer materials was also developed, which is expected to provide a guideline for developing NOD empirical expressions under other initial permanganate concentrations.

The end-product of permanganate reduction by aquifer materials is manganese dioxide, which might play an important role in 1) auto-decomposition of permanganate, and 2) passivation to the permanganate reaction with OAM due to its coating on the grain surface.

The result suggests that variations in experimental design will impact reported NOD values, and the kinetic nature of NOD reaction(s) cannot be ignored. Batch experimental determination of a temporal NOD should employ the expected permanganate concentration to be used in situ along with various permanganate to solid mass ratios. Assuming the same controlling factors also affect the oxidant stability in situ, the estimation of in situ permanganate NOD can then be obtained by linear extrapolation.

Table 3.3.1. Experimental details of long-term permanganate NOD

Material ID	Nominal Initial Concentration [g/L]	AM Mass [g]	Start Date	Sampling Duration [days]	Post-Experimental [2] Sample Analysis	Comments
Borden	1	10^3, 20, 30	15-Jan-04	125, 196, 146 (spiked)	Manganese content and dichromate COD test	
	10	20, 30		196, 196		
	20	20,30		196, 196		
DNTS	1	20, 30	28-Jan-04	186, 163 (spiked)	Manganese content and dichromate COD test	
	10	20, 30		186, 186		
	20	20, 30		186, 186		
EGDY[1]	10	15, 25	19-Apr-04	197, 197	Manganese content	Problembic reading in COD test
	20	15, 25		197, 197		
LAAP	1	20, 30	1-Dec-03	241, 241	NA	Problembic sampling
	10	20, 30		241, 241		
	20	20, 30		241, 241		
LC34-USU	12.7	10, 20, 30, 40, 50	8-Apr-03	323 (spiked)	Mixed, Chao's method, Respiked with 20 g/L	
	1	20, 30	18-Jul-03	215, 215	Manganese content, dichromate COD test	
	20	20, 30		158, 158		
LC34-LSU	12.7	10, 20, 30, 40	11-Apr-03	322 (spiked)	Mixed, Chao's method, Respiked with 20 g/L	
	1	20, 30	18-Jul-03	213, 213 (spiked)	Manganese content, dichromate COD test	
	20	20, 30		213		
MAAP	1	20, 30	6-Nov-03	226, 226	Manganese content and dichromate COD test	
	10	20, 30		226, 226		
	20	20, 30		226, 226		
NFF[1]	10	15, 25	12-Feb-04	61, 143	Manganese content	Problembic reading in COD test
	20	15,25		168, 168		
NIROP	1	30, 40	9-Jun-03	266	Manganese content and dichromate COD test	
	10	, 20, 30, 40,		321		
	20	20, 30		266		

Note:
1. 125 mL reactors used
2. foc analysis done but failed in consistency
3. Started on 12-Feb-04

Table 3.3.2. Estimated permanganate consumption rate (g-$KMnO_4$/kg/day).

	Fast			Slow	Maximum NOD			
	Avg	min	max	Avg	Average			Maximum
Borden	0.17	0.093	0.24	0.0034	2.12	±	0.57	2.79
DNTS	0.18	0.094	0.25	0.0014	2.28	±	0.59	2.83
EGDY	2.2	1.9	2.4	0.020	32.29	±	3.55	35.32
LC34-LSU	0.89	0.40	1.4	0.0035	11.42	±	2.67	14.46
LC34-USU	0.45	0.21	0.95	0.0012	5.50	±	1.97	9.34
MAAP	0.023	0.0029	0.064	0.00053	0.77	±	0.76	2.14
NFF	8.4	5.9	10	0.074	87.87	±	9.99	98.1
NIROP	0.12	0.080	0.19	0.00070	2.54	±	1.21	4.75

Table 3.3.3. Best-fitting parameters (k_{ox} and C_{OAM} for fast reaction, k_{ox} for slow reaction, and reduction factor) and other parameters of the kinetic model parameters.

Site	mass of aquifer (g)	Initial $KMnO_4$ (g/L)	porosity	bulk density (kg/L)	fast reaction			slow reaction			reduction factor
					C_{OAM} (g$KMnO_4$/kg	k_{ox} (L/g/day)	k_{OAM} (L/g/day)	C_{OAM} (g$KMnO_4$/kg)	k_{ox} (L/g/day)	k_{OAM} (L/g/day)	
Borden	20	1	0.82	0.47	0.56	0.37	0.152	6.40	0.00078	0.000054	0.000510
	30	10	0.73	0.71			0.135			0.000048	0.000512
	30	20	0.73	0.71			0.135			0.000048	0.000517
	20	20	0.82	0.47			0.152			0.000054	0.000513
DNTS	20	1	0.82	0.47	0.42	0.47	0.194	3.81	0.0028	0.00019	0.00210
	30	10	0.73	0.72			0.172			0.00017	0.00223
	20	10	0.82	0.47			0.194			0.00019	0.00190
	30	20	0.73	0.72			0.172			0.00017	0.00185
EGDY	15	10	0.96	0.11	5.01	0.37	0.179	29.47	0.0023	0.00018	0.000143
	15	20	0.96	0.11			0.179			0.00018	0.000122
	25	10	0.93	0.19			0.174			0.00018	0.000111
	25	20	0.93	0.19			0.174			0.00018	0.000122
MAAP	20	1	0.82	0.47	0.08	0.10	0.040	1.09	0.0030	0.00021	0.00703
	30	10	0.73	0.71			0.036			0.00019	0.00966
	20	10	0.82	0.47			0.040			0.00021	0.00522
	20	20	0.82	0.47			0.040			0.00021	0.00265

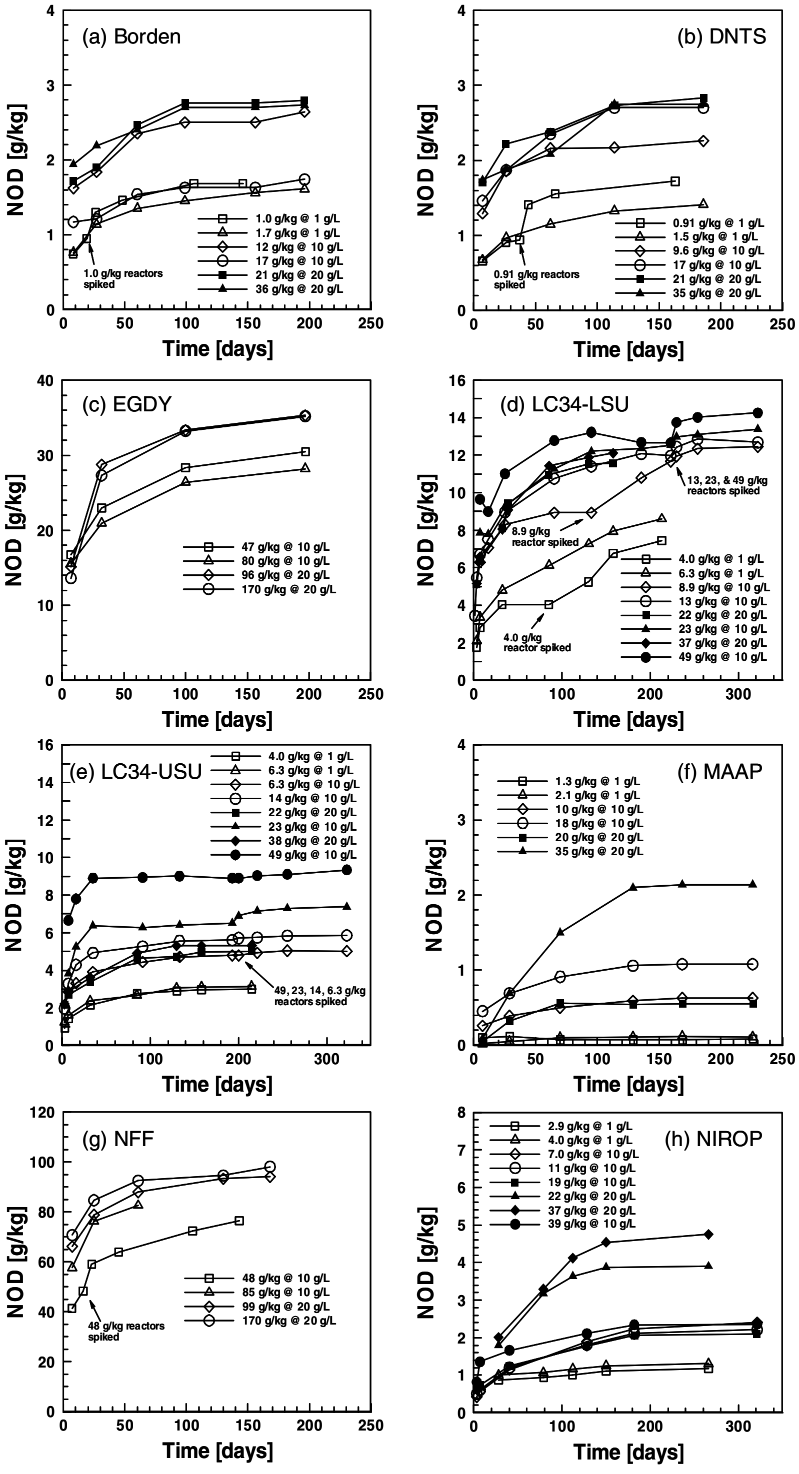

Figure 3.3.1. Long-term permanganate NOD profiles for each experimental series performed on the eight aquifer materials used in this investigation. Each data point represents the average from triplicate reactors. The legend for each profile indicates the oxidant to solids mass ratio and initial permanganate concentration used for each experimental series. Also noted on each panel is reactor spiking events. Error bars are not shown to avoid confusion.

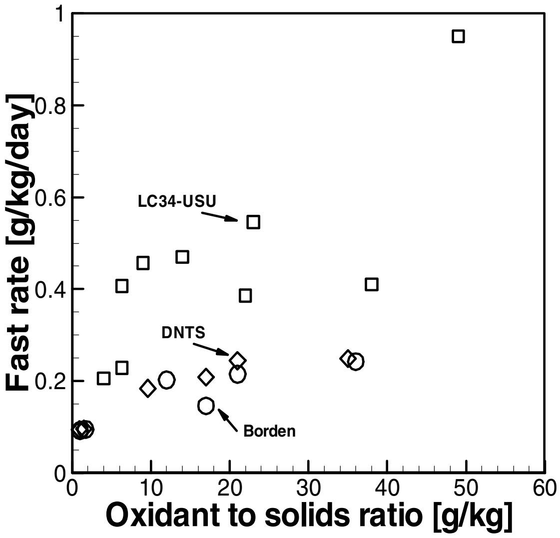

Figure 3.3.2. Scatter plot of the fast rate of permanganate consumption and the oxidant to solids mass ratio for each experimental series. The NOD expressed over the first 7 days was used to estimate the fast rate of permanganate consumption.

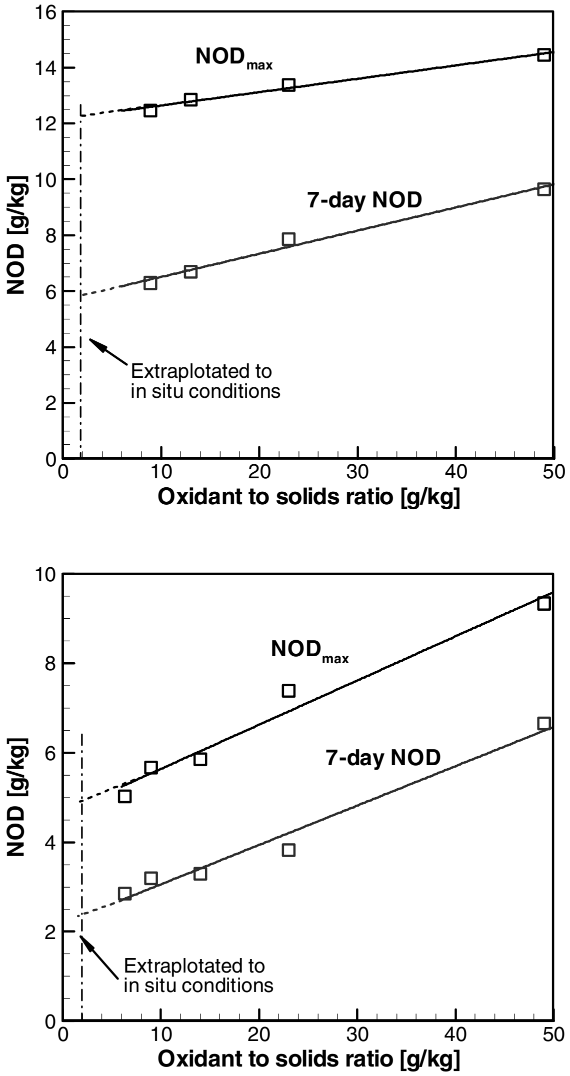

Figure 3.3.3. NOD_{max} and the 7-day NOD as functions of the oxidant to solids mass ratio for (a) LC34-LSU and (b) LC34-USU aquifer materials at an initial permanganate concentration of 12.7 g/L. The dashed lines are extrapolations of the linear relationship ($r^2 > 0.90$) to oxidant to solids mass ratio values representative of *in situ* conditions.

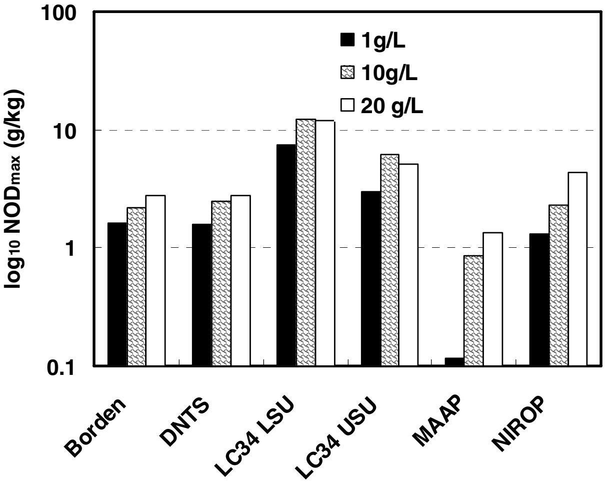

Figure 3.3.4. The impact of different initial permanganate concentrations on the average observed NOD_{max}.

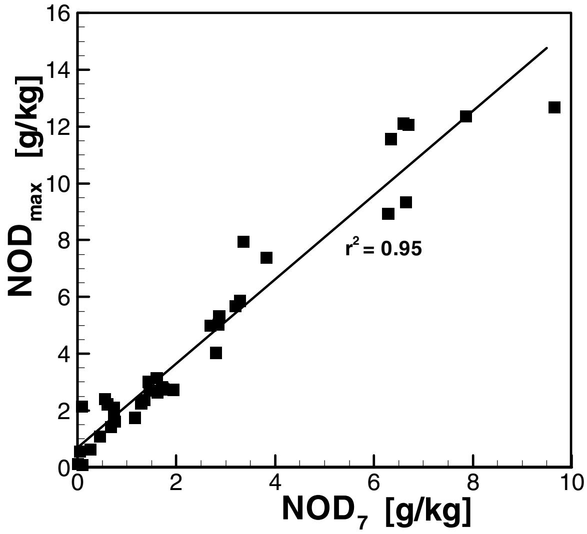

Figure 3.3.5. Scatter plot of the 7-day NOD and NOD_{max} data for all experimental sites.

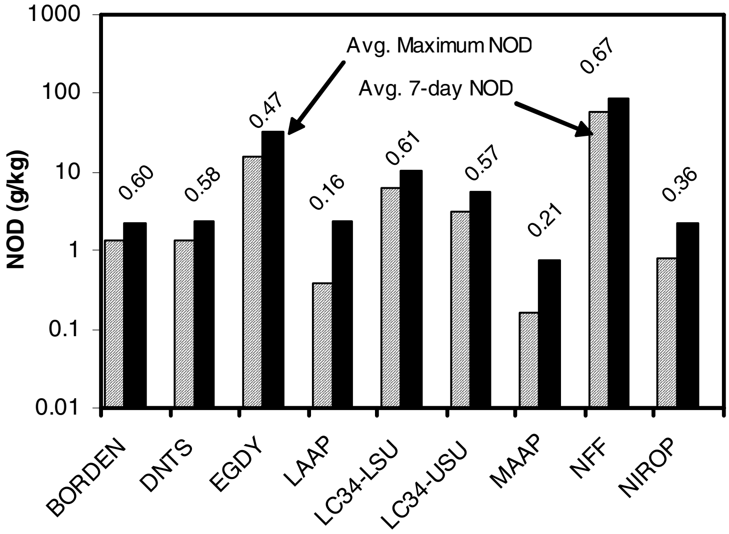

Figure 3.3.6. Observed maximum NOD and NOD at 7 days. The number above the bar indicates the ratio of the 7-day NOD value to the maximum NOD value.

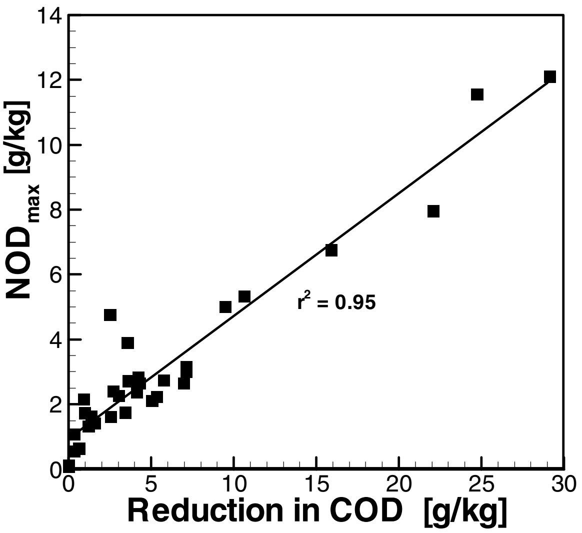

Figure 3.3.7. Reduction in COD test values after aquifer materials exposed to permanganate for Borden, DNTS, LC34-LSU, LC34-USU, MAAP, and NIROP aquifer materials compared with observed NOD$_{max}$ for each experimental series.

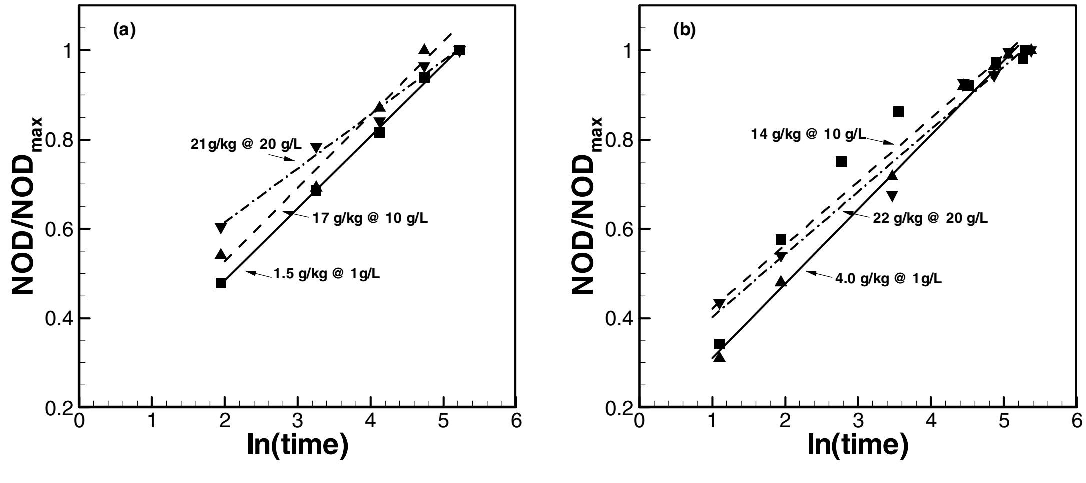

Figure 3.3.8. Best-fit logarithm functions to normalization NOD profiles for (a) DNTS and (b) LC34-USU aquifer materials.

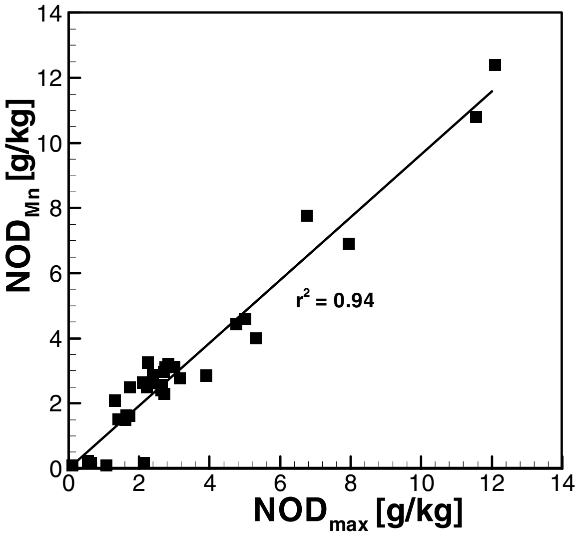

Figure 3.3.9. Scatter plot of NOD_{max} and the equivalent NOD based on the bulk soil manganese concentration after exposure to permanganate for >250 days.

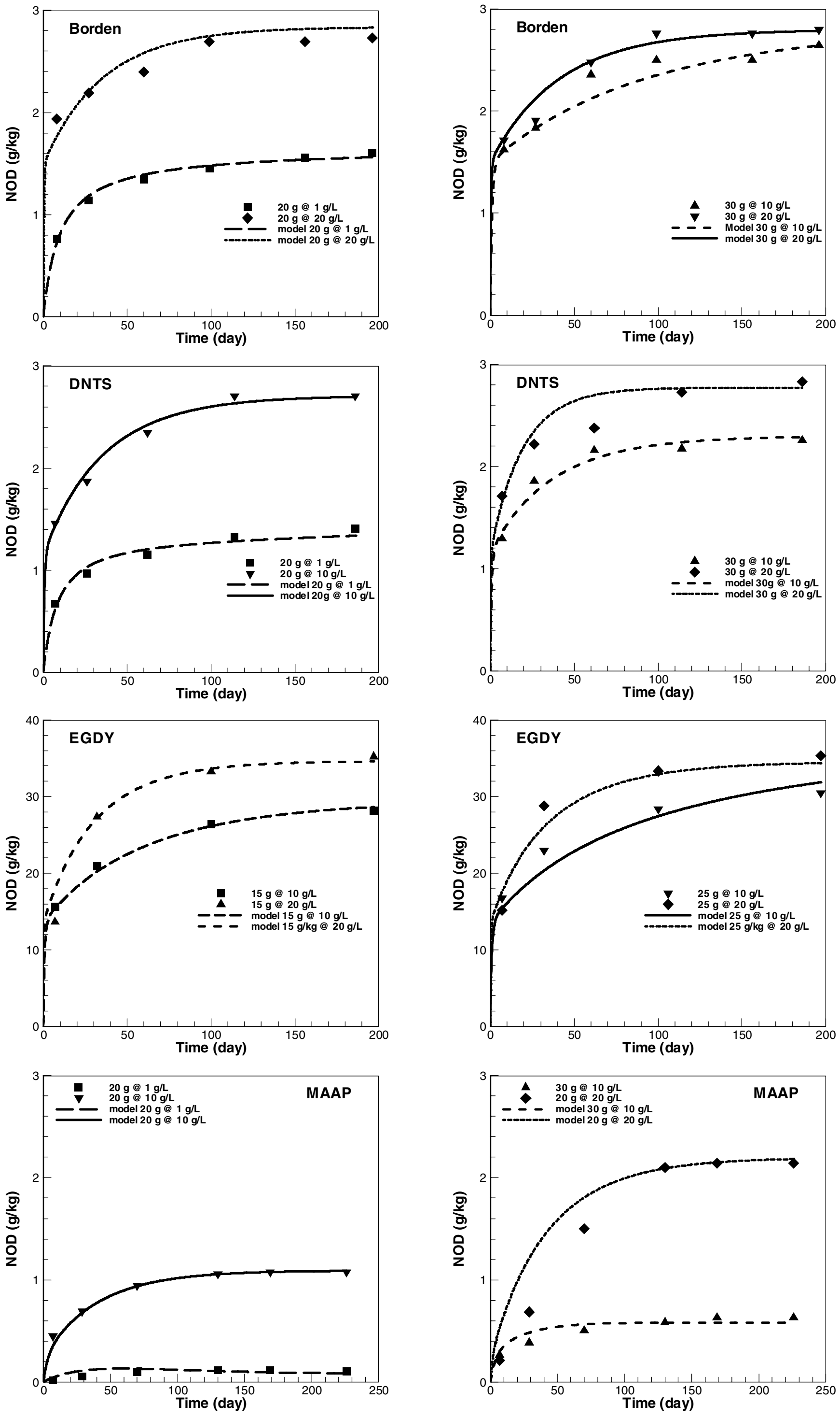

Figure 3.3.10. The observed and simulated NOD profiles for batch experiments with the Borden, DNTS, EGDY, and MAAP aquifer materials.

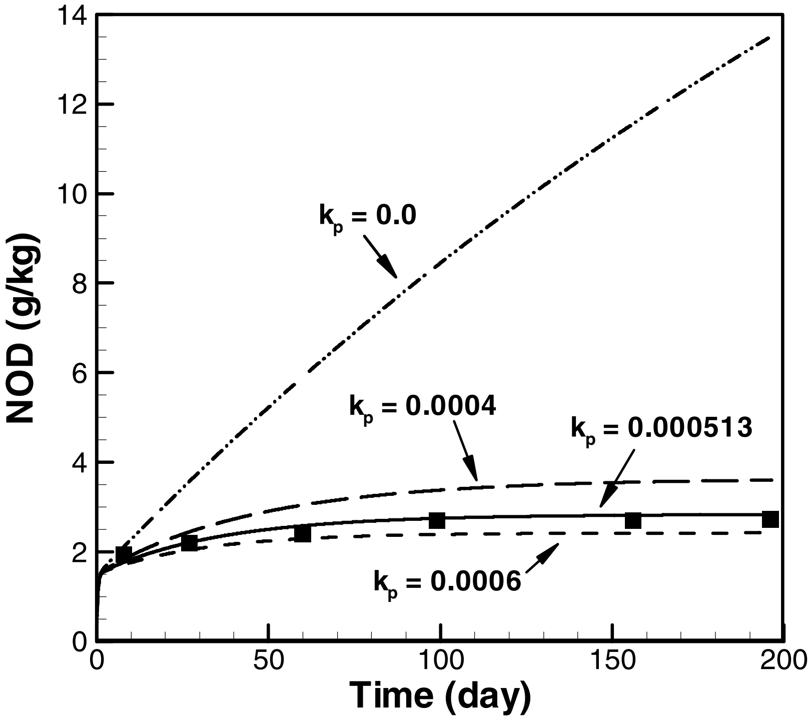

Figure 3.3.11. The influence of the change of reduction factor k_p on the simulated permanganate NOD profile. Square symbols represent the observed NOD values for the test with 20 g Borden aquifer material exposed to a $KMnO_4$ solution with an initial concentration of 20 g/L.

3.4 Permanganate COD Tests

As discussed in Chapter 2, the dichromate COD method has been able to provide reliable results for water and wastewater applications (APHA, 1998). Barcelona and Holm (1991) described modifications to the standard water/wastewater COD test to estimate the reduction capacity of aquifer materials. Our dichromate COD results, as shown in Chapter 2, indicated that these modifications could provide reliable estimates of the TRC of aquifer solids. However, a fraction of the complex natural organic matter, and various crystalline and amorphous inorganic components present in aquifer materials may be recalcitrant to permanganate (Christensen et al., 2000; Evanko and Dzomak, 1998; Blair et al., 1995) and therefore using the dichromate COD test to estimate permanganate consumption will lead to significant overestimation.

Permanganate was used as a specified oxidant in the COD test prior to dichromate (APHA, 1946; Burtle and Buswell, 1937); however, some reduced compounds such as acetic acid, propionic acid, butyric acid, stearate acid, and nitrogen species are not readily oxidized by permanganate (APHA, 1946; Burtle and Buswell, 1937; Eckenfelder and Hood, 1950). In response to the inability of permanganate to oxidize some forms of organic compounds in industrial wastewaters, non-uniformity of results and problems with manganese dioxide precipitates, permanganate was replaced by dichromate (Moore et al., 1949, 1951). However, permanganate is still used as a specified oxidant in the COD test for the water industry in Europe (European Environmental Agency, 1999), Japan (Fujimori et al., 2001), and China (Zhou, 1994) due to the advantages of a non-toxic waste stream and its ease of handling.

Considering that the dichromate COD test for aquifer solids is an extension from that used for water and wastewater, the work here attempts to extend the permanganate COD test used in the water and wastewater application to a test of aquifer solids since the ultimate permanganate consumption rather than dichromate demand by aquifer materials is of interest in permanganate treatment applications.

3.4.1 Methods

The developed permanganate COD test is similar in principle to the dichromate COD test described in Chapter 2. Aliquots of the dry ground solids (~1.5 g) were transferred to pre-cleaned reaction tubes and 10 mL of a 20% (w/w) concentrated sulfuric acid solution (EM Science) and 15 mL of a 10 g/L $KMnO_4$ solution was added. The potassium permanganate solution was prepared by adding analytical grade $KMnO_4$ (EM Science) to Milli-Q water and boiling for ~1 hour. The cooled solution was then filtered using a 0.45-mm glass fibre filter (Pall Corporation). Each reaction tube was sealed, inverted by hand 3 to 4 times and then heated at 85^oC for 2 hours (PMC, Model 350). We used an elevated temperature of 85^oC rather than 150 ^oC as used in the dichromate COD test to be consistent with the historical permanganate COD test for wastewater (APHA, 1946). After cooling, the reaction tubes were centrifuged for 1 hour at 4000 rpm (Beckman, Model TJ-6) to clear the supernatant solution for spectrophotometric measurement (Milton Roy, 20D) of un-reacted potassium permanganate at 525 nm. A standard curve using sodium oxalate (BDH Laboratories) was developed in parallel, and used to quantify the chemical oxygen demand. Sodium oxalate has a theoretical $KMnO_4$ demand of 0.4718 g/g (Method 4500; APHA, 1998) and based on the developed standard curve and the mass of aquifer material used, the $KMnO_4$ demand (g $KMnO_4$/kg of aquifer material) was determined. All tests were performed five times for each aquifer material.

A separate serie of experiments was also performed to confirm the theoretical $KMnO_4$ demand of sodium oxalate. These experiments involved adding between 0.002 to 0.200 g of sodium oxalate and the same volume and concentration of sulfuric acid and $KMnO_4$ solution as discussed above to reaction tubes. After digestion, the observed mass of $KMnO_4$ consumed per mass of sodium oxalate was determined to be 0.429 ± 0.047 g/g. This measured consumption is not statistically different from the theoretical $KMnO_4$ demand of sodium oxalate and therefore the theoretical demand of 0.4718 g/g was used in this effort.

As part of the development of this permanganate COD test method it was of interest to explore how the test method results varied due to changes in mass of aquifer material, initial permanganate concentration, and reaction duration. To assess these variations we performed a series of experiments using a sub-set of aquifer materials where the mass of aquifer material was varied from 1.0 to 2.0 g, the permanganate concentration was varied from 5 to 20 g/L, and the reaction duration was varied from 0.5 to 3.0 hours.

3.4.2 Results

The average results from the permanganate COD analyses are listed in Table 3.4.1. For comparison, the dichromate COD, Maximum NOD, and total reductive capacities (TRC) contributed from TOC, Fe, and Mn are also listed in Table 3.4.1. (Although TOC, Fe, and Mn were used to calculate the TRC, we acknowledge that only their reduced contents contribute to the TRC of each aquifer material). From Table 3.4.1, except for the results for LC34 USU aquifer material, the dichromate COD test results are 20 to 70% higher (avg. of 50%) than the permanganate COD test results which is not surprising since dichromate can oxidize a wider range of species relative to permanganate (APHA, 1998; Boyles, 1997). The average coefficient of variation for the permanganate COD test and the dichromate COD test are similar (12% compared to 9%) suggesting a comparable level of variability between the two methods.

Both the dichromate and permanganate COD test results are highly correlated with the overall maximum NOD (*r* of 0.978 and 0.996 respectively) indicating that both COD tests are potentially good predictors of the maximum NOD (Figure 3.4.1). This relationship between permanganate consumption and dichromate COD is consistent with the findings of Tucker (1984) in an investigation of the permanganate demand of pond waters. However, the results from the dichromate COD test overestimated the overall maximum NOD on average by 100% (range 20 to 280%) while the permanganate COD test, on average, slightly underestimated the overall maximum NOD by 10% (range -20 to +30%). The data also indicate that there is no statistically significant difference ($\alpha = 5\%$) between the results of the permanganate COD test and the overall maximum NOD. Therefore, as an absolute measure of the maximum NOD associated with an aquifer material, the permanganate COD test is superior to the dichromate COD test since the permanganate COD test result can be used directly as an estimate of the maximum NOD.

Similar to the overall maximum NOD, the dichromate COD and permanganate COD test results are highly correlated ($r > 0.91$) with the TOC and amorphous Fe content of each aquifer material (Figure 3.4.2). There was little correlation between the total Mn and/or total Fe content and the various test results ($r < 0.65$). This suggests that the organic matter and amorphous Fe contained in the aquifer materials used in this investigation were mainly responsible for oxidant consumption as captured by these COD tests. However, the dichromate COD test overestimates the TOC and amorphous Fe reductive capacity, while the results from the permanganate COD test behave in a similar fashion to the batch test results and underestimate the TOC and amorphous Fe reduction capacity. This suggests that even at an elevated temperature under acidic conditions permanganate appears to be reactive with only a portion of the TRC. Since dichromate can oxidize a wider range of species than permanganate, it is not surprising that the results from the dichromate COD test are higher then our estimated TRC consistent with the trends reported by Barcelona and Holm (1991).

Figure 3.4.3 presents the sensitivity of the permanganate COD test results for four aquifer materials to variations in reaction duration (0.5, 1.0, 2.0, and 3.0 hours), initial permanganate concentration (5, 10 and 20 g/L), and mass of aquifer material (1.0, 1.5, and 2.0 g). Note that this sensitivity investigation was performed relative to the permanganate COD test conditions discussed previously where a reaction duration of 2.0 hours, an initial permanganate concentration of 10 g/L, and a mass of aquifer material of 1.5 g were specified. As the reaction duration increased, the permanganate COD test results increased for all aquifer materials until the 2-hour reaction duration was reached and then stabilized (Figure 3.4.3a). The permanganate COD test protocol for water/waste water samples as described by APHA

(1946) specified a reaction period of 0.5 hours which is clearly too short for the heterogeneous reaction to reach completion in the aqueous-solid system investigated here. Similar to the impact of reaction duration, changes in initial permanganate concentration also influenced the permanganate COD estimate (Figure 3.4.3b). An initial permanganate concentration of 5 g/L produced permanganate COD estimates lower than those using an initial permanganate concentration of 10 or 20 g/L. This is presumably due to the concentration dependent reaction rate and at a permanganate concentration of 5 g/L complete oxidization of the permanganate oxidizable components in the aquifer materials over the 2-hour reaction duration was not achieved. For example, for the Borden aquifer material, the reacted $KMnO_4$ mass (0.0049 g, used to estimate NOD or permanganate COD value) over the reaction duration of 2 hours was much less than the unreacted $KMnO_4$ mass (0.045 g) remained in the reaction tube which was still available for further reaction. The permanganate COD test results were not significantly sensitive to the mass of aquifer material used (Figure 3.4.3c) except for the EGDY aquifer material. As shown in Figure 3.4.3a, the variability in the permanganate COD test results increased marginally as the reaction duration was increased from 2 to 3 hours, but increased considerably as the permanganate concentration was increased from 10 to 20 g/L, and the solids mass was increased or decreased from 1.5 g.

Supported by visual observations, we believe that the increased variability in the permanganate COD test results for a 3-hr reaction duration, a permanganate concentration of 20 g/L and a solids mass of 2.0 g is the result of interference by the manganese oxides produced during the oxidation process. These colloidal by-products may influence the test results by (1) promoting self-decomposition of permanganate which occurs in a strong acidic solution under elevated temperature conditions (Steward, 1965), and by (2) affecting our ability to quantify the permanganate concentration by spectrophotometry at a wavelength of 525 nm even though the reaction tubes were centrifuged for 1 hour at 4000 rpm. The first suspected interference would result in an increased demand of permanganate (positive bias), while the second interference would result in the quantification of an apparent higher permanganate concentration (negative bias). The high permanganate COD standard deviation for the 1.0 g sample size is likely related to the non-representative nature of this sample mass. Additional investigative efforts are presently underway to resolve the nature of this interference and develop corrective approaches.

3.4.3 Summary

Current methods used to determine permanganate NOD involve the use of well-mixed batch tests which are time consuming and subject to test variables (e.g., concentration, mass of oxidant to solid ratio, reaction duration, and mixing conditions) that significantly affect the results. The work here suggests that a modified chemical oxygen demand (COD) test method using permanganate can be used to determine the maximum permanganate NOD of an aquifer material quickly and economically. This proposed test method was used in a comparative study that involved eight different aquifer materials. The results showed that the proposed test method is superior to the dichromate COD test and can be used to directly estimate the maximum NOD for site screening and initial design purposes.

Based on this limited sensitivity investigation we recommend that a reaction duration of 2 hours, an initial permanganate concentration of 10 g/L, and a aquifer material sample size of 1.5 g be used in the permanganate COD test to estimate the maximum NOD of aquifer materials. In addition we acknowledge that potential interference of manganese oxides, a reaction by-product, variability in aquifer materials, and error in method may lead to large experimental variability.

Table 3.4.1. Summary of the maximum permanganate consumption as estimated from theoretical considerations of the reductive capacity of various aquifer species, the dichromate and permanganate chemical oxygen demand tests, and from the long-term permanganate NOD batch tests. All values are expressed in terms of g of $KMnO_4$ per kg of dry aquifer material.

Site ID	Theoretical Reductive Capacity					Dichromate-COD[1]			Permanganate COD			Maximum NOD			
	TOC	Fe_T	Fe (Am)	Mn_T	Mn (Am)	Avg		Stdev	Avg		Stdev	Average[2]			Maximum[3]
Borden	3.95	16.52	0.28	0.81	0.01	10.21	±	0.43	3.52	±	0.85	2.12	±	0.57	2.79
DNTS	4.61	60.22	0.34	0.29	<0.01	6.30	±	1.62	3.59	±	0.35	2.28	±	0.59	2.83
EDGY	37.53	37.00	1.12	1.34	0.15	54.48	±	1.25	32.58	±	0.69	32.29	±	3.55	35.32
LAAP	7.57	21.43	0.25	0.21	0.01	7.81	±	0.42	2.10	±	1.68	1.62	±	0.67	2.38
LC34 LSU	30.29	5.76	0.48	0.13	<0.01	30.19	±	0.41	13.36	±	0.48	11.42	±	2.67	14.46
LC34 USU	14.45	3.49	0.38	0.19	<0.01	11.09	±	0.32	11.32	±	1.32	5.50	±	1.97	9.3
MAAP	12.67	0.82	0.03	0.05	0.02	3.29	±	0.89	2.53	±	0.59	0.77	±	0.76	2.14
NIROP	5.18	12.18	0.71	0.57	0.06	7.25	±	0.52	4.34	±	0.48	2.54	±	1.21	4.75

Notes:

1. Average and standard deviation based on data from 5 tests of each aquifer material.
2. Average and standard deviation of the maximum NOD for all experimental trials
3. Overall maximum NOD of each aquifer materail

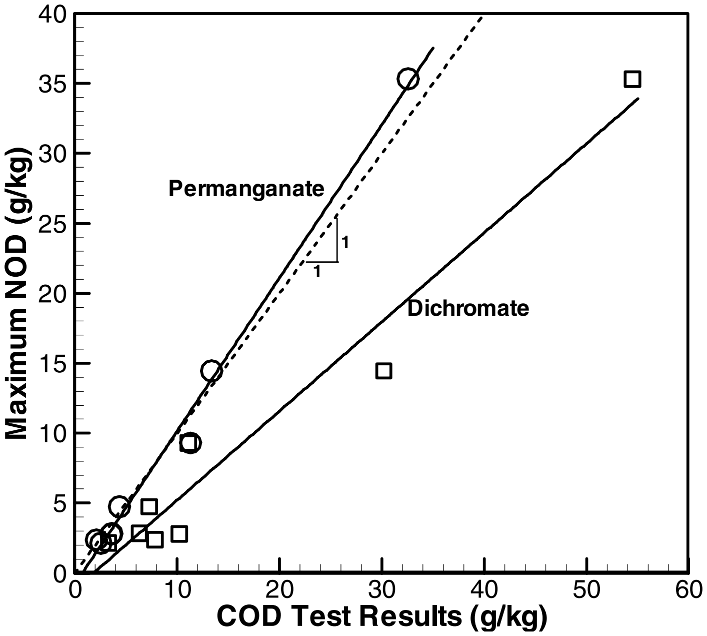

Figure 3.4.1. Scatter plot of the dichromate and permanganate chemical oxygen demand test results (average of 5 trials), and the overall maximum permanganate NOD from the long-term batch tests for each aquifer material. All values expressed as g-$KMnO_4$ /kg. Also shown are best-fit linear relationships for each COD test as described by (1) Overall maximum NOD = 0.64±0.14 x (dichromate COD value) – 1.15±3.14 with a $r^2 = 0.96$ for the dichromate test; and (2) Overall maximum NOD = 1.10±0.10 x (permanganate COD value) – 0.83±1.29 with a $r^2 = 0.99$ for the permanganate test.

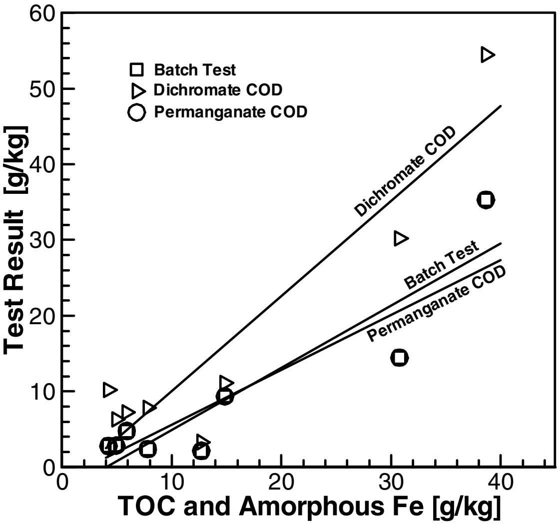

Figure 3.4.2. Scatter plot of the results from the dichromate COD test, the permanganate COD test, the long-term batch test (overall maximum NOD) and the sum of the TOC and the amorphous Fe content of each aquifer material. All values expressed as g-$KMnO_4$ /kg. Also shown are best-fit linear relationships as described by (1) Overall maximum NOD = 0.81 x TRC* – 2.8 with a r^2 = 0.83 for the batch test; (2) dichromate COD = 1.3 x TRC* – 2.5 with a r^2 = 0.86 for the dichromate COD test; and (3) permanganate COD = 0.73 x TRC* – 1.7 with a r^2 = 0.82 for the permanganate COD test; where TRC* is the contribution from TOC and amorphous Fe expressed in g/kg (see Table 3.4.1).

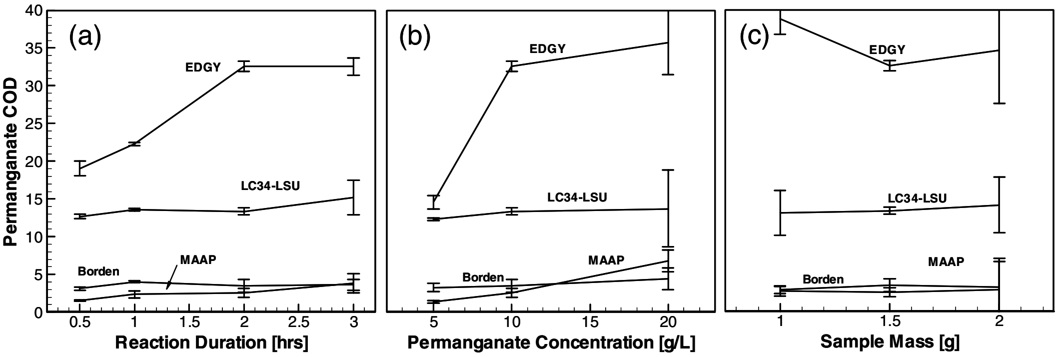

Figure 3.4.3. Sensitivity of the permanganate COD test results due to changes in (a) reaction duration, (b) initial permanganate concentration, and (c) sample mass of aquifer material. All test values are expressed in terms of g of $KMnO_4$ per kg of dry aquifer material. The error bars represent ± one standard deviation.

3.5 Short-Term Kinetic Investigations

3.5.1 Experimental Methods

To investigate the kinetics involved in the reaction between permanganate and aquifer materials, it is necessary to hold one of the two reactants constant or in excess in order to observe changes in the other reactant. Therefore, two series of experiments were conducted: (1) excess aquifer material experiments consisting of ~100 g of aquifer materials digested with various concentrations of permanganate solution (0.06 ~ 2 g/L), and (2) excess permanganate mass experiments consisting of an excess (~20 g/L) of permanganate mixed with various mass (10 ~ 25 g) of aquifer solids. All experiments were performed in replicates or triplicates using 300 mL reactor vessels in conjunction with 3.2 cm stir bar placed on a stir plate. If necessary, permanganate solutions were buffered with phosphates to maintain a neutral pH value.

Excess Aquifer Material Mass Kinetic Experiments

The mass of aquifer material used in these experiments was determined so that the various permanganate masses employed would be at least ten times less than the ultimate permanganate consumption as estimated from the results of the long-term NOD experiments and the permanganate COD tests. Each experimental run consisted of loading the aquifer material mass in the reactor and then adding the permanganate solution. Table 3.5.1 lists the aquifer material mass, solution volume, and permanganate concentration used for each experimental run. All $KMnO_4$ solutions were prepared by heating at 80^oC for ~1 hour, and then filtering the cooled solution through a 0.45-µm glass fiber filter (Pall Corp.). A phosphate buffer (sodium phosphate dibasic at 10 mM) was added to the permanganate solution to maintain a neutral pH (~7.2). At specified reaction times (nominally 2, 5, 10, 20, 40, 70, 120, 180 min) an aliquot (~2 mL) of the permanganate solution was extracted from the reactor with a syringe (LUER-LOK, Becton & Dickinson), and filtered through a 0.45 µm syringe filter (Acradisc, Pall Corp.). The permanganate concentration was quantified with a spectrophotometer (Milton Roy, 20D) at 525 nm.

Excess Permanganate Mass Kinetic Experiments

In these experimental runs two to three masses of aquifer material from each site were loaded into a reactor followed by the addition of a specified volume (between 100 to 150 mL) of a permanganate solution with a concentration of 20 g/L. After a specified reaction duration (nominally 5, 15, 30, 60 min) the experimental run was quickly terminated by filtering the slurry through a 6-µm filter paper (Whatman, VWR Lab) and rinsing the material retained on the filter with Milli-Q water until only a faint pink color persisted. The solid material remained on the filter paper was then transferred to aluminum trays, dried at 80°C for 24 hours, and ground in a porcelain mortar to pass through a 150-µm sieve. Aliquots of the ground aquifer material were then submitted for a dichromate-COD (DCOD) analysis. Table 3.5.2 lists the aquifer material mass, solution volume, and permanganate concentration used for each experimental run.

3.5.2 Results and Analysis

The data collected from the excess aquifer material mass and the excess permanganate mass kinetic experiments are shown in Figures 3.5.1 and 3.5.2. For the excess aquifer material experimental results each data point on Figure 3.5.1 is the average from duplicate experimental runs hence no error bars are shown. Data generated from the excess permanganate mass kinetic experiments indicated little difference between the DCOD values for each aquifer material mass used and thus these values were pooled. Therefore each data point on Figure 3.5.2 is the average of between six and nine DCOD values and the error bars indicate the standard deviation. Again, the aquifer material from the LAAP site proved to be problematic due to the high degree of fines which clogged the various filters used.

The data presented in Figure 3.5.1 clearly indicate that the consumption of permanganate by aquifer material is a function of the initial permanganate concentration, consistent with the observations from long-term batch experiments. As a first step to extract kinetic parameters from these data, we used the initial rate method (Levensipiel, 1999) to determine the reaction order with respect to permanganate and the observed rate coefficient with respect to permanganate (see Table 3.5.3). It can be seen that the reaction order, α, ranges from 0.22 to 1.0., while the magnitude of observed permanganate rate coefficient ranges from 0.011 to 0.111 $\text{min}^{-1}(\text{MnO}_4^-/\text{L})^{1-\alpha}$. It should be noted that the initial rate method as applied here requires the change of permanganate concentration at t = 0.0, and therefore its accuracy depends on the elapsed reaction time prior to the first sampling episode.

Data presented in Figure 3.5.2 clearly indicate that the DCOD test value dropped significantly over the first 5 minutes followed by a relatively slow decrease over the next 1 to 2 hours. For all materials, the relative drop of DCOD ranges from 8 to 30% over the first five minutes, and from 18 to 50% over the first 60 minutes, implying some “very fast” and “intensive OAM-consuming” reactions took place over the first 5 minutes. To extract kinetic parameters with respect to OAM from the data in Figure 3.5.2, the integral method (Levensipiel, 1999) was employed. This indicated that if the initial data point at t = 0 was ignored the data is well represented by a first-order kinetic model with the observed rate coefficients for each aquifer material ranging from 0.0016 to 0.0076 min^{-1} (Table 3.5.4). Unfortunately, the elapsed reaction time prior to the first sampling episode was 5 minutes during which time some surface reactions occurring on the order of seconds to minutes probably occurred. Therefore, insufficient data obtained during the first 5 minutes actually missed some potentially important kinetic information.

Under the assumptions used to extract the kinetic information and with the experimental condition for each run, the kinetic parameters with respect to permanganate and OAM were calculated and are listed in Table 3.5.5. Except for the NIROP aquifer material, the value of reaction rate coefficient with respect to permanganate is 1.20 – 10.0 times greater than that of OAM. These two reaction rate coefficients generally display a similar trend across all aquifer materials: the aquifer material with a high value of the reaction rate coefficient with respect to permanganate will also have a high value of the reaction rate coefficient with respect to OAM; however, there is no good relationship ($r^2 < 0.3$) between these two reaction rate coefficients.

Correlation analyses between the reaction order and these two reaction coefficients and potential underlying aquifer material characteristics were performed (Figure 3.5.3). As evident from Figure 3.5.3, the reaction order with respect to permanganate, α, is weakly related to TOC ($r^2 = 0.68$), indicating that the initial permanganate consumption rate is sensitive to TOC content. The reaction coefficient k_{oam} is weakly related with surface area ($r^2 = 0.63$), implying that oxidation of OAM is probably controlled by the available amount of active sites on the grain surfaces. The reaction coefficient $k_{MnO_4^-}$ is weakly correlated with total Fe ($r^2 = 0.62$), perhaps suggesting that the (reduced) metal (i.e., Fe) content might be a major factor affecting short-term permanganate consumption.

3.5.3 Summary

The permanganate consumption by the aquifer material on a time order of hours is a function of the initial permanganate concentration, as is consistent with the observations from long-term batch experiments. This short-term permanganate reaction with bulk oxidizable aquifer materials (OAM) does not follow the first-order rate law. The OAM depletes quickly on a time scale of minutes and then follows a pseudo-first order reaction rate law. The reaction parameters (i.e. reaction order, rate coefficients) of the kinetic model describing the permanganate consumption reaction by aquifer materials are functions of aquifer material characteristics, indicating that this reaction is mainly controlled by the available reactive sites on the solid grain surface, and that the content of (reduced) Fe may also play a major role in determining its reaction rate. We acknowledge that insufficient samples especially for the excess permanganate mass experiment during the early reaction time period may have resulted in our inability to capture more fully the short-term kinetic reaction between permanganate and aquifer materials.

Table 3.5.1. Experimental details for the excess aquifer material mass kinetic experiments.

	Aquifer Material Mass [g]	Solution Volume [mL]	Concentation [g $KMnO_4$ / L]
Borden	100	100	0.1, 0.2, 0.3, 0.4, 0.5
DNTS	100	100	0.1, 0.2, 0.3, 0.4, 0.5
EGDY	80	100	0.5, 1.0, 1.5, 2.5,3.0
LAAP	100	100	0.1, 0.15, 0.2, 0.25, 0.3
LC34-LSU	100	100	0.4, 0.6, 0.8, 1.0, 1.2
LC34-USU	100	100	0.06, 0.2, 0.4, 0.6, 0.8
MAAP	100	100	0.04, 0.05, 0.06, 0.08, 0.1
NFF	80	100	5.0, 5.5, 6.0, 6.5, 7.0
NIROP	100	100	0.1, 0.2, 0.3, 0.4, 0.5

Table 3.5.2. Experimental details for the excess permanganate mass kinetic experiments.

	Concentation [g $KMnO_4$ / L]	Solution Volume [mL]	Aquifer Material Mass [g]
Borden	20	130	15, 20
DNTS	20	100	10, 20
EGDY	20	150	15, 20, 25
LAAP	20	100	10, 15
LC34-LSU	20	150	15, 25
LC34-USU	20	150	10, 20
MAAP	20	100	20, 25
NFF	25	125	10, 20
NIROP	20	100	15

Table 3.5.3. Observed reaction rate coefficients and reaction order for the excess aquifer material mass kinetic experiments

	Order (α)	k_{obs} min^{-1} $(MnO_4/L)^{1-\alpha}$	r^2
Borden	0.45 ± 0.12	0.037 ± 0.007	0.98
DNTS	0.30 ± 0.12	0.027 ± 0.005	0.95
EGDY	0.47 ± 0.13	0.137 ± 0.100	0.98
LAAP	NA	NA	NA
LC34-LSU	0.33 ± 0.19	0.072 ± 0.009	0.91
LC34-USU	0.52 ± 0.09	0.019 ± 0.002	0.99
MAAP	0.37 ± 0.17	0.008 ± 0.003	0.94
NFF	1.00 ± 0.00	0.111 ± 0.011	0.93
NIROP	0.22 ± 0.11	0.011 ± 0.001	0.94

Table 3.5.4. Observed reaction rate coefficients for excess permanganate mass kinetic experiments.

	k_{obs} [min^{-1}]	r^2	Excess Concentration [g $KMnO_4$/L]
Borden	0.0016 ± 0.0019	0.86	20
DNTS	0.0059 ± 0.0013	0.99	20
EGDY	0.0032 ± 0.0005	0.99	20
LAAP	NA ± NA	NA	NA
LC34-LSU	0.0028 ± 0.0017	0.96	20
LC34-USU	0.0018 ± 0.0019	0.89	20
MAAP	0.0021 ± 0.0010	0.93	20
NFF	0.0076 ± 0.0048	0.96	25
NIROP	0.0030 ± 0.0017	0.91	20

Table 3.5.5. Reaction rate coefficients with respect to OAM and permanganate

	k_{oam}[1]	k_{MnO4}[2]
Borden	4.62E-04	4.95E-03
DNTS	2.62E-03	5.86E-03
EGDY	8.86E-04	4.07E-03
LAAP	-	-
LC34-LSU	1.14E-03	3.30E-03
LC34-USU	4.42E-04	2.39E-03
MAAP	7.68E-04	3.16E-03
NFF	4.03E-04	1.67E-03
NIROP	1.67E-03	2.08E-03

1. units of (1/min)(g of MnO_4^- / L of solution)$^{-\alpha}$

2. units of (1/min)(g of MnO_4^- / L of solution)$^{1-\alpha}$(L of system / g of OAM as $KMnO_4$).

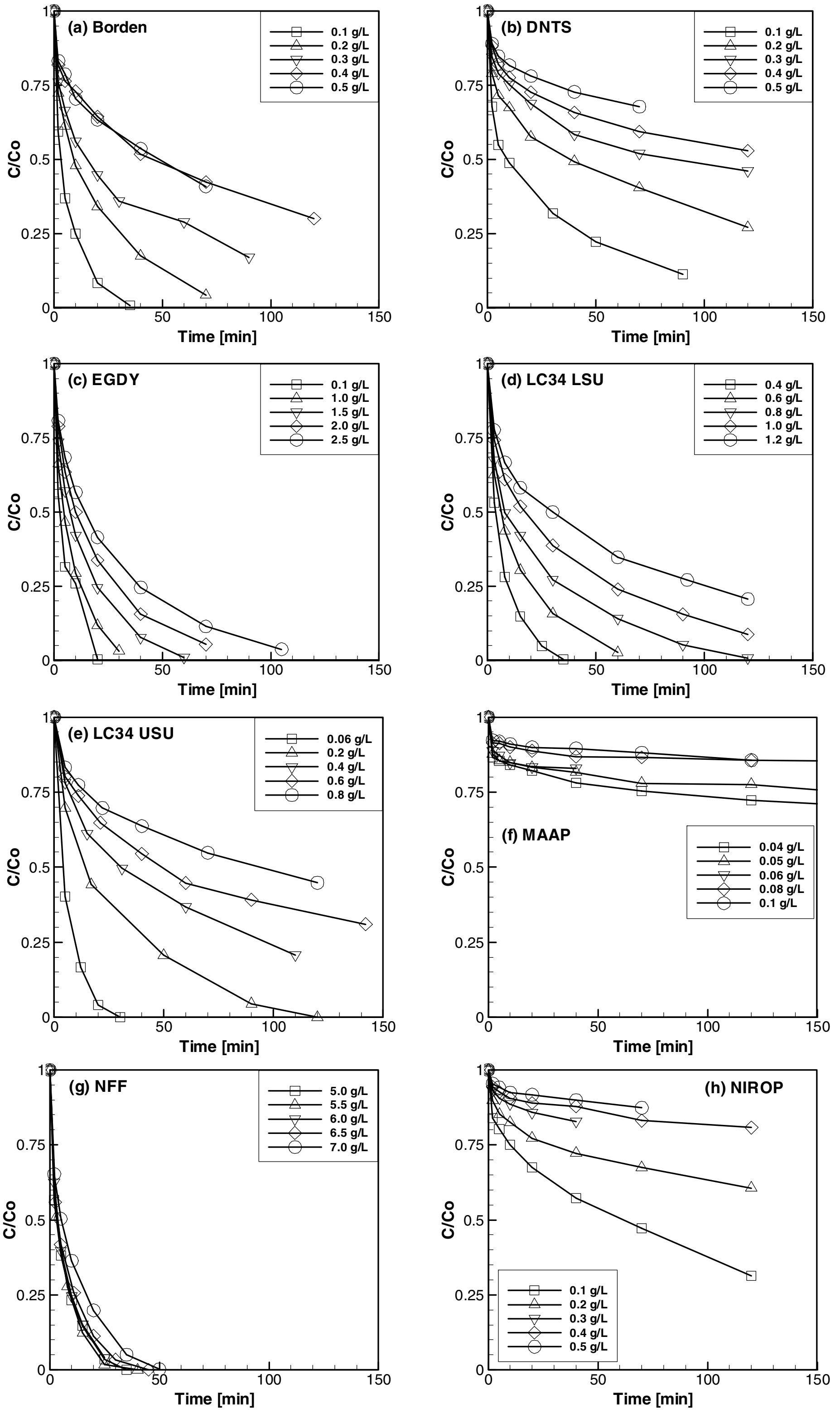

Figure 3.5.1. Permanganate concentration profiles generated from the excess aquifer material mass kinetic experiments. Each data point is the average from duplicate experiments.

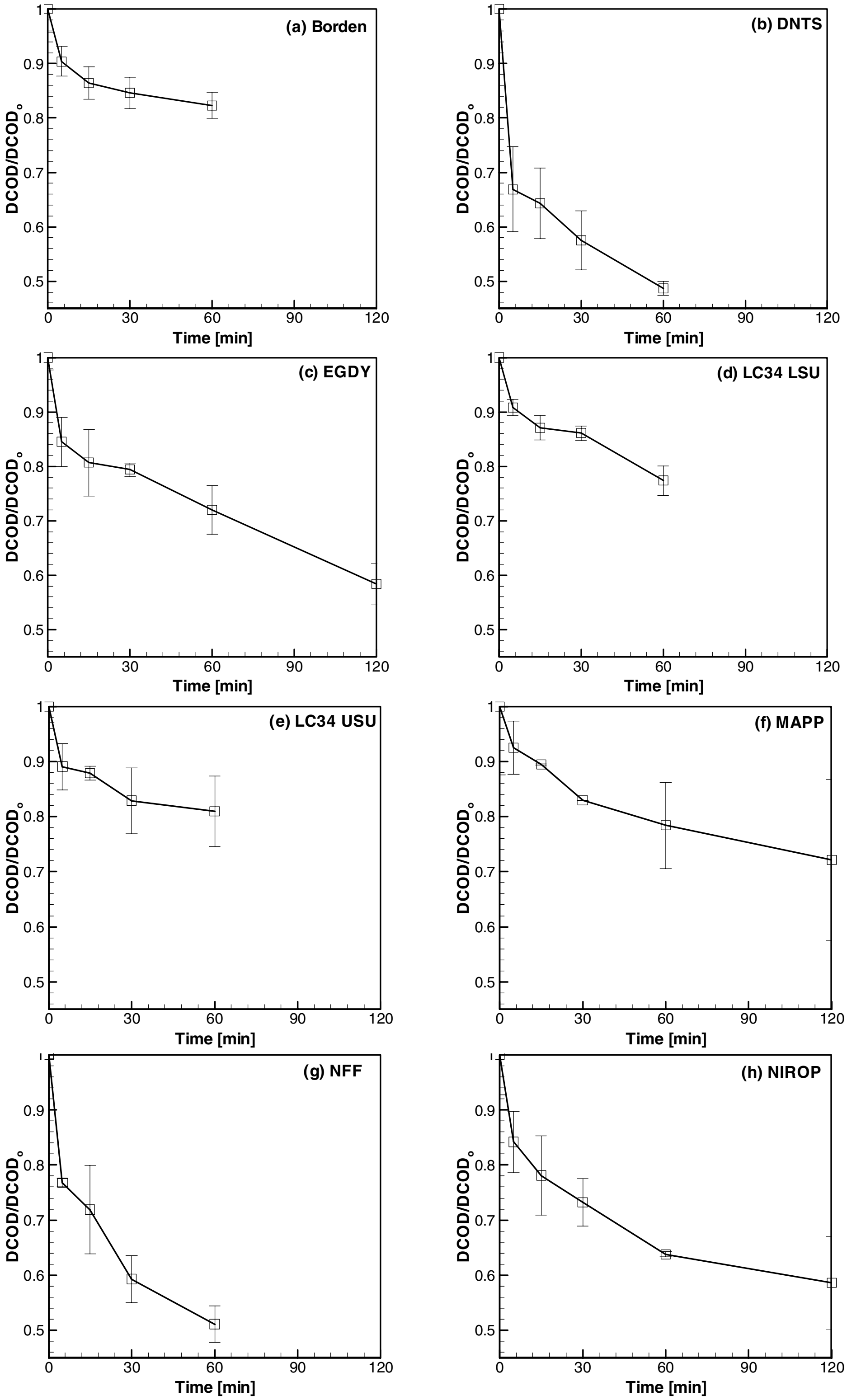

Figure 3.5.2. OAM data generated from the excess permanganate mass kinetic experiments. Each data point is the average from all aquifer material masses used. Error bars represent ±1 standard deviation.

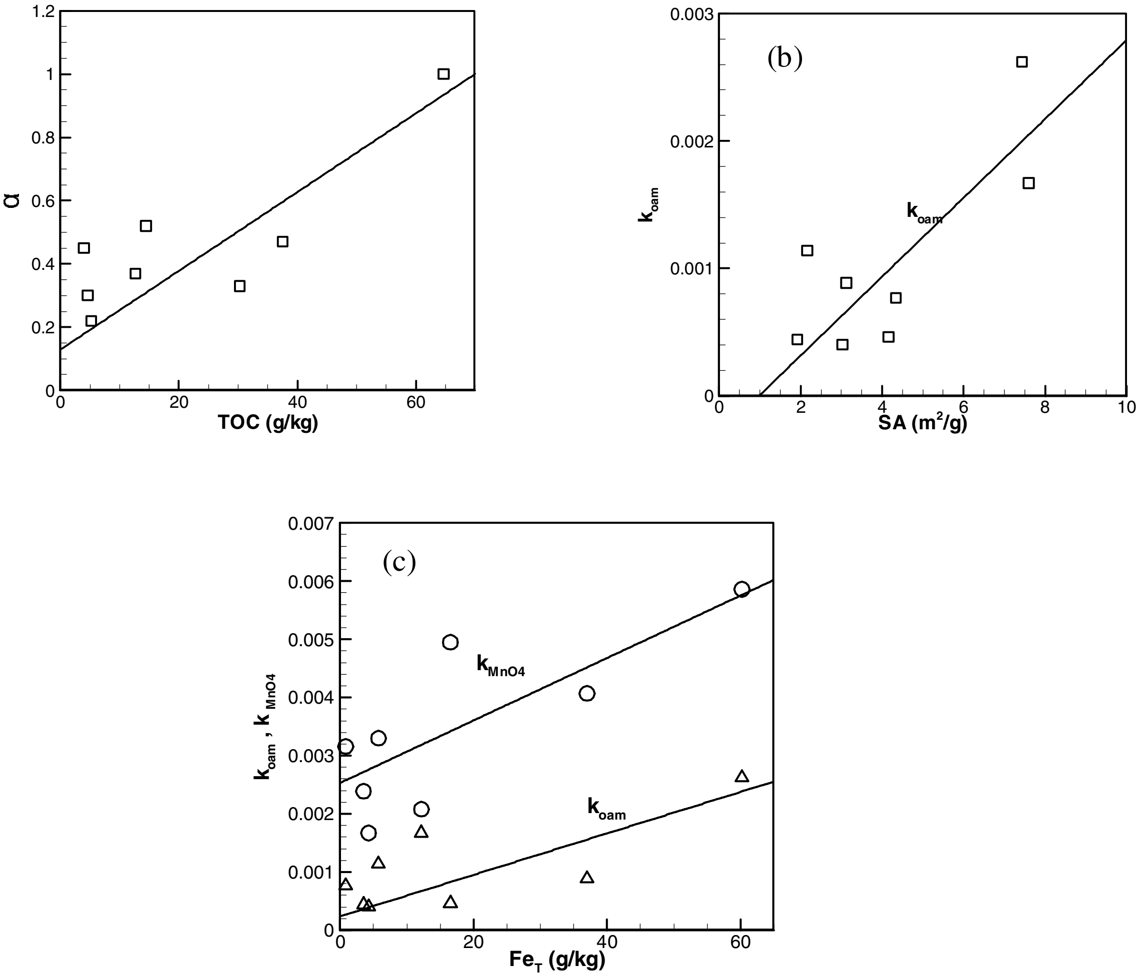

Figure 3.5.3. Scatter plots (a) the reaction order vs. TOC (r^2 = 0.68), (b) k_{oam} vs. surface area (r^2 = 0.63), and (c) k_{oam} vs. Fe_T (r^2 = 0.54) and $k_{MnO_4^-}$ vs. Fe_T (r^2 =0.62).

3.6 Column Investigations

3.6.1 Introduction

Compared to batch experimental systems, column experiments are generally considered to be more representative of *in situ* conditions since they provide more realistic aquifer material contact. Therefore, a series of permanganate column experiments were designed to complement and expand the findings of the batch experiments. Based on the batch permanganate experiments, aquifer materials from the following six sites were selected for these column experiments: MAAP, Borden, LC34-USU, LC34-LSU, EGDY, and NFF (listed in the order from lowest to highest maximum permanganate NOD).

3.6.2 Methods

A typical column (Figure 3.6.1) was constructed from a 40-cm long section of nominal 3.81 cm (1.5-inch) diameter transparent Plexiglas pipe equipped with four equally spaced sampling ports. Due to the high NOD associated with the EGDY and NFF aquifer materials as indicated from the batch test results, columns for these two materials were constructed from 12-cm long sections of nominal 2.54 cm (1-inch) diameter Schedule 40 PVC pipe to minimize experimental time. Permanganate source solutions were prepared by adding analytical grade $KMnO_4$ (EM Science) to Milli-Q water and boiling for ~1 hour. The cooled solution was filtered (0.45-μm glass fibre, Pall Corporation) and standardized by titration into a sulphuric acid and sodium oxalate solution (APHA, 1998).

To avoid problems associated with dry packing, homogenized aquifer material was wet with Milli-Q water to near saturation before use. Each column was packed in three stages: (1) the bottom 1.0 cm of the column (0.3 cm for the EGDY and NFF columns) was filled with 0.59 to 0.84 mm diameter glass beads (Potters Industries Ltd.) on top of which a thin layer of glass wool (Pyrex, VWR) was placed; (2) the next 38 cm (or 10 cm for the EGDY and NFF columns) was packed with aquifer material in 1 to 2 cm lifts compacted using a 1 cm diameter glass rod with the column attached to vertical vibrating rod; and (3) the top of the packed aquifer material was fitted with a 500-mm stainless steel screen, then filled with 0.59 to 0.84 mm diameter glass beads (Potters Industries Ltd.) and topped with a thin layer of glass wool (Pyrex, VWR). Both the bottom and top tubing couplers were fitted with a 500-mm stainless steel screen to prevent solids from escaping. Control columns filled exclusively with clean 0.59 to 0.84 mm diameter glass beads (Potters Industries Ltd.) were used to validate the experimental set-up and quantify apparatus/permanganate interactions.

Each column was operated in a continuous up-flow mode using a peristaltic pump (Cole-Parmer Instrument Co., Model No. 7553-80, 1-100 RPM, size 14 tubing) to control the rate of inflow, and a constant hydraulic head applied at the effluent end. Column experiments for each aquifer material were conducted in duplicate.

Table 3.6.1 summarizes the various column experiments performed. Prior to each experiment, the column was flushed with Milli-Q water until a stable flow rate was achieved (this process took about 1 to 5 hours). For a typical experiment trial the column was flushed with the permanganate source solution until sufficient permanganate breakthrough was observed, then flushed with Milli-Q water until no permanganate was detected (or no pink color appeared) in the effluent, and then flushed again with the same source solution until sufficient permanganate breakthrough was observed. The purpose of the second flush was to investigate the breakthrough behavior of permanganate in a system that was previously exposed to permanganate.

Two flow rates (high and low) were used for columns packed with MAAP aquifer materials to allow for different residence times to be investigated, while two permanganate concentrations (high and low) were flushed through the columns packed with EGDY aquifer materials to investigate the response to different permanganate concentrations.

At designed times, samples (with a typical volume of 0.2 to 0.5 mL) were taken and used to quantify permanganate concentration by spectrophotometry (Milton Roy Company, Spectronic 20D) at 525 nm with a method detection limit of 1.3 mg/L. For experiments that employed the longer columns, samples were collected from the mid-port (about 20 cm from the column influent) and from the effluent to investigate permanganate breakthrough at two locations, and for experiments that employed the shorter columns samples were only collected from the column effluent.

Tracer tests using sodium bromide solution (Fischer Scientific) at a constant concentration ranging from 50 to 100 mg/L were conducted to compare the tracer and permanganate breakthrough curves, as well as to evaluate hydrodynamic properties (porosity and dispersivity) of each aquifer material packed column. Bromide concentrations were determined by ion chromatography (IC) (Dionex AS4A-SC 4mm x 250 mm column; 1.8 mM sodium carbonate, 1.7 mM sodium bicarbonate eluate; 1.5 mL/min flow rate) with a MDL of 1.2 mg/L.

3.6.3 Results and Discussions

Temporal concentration profiles of permanganate and bromide (Br^-) obtained from the duplicate columns at identical sampling times were normalized to their respective source concentration and averaged. The resulting temporal profiles or breakthrough curves (BTCs) are shown in Figures 3.6.2 to 3.6.4, while Tables 3.6.2 to 3.6.4 list some characteristic properties of the tracer and permanganate BTCs for each experimental trial. Since the time to collect a sample ranged from 1 to 3 minutes, the characteristic properties listed in Tables 3.6.2 to 3.6.4 are accurate to within 0.009 to 0.108 pore volumes (PVs) for the high and low flow rates respectively.

In general for all cases, the arrival of permanganate at a given sampling location was delayed with respect to Br; an observation that is more apparent in the first flush BTC rather then the second flush BTC. After breakthrough, the permanganate concentration rapidly increased towards the source concentration, but showed extensive tailing in all but one case (i.e., the

MAAP aquifer material) and never reached the source concentration. This incomplete breakthrough (C/C_0 <100%) occurred despite at least 5 to more than 70 pore volumes (PVs) being flushed through various columns. This observation suggests that a slow reaction between the aquifer material and permanganate was still occurring at the end of each column trail and is consistent with our observations from the long-term batch experiments in which measurable permanganate consumption was observed for >200 days for most aquifer materials.

3.6.3.1 *Identification of Kinetic Regions*

Based on the observed BTCs shown in Figures 3.6.2 to 3.6.4, at least three kinetic regions are identifiable; a fast reaction region, an intermediate reaction region, and a slow reaction region. The extent and nature of these regions vary between the aquifer materials and we propose that a kinetic model for permanganate consumption by aquifer materials should consist of at least three parallel and independent reactions.

Evidence of Fast Reaction:

As shown in Tables 3.6.2 to 3.6.4, all column trials exhibited a delay in the arrival of permanganate at a given sampling location relative to Br. The delay between the first appearance of Br and permanganate during the first flush at the middle sample port was 0.25, 0.58, and 1.39 PVs for Borden, LC34-USU, and LC34-LSU aquifer materials respectively, while at the effluent location the delay was 0.26, 0.54, and 1.19 PVs for Borden, LC34-USU, and LC34-LSU. Since this delay is similar at the two sampling locations, it suggests that there is no residence time dependency related to this consumption and therefore is indicative of a fast reaction at the time scale of these observations.

When the EGDY aquifer material was flushed with the ~5 g $KMnO_4$/L solution the delay in the first appearance between Br and permanganate for the first flush was 0.76 PVs; however, when it was flushed with the ~1 g $KMnO_4$/L solution the delay increased to 2.76 PVs. While not completed scalable, this increase in the delay of the first appearance of permanganate indicates that this fast reaction behaves like an instantaneous permanganate sink which has a fixed permanganate demand that needs to be satisfied. Therefore it is not surprising that this fast reaction requires more volume of low concentration permanganate solution to fulfill its permanganate consumption requirements rather than less volume of a high concentration permanganate solution.

It is believed that liable oxidizable species or fast-reacting oxidizable aquifer material (OAM) loosely attached to solid grain surfaces of the aquifer material are responsible for this fast reaction. These oxidizable components may possibly include dissolved organic matter (DOC) and/or NOM, and dissolvable ferrous iron (Fe(II)), manganese (Mn(II)), and/or sulfur (S(0), S(I), and S(II)) (Christensen et al., 2000), which react with permanganate on a time scale of minutes (Stumm, 1992). The delay in the first appearance of permanganate during the second flush was less than the delay observed for the first flush indicating that some of the liable oxidizable species associated with the fast reaction were consumed during the first flush and therefore not available for permanganate consumption during the second flush.

Evidence of Intermediate Reaction(s):

Following the initial breakthrough or first appearance, the permanganate concentration increased rapidly with the shape of this rising portion of the BTC impacted by hydrodynamic dispersion and the reaction between permanganate and perhaps intermediate reacting OAM. These intermediate reacting OAM components may be organic matter, and reduced inorganic species (Fe, Mn, and S) which are possibly attached to the surface of the aquifer material (Stumm, 1992). This kinetic region may be considered active until the change in slope near the top of the BTC (as indicated by the inflection point). For example, it took about 0.9, 1.5, and 3.0 PVs from the first permanganate appearance to reach the change in slope for the Borden, LC34-USU, and LC34-LSU packed columns. This suggests that perhaps the LC34-USU aquifer material contains more intermediate OAM components than Borden but less than LC34-LSU. In situations where the aquifer material contains more OAM components, then this intermediate reaction would last longer and the shape of the rising portion of the BTC would be stretched as illustrated by the BTC for the EGDY and NFF aquifer material packed columns (Figure 3.6.3). For aquifer materials that contain little to no intermediate

OAM components, the shape of rising portion of the BTC after the initial delay should follow a similar shape to the Br BTC, as illustrated by the BTC for the MAAP aquifer material packed columns (Figure 3.6.4).

The shape of the rising portion of the BTC for the second flush BTC is quite different in most cases from that observed for the first flush BTC. For example the shape of the rising portion of the BTC for the second flush of the Borden and LC34-USU aquifer materials is very similar to their respective Br BTCs suggesting that any intermediate OAM, if present, was consumed during the first flush.

Evidence of Slow Reaction:

After the change in slope at the top of the BTC, all the BTCs exhibited a long tail where the change of permanganate concentration was small, clearly evidencing that a slow reaction was taking place. For some aquifer materials the slope of this slow reaction portion is relatively flat (e.g., the MAAP aquifer material), while for others the slope is more pronounced (e.g., the EGDY and NFF aquifer materials). Surprisingly the shape of this BTC tail is quite different between the first flush and second flush perhaps indicating that some of the slow OAM was depleted during the first flush. The OAM species associated with this slow reaction may be slowly reacting organic matter on grain surfaces, or organic matter and minerals containing reduced iron and manganese internal to the grains.

3.6.3.2 Estimation of Permanganate NOD

Based on a permanganate BTC, the NOD can be estimated from

$$\mathrm{NOD(t)} = \frac{1}{m_{aq}} \; C_o\, Q\, t - \int_0^t C_{Mn}(t)\; Q\, dt - (C_o + C_{Mn}(t))\, PV/2 \qquad (3.6.1)$$

where C_o is the permanganate source concentration [ML^{-3}], C_{Mn} is the permanganate concentration associated with the given BTC [ML^{-3}], Q is flow rate [L^3T^{-1}], PV is the column pore volume between the inlet and the sampling location [L^3], and m_{aq} is the mass of aquifer material packed in the column between the inlet and the sampling location. Eq. (3.6.1) was developed by considering a mass balance of permanganate mass entering the column (first term), permanganate mass crossing a sampling location (second term), and permanganate mass stored between the inlet and the sampling location (third term). The calculation of the mass of permanganate stored is approximate since the concentration profile within the column is unknown; however, after several PVs have been passed through the column or when the permanganate BTC concentration is close to the source concentration, this approximation results in an insignificant change in the estimated NOD. For example, if we assume that mass of permanganate stored can be estimated by the source concentration rather than by the average concentration, then the relative error in NOD after 2.0 PVs is <10% and decreases to <1% after 10 PVs. Table 3.6.5 lists the estimated permanganate NOD values for each flushing episode based on the duration of each episode (Table 3.6.1) and Eq. (3.6.1). Also listed in Table 3.6.5 is an NOD estimate using the observed slow permanganate consumption rate extrapolated until it intersects $C/C_o = 1$, and the overall maximum 7-day NOD and NOD_{max} observed from the batch experiments.

The data in Table 3.6.5 show that, except for the MAAP aquifer material, >60% of the NOD was expressed during the first flush indicating that a large portion of the observed permanganate consumption is relatively fast. This observation is consistent with the trends observed from our batch experiments in which over 60% of the maximum NOD was expressed within the first 7-days for all aquifer materials except for MAAP. The data also show that the use of a high permanganate concentration (5 g/L) in the EGDY column experiments generated a much higher NOD than when the lower permanganate concentration (1 g/L) was used (10.95 vs 4.56 g/kg). This again confirms that the NOD reaction is highly sensitive to the concentration of permanganate. The NOD estimated from the MAAP column experiments indicate that the lower flow rate generated a slightly higher NOD then when the high flow rate was used presumably a result of the longer residence time. The NOD estimated from the mid-port sampling location BTC and the effluent BTC (for Borden, LC34-LSU, LC34-USU aquifer materials) produced similar NOD values suggesting that the physical scale of these column trials is sufficient to capture the important NOD reaction processes.

Figure 3.6.5 displays the average NOD_{max} observed from batch experiments and the average NOD projected from column experiments. In all cases the average NOD_{max} observed from the batch experiments was 2.0 to 10.0 times greater than the NOD extrapolated from the column experiments. Moreover, even the average 7-day NOD_{max} observed from batch experiments (Table 3.6.5) is also greater than the average projected NOD for column experiments. This is consistent with the findings from Mumford et al. (2005) and is assumed to be related to the different aquifer material contact characteristics between batch and column tests. It is noted that the projected NOD estimates are based on the premise that the slow permanganate consumption rate observed at the end of the column experiment remains constant. If this rate does decrease then this assumption would lead to an underestimation of the NOD.

A correlation analysis indicates an excellent linear relationship ($r^2 = 0.99$) between both the average 7-day and maximum NOD from the batch tests and the extrapolated NOD from the column experiments (Figure 3.6.6). This suggests that permanganate consumption in a column system can be projected from batch system data using the following expression

$$NOD\ \text{(column)} = 0.61\, NOD_{\text{7-day average}}\ \text{(batch)} + 0.48 \quad (r^2 = 0.99) \qquad (3.6.2)$$

Furthermore, a good linear relationship between the NOD value projected from the column experiments and permanganate COD value is given by:

$$NOD\ \text{(column)} = 0.58\ \ PCOD - 2.98 \qquad (r^2 = 0.91) \qquad (3.6.3)$$

where PCOD is the permanganate COD test value (g-$KMnO_4$ / kg of dry aquifer materials). Since permanganate COD tests (Section 3.4) are easily and quickly implemented relative to batch experiments, Eq.(3.6.3) is expected to be more applicable than Eq. (3.6.2) for estimating the *in situ* permanganate consumption.

3.6.3.3 Overall Permanganate Consumption Rates

Overall permanganate consumption rates were calculated (Table 3.6.6) for each column experiment corresponding to: (1) the first appearance of permanganate which reflects the fast reaction rate, and (2) the tail of the permanganate BTC which reflects the slow permanganate rate. The fast permanganate consumption rate was calculated by assuming plug-flow conditions estimated by the delay in the first appearance of permanganate relative to Br as estimated from

$$r_{NOD}^{fast} = \left(QC_o(t_{Mn}^a - t_{Br}^a)/m_{aq}\right)\Big/(t_{Mn}^a - t_{Br}^a) = QC_o/m_{aq} \qquad (3.6.4)$$

where r_{NOD}^{fast} is the fast permanganate consumption rate, t_{Mn}^a and t_{Br}^a are the elapsed time with respect to the first arrival of permanganate and bromide at the sampling location. The slow consumption rate was estimated from the slope of NOD(t) as given by Eq. (3.6.1).

From data given in Table 3.6.6, the estimate of the fast consumption rate varies from 0.2 to 30 g/kg/day for the first flush BTCs, and was considerably less for the second flush BTCs for all trials, indicating that a majority of fast reacting OAM was consumed during the first flush. The slow permanganate consumption rates estimated for both the MAAP and Borden aquifer materials for the first and second flush are similar indicating that perhaps that the OAM related to the fast and intermediate reactions rates have been depleted at the end of the first flush; this was not the case for LC34-USU, LC34-LSU, EGDY, and NFF aquifer materials, and as is consistent with our observations discussed in Section 3.6.3.1.

3.6.4 Summary

The results from these permanganate column experiments suggest that there exist at least three kinetic regions controlling permanganate consumption by aquifer materials: a very fast reaction, an intermediate reaction(s), and a slow reaction. We believe that different reactive species in the aquifer materials are responsible for these three reactions: (1) the fast reaction may be controlled by labile organic species (possibly as dissolvable organic matter) and easily dissolved reduced metals (e.g., Fe, Mn, and S) loosely attached on the grain surfaces, (2) the intermediate reaction(s) may be controlled by organic species and inorganic compounds containing reduced metal (e.g., Fe, Mn, and S) bound on the grain surface, and (3) the slow reaction is associated with slowly reacting organic matter on grain surfaces, or organic matter and minerals containing reduced iron and manganese internal to the grains.

Permanganate consumption in these column experiments display some similar traits as we observed in the batch tests (e.g., sensitivity to concentration, and contact time), therefore, the prediction of permanganate consumption has been successfully realized based on the permanganate consumption in the batch systems as well as based on the permanganate COD test. However, permanganate NOD values estimated from the column trials are generally considerably less than those measured from the batch experiments. This difference is mainly ascribed to the solution/aquifer material contact differences between a column and a well-mixed batch reactor, and illustrates that results from well-mixed batch tests should be used with caution.

Finally, these column results indicated that >60% of the permanganate consumption occurred during the first flush suggesting that there may be an optimal approach to control the unproductive consumption of permanganate by aquifer materials through multiple-oxidant injection episodes.

Table 3.6.1. Summary of column experiments.

Aquifer Material	$KMnO_4$ (g/L)	Flow rate (mL/min)	Mass of material packed (g)	Length of the 1st flush (hrs)	Length of the 2nd flush (hrs)	Sampling location (distance from the influent location) (cm)
Borden	5.17	0.84	710	8.6	9.5	20, 38
EGDY	4.94	0.30	100	23.5	25.3	10
	0.95			23.5	48.5	
LC34-LSU	4.93 (1st flush) 5.47 (2nd flush)	0.83	620	36	27	20, 38
LC34-USU	4.95	0.77	720	10	10	20, 38
MAAP	5.28	0.75	710	7	5	38
	5.06	0.45		10	10	
NFF	5.02	0.30	79	31	32	10

Table 3.6.2. Characteristic BTC values for the Borden, LC34-LSU, and LC34-USU aquifer material column experiments.

Aquifer Material	Characteristic Value (PVs)	Tracer at the mid-port	Permanganate at the mid-port (1st flush)	Permanganate at the mid-port (2nd flush)	Tracer at the effluent	Permanganate at the effluent (1st flush)	Permanganate at the effluent (2nd flush)
Borden	First Appearance	0.85	1.10	0.90	0.97	1.23	1.02
	End of Trial	1.29	4.18	2.44	1.23	2.73	2.20
	Final BTC C/C_0	1.00	0.97	0.98	1.00	0.92	0.95
LC34-LSU	First Appearance	0.85	2.24	1.49	0.79	1.98	1.22
	End of Trial	1.49	21.55	16.14	1.31	11.32	8.49
	Final BTC C/C_0	1.00	0.94	0.97	1.00	0.91	0.95
LC34-USU	First Appearance	0.80	1.38	1.01	0.94	1.48	1.09
	End of Trial	1.38	5.74	6.69	1.34	3.02	3.52
	Final BTC C/C_0	1.00	0.92	0.98	1.00	0.85	0.95

Table 3.6.3. Characteristic BTC values for the EGDY and NFF aquifer material column experiments.

Aquifer Material	Characteristic Value (PVs)	Tracer (for high MnO_4^- conc.)	Permanganate at high conc. (1st flush)	Permanganate at high conc. (2nd flush)	Tracer (for low MnO_4^- conc.)	Permanganate at low conc. (1st flush)	Permanganate at low conc. (2nd flush)
EGDY	First Appearance	0.42	1.18	0.69	0.42	3.18	0.51
	End of Trial	2.27	25.64	27.82	2.27	26.00	52.91
	Final BTC C/C_0	1.00	0.86	0.94	1.00	0.61	0.87
NFF	First Appearance	0.58	10.35	1.71	-	-	-
	End of Trial	2.62	27.02	27.89			
	Final BTC C/C_0	1.00	0.73	0.91			

Table 3.6.4. Characteristic BTC values for the MAAP aquifer material column

Aquifer Material	Characteristic Value (PVs)	Tracer at high flow rate	Permanganate at high flow rate (1st flush)	Permanganate at high flow rate (2nd flush)	Tracer at low flow rate	Permanganate at low flow rate (1st flush)	Permanganate at low flow rate (2nd flush)
MAAP	First Appearance	0.80	0.87	0.83	0.80	0.83	0.81
	End of Trial	1.36	2.20	1.57	1.53	1.89	1.89
	Final BTC C/C_0	1.00	1.00	0.99	1.00	0.99	1.00

Table 3.6.5. NOD (g/kg) estimated from the permanganate BTCs using Eq. (3.6.1). The NOD projected was estimated by extrapolating the rate of slow permanganate consumption until it intersected $C/C_o = 1$.

Aquifer Material		1st flush (g/kg)	2nd flush (g/kg)	Sum of two flush trials (g/kg)	NOD projected (column) (g/kg)	7-day NOD$_{max}$ (batch) (g/kg)	NOD$_{max}$ (batch) (g/kg)
Borden	Mid-port	0.73	0.18	0.91	0.92	1.94	2.79
	Effluent	0.81	0.28	1.09	1.10		
EGDY	C_0 = 5 g/L	7.92	3.03	10.95	11.85	16.75	35.32
	C_0 = 1 g/L	2.71	1.85	4.56	5.03		
LC34-LSU	Mid-port	4.65	1.95	6.60	6.91	9.65	14.46
	Effluent	4.43	2.14	6.57	6.99		
LC34-USU	Mid-port	1.14	0.37	1.51	1.55	6.20	9.34
	Effluent	1.05	0.43	1.48	1.52		
MAAP	High flow	0.07	0.07	0.15	0.15	0.45	2.14
	Low flow	0.12	0.10	0.22	0.22		
NFF	C_0 =5.2 g/L	25.50	7.42	32.93	36.55	70.80	98.18

Table 3.6.6. Overall permanganate consumption (NOD) rates.

Aquifer Material	Sample port	Fast NOD rate (g/kg/day)		Slow NOD rate (g/kg/day)	
		First Flush	Second Flush	First Flush	Second Flush
Borden	Mid-Port	3.9	0.93	0.31	0.37
	Effluent	1.8	0.45	0.21	0.20
EGDY	High Conc.	14	8.4	3.1	1.4
	Low Conc.	3.6	0.73	1.6	0.61
LC34-LSU	Mid-Port	11	8.6	1.0	0.52
	Effluent	5.7	3.7	0.90	0.52
LC34-USU	Mid-Port	5.1	1.6	1.1	0.36
	Effluent	2.8	1.0	0.81	0.32
MAAP	High Flow Rate	0.64	0.29	0.053	0.039
	Low Flow Rate	0.16	0.056	0.036	0.036
NFF	Effluent	28	18	7.6	2.6

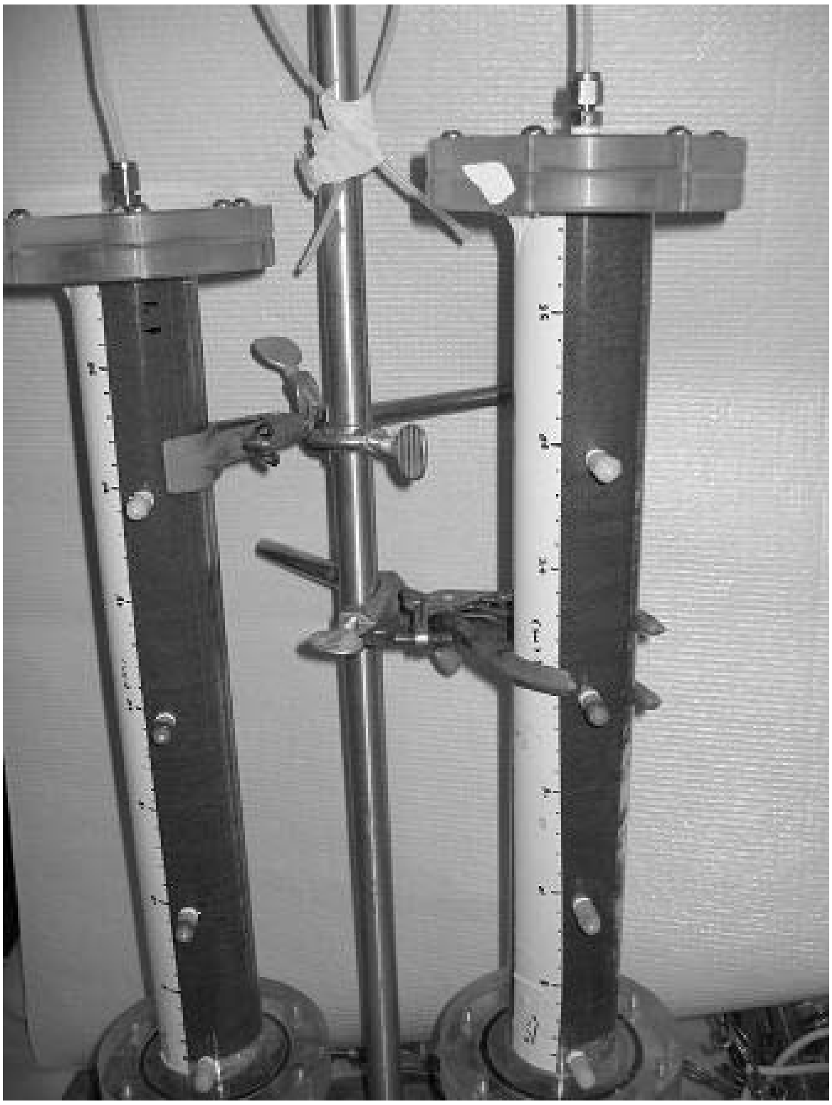

Figure 3.6.1. Typical columns used in permanganate experiments. Each column has a length of 40 cm and an inner diameter of 3.81 cm, and is equipped with four equally spaced sampling ports along its length.

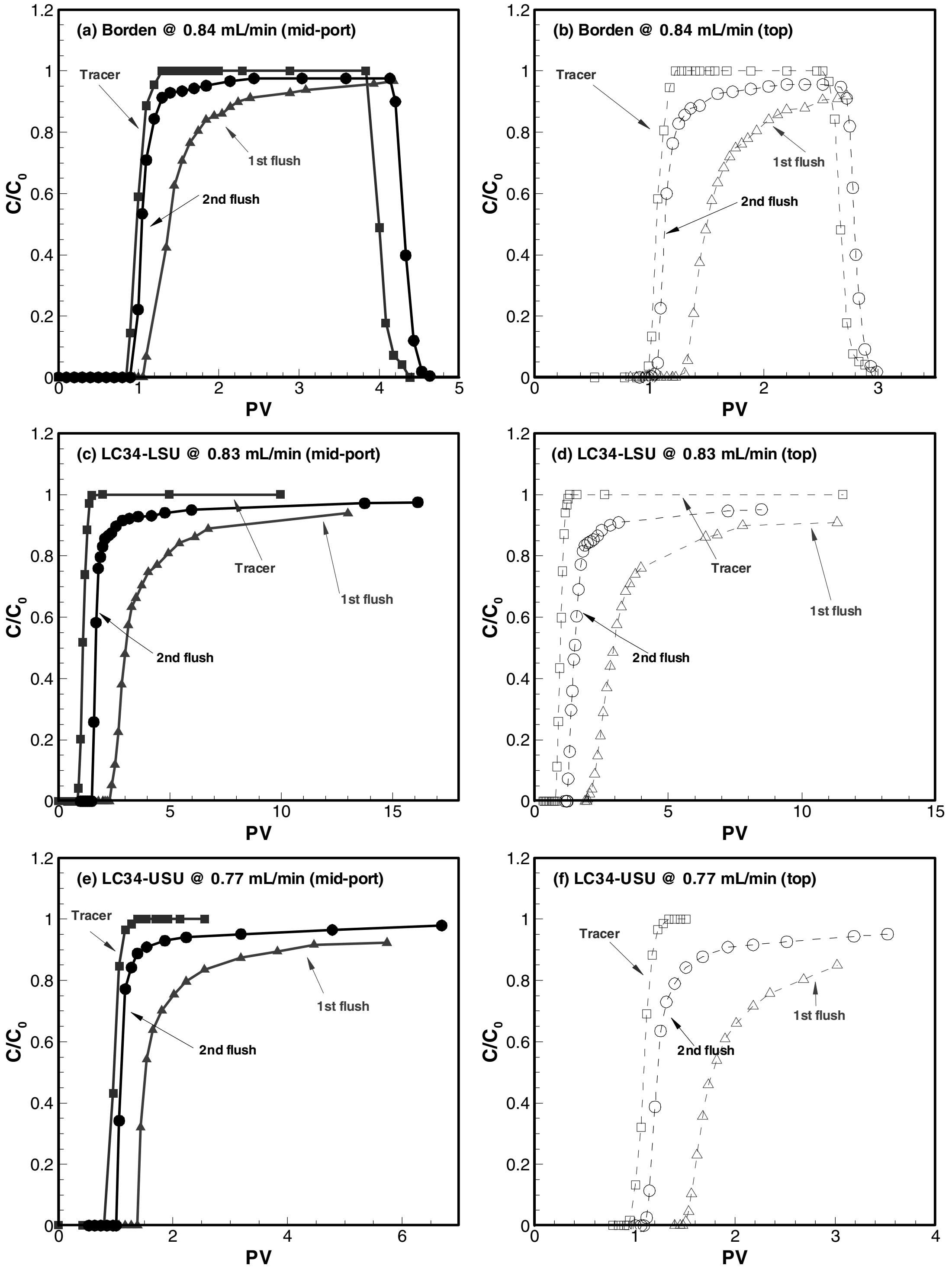

Figure 3.6.2. Permanganate and bromide breakthrough curves for: (a) and (b) Borden aquifer material, (c) and (d) LC34-LSU aquifer material, and (e) and (f) LC34-USU aquifer material.

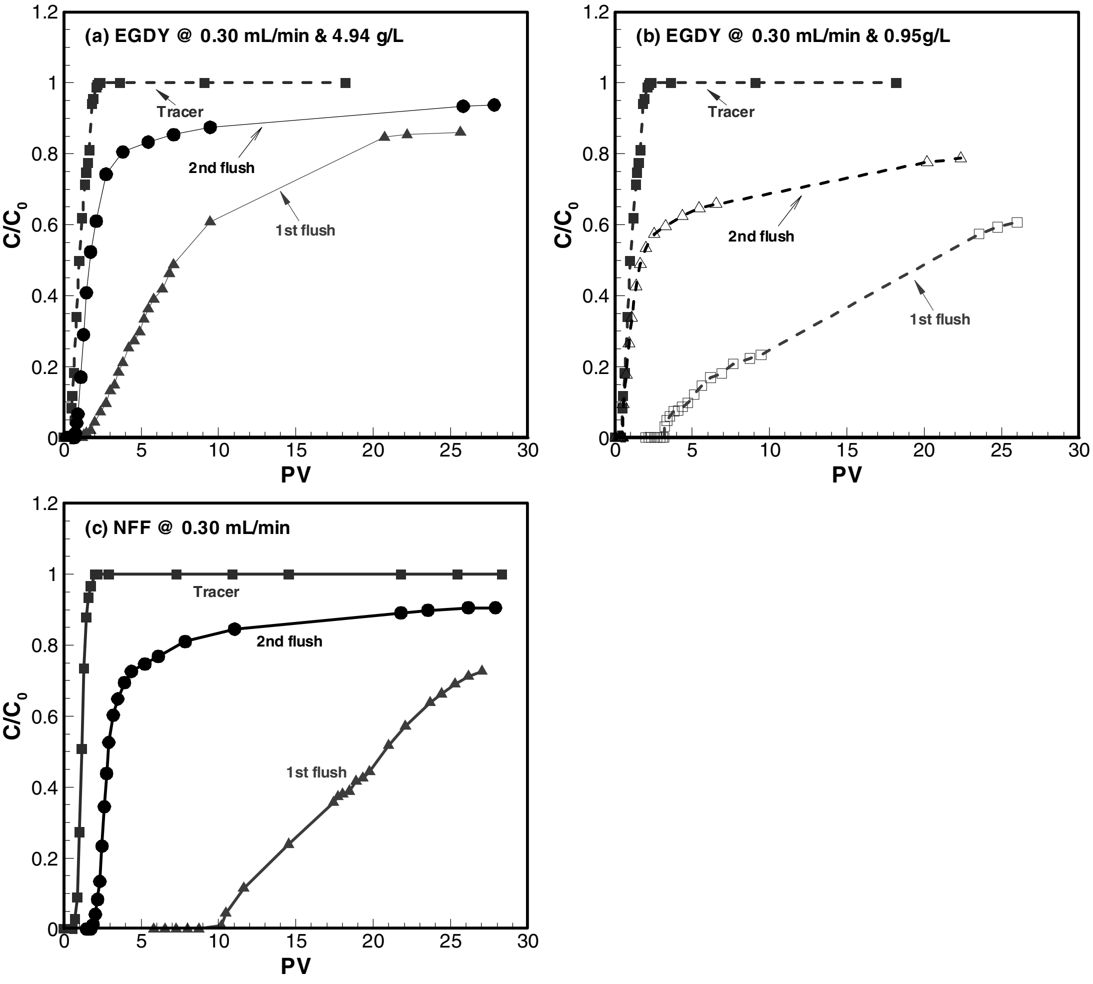

Figure 3.6.3. Permanganate and bromide breakthrough curves for: (a) and (b) EGDY aquifer material, and (c) NFF aquifer material.

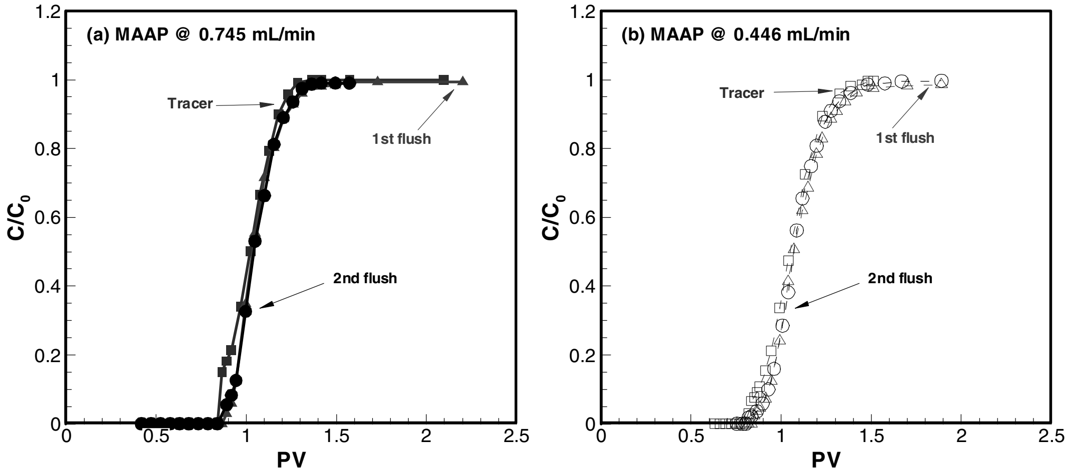

Figure 3.6.4. Permanganate and bromide breakthrough curves for MAAP aquifer material.

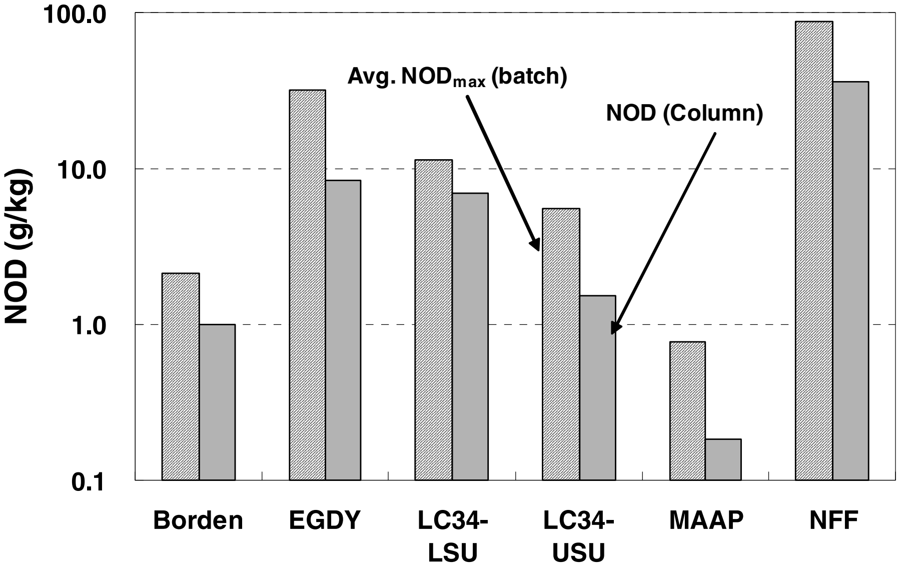

Figure 3.6.5. Permanganate NOD from batch and column systems. The column NOD was estimated by extrapolating the rate of slow permanganate consumption until the effluent permanganate BTC intersected $C/C_o = 1$.

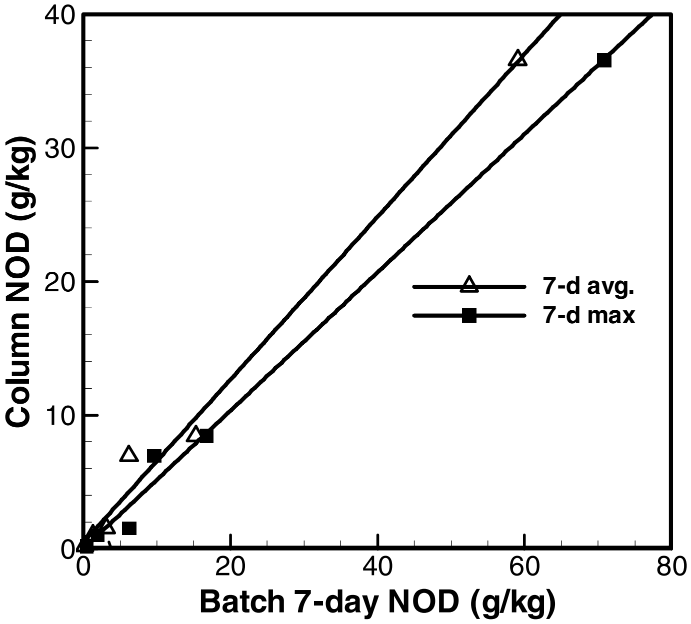

Figure 3.6.6. Scatter plot of the average 7-day NOD and the maximum 7-day NOD results from the batch tests and the NOD projected from the column experiments. Also shown are best fit linear relationships between the column NOD and the average 7-day NOD ($r^2 = 0.99$) and the maximum 7-day NOD ($r^2 = 0.99$).

Chapter 4

Interactions of Hydrogen Peroxide and Aquifer Materials

4.1 Overview

This chapter addresses the interaction between hydrogen peroxide and aquifer materials, and begins with a background review on relevant hydrogen peroxide reactions, applications in groundwater remediation, and decomposition in the subsurface. Following this review, results from a series of bench-scale experiments designed to investigate hydrogen peroxide fate in the subsurface environment are discussed. Batch experiments with mixtures of hydrogen peroxide and non-autoclaved or autoclaved aquifer materials from eight sites provided an overall understanding of hydrogen peroxide behaviour in the presence of aquifer materials. The impact of chelating reagents to enhance the stability of hydrogen peroxide was also evaluated under several scenarios. Finally, results from column experiments designed to complement and expand the findings of the batch experiments are presented, along with a mathematical model developed to capture hydrogen peroxide decomposition.

4.2 Background

While the first use of hydrogen peroxide in groundwater occurred in the late 1980s as an oxygen source for in situ biodegradation of contaminants (Nyer and Vance, 1999), there exist very few examples of direct field application of hydrogen peroxide alone as an oxidant in environmental engineering although theoretically hydrogen peroxide has a relatively high oxidation potential (Jones, 1999). Two approaches associated with hydrogen peroxide

(Fenton's and Fenton-like approaches) have been explored and widely applied in subsurface remediation since the first report on hydrogen peroxide use for ISCO in the 1990s (Watts et al., 1990). Watts and Teel (2005) proposed the term "Catalyzed Hydrogen Peroxide Propagations (CHP)" to unify these two approaches because the principle of these two approaches is that the catalysis of high concentrations of hydrogen peroxide generates a suite of reactive oxygen species through propagation reactions (as will detailed in sub-sections 4.2.2 and 4.2.3), which are hypothesized to be responsible for destroying target contaminants in the subsurface (Pignatello et al., 2006; Smith et al., 2002). In subsurface remediation, only thermal Fenton's processes rather than photochemical processes are applicable since light can not penetrate the subsurface beyond a few millimeters (Pignatello et al., 2006). Therefore, the following review focuses only on the ISCO thermal Fenton's processes.

4.2.1 General Properties and Reactions

Hydrogen peroxide is a clear, colorless liquid, and is completely miscible with water. Some of other physical properties of hydrogen peroxide are listed in Table 4.2.1. The hydrogen peroxide half-reaction is given by

$$H_2O_2 + 2H^+ + 2e^- \rightarrow 2H_2O \qquad E^o = 1.78 \text{ V} \qquad (4.2.1)$$

Hydrogen peroxide alone is actually a relatively weak oxidant due to its high activation energy (Jones, 1999) and is not effective for certain refractory contaminants at high concentrations because of the low reaction rate (Neyens and Baeyens, 2003). Therefore, three methods are used to increase its activity by converting it into different and more active species (Strukul, 1992): (1) by the reaction of hydrogen peroxide with certain metals capable of generating metal peroxy or hydroperoxy; (2) by producing highly reactive metal-oxo species that use hydrogen peroxide as a mono-oxygen donor; and (3) by using one-electron redox couples (e.g., Fe(II)/Fe(III), Ce(III)/Ce(IV), and Ti(II)/Ti(III)) to promote the radical decomposition of hydrogen peroxide. This third method for increasing the reactivity of hydrogen peroxide is called Fenton's reagent and has been widely used in wastewater treatment for several decades (Neyens and Baeyens, 2003; Jones, 1999).

Depending on temperature, pH and the presence of impurities, hydrogen peroxide can disproportionate into water and oxygen with an energy release (-98.3kJ/mol),

$$2H_2O_2 \rightarrow 2H_2O + O_2 \tag{4.2.2}$$

The mechanism for this reaction is that two hydrogen peroxide molecules react with each other, with one acting as the reductant and the other as the oxidant. Although this decomposition reaction is favorable for in situ bioremediation (Jones, 1999; Korom et al., 1996; Pardieck et al., 1992), it is not desirable for ISCO because oxygen may not be an effective oxidant for certain target organic contaminants (e.g., PAHs) in the subsurface (Kakarla et al., 2002).

In an alkaline solution, hydrogen peroxide can dissociate to produce a hydrogen ion and hydroperoxide anion according to (Jones, 1999)

$$H_2O_2 \rightarrow H^+ + HO_2^- \tag{4.2.3}$$

while in a strongly acidic non-aqueous solution, hydrogen peroxide can be protonated to the equivalent hydroxyl cation (Jones, 1999) following

$$H_2O_2 + H^+ \rightarrow H_3O_2^+ \tag{4.2.4}$$

In addition, hydrogen peroxide may behave to some extent as both electrophile and nucleophile, which arises from the easily polarized O-O bond and the undissociated hydrogen peroxide molecular, respectively (Jones, 1999).

4.2.2 Fenton's Reactions

The classic Fenton's reagent, consisting of hydrogen peroxide with an iron (II) catalyst (usually ferrous sulfate), is the most commonly used oxidant in the water and wastewater industry. The mechanism behind the Fenton's system is generally believed to be described by the Harber-Weiss reactions (Neyens and Baeyens, 2003), which suggests that the hydroxyl radicals formed in the system promote its oxidizing ability. However, there is still some uncertainty surrounding the very existence of the free hydroxyl radical ($OH^\bullet$) as the active intermediate (Rodriguez et al., 2003), and therefore Fenton's chemistry is actually still unsolved (Ensing et al., 2003). Nevertheless, the reactions in a pure Fenton's system (in the absence of reductants) are described by the following (Jones, 1999):

$$Fe^{2+} + H_2O_2 \rightarrow Fe(OH)^{2+} + OH^{\bullet} \qquad (4.2.5)$$

$$OH^{\bullet} + Fe^{2+} \rightarrow Fe(OH)^{2+} \qquad (4.2.6)$$

$$Fe(OH)^{2+} + H^{+} \rightarrow Fe^{3+} + H_2O \qquad (4.2.7)$$

Walling (1975) simplified the overall Fenton's chemistry by accounting for the dissociation water

$$2Fe^{2+} + H_2O_2 + 2H^{+} \rightarrow 2Fe^{3+} + 2H_2O \qquad (4.2.8)$$

Eq. (4.2.8) suggests that the presence of H^+ is required for the decomposition of hydrogen peroxide, indicating the need for an acidic environment to produce a maximum amount of hydroxyl radicals. Chen et al. (2001) pointed out that the decrease of soil pH could decelerate the decomposition rate of hydrogen peroxide. Indeed, the standard Fenton's system with iron (II) in an acidic solution has the most efficient reaction stoichiometry for free-radical generation (Teel et al., 2001). Numerous applications of Fenton's reagents in wastewater treatment and subsurface remediation have shown that the best pH range is 3-5 (Teel et al., 2001; Gallard and De-Laat, 2000; De-Laat and Gallard, 1999) or 2-4 (Siegrist et al., 1999). However, Pignatello et al. (2006) pointed out that this is an incorrect concept because the Fe(II) initiated reaction is pH independent below pH ~3 and increases in rate with pH above 3 until it reaches a plateau at about pH 4. This plateau value in the reaction rate at pH 4 is about 7 times greater than at pH 3.

The generation rate of hydroxyl radicals or the decomposition of hydrogen peroxide initiated by iron (II) is often the limiting factor in the Fenton's chemistry (k = 76 M^{-1} S^{-1} for Eq. (4.2.9) at pH = 3) (Walling, 1975). A similar conclusion was also obtained by Kang et al. (2002) when they listed 28 reactions (including Eqs.4.2.10 to 4.2.18) involved in the

Fenton's oxidation of phenol and monochrophenols. For each reaction, the overall second-order reaction is generally used to describe the mass action law. For example, the decomposition rate law for the hydrogen peroxide reaction as given by Eq. (4.2.8) is (Jones, 1999)

$$\frac{d[H_2O_2]}{dt} = -k[H_2O_2][Fe(II)] \tag{4.2.9}$$

4.2.3 Modified Fenton's Reagent

Generally, any modification to the standard Fenton's reagent is a "modified Fenton's reagent". Due to the presence of competing organics and mineral surfaces that are reactive to hydrogen peroxide, dosage of hydrogen peroxide used for ISCO usually range from 2% to 12% (Watts and Teel, 2006) to accomplish the desired oxidation of target contaminants. This "modified Fenton's reagent" with a high concentration of hydrogen peroxide (Watts and Teel, 2005; Smith et al., 2004) has been commonly used in ISCO. In addition, over the past several years, a variety of studies have made great efforts to enhance the mobility of catalysts (i.e., ferrous iron) as well as the stability of hydrogen peroxide in the subsurface by decreasing its catalyzed decomposition rate over a wide range of pH (Kakarla et al., 2002; 1997; Watts et al., 1999a; b; c). This "modified Fenton's reagent" is actually catalyst-modified Fenton's reagent. Other "modified Fenton's reagents" include photoassisted Fenton's reagent, solid iron(II) catalyzed Fenton's reagent, and electro-Fenton's reagent (Pignatello et al., 2006).

In applying Fenton's chemistry when other reductants exist (e.g., organic contaminants - RH), the soluble iron will be oxidized very slowly compared to the absence of the reductants (Chen et al., 2001; Weeks et al., 2000), and hydroxyl radicals will react strongly with dissolved organic compounds. The overall reactions can be described by the following (Pignatello et al., 2006; Neyens et al, 2003; Chen et al., 2001; Jones, 1999)

$$Fe^{2+} + H_2O_2 \rightarrow Fe^{3+} + OH^- + OH^\bullet \tag{4.2.10}$$

$$Fe^{2+} + OH^\bullet \rightarrow Fe^{3+} + OH^- \tag{4.2.11}$$

$$OH^\bullet + H_2O_2 \rightarrow H_2O + OOH^\bullet \tag{4.2.12}$$

$$OH^\bullet + OH^\bullet \rightarrow H_2O_2 \tag{4.2.13}$$

$$Fe^{3+} + H_2O_2 \rightarrow Fe^{2+} + OOH^\bullet + H^+ \tag{4.2.14}$$

$$OH^\bullet + RH \rightarrow H_2O + R^\bullet \quad \text{(chain propagation)} \tag{4.2.15}$$

$$R^\bullet + H_2O_2 \rightarrow ROH + OH^\bullet \quad \text{(chain propagation)} \tag{4.2.16}$$

$$R^\bullet + R^\bullet \rightarrow RR \quad \text{(dimmer product) (non-chain termination)} \tag{4.2.17}$$

$$R^\bullet + Fe^{3+} \rightarrow Fe^{2+} + product \quad \text{(regenerate Fe}^{2+}\text{ for chain initiation)} \tag{4.2.18}$$

The hydroperoxyl radical ($OOH^\bullet$) produced in these reactions is also a strong oxidant which may further decompose through Eq. (4.2.19) to the superoxide anion and the hydrogen ion (Petigara et al., 2002; Watts et al., 1999; 2005), and it could also compete with the hydroxyl radical for the reductants in the system (Jones, 1999) although it is generally ignored.

Watts et al. (1999a) demonstrated that a modified Fenton's chemistry (high hydrogen peroxide concentration chelated with the mixture of ammonium sulfate [$(NH_4)_2SO_4$] and monobasic sodium phosphate [KH_2PO_4]) could promote coexisting redox reactions involving the potential reductants such as the superoxide anion and the hydroperoxide anion, which are produced through the reaction (4.2.12) followed by

$$OOH^\bullet \leftrightarrow OO^{\bullet -} + H^+ \tag{4.2.19}$$

$$OOH^\bullet + Fe^{2+} \rightarrow HOO^- + Fe^{3+} \tag{4.2.20}$$

Although hydroxyl radical-mediated oxidation has been the degradation mechanism most commonly associated with Fenton's reagent, the hydroxyl radical is unlikely to react with non-aqueous phase contaminants (Sheldon and Kochi, 1981) because it reacts at diffusion-controlled rates and is not reactive with sorbed compounds (US DOE, 1999; Watts et al., 1999a; Sedlak and Andren, 1994). However, rapid destruction of DNAPLs such as TCE and carbon tetrachloride has been demonstrated with the modified Fenton's reagent (Watts et al., 2005; Yeh et al., 2003). Recent studies have shown that the superoxide and hydroperoxide anions are the reactive species in modified Fenton's reagent and can be used to promote desorption and degradation of recalcitrant organic contaminants such as carbon tetrachloride DNAPL (Smith et al., 2004, 2006; Kakarla et al., 2002). Therefore, the generation of hydroxyl radicals, superoxide ions, and hydroperoxide ions provide a reaction matrix where oxidants, reductants, and nucleophiles co-exist, making CHP a near-universal treatment system (Watts and Teel, 2006).

4.2.4 Fenton-Like Approaches

For Fenton-like reagent, $[H_2O_2]_0 >> [Fe(II)]_0$ in the presence of iron oxides (Rodrigues et al., 2003), or only a Fe^{3+}/H_2O_2 mixture (Ensing et al., 2003). The initiation of the Fenton-like reaction is hydrolysis which forms the iron(III) intermediate rather than the O-O bond breaking in the Fenton's chemistry as described by Eq. (4.2.5) or Eq. (4.2.8). This well accepted reaction can be written as (Ensing et al., 2003; Kwan and Voelker, 2003; Jones, 1999)

$$Fe(III) + H_2O_2 \rightarrow [Fe^{(III)}OOH]^{2+} + H^+ \qquad (4.2.21)$$

The pathway for the decomposition or transformation of the iron (III) hydroperoxy complex until recently was still not fully understood. Many studies (Ensing et al., 2003; Kwan and Voelker 2003; De-Laat and Gallard, 1999) tend to believe that it may homolyze at the Fe(III)-O bond via the reaction

$$[Fe^{(III)}OOH]^{2+} \rightarrow Fe^{2+} + OOH^{\bullet} \qquad (4.2.22)$$

Through the reaction Eq.(4.2.22), Fe(II) is formed and the initiation of Fenton's chemistry is also achieved. However, it was also hypothesized that the bond breaking of the iron(III) intermediate may also take place at the O-O bond rather than at Fe-O bond to produce the ferryl (Fe(IV) or Fe(V) oxide) ion and the free hydroxyl radical (Ensing et al., 2003).

With the reactions given by Eqs.(4.2.21) and (4.2.22) and the fact that iron (III) can be produced in the chain reactions of Fenton's reagent, Fenton's chemistry and Fenton-like chemistry often occur simultaneously. Therefore, although the initiation of the radical-generating reactions is apparently different, it is still proposed that Fenton's and Fenton-like chemistry have similar mechanisms (Watts and Teel, 2005; Pignatello et al., 2006; Kwan and Voelker, 2003). A schematic of these reactions is shown in Figure 4.2.1. It is also noted that under acidic conditions, soluble Fe(III) will represent the largest fraction of total Fe(III) in a Fenton's or Fenton-like system (De-Laat and Gallard, 1999), while at neutral pH conditions Fe(III) may precipitate. This is especially true for iron oxyhydroxide minerals in the subsurface, as the iron oxyhydroxide mineral will be dissolved at acidic pH to produce Fe^{2+}, which then catalyzes hydrogen peroxide. To explain the chemical oxidation in Fenton-like systems in which Fe(III) exists in the solid phase (neutral pH) , it was proposed that hydrogen peroxide is catalyzed on the surface of iron oxyhyoxide minerals through surface interaction processes (Yeh et al., 2003; Chen and Watts, 2000; Lin and Gurol, 1998). Miller and Vallentine (1995) proposed that HO_2/O_2^- could also diffuse into the bulk solution to generate free hydroxide radicals by reacting with hydrogen peroxide.

4.2.5 CHP-ISCO Use in Subsurface Remediation

CHP-ISCO has been widely used to remediate groundwater contaminated with various contaminants (Pignatello et al., 2006; ESTCP, 1999; Watts and Teel, 2005; 2006; US EPA, 2004a; 2004b; 1998; WSTC, 2004; Watts et al., 2002; Yeh et al., 2002; Groher, 2001; ITRC, 2000; 2001; US DOE, 1999).

Many studies on the application of Fenton's or modified Fenton's reagents in subsurface remediation have focused on parameters affecting the treatment system for particular contaminants. For example, Bogan and Trbovic (2003) detected PAH degradability with Fenton's reagent under the impacts of total organic carbon, humin, and soil porosity, while Quan and Watts (2003) confirmed that dosage requirements of hydrogen peroxide for soil treatment increase as a function of contaminant hydrophobicity. Miller and Valentine (1995) investigated the oxidation behavior of quinline and nitrobenzene in aqueous solutions in the presence of hydrogen peroxide and fine aquifer materials used as filter media. They observed phenomena that the lifetime of hydrogen peroxide was prolonged after the filter media was treated with the acidified hydroxylamine, which can remove manganese oxides, another catalyst of hydrogen peroxide, from the media surface. In a bench-scale experiment, Gates and Siegrist (2002) evaluated the impact of hydrogen peroxide dose, TCE concentration, and reaction time on the TCE oxidation in fine-grained soils with low-permeability. The experimental work conducted by Cirmi and Siegrist (2005) indicated that the interactions of variables (especially the oxidant load/DNAPL load interaction and the oxidant load/media type interaction) could significantly influence oxidation effectiveness and efficiency.

Kakarla and Watts (1997) performed a series of column experiments to investigate the migration depth of Fenton-like reactions with four hydrogen peroxide stabilizers. They concluded that hydrogen peroxide could move to a deeper depth with monobasic potassium phosphate than with three other stabilizers (i.e., dibasic potassium phosphate, sodium tripolyphosphate, and silicic acid). In addition, a solution with a hydrogen peroxide concentration of about 5~20% w/w was found to have a better efficiency with modified Fenton's reagent compared with a high hydrogen peroxide concentration (Kakarla et al., 2002).

The ubiquitous existence of transition metal (i.e., iron and manganese) minerals in subsurface makes it possible for Fenton's or Fenton-like reactions to take place without the addition of iron species during CHP-ISCO applications (Watts and Teel, 2005). Iron minerals have been studied recently as catalysts in modified Fenton's systems with the addition of a concentrated hydrogen peroxide to promote Fenton's or Fenton-like reactions. Miller and Valentine (1999, 1995) found that quinoline and nitrobenzene were degraded by hydrogen peroxide catalyzed by aquifer materials and the iron mineral goethite (α-FeOOH), which is a common form of iron oxide minerals found in oxic aquifers. Hematite and magnetite in soils are also able to catalyze the decomposition of hydrogen peroxide and initiate the Fenton-like oxidation of pentachlorophenol (PCP) and chlorobenzenes (Watts et al., 1997; 1999c). Kakarla and Watts (1997) experimentally concluded that a high iron content in the subsurface is a critical but not the only parameter for modified Fenton-like approaches. Chen et al. (2001) observed that the soil-induced Fenton's reaction did not efficiently destroy volatile organic carbon (VOC) contaminants in a soil column, but rather promoted an "air-sparging process" of VOC removal; however, they did not further investigate the reason for this phenomenon. The failure to oxidize VOCs in the study by Chen et al. (2001) is probably because their experimental soils contained high concentrations of iron and manganese which serve as hydrogen peroxide scavengers. Once again this demonstrates that the choice of a remediation method is always site-specific.

Three patented and commercial approaches are commonly used to apply Fenton's reagent in subsurface remediation (ITRC, 2001; Siegrist et al., 1999). The first method uses an injector to inject a hydrogen peroxide solution and ferrous iron at the same location so that the chemicals mix before reaching the target zone. In the second method, a more mobile form of ferrous iron is injected into subsurface initially and the hydrogen peroxide solution is injected after the subsurface condition is favorable for Fenton's reaction. In the third method, a mixture of hydrogen peroxide, an iron catalyst, and other proprietary compounds are injected in one step through a direct-push probe (ITRC, 2001).

4.2.6 Mechanisms of H_2O_2 Decomposition in the Subsurface

The rapid decomposition of hydrogen peroxide in soils may limit the application of Fenton's reagent for in situ chemical remediation of contaminated sites. The presence of iron minerals (e.g., goethite, magnetite, and hematite) or other transition metals (Mn(II, IV), Ti(III)) in a peroxide system can significantly facilitate contaminant oxidation via catalysis (Watts et al., 2005; Baciocchi et al., 2003; Teel et al., 2001; Gallard and De-Laat, 2000; Lin and Gurol 1998). Furthermore, studies have indicated that aquifer organic matter (AOM) or natural organic matter (NOM) can give rise to complex interactions and its impact on the oxidation effectiveness and efficiency depend on the concentration of the NOM (Kwan and Voelker 2003; Petigara et al. 2002), or may have no significant effect (Huling et al., 2001). The effect of humic acid on the oxidation rate and extent depends on its concentration, and that humic acid can act as a free radical scavenger, a radical chain promoter, and a catalytic site inhibitor (Valentine and Wang, 1998; Voelker and Sulzberger, 1996). In addition, microbioactivity may also be responsible for hydrogen peroxide decomposition (Vogt et al., 2004; Petigara et al. 2002).

The mechanisms of hydrogen peroxide decomposition are complicated by the presence of various reductants and catalysts. Four types of mechanisms are potentially responsible for the hydrogen peroxide decomposition: (1) the oxidation of hydrogen peroxide to oxygen, (2) Harber-Weiss reaction (as shown in Eq.4.2.9), (3) the catalase-type reaction, and (4) the peroxidase-type reaction (Petigara et al., 2002). The catalase-type decomposition occurs when free hydroxyl radicals generated by the Harber-Weiss reaction react with excess hydrogen peroxide and the overall reaction products will be oxygen and water. The peroxidase-type reaction responsible for hydrogen peroxide decomposition can be written as (Petigara et al., 2002)

$$S_{RED} + H_2O_2 \rightarrow S_{OX} + H_2O \qquad (4.2.23)$$

where S_{RED} represents the soil constituents (usually reductants), and S_{OX} represents the oxidized substrates.

Lin and Gurol (1998) demonstrated that the decomposition rate of hydrogen peroxide in the presence of goethite was proportional to the concentration of the goethite surface sites and hydrogen peroxide. Kwan and Voelker (2003) showed that the generation rate of hydroxide radicals was proportionally related to the product of the hydrogen peroxide concentration and the solid concentration containing iron-oxides; however, this radical generation rate did not equal to the decomposition rate of hydrogen peroxide. De-Laat and Gallard (1999) summarized that four steps are involved in the catalytic decomposition of hydrogen peroxide by soluble Fe(III): (1) the hydrolysis of Fe(III); (2) the initiation step; (3) the propagation step; and (4) the recombination step. For each reaction step, an overall second-order reaction was used to describe the kinetic model. The concentration-time profile for a particular species is described with a lumped equation of all the step reactions involving that species (Gallard and De-Laat, 2000).

Table 4.2.1. Physical properties of commercial hydrogen peroxide (after Strukul et al., 1992).

Property	Hydrogen peroxide concentration (wt%)		
	35	50	70
Density at 20°C	1.1312	1.1953	1.2886
Viscosity at 20°C (mPa s)	1.11	1.17	1.23
Freezing point (°C)	-33	-52.2	-40.3
Boiling point (°C)	107.9	113.8	125.5

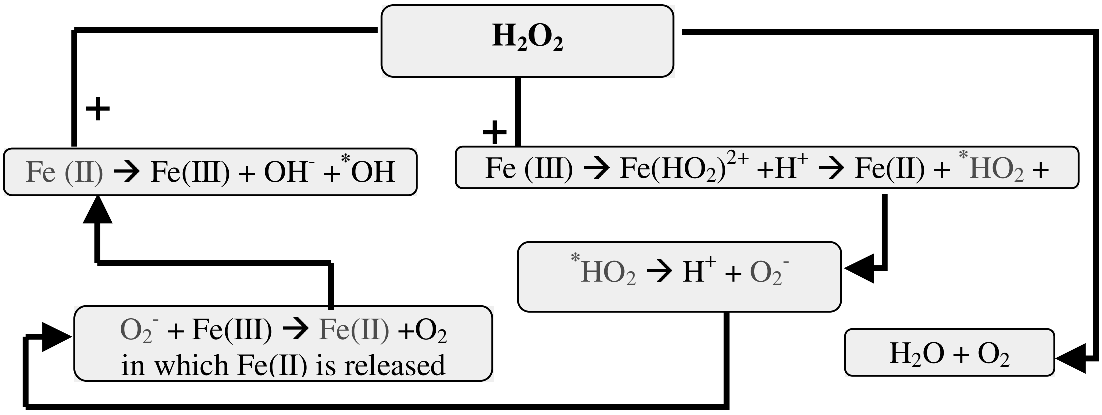

Figure 4.2.1. Schematic diagram for Fenton [Fe(II)] and Fenton-like [Fe(III)] reactions.

4.3 H_2O_2 Decomposition in the Presence of Aquifer Materials in Batch Systems

4.3.1 Methods

Two sets of experiments were performed: one with non-autoclaved aquifer materials and the other with autoclaved aquifer materials. The autoclaved aquifer materials were obtained by autoclaving (Castle®, MDT Steam Sterilizer) the corresponding air-dried aquifer materials for about 30 minutes. For each set of experiments, 15 g of dried aquifer material and 80 mL of a hydrogen peroxide solution (2.0%) were added to a 110 mL amber reactor fitted with a Teflon cap. The hydrogen peroxide solution was made from a stock 30% hydrogen peroxide solution (VWR, Toronto, Canada). The initial pH of the H_2O_2 solution was adjusted to 3.0 ± 0.2 using 1.0 N NaOH and 1.0 N H_2SO_4. All experiments were performed in replicates (for autoclaved aquifer materials), or triplicates (for non-autoclaved aquifer materials).

All reactors were placed on a reciprocal shaker (Eberbach Corp., Ann Arbor, Michigan). At designated times, an aliquot of the soild/aqueous solution (~0.5 mL) was removed with a syringe and filtered through a 0.45 μm filter (Nalgene). The concentration of hydrogen peroxide in the filtrate was quantified with an iodiometric titration method (Schumb et al., 1995). The solution pH was monitored throughout the course of each experiment using a pH meter (Model 81-02, Orion). In addition, an aliquot of solution (~5 mL) was taken from each batch reactor within the first hour, filtered through a 0.45 μm filter (Nalgene) and used to quantify total iron (Fe) and manganese (Mn) dissolved concentrations using an inductively coupled plasma (ICP) emission spectroscopy with a Spectro Flame instrument (Spectro Analytical, Fitchburg, MA) with a method detection limit (MDL) of 0.1 mg/L for Fe and 0.01 mg/L for Mn, respectively.

A third set of experiments was performed to investigate changes in the bulk reduction capacity to each aquifer material to prolonged exposure to hydrogen peroxide. In this set of experiments, a series of reactors containing 80 mL of a 2% H_2O_2 solution (initial pH 3.0) and 15 g of non-autoclaved aquifer materials (DNTS, EGDY, LC34 USU, MAAP, and NIROP) were shielded from light for two weeks (triplicates for each aquifer material) and gently shaken on a reciprocal shaker for one hour daily. After the two-week reaction period, aquifer materials in these reactors were rinsed three times with Milli-Q water, and dried at 80^{o}C to a constant weight. After cooling to room temperature, dichromate COD tests were performed on these dried aquifer materials using the method presented in Chapter 2.

4.3.2 Results and Discussion

The hydrogen peroxide concentration decreased in an approximately exponential fashion in all experiments with either autoclaved or non-autoclaved aquifer materials indicating that hydrogen peroxide decomposition follows a pseudo first-order rate law (Figure 4.3.1), and is consistent with other observations (Jung and Thomson, 2004; Miller and Valentine, 1999; Barcelona and Holm, 1991). The best-fit first-order reaction rate coefficients are listed in Table 4.3.1 and presented graphically in Figure 4.3.2. They were determined by fitting

$$\ln([H_2O_2]/[H_2O_2]_o) = -k_{obs}t \qquad (4.3.1)$$

to the observations, where k_{obs} is the observed first-order reaction rate coefficient, and $[H_2O_2]$ and $[H_2O_2]_o$ are hydrogen peroxide concentrations at time t and time zero, respectively. The total dissolved iron and manganese concentrations representative of conditions within the first hour for experiments using the non-autoclaved aquifer materials are presented in Figure 4.3.3. Based on the these data, the reaction rate coefficients for hydrogen peroxide span from a k_{obs} of 0.01 to 1.0 /hr and can be classified as: 1) very high (NIROP, k_{obs} ~ 1.0 /hr), 2) high (NFF, k_{obs} ~ 0.3 /hr), 3) medium (EGDY and MAAP, k_{obs} ~ 0.1 /hr), 4) low (LC34-LSU and LC34-USU, k_{obs} ~ 0.03 /hr), and 5) very low (Borden and DNTS, k_{obs} ~ 0.02 /hr).

The observed hydrogen peroxide decomposition rate coefficients for the autoclaved materials were generally 0.3 to 62.4% less than those for non-autoclaved materials (Table 4.3.1 and Figure 4.3.2). This difference was statistically significant (α = 5%) for the EGDY, LC34-LSU, LC34-USU, and NFF materials, suggesting that a fraction of the hydrogen peroxide reactivity may be attributed to mechanisms related to biological activity (Vogt et al., 2004; Petigara et al. 2002). Pardieck et al. (1992) proposed that the possible bio-mechanism for the decay reactions of hydrogen peroxide was via particle-associated microorganisms or enzymes. Interestingly, the TOC content of the EGDY, LC34-LSU, LC34-USU, and NFF aquifer materials are relatively higher than the other aquifer materials used in this investigation (Table 2.3), implying that a larger biological-related decomposition component may be associated with aquifer materials with a larger NOM content. Autoclaving of the aquifer materials with high temperature steam (121^{o}C) may have resulted in a change of the soil fabric or potential loss of natural organic matter, and therefore a definitive conclusion on the overall rate of biological related hydrogen peroxide decomposition is not possible based on these data. Unless specified, the following discussion is based on the results using non-autoclaved aquifer materials.

In less than an hour after the start of each experiment, the solution pH increased due to the strong aquifer material buffering capacity from the initial pH of 3.0 to a stable value, which was close to the corresponding soil pH for each aquifer material (e.g., 6.4 for Borden, 4.2 for DNTS, 5.4 for EGDY, 7.5 for LC34-LSU and LC34-USU, 3.5 for MAAP, and 8.5 for NIROP) except for the NFF aquifer material, where a stable pH of ~ 2.3 was observed. This reduction in pH is possibly a result of the oxidation of NOM in the NFF aquifer material that generates sufficient acidity to reduce the pH in this batch system (WSTC, 2004). Note that the NFF aquifer material has a low soil pH of 3.7 (see Table 2.3 in Chapter 2) and the highest NOM content of all the aquifer materials used in this investigation. Nevertheless, the pH results illustrate that *in situ* pH control will be difficult to achieve during the injection of hydrogen peroxide into aquifer materials with a high buffering capacity as suggested by Nyer and Vance (1999), and will be problematic in situations where an optimal reaction pH between 3 to 4.5 due to iron chemistry and the weak acid characteristics of hydrogen peroxide are required for treatment.

Watts and Teel (2005) discussed the role of NOM on hydroxyl radical scavenging and concluded that its impact is a function of the state of the organic matter, the nature of the hydrogen peroxide catalyst, and other factors. Furthermore, it has been demonstrated that humic acid can act as a free radical scavenger, a radical chain promoter, and a catalytic site inhibitor (Valentine and Wang, 1998; Voelker and Sulzberger, 1996). The data generated in this study suggest a weak relationship (r^2 = 0.61) between the observed hydrogen peroxide decomposition coefficient and TOC content, indicating that perhaps hydrogen peroxide might decay quickly in the presence of aquifer materials containing high NOM content. Therefore, it can be concluded from this investigation that NOM content may have a negligible impact on hydrogen peroxide decomposition for low TOC materials (e.g., Borden, DNTS, and NIROP materials) which is consistent with the studies of Huling et al (2001), or may accelerate the hydrogen peroxide decomposition for high TOC content materials (e.g., EGDY, LC34-LSU, LC34-USU, MAAP, NFF). Humic acids associated with aquifer organic matter might be responsible for the hydrogen peroxide decomposition in these aquifer materials (Valentine and Wang, 1998). Evidence of the role of NOM in the decomposition of hydrogen peroxide is given by the change in dichromate COD test results (Figure 4.3.4) of the DNTS, EGDY, LC34-USU, MAAP, and NIROP aquifer materials after exposure to a 2.0% hydrogen peroxide solution for a two-week period. As discussed in Chapter 2, the dichromate COD (DCOD) results are highly correlated to the TOC content of these aquifer materials, and therefore changes in the DCOD results are assumed to reflect the changes in TOC content of the aquifer materials. Figure 4.3.4 clearly shows that after the 2-week exposure to hydrogen peroxide, a statistically significant decrease (α = 5%) in the DCOD test results for EGDY, LC34-USU, and MAAP aquifer materials ranging from 37% to 76% was observed. Insignificant change was observed for the DNTS and NIROP aquifer materials (less than 8.0%). It is interesting to note that the significant DCOD change occurred for the aquifer materials containing >0.70 mg/g TOC content, supporting the previous conclusion that NOM (possibly humic acids) may have a negligible impact on hydrogen peroxide decomposition for low TOC materials, or may accelerate the hydrogen peroxide decomposition for high TOC materials.

A correlation analysis between k_{obs} and the various aquifer material properties which are believed to be responsible for the reaction with hydrogen peroxide was performed. In most cases the correlation coefficient was <0.6; however, some correlation coefficients could be greatly improved if data from NIROP, NFF, and MAAP aquifer materials were excluded from the analysis (Figure 4.3.5). This modified correlation analysis indicates that in general the hydrogen peroxide decomposition rate coefficient is highly correlated ($r^2 > 0.98$) with the amorphous Fe and amorphous Mn content, and mildly correlated with the TOC content (as discussed above). Non-crystalline minerals can be characterized by high cation exchange capacity, surface area, and reactivity with organics, and they are generally formed on the grain surface of aquifer materials due to precipitation. These characteristics may be responsible for the high reactivity with hydrogen peroxide and is consistent with findings reported by others (Valentine and Wang, 1998; Miller and Valentine, 1995; Ravikumar and Gurol, 1994).

As indicated above, specific properties of the aquifer materials are presumed to affect the reactivity of hydrogen peroxide. The NIROP aquifer material contains a significant amount of carbonate minerals (as calcite and dolomite) as confirmed by its high total carbon (TC) and low TOC content, which can serve as a sink of hydrogen peroxide (Seol et al., 2003). In addition, the NIROP aquifer material has also been strongly weathered (visual inspection; Reardon, 2006), and has the highest value of bulk surface area and cation exchange capacity (CEC) of all other aquifer materials except for LAAP (Table 2.3 in Chapter 2), implying that there exists a large quantity of reactive sites on the surface of each grain. Moreover, due to the strong buffering capacity, the solution pH in the batch reactors containing the NIROP aquifer material was quite high (8.5 to 9.0), which can also increase hydrogen peroxide decomposition (Chen et al., 2001). As such, these three factors (i.e., high carbonate content, high surface area and CEC, and high soil pH) are responsible for the highest decomposition rate (1.16/hr) of all the aquifer materials used in this study. Petigara et al. (2002) showed that hydrogen peroxide decayed rapidly in the presence of soils with a high TOC content, and decayed much slower in the presence of soil with a lower TOC content, and therefore it is not surprising for the NFF and EGDY aquifer materials to have high decomposition rate coefficients since both aquifer materials contain high organic matter and iron contents. Based on the aquifer material characterization data, the behavior of hydrogen peroxide in the presence of the LC34-USU, LC34-LSU, and MAAP aquifer materials should be similar; however, the hydrogen peroxide decomposition rate coefficient in the presence of the MAAP aquifer material is much higher due to the higher dissolved Mn concentration in the reactor solution for the MAAP aquifer material than for the LC34-LSU and LC34-USU aquifer materials (Figure 4.3.3) even though the MAAP aquifer material itself contains a relatively low content of total Fe and Mn. This is consistent with the interaction between hydrogen peroxide and soluble Fe reported by Watts and Teel (2005). The low hydrogen peroxide decomposition rate coefficients observed for the Borden and DNTS aquifer materials are attributed to their low TOC content and dissolvable Fe and Mn content.

A multiple linear regression analysis was performed on the observed hydrogen peroxide reaction rate coefficients with the various aquifer material characteristics. No significantly statistical model could be obtained unless data from NIROP and NFF aquifer materials were excluded. These two aquifer materials had the largest observed reaction rate coefficients (0.3 and 1.2 /hr) and their exclusion indicates that perhaps the hydrogen peroxide decomposition mechanisms are significantly different for these materials. In general, the observed reaction rate coefficients could be expressed by combinations of TOC, total Fe and total Mn contents, amorphous Fe and Mn contents, surface area, and CEC (Table 4.3.2). Each of these characteristics alone (except for amorphous Fe and Mn) did not yield a satisfactory relationship ($r^2 < 0.62$) for the hydrogen peroxide decomposition rate coefficient, indicating that hydrogen peroxide decomposition is a result of the combined influence of various aquifer material characteristics. Table 4.3.2 lists various expressions for the observed hydrogen peroxide decomposition rate coefficient using data from only 4, 5, and 6 aquifer materials. When data from 4 aquifer materials were considered the best-fit expressions involved combinations of surface area, total Fe and amorphous Mn. When an additional aquifer material was added to the analysis, a series of the best fit expressions were obtained, one of simplest involved only amorphous Fe given by:

$$k_{obs} = 0.0899 \bullet [\text{Amorphous F}e] - 0.0126 \qquad (r^2 = 0.99) \qquad (4.3.2)$$

where amorphous Fe is expressed in terms of mg/g, ranging from 0.29 to 1.2 mg/g. Moreover, if data from 6 aquifer materials (i.e., Borden, DNTS, EGDY, LC34-LSU, LC34-USU, and MAAP) were used, only the following statistically significant expression was generated:

$$k_{obs} = 0.613 \bullet \mathrm{TOC} - 0.00949 \bullet \mathrm{CEC} + 0.0385 \qquad (r^2 = 0.94) \qquad (4.3.4)$$

where CEC is the cation exchange capacity (cmol/kg), and TOC is expressed in terms of mg/g. Equation 4.3.2 is suitable for practical use since it is the simplest; however, Equation (4.3.4) involves data from 6 rather than 5 aquifer materials and thus may provide a more representative estimate.

A multiple linear regression analysis was also performed on the observed hydrogen peroxide reaction rate coefficients obtained from the autoclaved aquifer materials. Similar to non-autoclaved aquifer materials, the hydrogen peroxide decomposition rate coefficient for the autoclaved aquifer materials could be expressed in terms of amorphous Fe and amorphous Mn (Table 4.3.2). As noted above, the hydrogen peroxide decomposition rate coefficient for autoclaved aquifer materials was generally less than those for non-autoclaved aquifer materials, suggesting that there may be a biological influence, and the observed hydrogen peroxide decomposition rate coefficient for non-autoclaved aquifer materials, k_{obs}, might be written as

$$k_{obs} = k_{obs}^{bio} + k_{obs}^{other} \qquad (4.3.5)$$

where k_{obs}^{bio} and k_{obs}^{other} are hydrogen peroxide decomposition rate coefficients due to biological activity, and non-biological factors, respectively. Once again, detailed research into the potential biological component was beyond the scope of this thesis.

4.3.3 Summary

Hydrogen peroxide concentration decreases in an approximately exponential fashion, following a first-order or pseudo first-order kinetic reaction. *In situ* pH control will be difficult to achieve during the injection of hydrogen peroxide into aquifer materials with a high buffering capacity.

The decomposition of hydrogen peroxide in the presence of aquifer materials is strongly correlated to the content of amorphous Fe and Mn rather than their crystalline forms, and is weakly related to the content of total organic matter. Moreover, natural organic matter may have a negligible influence on hydrogen peroxide decomposition for low TOC aquifer materials or may accelerate the hydrogen peroxide decomposition for high TOC aquifer materials. Finally, biological activity may play a role in the hydrogen peroxide decomposition in the presence of aquifer materials containing high NOM, although investigations with little data could not achieve a conclusive statement about the biological related hydrogen peroxide decomposition.

Multiple linear regression analyses based on the batch experiment results with the aquifer materials from six sites were performed and a variety of expressions for hydrogen peroxide decomposition rate coefficients were generated. These relationships can be used to predict hydrogen peroxide decomposition rate coefficients, given aquifer material properties.

Table 4.3.1. Observed hydrogen peroxide reaction rate coefficients in the presence of autoclaved and non-autoclaved aquifer material (15 g solids, 80 mL of 2.0% H_2O_2 solution with an initial pH of 3.0).

Site	Autoclaved		Non-Autoclaved		Statistical difference (t-test 95%)
	k_{obs} (hr^{-1})	r^2	k_{obs} (hr^{-1})	r^2	
Borden	0.0122 ± 0.0037	0.92	0.0178 ± 0.0090	0.79	No
DNTS	0.0136 ± 0.0084	0.85	0.0188 ± 0.0085	0.82	No
EGDY	0.0602 ± 0.0100	0.94	0.0955 ± 0.0145	0.95	Yes
LC34-LSU	0.0161 ± 0.0021	0.97	0.0261 ± 0.0038	0.95	Yes
LC34-USU	0.0179 ± 0.0028	0.95	0.0260 ± 0.0043	0.94	Yes
MAAP	0.0758 ± 0.0124	0.96	0.0856 ± 0.0135	0.96	No
NFF	0.205 ± 0.021	0.98	0.267 ± 0.005	1.00	Yes
NIROP	1.16 ± 0.011	1.00	1.16 ± 0.12	0.98	No

Table 4.3.2. Multiple linear regression equations for the observed hydrogen peroxide reaction rate coefficient (1/hr) as a function of various aquifer material characteristics. All regression coefficients are statistically significant at the 5% LOS.

	Combinations	$k_{obs} = a*A + b*B + c*C + d*D + e*E + f*F + g*G + h*H + i*I + const$										r^2	Aquifer materials used[1]
		a	b	c	d	e	f	g	h	i	const		
Non-Autoclaved	A	5.16E-02									1.80E-02	0.73	four sites[2]
	C			2.57E+00							4.11E-03	0.77	
	B, D		2.96E-02		-7.13E-03						3.79E-02	1.00	
	D, F				-6.95E-03		5.13E-04				3.77E-02	1.00	
	C			4.63E+00							-1.01E-02	0.99	five sites[3]
	A	2.79E-01									6.00E-03	0.61	
	I									9.86E-01	1.94E-02	0.98	
	H								8.98E-02		-1.26E-02	0.99	
	A, D, H	-1.09E-01			-1.49E-03				1.10E-01		-6.34E-03	1.00	
	D, F, I				-8.51E-03		6.53E-04			7.53E-01	3.85E-02	1.00	
	D, F, G				-2.27E-02		1.90E-03	4.67E-02			5.92E-02	1.00	
	A, E	6.13E-01				-9.49E-03					3.85E-02	0.94	six sites[4]
Autoclaved	A	1.67E-01									5.50E-03	0.57	five sites[3]
	C			2.85E+00							-4.89E-03	0.98	
	H								5.52E-02		-6.40E-03	0.98	
	I									6.09E-01	1.32E-02	0.98	
	A, E	4.38E-01				-7.90E-03					3.48E-02	0.85	six sites[4]

NOTE: A: TOC (%g/g)
B: Total Fe + Total Mn (mmol/g)
C: Amorphous Fe + Amorphous Mn (mmol/g)
D: Surface area (m^2/g)
E: Cation Exchange Capacity (CEC) (cmol/kg)
F: Total Fe (mg/g)
G: Total Mn (mg/g)
H: Amorphous Fe (mg/g)
I: Amorphous Mn (mg/g)
1: If NFF and NIROP data were included, a poor correlation was achieved in all cases investigated.
2: Data from four aquifer materials (i.e., Borden, DNTS, LC34-LSU, and LC34-USU)
3: Data from five aquifer materials (i.e., Borden, DNTS, EDGY, LC34-LSU, and LC34-USU)
4: Data from six aquifer materials (i.e., Borden, DNTS, EDGY, LC34-LSU, LC34-USU, and MAAP)

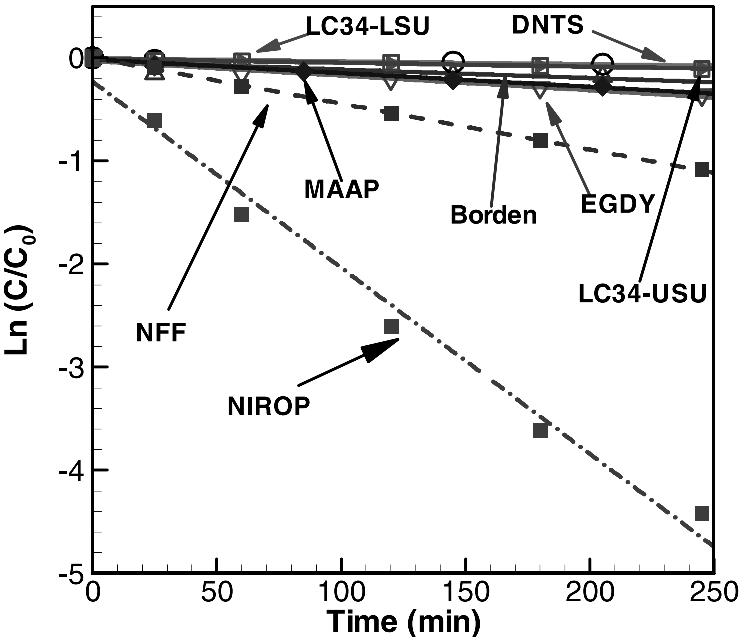

Figure 4.3.1. Hydrogen peroxide decomposition profiles for non-autoclaved aquifer materials.

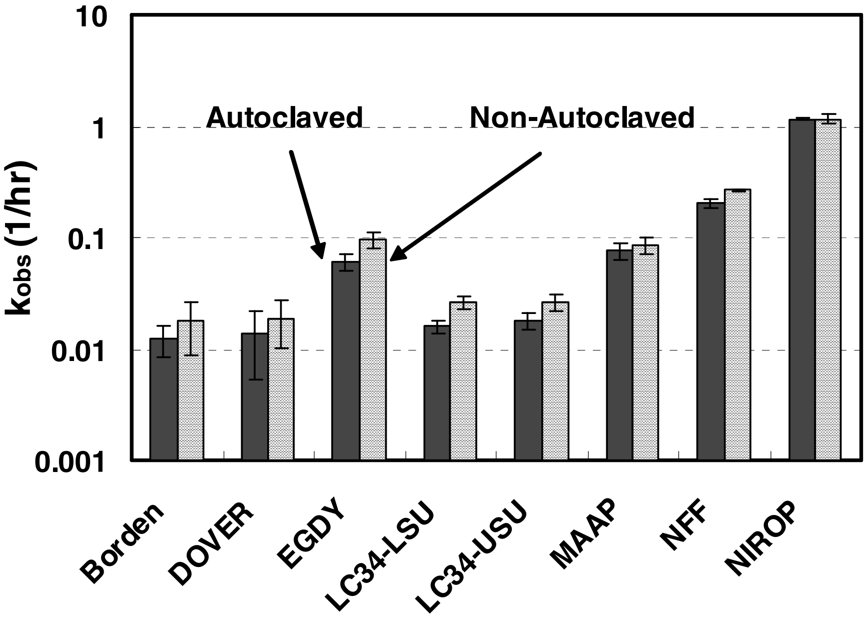

Figure 4.3.2. Hydrogen peroxide decomposition rate coefficients for autoclaved and non-autoclaved aquifer materials.

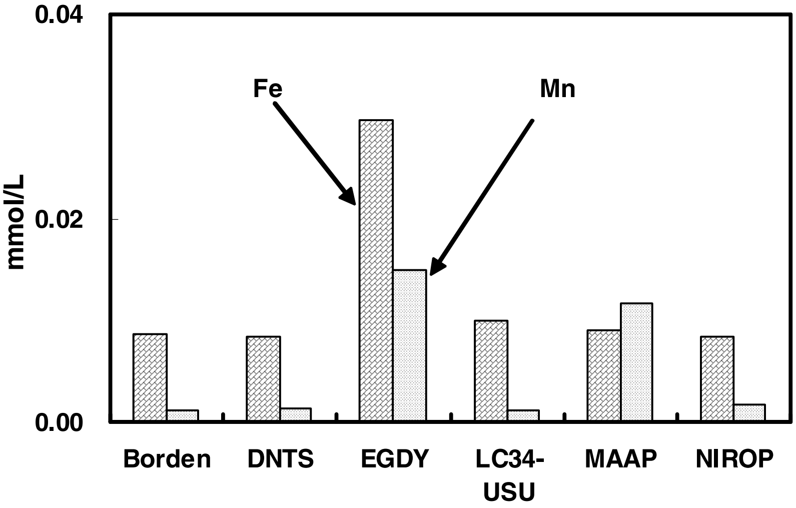

Figure 4.3.3. Total Fe and Mn dissolved concentrations in batch reactors within the first hour.

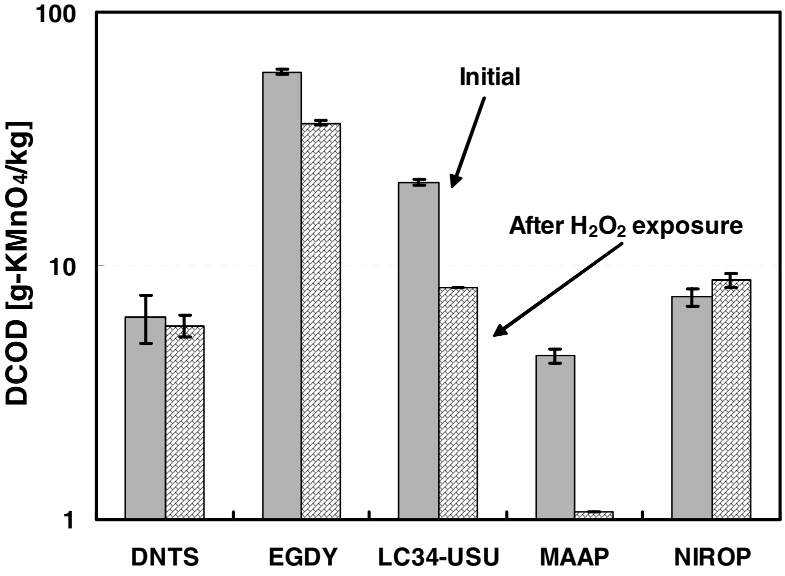

Figure 4.3.4. Dichromate COD test results for selected aquifer materials prior and after exposure to hydrogen peroxide for two-weeks. The error bars represented ± one standard deviation.

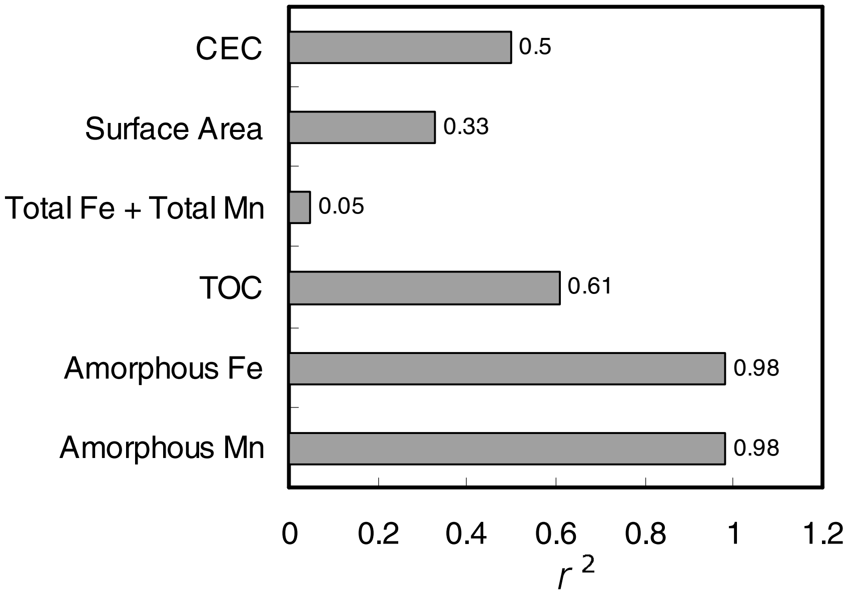

Figure 4.3.5. Results of correlation analysis of the hydrogen peroxide decomposition rate coefficients in the presence of non-autoclaved aquifer materials with an initial hydrogen peroxide concentration of 2% and a pH of 3.0. Data for the aquifer materials from NIROP, NFF, and MAAP are excluded from this analysis.

4.4 Enhanced Stability of Hydrogen Peroxide

4.4.1 Introduction

As discussed in Section 4.2, the successful application of hydrogen peroxide-based ISCO is limited by the instability of hydrogen peroxide (Pignatello et al., 2006; Watts et al, 2006), and many efforts have been undertaken to enhance the stability of hydrogen peroxide in subsurface environments (Kakarla et al., 1997; 2002; Watts et al., 1999a, b, c). Ethylenediaminetetraacetic (EDTA) is a popular chelating agent used to reduce the decomposition of hydrogen peroxide by suppressing the catalytic activity of naturally-occurring transition metals (Watts and Teel, 2005; Ramo, 2003; Jones and Williams, 2002); however, calcium ions may interfere with its chelating efficiency and EDTA is not easily biodegradable and therefore its accumulation in the natural environment is a concern (Jones and Williams, 2002). An inorganic mixture of ammonium sulfate and monobasic sodium phosphate has been also used to stabilize hydrogen peroxide (Watts et al., 1999c). Of the four inorganic compound stabilizers (i.e., monobasic potassium phosphate, dibasic potassium phosphate, sodium tripolyphosphate, and silicic acid) for hydrogen peroxide, monobasic phosphate was found to propagate hydrogen peroxide the longest distance in soil columns (Kakarla et al., 1997); however, it was depleted by adsorption, and may also function as a radical scavenger (Watts et al., 1999c). A comprehensive evaluation of 50 chelating reagents indicated that nitrilotriacetic (NTA) and hydroxyethliminodiacetic (HEIDA) were the most effective chelating reagents for iron (Sun and Pignatello, 1992), and EDTA had a comparable chelating efficiency to NTA (Tandy et al., 2006a). Although the application of chelating reagents has been intensively studied, the long-term potential impact of these chelating reagents on the environment has not been evaluated (Watts and Teel, 2005) and in recent years concern for potential environmental impacts have resulted in a search for "green" hydrogen peroxide stabilizers (Ramo, 2003; Jones and Williams, 2002).

While currently used or proposed cheating reagents are either poorly biodegradable (eg., EDTA), associated with health issues (e.g., cancer-causing agent, NTA), or are not very effective (e.g., citrate) (Vandeviviwre et al., 2001), a newly available and environment-friendly chelating agent, S,S'-ethylenediaminedisuccinate (EDDS) is readily-biodegradable, does not lose its chelating efficiency for transition metals in the presence of calcium ions (Jones and Williams, 2002), and has been proposed as an alternative chelating agent to EDTA in other industrial applications (Grcman, et al., 2003; Jones and Williams, 2001; 2002; Ramo, 2003). For example, in ex-situ washing of soils contaminated with heavy metals, EDDS showed the best extraction efficiency compared to other chelating agents such as nitrilotriacetic acid (NTA) and EDTA (Tandy et al., 2004; 2006a). EDDS has also been found to be more effective when used during phytoextraction of heavy metals in soils than EDTA (Tandy et al., 2006b; Grcman et al., 2003; Kos and Lestan, 2003), while NTA and citric acid showed insignificant chelating efficiency on the uptake of transition heavy metals (Meers et al., 2005). Recent studies have shown that EDDS effectively prevents the contact of transition metals with hydrogen peroxide, and can be used as an excellent stabilizer for hydrogen peroxide over a wide pH range in the pulp and paper industry (Jones and Williams, 2002; Ramo, 2003). According to our knowledge EDDS has never been used in ISCO applications with hydrogen peroxide. Therefore, the experiments we performed in this study were designed to explore the applicability of EDDS as a chelating agent for hydrogen peroxide stabilization during ISCO. To compare the stabilizing effects of EDDS on hydrogen peroxide decomposition we used EDTA, one of the most commonly used chelating agents (Watts and Teel, 2005).

Figure 4.4.1 shows the molecular structure and acidity constants for EDTA and EDDS, and indicates that EDDS is a close isomer to EDTA. Commercial EDDS has been available from Octel Performance Chemicals Company, Cheshire, UK (http://www.octel-pc.com) in recent years.

4.4.2 Methods

As discussed in Section 4.3, hydrogen peroxide decomposition rate coefficients in the presence of the various aquifer materials used in this study span the range from 0.018 to 1.16 hr^{-1}. Based on these data, five representative aquifer materials (DNTS, EGDY, LC34-USU, MAAP, and NIROP) were chosen to investigate the enhanced stability of hydrogen peroxide. Prior to use, aquifer materials were air-dried to a constant weight, and only materials passing the US No. 10 standard sieve (<2 mm) were used.

Solutions used in these experiments were prepared with the use of 30% hydrogen peroxide (VWR, Toronto, Canada), ferrous sulfate heptahydrate (J.T. Baker, Phillipsburg, NJ), EDTA (BDH, Toronto, Canada), and EDDS (Fluka Chemika, Sigma-Aldrick, Steinheim, UK). In addition, 1 N sodium hydroxide solution and 1 N sulfuric acid solution were used for initial pH adjustment as required.

This study investigated the stability of hydrogen peroxide in four different experimental solution matrices (Table 4.4.1):

1. a solution with an initial pH of 3.0 and a hydrogen peroxide concentration of 2.0% (Experimental Series 1, which has been addressed in Section 4.3);
2. a solution with an initial pH of 3.0, hydrogen peroxide concentration of 2.0%, and either EDTA or EDDS added in a ratio of 0.5 mmol or 1.0 mmol per kg of aquifer material, respectively (Experimental Series 2, 3, and 4);
3. a solution with an initial pH of 3.0, hydrogen peroxide concentration of 2.0% mixed with ferrous iron in a weight ratio of Fe^{2+}/H_2O_2 of 0.005 or 0.02 (Experimental Series 5 and 6); and
4. a solution with an initial pH of 3.0, hydrogen peroxide concentration of 2.0%, ferrous iron in a weight ratio of Fe^{2+}/H_2O_2 of 0.005, and EDDS in a ratio of 0.5 mmol EDDS per kg of aquifer material (Experimental Series 7).

Each experiment was performed in triplicate and consisted of adding 15 g of aquifer material and 80 mL of the appropriate solution into a 110 mL amber reactor fitted with a Teflon cap. The experimental procedure for Series 2 to 4 is the same as that used for the Series 1 experiments which was described in Section 4.3 for the non-autoclaved aquifer materials.

4.4.3 Results and Discussions

The hydrogen peroxide concentration profiles corresponding to the four different solution matrices for each aquifer material are shown in Figure 4.4.2. These profiles all show some level of hydrogen peroxide decomposition which can be captured by a pseudo first-order kinetic model. The best-fit first-order reaction rate coefficients are listed in Table 4.4.1 and visually displayed in Figure 4.4.3. Similar to the observations for Experimental Series 1 as discussed in Section 4.3.2, in less than an hour after the start of each experiment, the solution pH in Experimental Series 2 to 4 increased due to the strong aquifer material buffering capacity from the initial pH of 3.0 to a stable value, which was less than but close to the corresponding soil pH for each aquifer material (e.g., 4.2 for DNTS, 5.4 for EGDY, 7.5 for LC34-USU, 3.5 for MAAP, and 8.5 for NIROP), again suggesting that *in situ* pH control will be difficult to achieve during the injection of hydrogen peroxide into aquifer materials with a high buffering capacity.

Based on the data in Table 4.4.1, there is no statistically significant difference ($\alpha = 5\%$, t-test) between the observed hydrogen peroxide first-order rate constants for the two chelating agents (EDTA and EDDS) used in this investigation (Experimental Series 2 and 3). This suggests that EDDS has a comparable chelating efficiency to EDTA in the presence of various aquifer materials. Figure 4.4.4 shows that the addition of EDTA resulted in an increase of the dissolved phase concentrations of transition metals (Fe and Mn) in each experimental system which is similar to the results we obtained for EDDS (not shown). This increase in metal concentration is because chelating reagents complex with metal ions in the solid phase and extract them from aquifer materials (Stumm and Morgan, 1995). Compared to uncomplexed forms of these metals, the catalytic activity of these complexed metals with respect to hydrogen peroxide reactivity is suppressed in the aqueous phase (Jones and

Williams, 2002; Ramo, 2003).

As other studies have illustrated, the presence of chelating agents in the aqueous phase can reduce the availability of transitional metals to react with hydrogen peroxide (Jones and Williams, 2002; Ramo, 2003), and therefore increase the stability of hydrogen peroxide in situations where naturally-occurring transitional metals are involved. In this investigation with the presence of various aquifer materials, the addition of chelating reagents resulted in a significant drop in the hydrogen peroxide decomposition rate coefficient (Experimental Series 2, 3, and 4). For example, in the case of the addition of 0.5 mmol/kg EDDS, the hydrogen peroxide decomposition rate coefficient was reduced by about 97% for MAAP, 82% for DNTS, 73% for EGDY, 24% for LC34-USU, and 82% for NIROP aquifer materials. Although the addition of a higher dosing of the chelating reagent (1.0 compared to 0.5 mmol/kg EDDS) generally produced a slightly lower hydrogen peroxide decomposition rate coefficient, the difference between these rate coefficients was not statistically significant (α = 5%, t-test). Both the DNTS and NIROP aquifer materials have a relatively low TOC content (0.28 mg/g and 0.30 mg/g respectively), and therefore the main factors influencing hydrogen peroxide decomposition in the presence of these aquifer materials is their amount of dissolvable Fe and Mn; hence the use of chelates for these aquifer materials is beneficial. The EGDY aquifer material has a relatively high TOC content (2.28 mg/g) and amorphous Fe and Mn content which leads to a high dissolved Fe and Mn concentration (see Figure 4.4.4) which can be affected by the chelating agents and therefore improvements in hydrogen peroxide stability are realized. Although the MAAP aquifer material contains an relatively average TOC content (0.77 mg/g) and a relatively low content of total Fe and Mn as well as amorphous Fe and Mn, it has a high dissolvable Fe and Mn content as confirmed by high concentrations of dissolved Fe and Mn present in the solution (see Figure 4.4.4). The LC34-USU aquifer material also has a relatively average TOC content (0.87 mg/g), but the dissolved Fe and Mn concentrations are quite low (see Figure 4.4.4), so the influence of chelating reagents to stabilize hydrogen peroxide is relatively insignificant compared to the other aquifer materials used in this study.

The addition of ferrous iron generally resulted in a significant increase in the hydrogen peroxide decomposition rate coefficient which increased with the amount of ferrous iron added (Experimental Series 5 and 6). For example, in comparison to the case with no addition of iron or chelating reagent, the addition of iron at the weight ratio of 0.005 (Fe^{2+}/H_2O_2) increased the hydrogen peroxide decomposition rate coefficient by approximately 100% for the MAAP aquifer material, and by 200% for the DNTS and LC34-USU aquifer materials. Surprisingly, the addition of ferrous iron did not increase the hydrogen peroxide decomposition rate coefficient for the NIROP aquifer materials. In fact as the amount of iron was increased, the hydrogen peroxide decomposition rate coefficient decreased. This may be due to experimental error and variability or may be related to the high soil pH, the high CEC and bulk surface area, and the high carbonate content associated the NIROP aquifer materials, resulting in an unknown mechanism.

When both the chelating reagent and ferrous iron were added (e.g., ferrous iron was added according at a weight ratio of 0.02 (Fe^{2+}/H_2O_2), and EDDS was added according to the ratio of 0.5 mmol EDDS per kg of solids), the hydrogen peroxide decomposition rate was higher than when only the EDDS was added, and lower then when only the ferrous iron was added. This observation further supports the above findings that ferrous iron accelerates hydrogen peroxide decomposition, and that chelating reagents (i.e., EDDS) can stabilize hydrogen peroxide in the presence of various aquifer materials by suppressing the catalytic activity of metals (e.g., iron and manganese).

4.4.4 Summary

This investigation of the enhanced stability of hydrogen peroxide demonstrated that the addition of ferrous iron generated the largest hydrogen peroxide decomposition rate coefficients, while the presence of a chelating agent (EDDS or EDTA) generated the lowest hydrogen peroxide decomposition rate coefficients. Even for the high pH and carbonate rich NIROP aquifer material, the hydrogen peroxide decomposition rate was still decreased by an order of magnitude (from 1.2 to 0.2 / hour) with chelate addition.

Fenton's Reagent (a mixture of hydrogen peroxide, ferrous iron, and sulfuric acid) is used widely in water and wastewater treatment, and has gained popularity as an oxidant for ISCO applications (Chen et al., 2001; Pignatello, 2006). However, Watts and Teel (2005) determined that the optimal treatment environment in the presence of most natural aquifer materials was not to add ferrous iron. The experimental results from this investigation show that the stability of hydrogen peroxide is greatly degraded when ferrous iron was added to the system, and therefore we also recommend that if the site geochemistry is favorable that additional ferrous iron not be used.

It is recommended that EDDS be considered as an alternative chelating agent for stabilizing hydrogen peroxide in ISCO application since: (1) EDDS has been proven to be easily biodegraded (Jones and Williams, 2002); and (2) our results show that EDDS is comparable to EDTA in terms of chelating efficiency for transition metals (Fe and Mn) in the presence of various aquifer materials. The application of EDDS is especially effective in reducing the hydrogen peroxide decomposition rate for those materials with low TOC and/or high amorphous iron and manganese contents.

Table 4.4.1. First-order reaction rate coefficients (1/hour) for hydrogen peroxide decomposition in batch experiments.

			Fe^{2+}/H_2O_2	DNTS		EDGY		LC34-USU		MAAP		NIROP	
Series	H_2O_2	Chelate	Ratio [w/w]	Avg	95% CI	Avg	95% CI	Avg	95% CI	Avg	95% CI	Avg	95% CI
1	2%	-	-	0.0188	± 0.008	0.0955	± 0.014	0.0260	± 0.0043	0.0856	± 0.0135	1.16	± 0.12
2	2%	1.0 mmol/kg EDTA	-	0.00437	± 0.0011	0.0268	± 0.005	0.0192	± 0.0014	0.00328	± 0.0004	0.161	± 0.037
3	2%	1.0 mmol/kg EDDS	-	0.00331	± 0.0007	0.0260	± 0.002	0.0238	± 0.0009	0.00462	± 0.0008	0.177	± 0.034
4	2%	0.5 mmol/kg EDDS	-	0.00288	± 0.0003	0.0235	± 0.002	0.0197	± 0.0003	0.00279	± 0.0008	0.213	± 0.04
5	2%	-	0.005	0.0547	± 0.01	0.0736	± 0.01	0.0876	± 0.01	0.164	± 0.012	0.708	± 0.04
6	2%	-	0.02	0.919	± 0.177	1.06	± 0.119	0.306	± 0.031	1.10	± 0.125	0.461	± 0.028
7	2%	0.5 mmol/kg EDDS	0.02	0.420	± 0.048	0.345	± 0.031	0.230	± 0.021	0.450	± 0.04	0.364	± 0.042

EDTA (MW = 292 g/mol)

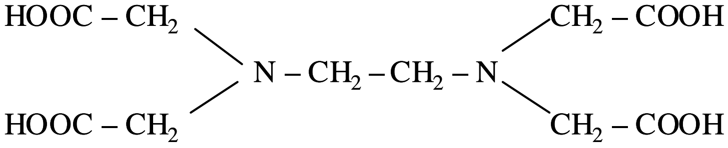

EDDS (MW = 292 g/mol)

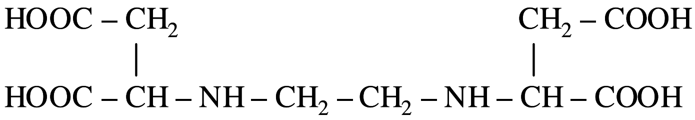

$$\mathrm{HOOC-\overset{\overset{\displaystyle HOOC-CH_2}{|}}{C}H-NH-CH_2-CH_2-NH-\overset{\overset{\displaystyle CH_2-COOH}{|}}{C}H-COOH}$$

	EDDS	EDTA
pK_1	2.4	2.1
pK_2	3.9	3.0
pK_3	6.8	6.4
pK_4	9.8	10.4

Figure 4.4.1. Molecular structure and acidity constants for ethylenediaminetetraacetic acid (EDTA) and ethylenediaminedisuccinic acid (EDDS) (25^0C) (adapted from Vandevivere et al., 2001)

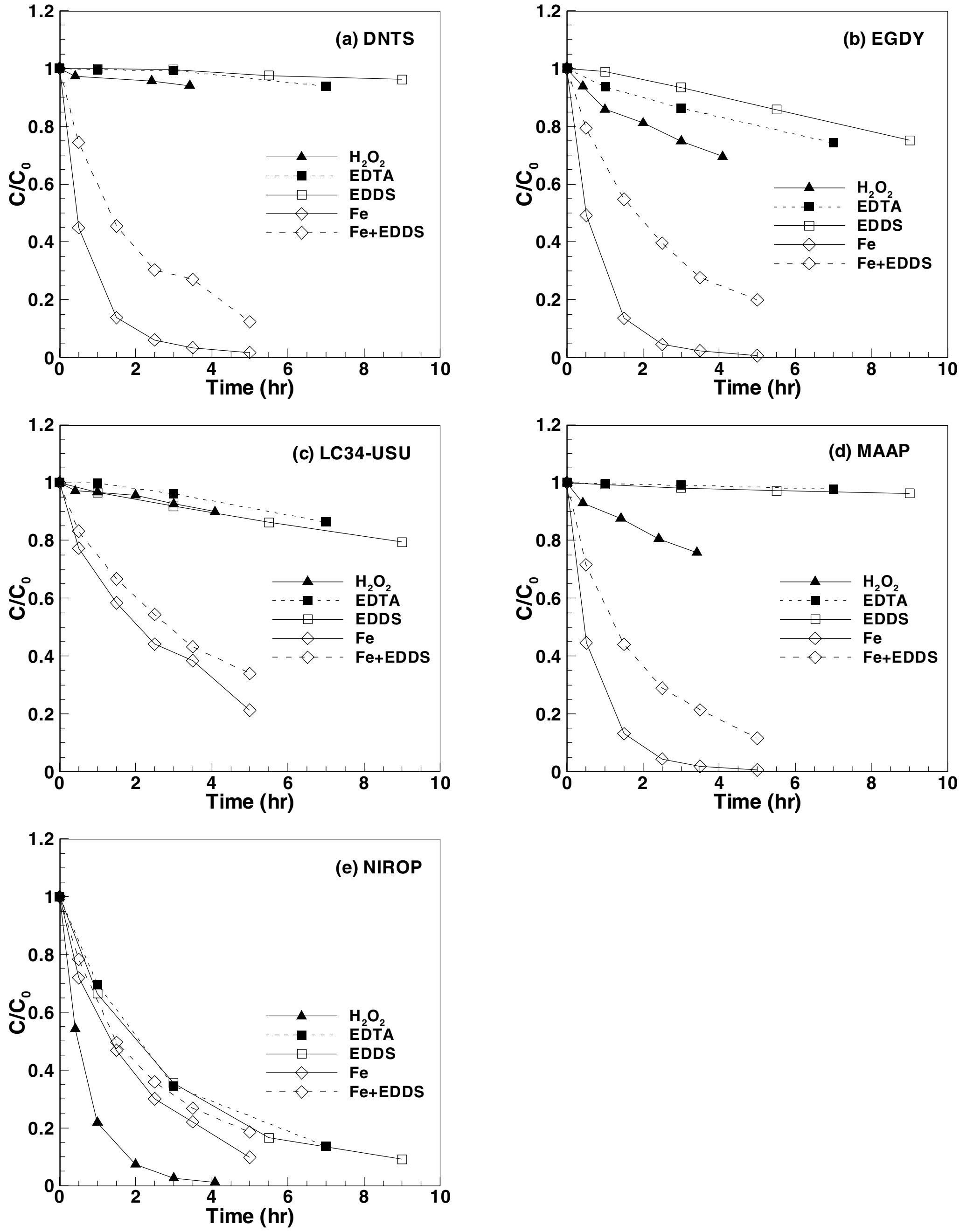

Figure 4.4.2. Hydrogen peroxide profiles in the presence of (a) DNTS aquifer materials, (b) EGDY aquifer materials, (c) LC34-USU aquifer materials, (d) MAAP aquifer materials, and (e) NIROP aquifer materials. Each data point is the average from triplicate experiments. EDDS was added at 0.5 mmol EDDS per kg of solids, EDTA was added at 1.0 mmol per kg of solids, and ferrous iron was added at a weight ratio of 0.02 (Fe^{2+}/H_2O_2).

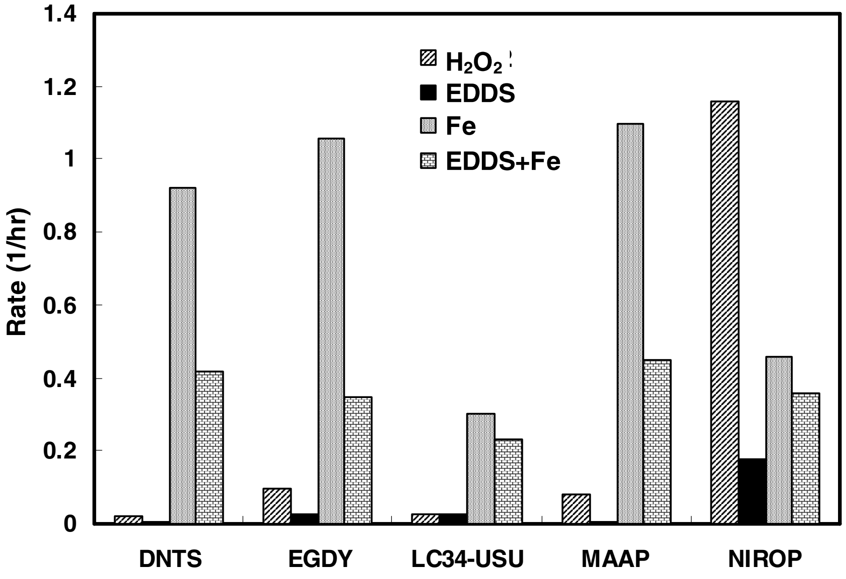

Figure 4.4.3. Observed reaction rate coefficients in the presence of aquifer materials for Experimental Series 1, 4, 6 and 7. EDDS was added at 0.5 mmol EDDS per kg of solids, and ferrous iron was added at a weight ratio of 0.02 (Fe^{2+}/H_2O_2).

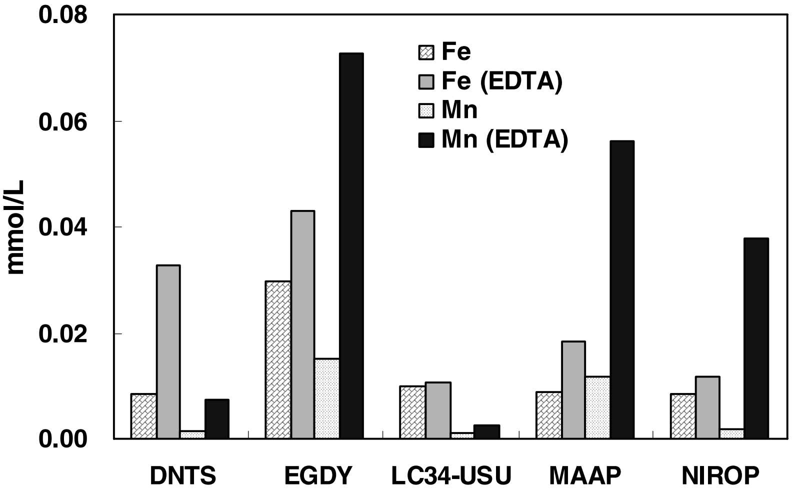

Figure 4.4.4. Total Fe and Mn dissolved concentrations from Experimental Series 1 and 2. EDTA was added at 1.0 mmol EDTA per kg of solids. Samples were taken within the first hour.

4.5 Column Experiments

4.5.1 Introduction

As indicated in Sections 4.3 and 4.4, hydrogen peroxide in the presence of aquifer materials decomposes at a rate that is well-represented by a pseudo-first order mass action law, and the addition of EDDS improves the stability of hydrogen peroxide by reducing the decomposition rate. Relative to batch reactor systems, results from aquifer material packed columns are considered more representative of *in situ* conditions since they provide more realistic aquifer material contact, and therefore column experiments were designed to complement and expand the findings from the batch experiments.

Aquifer materials from EGDY, LC34-LSU, LC34-USU, NIROP, and MAAP were chosen for these column experiments. These five aquifer materials span the spectrum of geochemical conditions of the ten aquifer materials used in this study; (1) The EGDY aquifer material has a high TOC content while the NIROP aquifer material has a high soil pH and carbonate content, (2) the MAAP aquifer material contains relatively low total transition metals (e.g., Fe and Mn), and (3) the aquifer materials from LC34-LSU and LC34-USU contain a TOC and transition metal content (e.g., Fe and Mn) close to the average of those used in this study.

4.5.2 Methods

Figure 4.5.1 shows the typical column setup used in this investigation. All columns were constructed from 11 to 13 cm long sections of nominal 2.54 cm (1-inch) diameter Schedule 40 PVC pipe. The top and bottom of each column were constructed from PVC fittings tapped to accommodate 1.1 cm (7/16") stainless steel tubing couplers (Swagelok). To avoid problems associated with dry packing, homogenized aquifer material was wet with Milli-Q water to near saturation before use. Each column was packed in three stages: (1) the bottom tubing coupler was fitted with a 500 µm stainless steel screen, a thin layer of glass wool (Pyrex, VWR) and a 0.2 cm layer of 0.59 to 0.84 mm glass beads (Potters Industries Ltd.), (2) the next 10 cm was packed with aquifer material in 1 to 2 cm lifts compacted using a 1 cm diameter glass rod with the column attached to vertical vibrating rod; and (3) above the aquifer material the top of the column was fitted with a 500 µm stainless steel screen, topped with glass wool (Pyrex, VWR) and 0.59 to 0.84 mm glass beads (Potters Industries Ltd.).

Each column was operated in a continuous up-flow mode using a peristaltic pump (Cole-Parmer Instrument Co., Model No. 7553-80, 1-100 RPM, size 14 tubing) to control the rate of inflow, and a constant hydraulic head applied at the effluent end. Column experiments for each aquifer material were conducted in duplicate.

Two types of hydrogen peroxide source solutions were prepared: (1) a *hydrogen peroxide only* solution consisting of a hydrogen peroxide (VWR, Toronto, Canada) concentration of ~2.4% (w/w) and pH of 3.0, and (2) a *hydrogen peroxide and EDDS solution* consisting of a hydrogen peroxide concentration of ~2.4%, pH of 3.0, and an EDDS (Fluka Chemika, Sigma-Aldrick, Steinheim, UK) concentration of ~7.5 mM. The solution pH was adjusted with 1 N H_2SO_4 (Fischer Scientific) solution, and 1N NaOH solution (Fischer Scientific).

Each column was flushed with Milli-Q water at the specified flow rate for up to 5 hours prior to injection of the hydrogen peroxide solution. Samples (with a volume of 0.2 to 0.3 mL) were periodically taken from the effluent to determine hydrogen peroxide concentration (iodometric method, Schumb et al., 1995), and pH (pH meter Model 81-02, Orion). For a typical sample volume of 0.2 to 0.3 mL the hydrogen peroxide method detection limit (MDL) was 0.05%.

For the LC34-LSU, LC34-USU, and MAAP aquifer materials two flow rates were used (high and low) to allow for different resident times to be investigated (Table 4.5.1). For each flow rate, the column was flushed with the source solution until a stable or near stable hydrogen peroxide concentration in the effluent was observed, then flushed with Milli-Q water until no hydrogen peroxide was detected in the effluent, and then flushed again with the same source solution until a stable hydrogen peroxide concentration in the effluent was observed. The purpose of the second flush was to investigate the breakthrough behavior of hydrogen peroxide in a system that was previously exposed to hydrogen peroxide.

Tracer tests using a sodium bromide solution at a constant concentration of 50 to 100 mg/L (Fischer Scientific) were conducted to compare the breakthrough behavior between a conservative tracer and the hydrogen peroxide solution as well as to evaluate hydrodynamic properties (porosity and dispersivity) of each aquifer material packed column. Bromide concentrations were determined by ion chromatography (IC) (Dionex AS4A-SC 4mm x 250 mm column; 1.8 mM sodium carbonate, 1.7 mM sodium bicarbonate eluate; 1.5 mL/min flow rate) with a MDL of 1.2 mg/L.

As demonstrated in the batch experiments (Sections 4.3.2 and 4.4.3), dissolved Fe and Mn played a significant role in the decomposition of hydrogen peroxide, especially for the MAAP aquifer material. Therefore, an additional column experiment with the MAAP aquifer material was performed to investigate the influence of dissolved metals (e.g., Fe and Mn) on hydrogen peroxide decomposition in the column system. A low flow rate (0.22 mL/min) was used for this experiment, and the columns were flushed with a *sulfuric acid* solution (pH = 3.0) for about 2 hours to decrease the dissolved metal (Fe and Mn) concentration produced in this column system, and then flushed with the *hydrogen peroxide only* solution. When the effluent hydrogen peroxide concentration reached a nearly stable value, a solution sample (~ 5 mL) from each column effluent was taken, filtered (0.45 μm filter (Nalgene)), and used to quantify Fe and Mn concentrations with an inductively coupled plasma (ICP) emission spectroscopy with a Spectro Flame instrument (Spectro Analytical, Fitchburg, MA), which had a MDL of 0.01 mg/L for Mn and 0.1 mg/L for Fe. For comparison, samples were also taken from the effluent of the MAAP column experiments flushed with the *hydrogen peroxide only* solution and the *hydrogen peroxide and EDDS* solution, and the dissolved Fe and Mn concentrations were determined.

4.5.3 Results and Discussion

4.5.3.1 General Observations

Temporal concentration profiles of hydrogen peroxide and bromide (Br) obtained from the duplicate columns at identical sampling times were averaged for the MAAP, LC34-LSU, and LC34-USU aquifer materials and are shown in Figure 4.5.2. No hydrogen peroxide was detected in the effluent from the columns packed with EGDY and NIROP aquifer materials after flushing for ~10 hours (~14 and 10 pore volumes for the columns containing EGDY and NIROP aquifer material, respectively) with the *hydrogen peroxide only* solution. The high hydrogen peroxide decomposition rate in the presence of EGDY and NIROP aquifer materials is the result of the high TOC (~3 mg/g) and transition metal (e.g., Fe and Mn) content in the EGDY aquifer material, and high surface area, high CEC, and the strong buffering capability (pH 8.5 to 9.0) of the NIROP aquifer material where the carbonates act as a scavenger (sink) for hydroxyl radicals (Seol et al., 2003; Watts and Teel, 2005). When the *hydrogen peroxide and EDDS* solution was used, hydrogen peroxide breakthrough in the columns packed with NIROP and EGDY aquifer material was observed with stable effluent concentrations of 0.01% and 0.1% respectively. This is consistent with the batch test results which indicated that the addition of EDDS improves the stability of hydrogen peroxide in the presence of these aquifer materials.

The first appearance of hydrogen peroxide and the Br tracer as defined by a detectable concentration in the effluent (0.05% for hydrogen peroxide, and 1.2 mg/L for Br) are listed in Table 4.5.2 for the LC34-LSU, LC34-USU, and MAAP aquifer materials. Since the time required to collect a typical sample volume was 1 minute for the fast flow rate and 3 minutes for the slow flow rate, the first appearance is accurate within 0.014 to 0.12 pore volumes (PVs) for the fast and slow flow rates, respectively. The delay in the first appearance of the first-flush *hydrogen peroxide only* solution relative to Br varies from 0.07 to 0.98 PVs at the high flow rate, and from 0.10 to 2.04 PVs at the low flow rate. This delay is markedly less for the second-flush of the *hydrogen peroxide only* solution where a delay from zero to 0.19 PVs was observed at the high flow rate, and a delay from 0.05 to 0.34 PVs was observed at the low flow rate. In both flushing episodes the delay in the first appearance of hydrogen peroxide was accentuated at the lower flow rates due to the longer contact time with aquifer materials. The cause of this delay is related to the presence of labile species associated with the aquifer material which contribute to an increased consumption of hydrogen peroxide during the first flush relative to the second flush. These labile species may include reactive organic matter which contributes to the consumption of hydrogen peroxide through redox reactions during the first-flush episode, and transition metals (e.g., Fe and Mn) which promote hydrogen peroxide decomposition (Watts and Teel, 2005). Some of the transition metals are in the dissolved form and are removed from the column system during the first flush (Table 4.5.3). Evidence of the removal of dissolved metals (Fe and Mn) from the column system is presented later in this section when the results from the additional MAAP column experiment are discussed.

When the *hydrogen peroxide and EDDS* solution was used, the delay in the first appearance of hydrogen peroxide varied from 0.07 to 0.34 PVs for the first flush, and from zero to 0.15 PVs for the second flush. In all cases the presence of EDDS resulted in a delay less than or equal to the delay observed during the first flush with the *hydrogen peroxide only* solution. For example, under the low flow rate the first appearance of hydrogen peroxide in the presence of EDDS for the LC34-LSU and MAAP aquifer materials was about 0.08 and 1.7 PVs ahead of the first appearance of hydrogen peroxide with the *hydrogen peroxide only* solution. It is interesting to note that delay in the first appearance of hydrogen peroxide for the first flush with the *hydrogen peroxide and EDDS* solution is nearly identical to the delay for the second flush with the *hydrogen peroxide only* solution for the LC34-LSU, LC34-USU, and MAAP aquifer materials. This suggests that the presence of EDDS causes the dissolved iron and manganese which were active during the first flush with the *hydrogen peroxide only* solution to be less available for the reaction with hydrogen peroxide by suppressing their catalytic activity.

As shown in Figure 4.5.2, once the initial breakthrough was established for each column trial, the hydrogen peroxide concentration increased to a constant value representative of stable or steady-state conditions. This steady-state effluent concentration depends on the flushing solution and flow rate, but is consistent between the first and second flushing episodes. For example, the steady-state concentration is ~80% of the inflow concentration when the LC34-LSU and LC34-USU aquifer materials are flushed under a high flow rate, and <60% when flushed under the low flow rate. This difference in steady-state effluent concentration is related to the longer residence time for the low flow rate which allows for increased interaction between hydrogen peroxide and the aquifer material. The addition of EDDS to the flushing solution resulted in much higher steady-state hydrogen peroxide concentrations relative to the *hydrogen peroxide only* solution.

As discussed above, hydrogen peroxide decomposition in the presence of aquifer materials (especially MAAP solids) are associated with the existence of dissolved metals (e.g., Fe and Mn) which originate from the aquifer solids. This is especially true for the MAAP aquifer material which produced high concentrations of dissolved Fe and Mn in the batch reactor solution and in the column effluent. The impact of the dissolved Fe and Mn concentrations on hydrogen peroxide reactivity was investigated using the additional MAAP column experiment. The temporal hydrogen peroxide concentration profile produced from this additional experiment is shown on Figure 4.5.2 (f), and pH and dissolved metal (Fe and Mn) data are listed in Table 4.5.3.

For the column treated with the *sulfuric acid* solution (pH = 3.0), the first appearance of hydrogen peroxide in the column effluent (0.97 PV) was nearly identical to that for the first flush with the *hydrogen peroxide and EDDS* solution (0.95 PV), and for the second flush with the *hydrogen peroxide only* solution (0.95 PV) (Table 4.5.3). The shape of the rising portion of the hydrogen peroxide profile for the column treated with the *sulfuric acid* solution is almost identical to that produced by the first flush with the *hydrogen peroxide only* solution, suggesting that the quantity of hydrogen peroxide used in actual ISCO application may be considerably decreased by performing an acidic flush prior to the injection of hydrogen peroxide. The effluent pH ranged from 3.3 to 4.2 with an average value of 3.7 of all column observations, indicating that an acidic condition remained within the column, and that the pH condition was suitable for Fenton's reaction (Pignatello et al., 2006; Watts and Teel, 2005). Under this acidic condition, more dissolved metals (including Fe and Mn) would be released from aquifer solids and then removed from the column system by the acidic flush (Nicholson et al., 2003), leading to a low content of Fe and Mn remained within the column and an decrease of the unproductive depletion of hydrogen peroxide by aquifer materials. When the effluent hydrogen peroxide concentration stabilized, the total dissolved concentration of Fe and Mn for the flush with the *hydrogen peroxide only* solution following the treatment with the *sulfuric acid* solution was 0.18 mmol/L, which is less than that (0.34 mmol/L) for the first-flush with the *hydrogen peroxide only* solution but greater than that (0.05 mmol/L) for the second-flush with the *hydrogen peroxide only* solution. A reasonable explanation for this observation is that a portion of the dissolvable metals (Fe and Mn) in the MAAP aquifer material were removed from the column during the initial flush with the *sulfuric acid* solution. The results from the batch experiments as presented in Table 4.4.1 (Section 4.4) indicated that the hydrogen peroxide decomposition rate coefficient increases as the transition metal (Fe and Mn) concentration in the system increases, and therefore it is not surprising that with the high dissolved metal concentration (0.34 mmol/L) the first appearance of hydrogen peroxide during the first-flush with the *hydrogen peroxide only* solution lags behind the second-flush with the *hydrogen peroxide only* solution. Interestingly, all these three dissolved metal concentration values are much less than that (0.75 mmol/L) for the first-flush with the *hydrogen peroxide and EDDS* solution, and the first appearance of hydrogen peroxide for the column experiments with the *hydrogen peroxide and EDDS* solution was nearly identical to that for the second-flush with the *hydrogen peroxide only* solution. This suggests that the presence of EDDS causes the dissolved iron and manganese to be less available for the reaction with hydrogen peroxide by suppressing their catalytic activity. This high metal concentration (0.75 mmol/L) in the column effluent solution for the *hydrogen peroxide and EDDS* solution compared to the other cases is because EDDS complexes metal ions in the solid phase and extracts them from aquifer materials. This observation is consistent with the results form the batch system discussed in Section 4.4.

4.5.3.2 Observed H_2O_2 Decomposition Rate Constants

As concluded from the batch experiments, the decomposition of hydrogen peroxide in the presence of aquifer materials follows the first-order rate law, given as

$$\frac{dC}{dt} = -k_{obs} C \tag{4.5.1}$$

where k_{obs} is the observed rate coefficient for hydrogen peroxide [1/T], C is the hydrogen peroxide concentration [% w/w], and t is time [T]. Assuming minimal dispersion, the transport of hydrogen peroxide in the column can be expressed as

$$\frac{\partial C}{\partial t} = -v_x \frac{\partial C}{\partial x} - k_{obs} C \tag{4.5.2}$$

where x is aligned with the direction of flow in the column [L], and v_x is velocity [L/T]. At steady-state, or when stable hydrogen peroxide conditions are established, Eq. (4.5.2) can be expressed as

$$\frac{dC}{dt_r} = -k_{obs} C \tag{4.5.3}$$

where t_r is travel time in the column [T], and the observed hydrogen peroxide reaction rate coefficient can then be calculated from

$$k_{obs} = -\frac{1}{t_r(x = L)} \ln \frac{C_{eff}^s}{C_o} = -\frac{v_x}{L} \ln \frac{C_{eff}^s}{C_o} \tag{4.5.4}$$

where C_{eff}^s is the stable hydrogen peroxide concentration in the effluent, C_o is hydrogen peroxide influent concentration, and L is the length of the column.

Table 4.5.4 lists the calculated hydrogen peroxide reaction rate coefficients using Eq. (4.5.4) and the breakthrough curve data shown on Figure 4.5.2, and additional data for the NIROP and EGDY aquifer materials. As expected, the addition of EDDS to the source solution produced a decrease in the reaction rate coefficient. For example, the reaction rate coefficients for columns packed with MAAP, LC34-USU, LC34-LSU aquifer materials were reduced by 38, 20, and 10% respectively with the addition of EDDS. The hydrogen peroxide decomposition rate coefficients for EGDY and NIROP were decreased from greater than 200 day^{-1} to less than 160 day^{-1} by the addition of EDDS.

4.5.3.3 Comparison of the Hydrogen Peroxide Decomposition in Column and Batch Systems

Along with the calculated hydrogen peroxide reaction rate coefficients from the column experiments, the observed decomposition rate coefficients obtained from batch experiments (Sections 4.4.3 and 4.4.4) are also listed in Table 4.5.4.

For all aquifer materials, the hydrogen peroxide reaction rate coefficients based on the column data are much greater (>18% for the *hydrogen peroxide only* solution, and >1500% for *hydrogen peroxide and EDDS* solution) than those estimated from the batch test data. This increase is a direct result of higher mass of aquifer material to solution mass ratio in the column experiments, which leads to higher decomposition rate coefficients. To remove this influence, all decomposition rate coefficients from both column and batch experiments were divided by the corresponding mass of aquifer materials used in each system, and for comparison these normalized decomposition rate coefficients are also listed in Table 4.5.4. It can be seen that after this normalization, the hydrogen peroxide reaction rate coefficients based on the column data are greater (>28% for the *hydrogen peroxide only* solution except for the MAAP aquifer material, and >58% for *hydrogen peroxide and EDDS* solution) than those estimated from the batch test data. As discussed in Section 4.3.2, the MAAP aquifer material contains a relatively low content of total Fe and Mn but a relatively high content of dissolvable Fe and Mn, leading to a high concentration level of dissolved Mn and Fe in the solution of the corresponding batch reactors (Figure 4.3.3). The dissolved Fe and Mn were retained in the reactors throughout the reaction process for batch experiments while these species were likely removed from the column, resulting in differing hydrogen peroxide decomposition for these two systems.

Acknowledging the limited data availability, a correlation analysis was performed between the observed hydrogen peroxide decomposition rate coefficients generated from the batch and the column experiments. The results from this analysis indicated a weak correlation for the *hydrogen peroxide and EDDS* solution (r = 0.8, n = 4), and for the *hydrogen peroxide* *only* solution (r = 0.6, n = 4); neither of these correlations produced statistically significant linear relationships. However, for the normalized decomposition rate coefficient, the correlation coefficient for the *hydrogen peroxide and EDDS* solution increased from r = 0.8 to r = 0.88, but decreased from r = 0.6 to <0.5 for the *hydrogen peroxide only* solution.

Contrary to the good correlation between the hydrogen peroxide decomposition rate coefficients from the column and batch systems for the *hydrogen peroxide and EDDS* solution, a poor correlation was obtained for the *hydrogen peroxide only* solution. This may be due to the combined influence of the EDDS stabilizing effect on hydrogen peroxide and the solution/aquifer material contact difference between column and well-mixed batch reactor systems. The presence of EDDS causes the dissolved Fe and Mn to be less available for the reaction with hydrogen peroxide by suppressing their catalytic activity in both experimental systems, and thus provides a relatively comparable reaction environment for hydrogen peroxide in these two systems. As mentioned previously, without EDDS addition, the differing concentrations of dissolved Fe and Mn in the batch and column systems likely led to completely different reaction conditions for hydrogen peroxide.

4.5.4 Summary

The results from these column experiments clearly demonstrate that the addition of EDDS was able to successfully stabilize hydrogen peroxide in the presence of the aquifer materials used in this study. This is especially true for the EGDY and NIROP aquifer materials where we were unable to propagate hydrogen peroxide through a 10-cm long column with the *hydrogen peroxide only* solution, but were able to achieve some level of breakthrough with the *hydrogen peroxide and EDDS* solution. Therefore, the use of EDDS as a green chelating agent appears to be promising for *in situ* applications involving the injection of hydrogen peroxide.

The transport of transition metals (Fe and Mn) associated with the application of hydrogen peroxide, especially when an acid flush was conducted prior to hydrogen peroxide, was observed in this investigation. Since Fe and Mn can promote the decomposition of hydrogen peroxide depending on their form (e.g., solid and soluble) and their content within the system, this transport of dissolved metals (Fe and Mn) is expected to affect the behavior of hydrogen peroxide within the subsurface environment.

When a chelating reagent (i.e., EDDS) was used, a relationship related to the hydrogen peroxide decomposition rate coefficient obtained from column systems to batch system data was developed. The hydrogen peroxide decomposition rate coefficients generated from the column data are significantly higher than those generated from the batch test data due to the solution/aquifer material contact difference between a column and a well-mixed batch reactor. This is a clear indication that the use of batch test data for design is questionable since column experiments can provide more realistic aquifer material contact and therefore are believed to mimic *in situ* conditions better than batch tests.

Table 4.5.1. Summary of flow rates (mL/min) used for the hydrogen peroxide column trials.

Solution		EGDY	LC34-LSU	LC34-USU	MAAP	NIROP
H_2O_2	high	0.41	0.57	0.65	0.43	0.33
H_2O_2	low		0.26	0.23	0.22	
H_2O_2 + EDDS	high	0.41	0.57	0.65	0.22	0.33
H_2O_2 + EDDS	low		0.26	0.23		

Table 4.5.2. First appearance (in pore volumes) of the bromide tracer and hydrogen peroxide in the column effluent as defined by a detectable concentration in the effluent (0.05% for hydrogen peroxide, and 1.2 mg/L for Br).

Site	Flow Rate (mL/min)	Porosity	Tracer	H_2O_2 only		H_2O_2 + EDDS	
				1st flush	2nd flush	1st flush	2nd flush
LC34-LSU	0.26	0.32	0.64	0.80	0.69	0.72	0.69
LC34-LSU	0.57		0.67	0.77	0.70	0.74	0.67
LC34-USU	0.23	0.36	NA	0.82	0.63	0.69	0.63
LC35-USU	0.65		0.64	0.71	0.71	0.71	0.64
MAAP	0.22	0.32	0.61	2.65	0.95	0.95	0.75
MAAP	0.43		0.74	1.72	0.93	-	-

Table 4.5.3. Observations from the MAAP column experiments with a flow rate of 0.22 mL/min. The effluent pH, dissolved total Fe, and dissolved total Mn were measured after the hydrogen peroxide concentration in the effluent reached a stable value.

Run	First appearance of H_2O_2 in the effluent (PV)	pH	Dissolved Fe (mg/L)	Dissolved Mn (mg/L)	Dissolved Fe + Mn (mmol/L)
1st flush with the H_2O_2 solution only	2.65	3.3	1.44	17.07	0.34
2nd flush with the H_2O_2 solution only	0.95	3.7	0.45	2.15	0.05
1st flush with the EDDS + H_2O_2 solution	0.95	3.6	9.98	31.46	0.75
1st flush with the H_2O_2 solution only after the 2 hours H_2SO_4 flush	0.97	4.2	0.06	9.93	0.18

Table 4.5.4. Observed reaction rate coefficients from selected batch and column experimental systems. (Note: the normalized decomposition rate coefficient are obtained by dividing the corresponding rate coefficients by the aquifer material mass loaded in columns and batch reactors)

System			EDGY	LC34-LSU	LC34-USU	MAAP	NIROP
Observed (Unit: 1/day)	Column	H_2O_2	>210	10.97	11.83	2.27	>205
		H_2O_2 + EDDS	112.60	9.70	9.35	1.41	158.50
	Batch	H_2O_2	2.29	0.69	0.62	2.05	27.84
		H_2O_2 + EDDS	0.62	-	0.57	0.11	4.25
Normalized (Unit: 1/day/g)	Column	H_2O_2	>2.10	0.14	0.15	0.03	>2.59
		H_2O_2 + EDDS	1.13	0.13	0.12	0.02	2.01
	Batch	H_2O_2	0.15	0.05	0.04	0.14	1.86
		H_2O_2 + EDDS	0.04	-	0.04	0.01	0.28

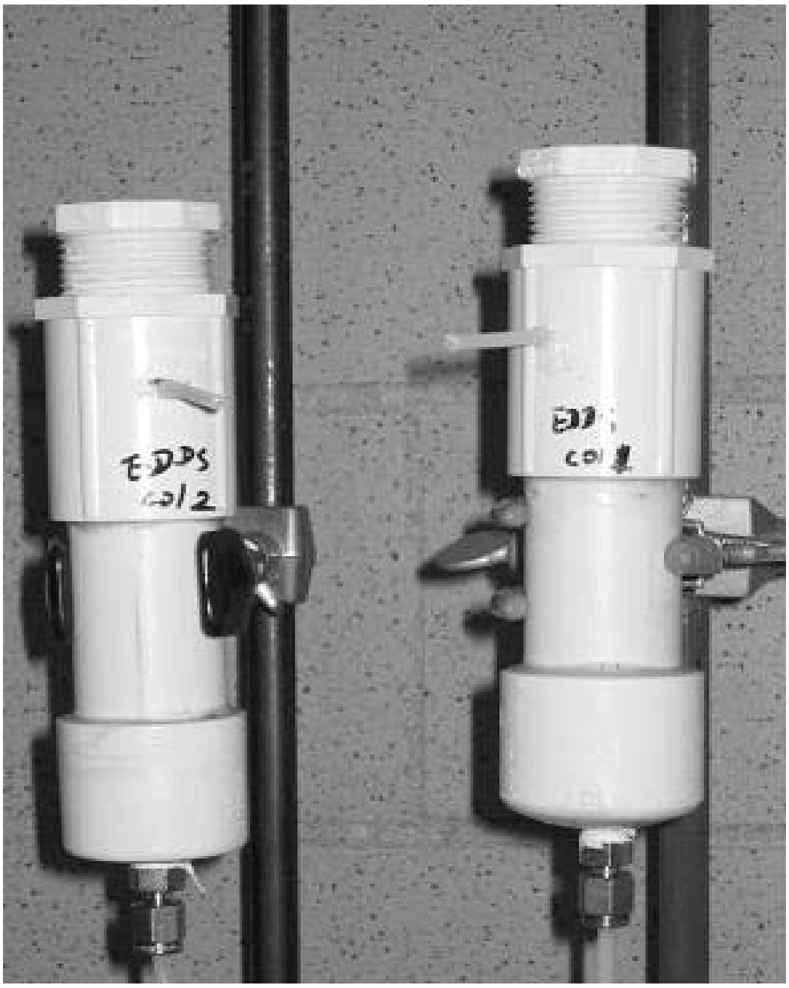

Figure 4.5.1. Typical setup for hydrogen peroxide column experiments.

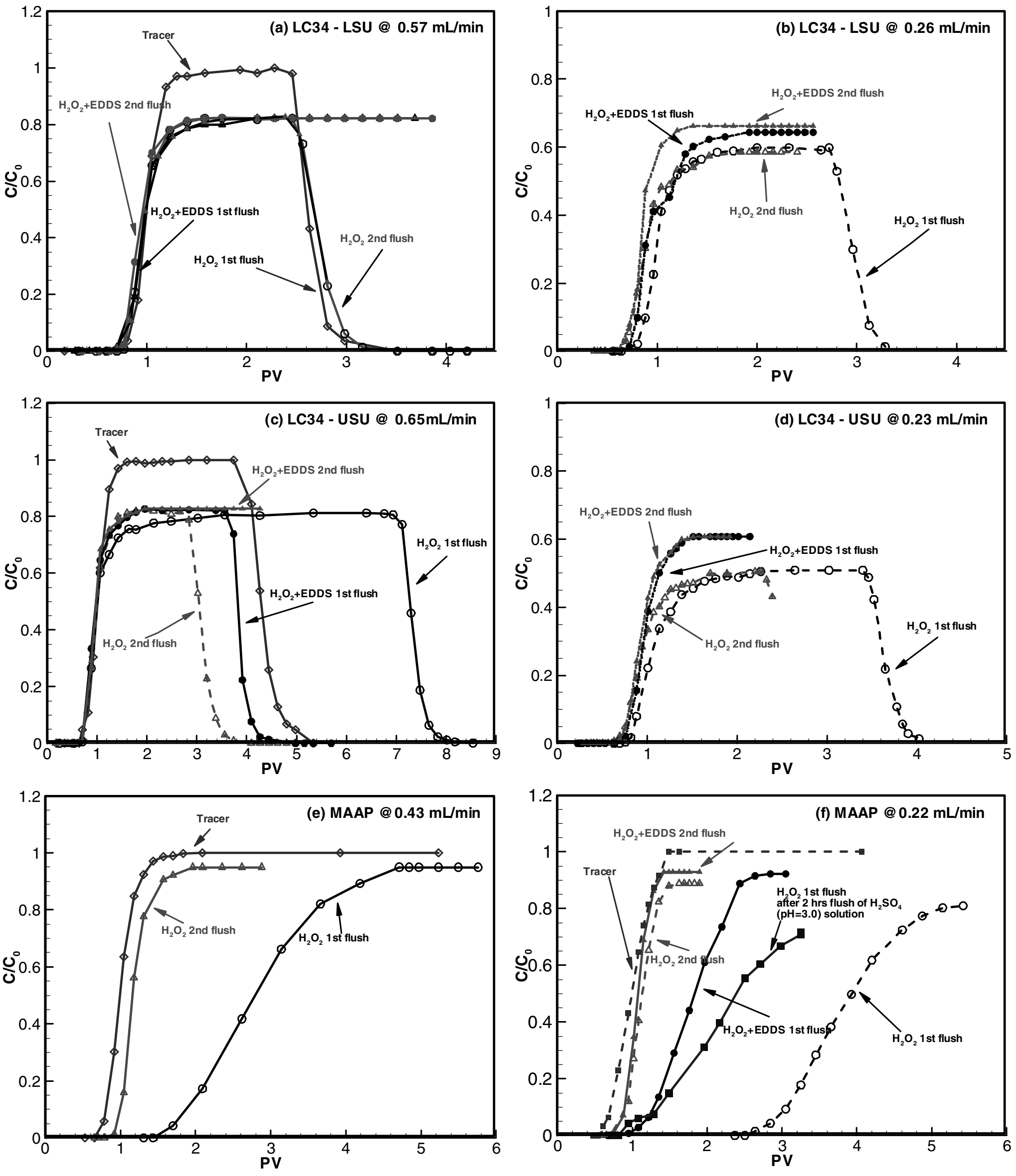

Figure 4.5.2. Hydrogen peroxide and bromide breakthrough curves for the column trials performed: (a) and (b) high and low flow rate for the LC34-LSU aquifer material, (c) and (d) high and low flow rate for the LC34-USU aquifer material, (e) and (f) high and low flow rate for the MAAP aquifer material. Also shown in (f) are results from the additional MAAP aquifer material column experiments where the column was first flushed with a H_2SO_4 solution (pH = 3.0) for two hours prior to a solution of hydrogen peroxide.

4.6 Modeling

Models are especially important in understanding the oxidant behavior in subsurface systems, not only because they allow the complex subsurface system to be economically investigated and the observed data to be reproduced, but also because they provide a tool for the appropriate design of ISCO systems.

The transport of hydrogen peroxide in a one-dimensional subsurface system can be described using the advective-dispersion equation as expressed by:

$$\frac{\partial C}{\partial t} = D\frac{\partial^2 C}{\partial x^2} - v\frac{\partial C}{\partial x} - k_{obs}C \tag{4.6.1}$$

where k_{obs} is the hydrogen peroxide decomposition rate coefficient [1/T]; v is the linear groundwater velocity [L/T] which is identical to the velocity of the tracer and can be calculated from q/θ (q is the Darcy velocity and θ is the effective porosity); $D = \alpha_x v$ is the coefficient of hydrodynamic dispersion; and α_x is the hydrodynamic dispersivity.

Under the boundary conditions of $C\big|_{x=0,t} = C_0$ and $C\big|_{x=\infty,t} = 0$, and the initial condition of $C\big|_{x,t=0} = 0$, the analytical solution for Eq. (4.6.1) is (Domenico and Schwartz, 1998):

$$\frac{C}{C_0} = \frac{1}{2}\exp \quad \frac{x}{2\alpha_x} \quad 1 - \quad 1 + \frac{4k_{obs}\alpha_x}{v} \quad ^{1/2} \quad \text{erfc} \quad \frac{x\text{-}vt(1+4k_{obs}\alpha_x / v)^{1/2}}{2(\alpha_x vt)^{1/2}} \tag{4.6.2}$$

For conservative species (e.g., bromide, chloride etc.), Eq.(4.6.2) can be simplified to:

$$\frac{C}{C_0} = \frac{1}{2} \text{erfc} \ \frac{x\text{-}vt}{2(\alpha_x vt)^{1/2}} \tag{4.6.3}$$

The hydrodynamic dispersive coefficient and effective porosity for each aquifer material packed column was estimated by calibration to the corresponding tracer breakthrough curve (BTC) using Eq.(4.6.3). The hydrogen peroxide BTC was calculated using Eq.(4.6.2) and the decomposition rate coefficient data listed in Table 4.5.4. The simulated BTCs for LC34-LSU, LC34-USU, and MAAP are shown on Figure 4.6.1 and agree well with the experimental observations, and in particular, the model is able to reproduce the first arrival of hydrogen peroxide and the rising portion of BTCs. This indicates that the model represented by Eq. (4.6.2) is adequate for describing the hydrogen peroxide transport in these column systems.

It is interesting to note that for the MAAP aquifer material, the model simulates the observations of the second flush much better than that of the first flush. As discussed in Section 4.5, accompanying the propagation of hydrogen peroxide in the column was the transport of dissolved Fe and Mn during each flushing episode, which continuously changed the aquifer material characteristics throughout both flushing episodes, but this change was more pronounced during the first flush. Acknowledging that the model given by Eq.(4.6.2) does not consider these changing characteristics (e.g., Fe and Mn contents), it is not surprising that the model generated adequate results for the second flush but not for the first flush. Compared to the MAAP aquifer material, the LC34-LSU and LC34-USU aquifer materials contain a relatively small amount of dissolvable Fe and Mn (see Figure 4.3.3), and therefore the characteristics associated with these two aquifer materials remained relatively stable, leading to relatively good comparison to the model BTCs.

Based on the above discussion, an accurate model for hydrogen peroxide transport in the subsurface appears to be the one which could account for the content and form of transition metals (Fe and Mn) in the system. However, quantifying this change of aquifer material characteristics is quite difficult and is perhaps the reason why there are very few mathematical models describing hydrogen peroxide transport in the subsurface.

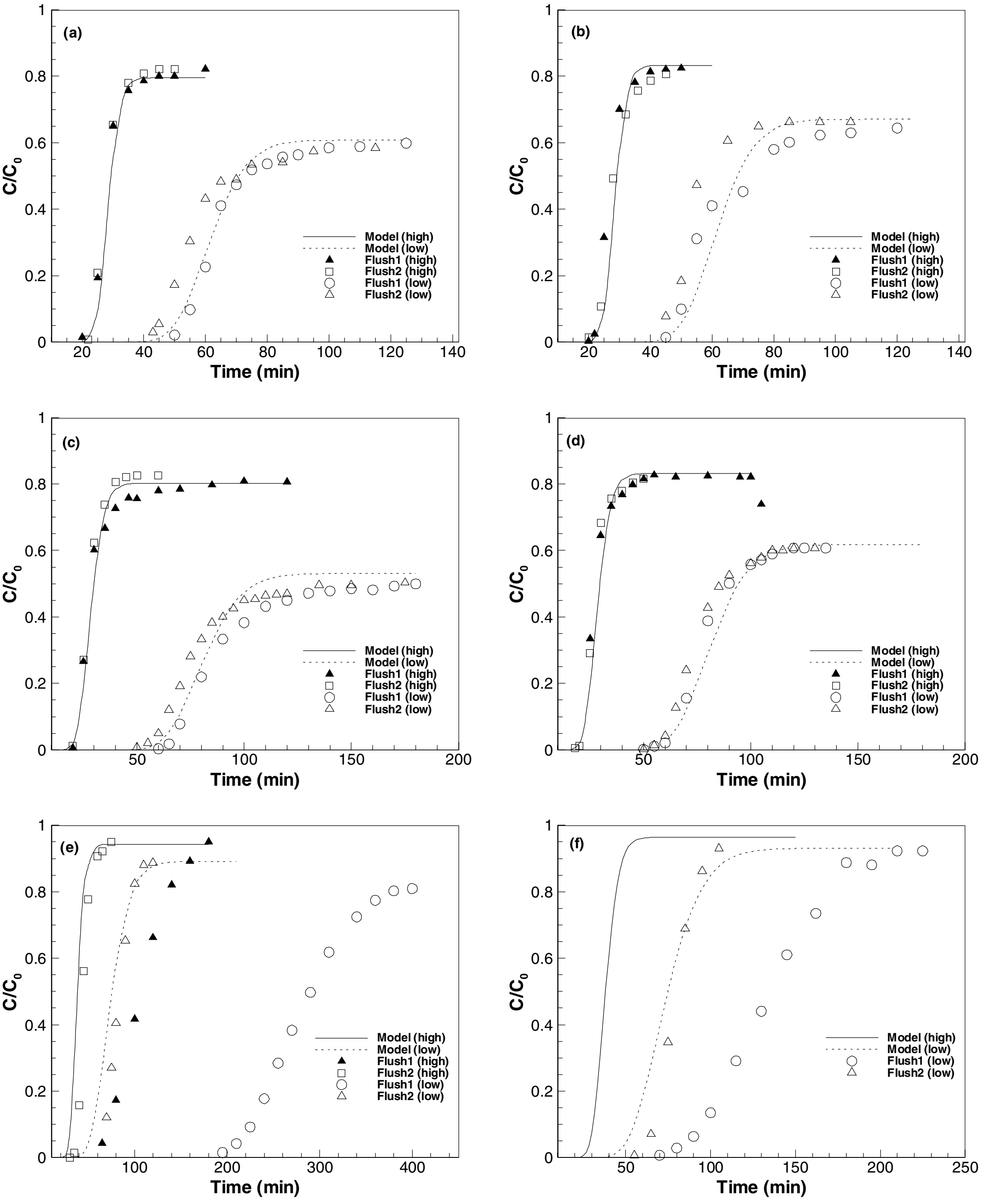

Figure 4.6.1. Calculated and observed hydrogen peroxide breakthrough curves for columns: (a) without and (b) with EDDS application for the LC34-LSU aquifer material, (c) without and (d) with EDDS application for the LC34-USU aquifer material, (e) without and (f) with EDDS application for the MAAP aquifer material.

Chapter 5

Conclusions and Implications, Recommendations, and Contributions

Based on a series of bench-scale experiments with the aquifer materials collected from 10 sites throughout the North America, a number of conclusions and implications, recommendations, and significant contributions concerning the interaction between aquifer materials and permanganate or hydrogen peroxide are summarized in this chapter.

5.1 Conclusions and Implications

5.1.1 Permanganate / Aquifer Material Interactions

A modified chemical oxygen demand (COD) test method using permanganate was developed and was demonstrated to be able to quickly and economically determine the maximum permanganate NOD. The maximum permanganate NOD observed from the long-term batch experiments ranged from approximately 2 to 100 g-$KMnO_4$ per kg of dry aquifer material, while for most aquifer materials the typical permanganate NOD was < 35 g/kg.

The mass loading ratio, the initial permanganate concentration, and the type and form of reduced aquifer material species were the main factors controlling permanganate consumption rates at the bench-scale. In terms of aquifer material characteristics, an empirical expression for the maximum permanganate NOD at an initial permanganate concentration of 20 g/L was developed.

The overall long-term permanganate NOD profiles observed from the batch experiments demonstrated a characteristic fast rise followed by a lengthy period of slow increase. Based on these observations and other supporting evidence, a conceptual kinetic NOD model consisting of a fast and a slow reactive component was developed. The end-product of permanganate reduction, manganese dioxide (MnO_2) was deemed to play an important role in the consumption of permanganate through both an auto-catalytic reaction and passivation due to manganese dioxide coatings on the solid grain surfaces.

The results from a series of short-term kinetic experiments demonstrated that permanganate consumption is controlled a fast reaction occurring on the order of minutes to hours. This reaction does not necessarily follow a first-order rate law. The OAM was found to deplete quickly on the order of minutes and followed a pseudo-first order reaction law. The reaction parameters (rate coefficients and reaction order) were found to correlate weakly with aquifer material characteristics.

The breakthrough curves (BTCs) generated from permanganate column experiments demonstrated that permanganate consumption appears to be controlled by three different reaction rates: a fast reaction rate that is responsible for the distinct delay between the first appearance of a conservative tracer and permanganate, an intermediate rate that controls the shape of the rising limb of the BTC, and a slow reaction rate that controls the shape of the BTC tail. It is likely that different reactive species in aquifer materials are responsible for these three reactions: the fast reaction may be controlled by labile organic species and easily dissolvable reduced metals loosely attached on the grain surfaces, the intermediate reaction may be controlled by organic species and reduced inorganic compounds bound on the grain surfaces, and the slow reaction is associated with slowly reacting organic matter and/or minerals containing reduced elements (e.g., Fe, Mn, and S etc.) internal to the grains.

Permanganate consumption in the column systems demonstrated some similarities to the consumption in the batch systems (e.g., sensitive to source concentrations and contact time, and controlled by a fast reaction over a relatively short period). However, NOD values estimated from column experiments are considerably less than those from batch experiments, and therefore the results from batch experiments should be used with caution for design. A good linear relationship between the 7-day permanganate NOD observed from batch systems and the total permanganate NOD estimated from column systems was developed and can be used to estimate the column permanganate NOD from batch data.

The findings from the study suggest that for initial site screening and design purposes, the maximum permanganate NOD can be quickly determined by the proposed permanganate COD test, or estimated through the developed empirical expressions using the corresponding dichromate COD value and TOC content. However, since the kinetic nature of permanganate NOD reactions cannot be ignored and variations in test design will impact the reported NOD values, batch experimental determination of intermediate permanganate NOD values should employ the expected *in situ* permanganate concentration to be used in the ISCO application along with varying permanganate to aquifer solid mass ratios. The estimation of *in situ* permanganate NOD can then be achieved by extrapolation, assuming the same controlling factors are expected to affect oxidant stability *in situ*. In addition to experimental measurements, the intermediate NOD can also be estimated either from empirical equations or on the basis of the developed kinetic models.

Both batch and column results indicated that a majority of the permanganate consumption occurred during a relatively short period after the start of experiments suggesting that there is an optimal approach to control the unproductive consumption of permanganate by aquifer materials through multiple low concentration oxidant injection episodes.

5.1.2 Hydrogen Peroxide / Aquifer Material Interactions

The batch system results with eight aquifer materials indicated that hydrogen peroxide concentration decreases in an approximately exponential fashion, and follows a pseudo first-order mass action law. *In situ* low pH control would be difficult to achieve during the injection of hydrogen peroxide into aquifer materials with high buffering capacities.

The decomposition of hydrogen peroxide is also highly correlated with the amorphous Fe and Mn content rather than their crystalline forms, and is weakly correlated with the TOC content. It is likely that humic acids rather than all types of natural organic matter are responsible for hydrogen peroxide decomposition. Moreover, the data shows that natural organic matter may have a negligible impact on hydrogen peroxide decomposition for low TOC aquifer materials or may accelerate the hydrogen peroxide decomposition for high TOC aquifer materials. A multiple linear regression analysis approach was used to generate various functional relationships that relate the hydrogen peroxide decomposition rate coefficient to aquifer material properties (i.e., TOC, total Fe and Mn or amorphous Fe and Mn contents, surface area, cation exchange capacity), and these relationships can be used as predictive tools to estimate hydrogen peroxide decomposition rate coefficients.

The results from both batch and column experiments clearly demonstrated that the addition of EDDS was able to stabilize hydrogen peroxide in the presence of the aquifer materials used in this study. This is especially true for the EGDY aquifer material (high TOC and high transition metal contents) and the NIROP aquifer material (high carbonates, CEC and surface area, and soil pH) where it was unable to propagate hydrogen peroxide through a 10-cm long column with the *hydrogen peroxide only* solution, but were able to achieve some level of breakthrough with the *hydrogen peroxide and EDDS* solution. Moreover, the batch experimental results indicated that hydrogen peroxide can be significantly stabilized with EDDS or EDTA for those aquifer materials either with a relatively low TOC content or with high dissolvable Fe and Mn contents.

In general, hydrogen peroxide decomposition rate coefficients from the column data were significantly higher than those generated from the batch test data due to the solution/aquifer material contact differences between a column and a well-mixed batch reactor, indicating that care must be taken for the direct use of batch results. No scaling relationships between the batch and column test results were determined, suggesting little transferability between these two systems.

The release of dissolvable Fe and Mn from aquifer solids and the transport of dissolved metals (Fe and Mn) were investigated. Because Fe and Mn can react with hydrogen peroxide depending on their form (e.g., solid and dissolved) and content in the system, this migration of dissolved metals is expected to play an important role on the behavior of hydrogen peroxide within subsurface environments. It was also found that the application of an acidic solution flush prior to the hydrogen peroxide injection could enhance the mobility of dissolvable Fe and Mn, and therefore induce benefits for CHP-ISCO applications by providing a favorable pH condition as well as reducing the unproductive depletion of hydrogen peroxide.

A simple advective-dispersive mathematical model was able to describe the hydrogen peroxide transport in the column systems, and was especially able to capture the first arrival of hydrogen peroxide and the rising portion of the BTCs. However, a comprehensive model for the hydrogen peroxide transport in the subsurface appears to be the one which could be coupled with the content and form of transition metals (Fe and Mn) in the system.

The study suggests that at least two ways could be used to control the unproductive depletion of hydrogen peroxide: (1) use of hydrogen peroxide stabilizers especially green stabilizers (i.e., EDDS), and/or (2) for aquifer systems with low buffering capacity, use of an acid flush prior to the hydrogen peroxide injection. Finally, due to little transferability between batch and column data, data from batch tests might be misleading and column systems should be used to determine hydrogen peroxide decomposition reaction rate coefficients.

5.2 Recommendations

The results presented in this thesis highlight the ability of enhancing the stability of hydrogen peroxide with ‘green’ stabilizers, and the importance of considering the kinetic nature of permanganate NOD reaction process in ISCO design and application. Although some scaling relationships between batch and column results were developed, both permanganate and hydrogen peroxide experiments clearly indicate that batch test data for ISCO system design should be used with care since column experiments are believed to mimic *in situ* conditions better. Future effort is required to develop scaling relationships from the batch and/or column results to pilot or field situations.

Although an empirical NOD expression with a 20 g/L $KMnO_4$ solution was developed in this thesis study, the lack of proper data for other concentrations limits the development of a unified empirical expression for permanganate NOD. To achieve such an empirical NOD expression, additional experiments need to be performed using a range of permanganate concentrations. Following a similar procedure for developing the empirical expression with respect to the 20 g/L $KMnO_4$ solution, a series of NOD expressions corresponding to other permanganate concentrations could be developed. A correlation analysis relating (the parameters in) these expressions to permanganate concentrations could be then performed and to determine a unified empirical NOD expression.

Further research on the theoretical permanganate NOD kinetic model is needed. The nature of three kinetic regions of permanganate consumption observed in the column experiments has not yet been mathematically expressed by a unified kinetic model. The long-term permanganate NOD kinetic expression was only a conceptual model, and the complete role of manganese dioxide (MnO_2) in influencing the permanganate / aquifer material interactions remains unsolved. Moreover, the kinetic NOD expressions proposed in this thesis describe separately the permanganate consumption over a short-term (minutes to hours) and a long-term (> one week). As such, future research should focus on a construction of a comprehensive kinetic model accounting for both short-term and long-term permanganate consumption.

This study showed that comprehensive modeling of hydrogen peroxide transport in the subsurface will be hampered by the lack of sufficient knowledge concerning the role of transition metals (i.e., Fe and Mn), and therefore this area deserves more effort in the future. To model permanganate transport, a simple first-order permanganate NOD expression is simply not sufficient to capture the observed consumption profile, and thus the kinetic models presented in this study are recommended.

Given the applicability of EDDS to enhance hydrogen peroxide stability in the presence of uncontaminated aquifer materials, more research is required to demonstrate its application for contaminated aquifer materials. Experimental data are needed to support the persistence of EDDS (or other potential hydrogen peroxide stabilizers) throughout a complete ISCO application. Moreover, to achieve CHP-ISCO cost-effective implementations, optimal dosage of the hydrogen peroxide stabilizer also deserves attention.

It is uncertain whether biological activity plays a role in hydrogen peroxide decomposition in the presence of aquifer materials. Many questions such as how and what microorganisms present in the subsurface affect the fate of hydrogen peroxide need to be addressed.

5.3 Significant Contributions

- A multi-site comprehensive investigation into the interaction between aquifer materials and two of the most commonly used ISCO oxidants, permanganate and hydrogen peroxide was performed in this study. Robust bench-scale methods were proposed to quantify permanganate consumption and hydrogen peroxide decomposition in the presence of aquifer materials.

- A range of the maximum permanganate NOD values by typical aquifer materials was presented, and empirical expressions for permanganate NOD were developed. The study revealed the main controlling factors (mass loading ratio, the initial permanganate concentration, and the type and form of reduced aquifer material species) for permanganate consumption rates at the bench-scale.

- An innovative and economical method using a permanganate COD test was developed and demonstrated to quickly estimate permanganate NOD for ISCO site screening and initial design purposes.

- A comprehensive investigation into the kinetic behavior of permanganate in both batch and column systems was performed. The results showed the multiple-component kinetic nature of permanganate consumption by aquifer materials. Also for the first time, this study derived the kinetic rate law for describing the permanganate reaction with aquifer materials, and experimentally investigated this kinetic reaction over a short-term scale (minutes to hours).

- An evaluation on the potential applicability of an environmentally-friendly chelating reagent (i.e., EDDS) to stabilize hydrogen peroxide in the presence of various aquifer materials for ISCO groundwater remediation was performed. The results showed that EDDS appears to be promising for *in situ* applications involving the injection of hydrogen peroxide into the subsurface environment.

- A comparative investigation of the behavior of hydrogen peroxide and associated aquifer material characteristics in both batch and column systems was performed. Based on batch system results, a series of empirical expressions for the hydrogen peroxide decomposition coefficient in terms of various aquifer material characteristics was developed. These expressions can be used as tools for predicting hydrogen peroxide decomposition behavior in the presence of aquifer.

- Batch-to-column scaling factors were developed to extend the results obtained from relatively fast and economical batch tests to physically representative *in situ* conditions. These scaling relationships could serve as an engineering tool for ISCO design and implementations.

Appendix A

Grain Size Distributions

The grain size distribution was determined by ASTM Method D422-63 with a 152 hydrometer.

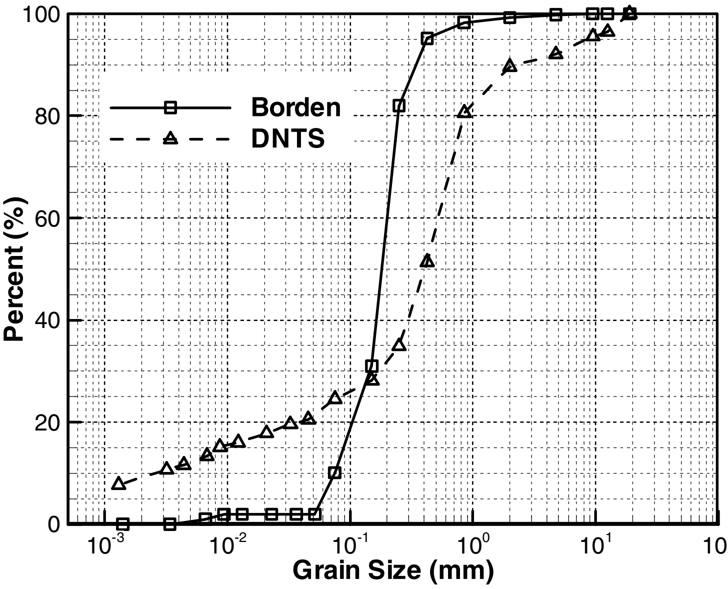

Figure A.1 Grain size distribution for the Borden and DNTS aquifer materials

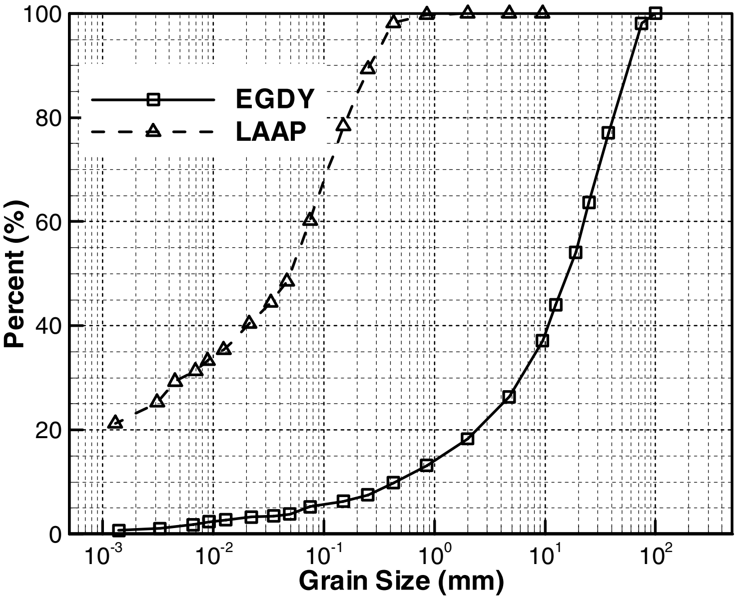

Figure A.2 Grain size distribution for the EGDY and LAAP aquifer materials

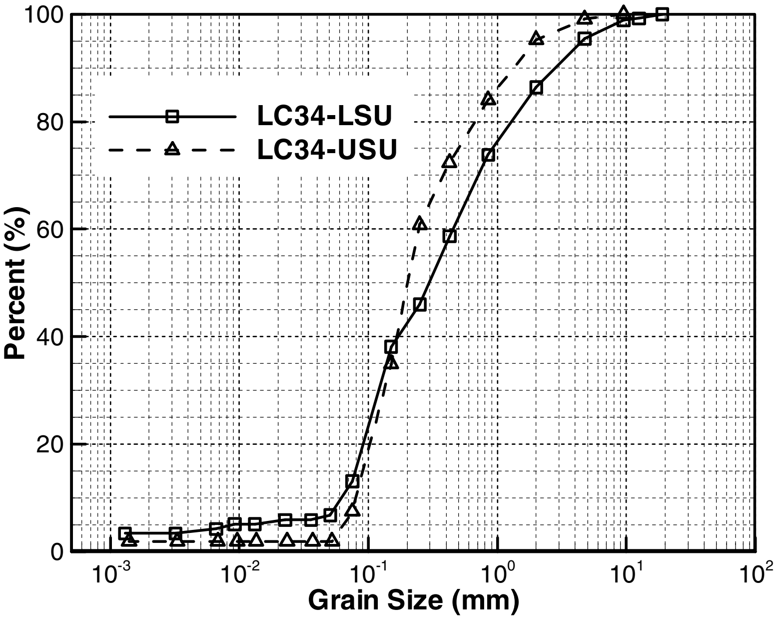

Figure A.3 Grain size distribution for the LC34-LSU and LC34-USU aquifer materials

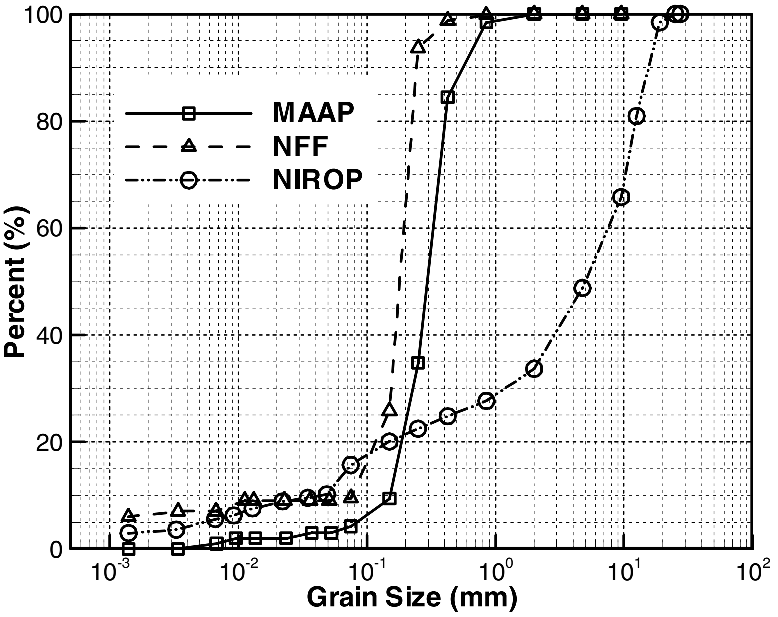

Figure A.4 Grain size distribution for the MAAP, NFF, and NIROP aquifer materials

Appendix B
Interpretation of XRD Diffractograms

Using a computerized search, each sample's diffractogram was compared to the powder diffraction file maintained by the International Centre for Diffraction Data (ICDD). The software searches for all minerals composed of elements chosen by the user and then overlays the reference diffractogram onto the sample diffractogram. Several different sets of elements were used as outlined below. Elements that are underlined and in bold font are "must contain" elements for the reference file search. Elements in normal type are "may contain" elements.

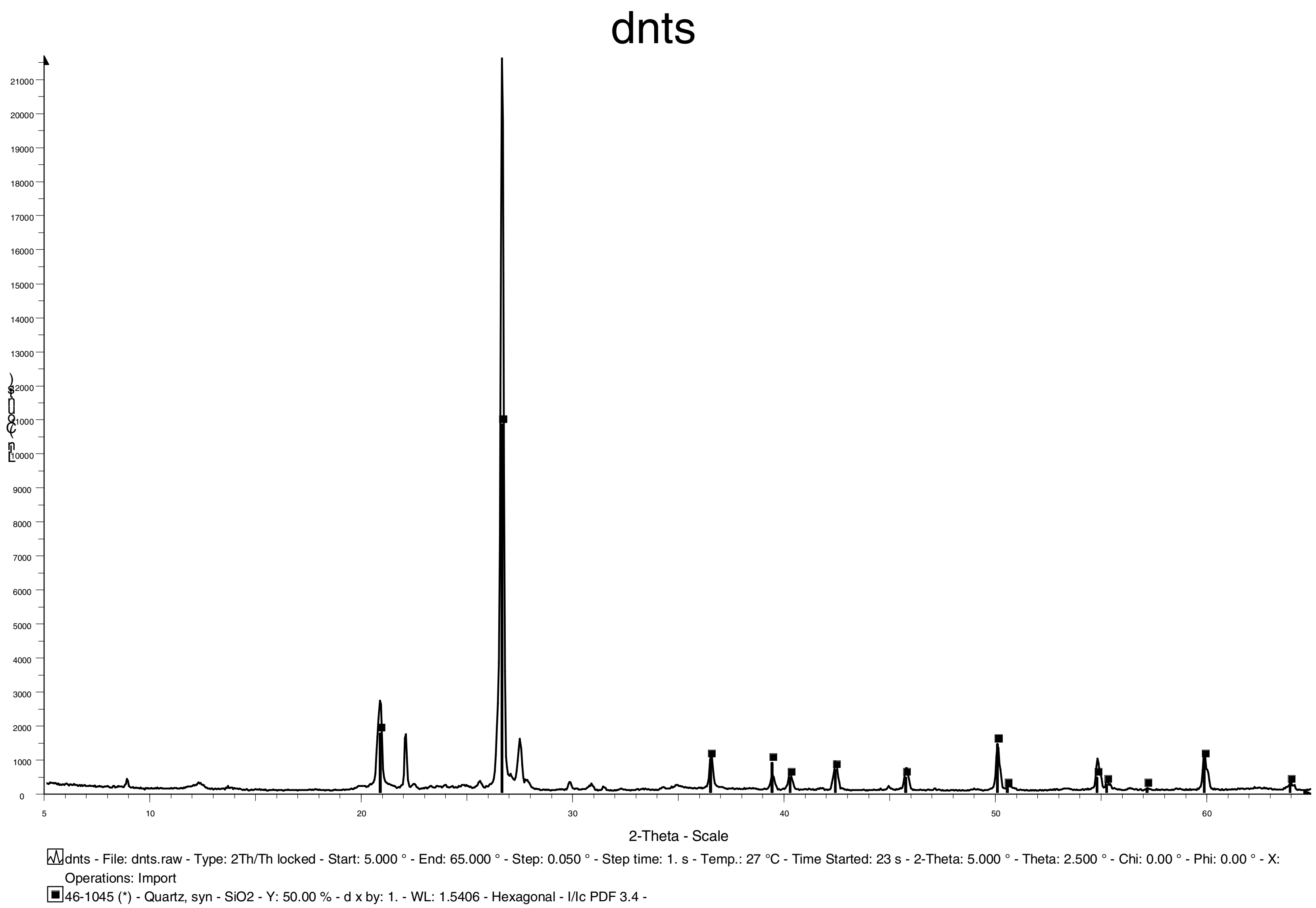

Figure B.1. XRD trace for the DNTS aquifer material.

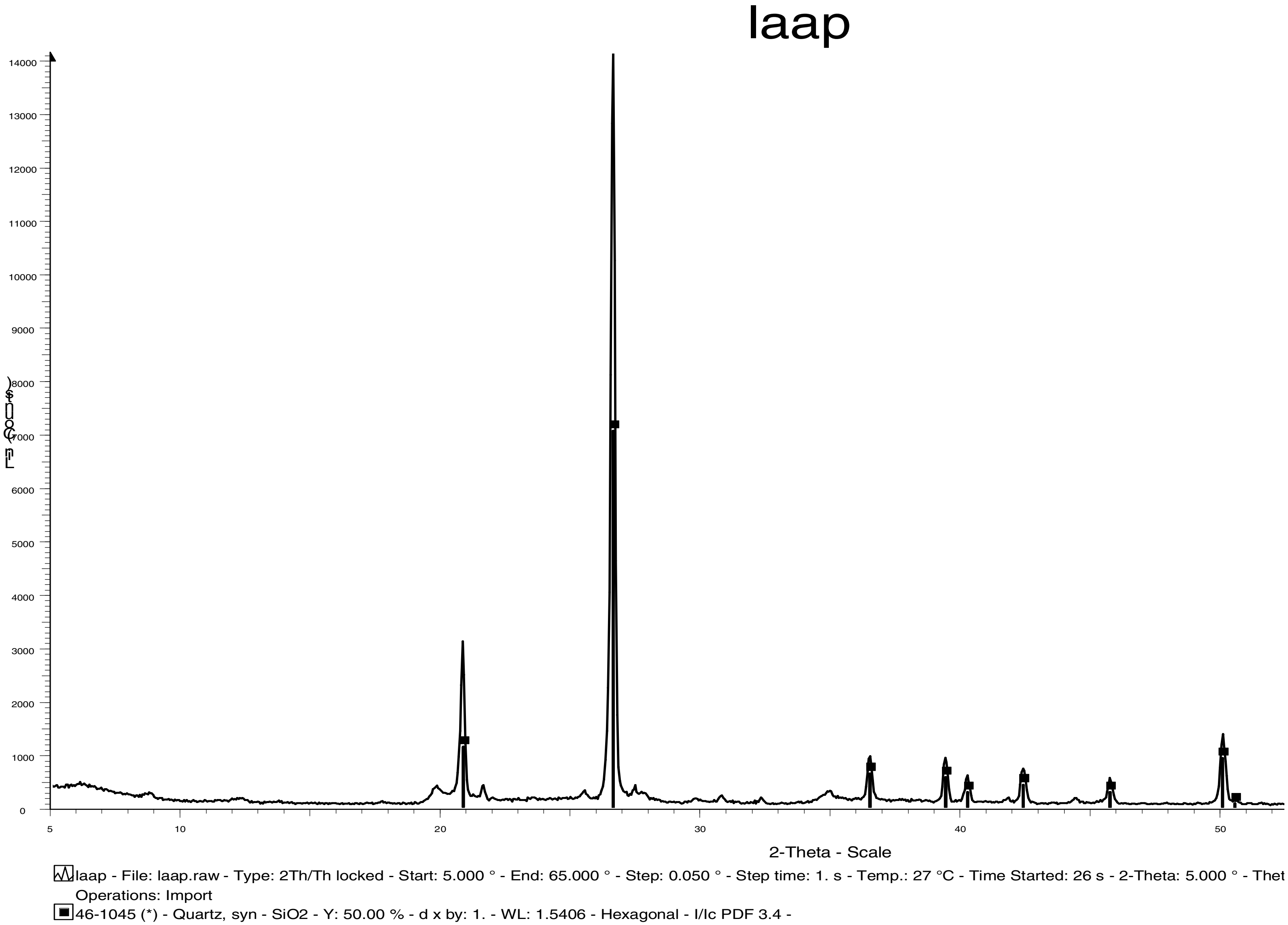

Figure B.2. XRD trace for the LAAP aquifer material

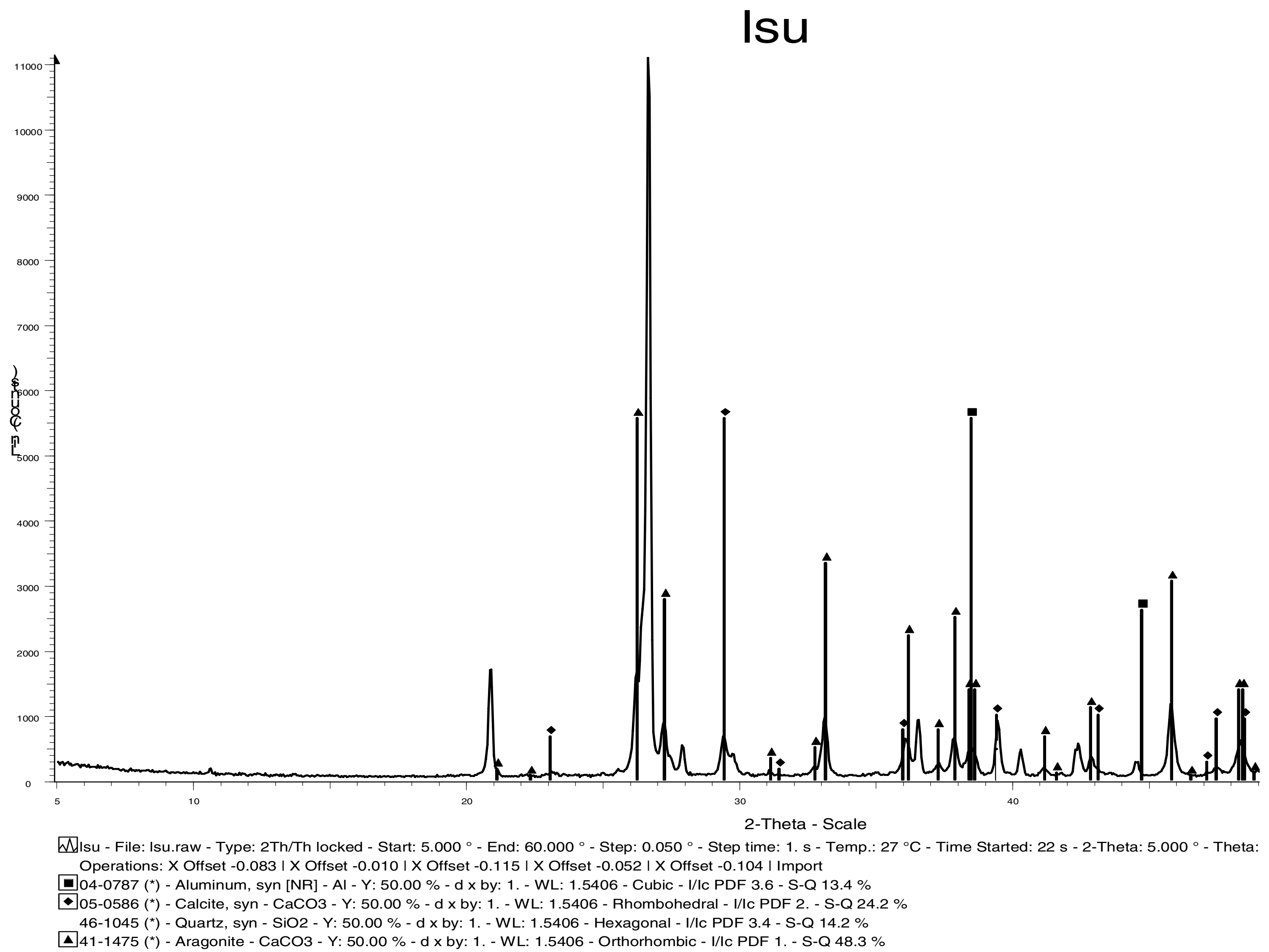

Figure B.3. XRD trace for the LC34-LSU aquifer material.

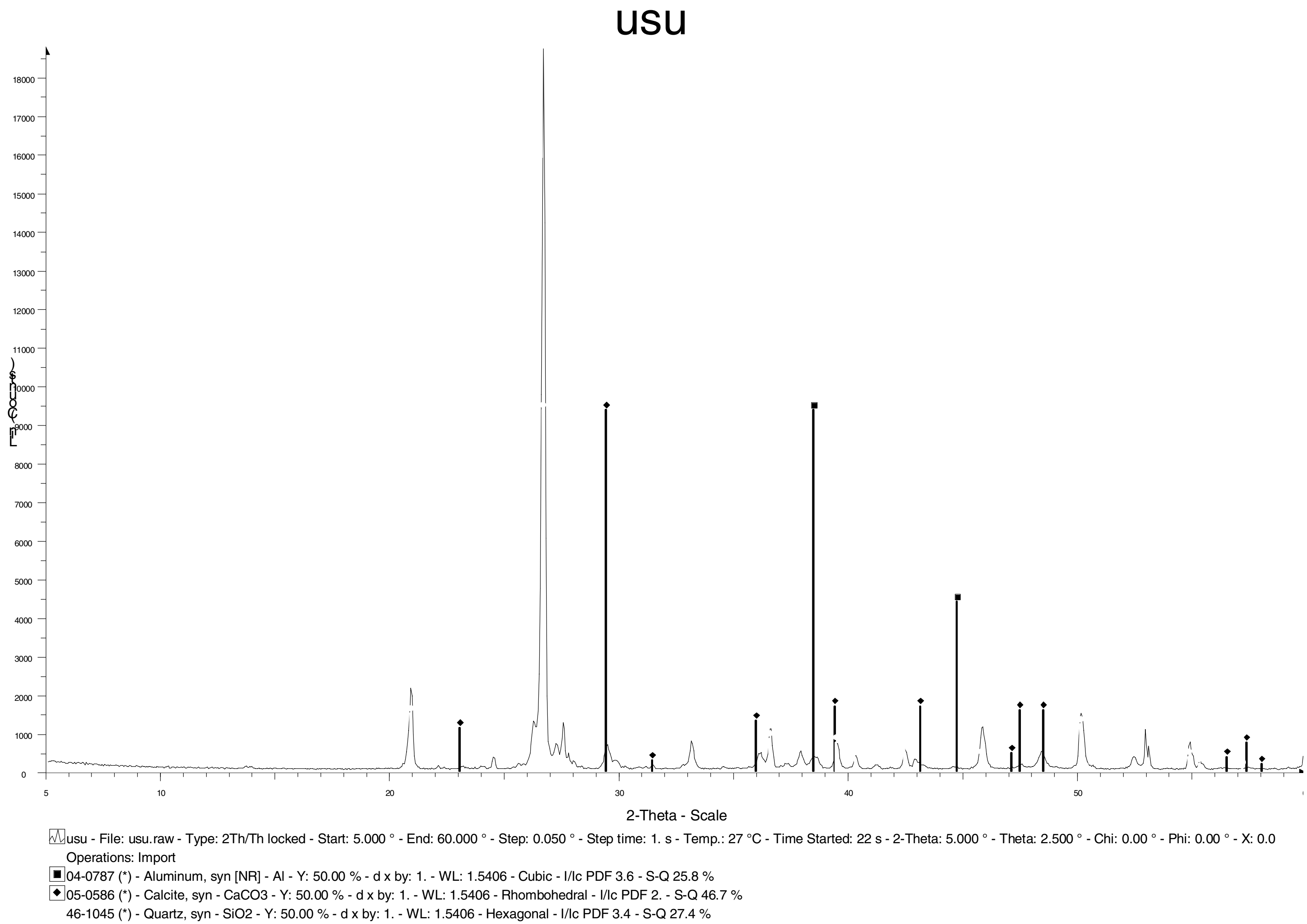

Figure B.4. XRD trace for the LC34-LSU aquifer material.

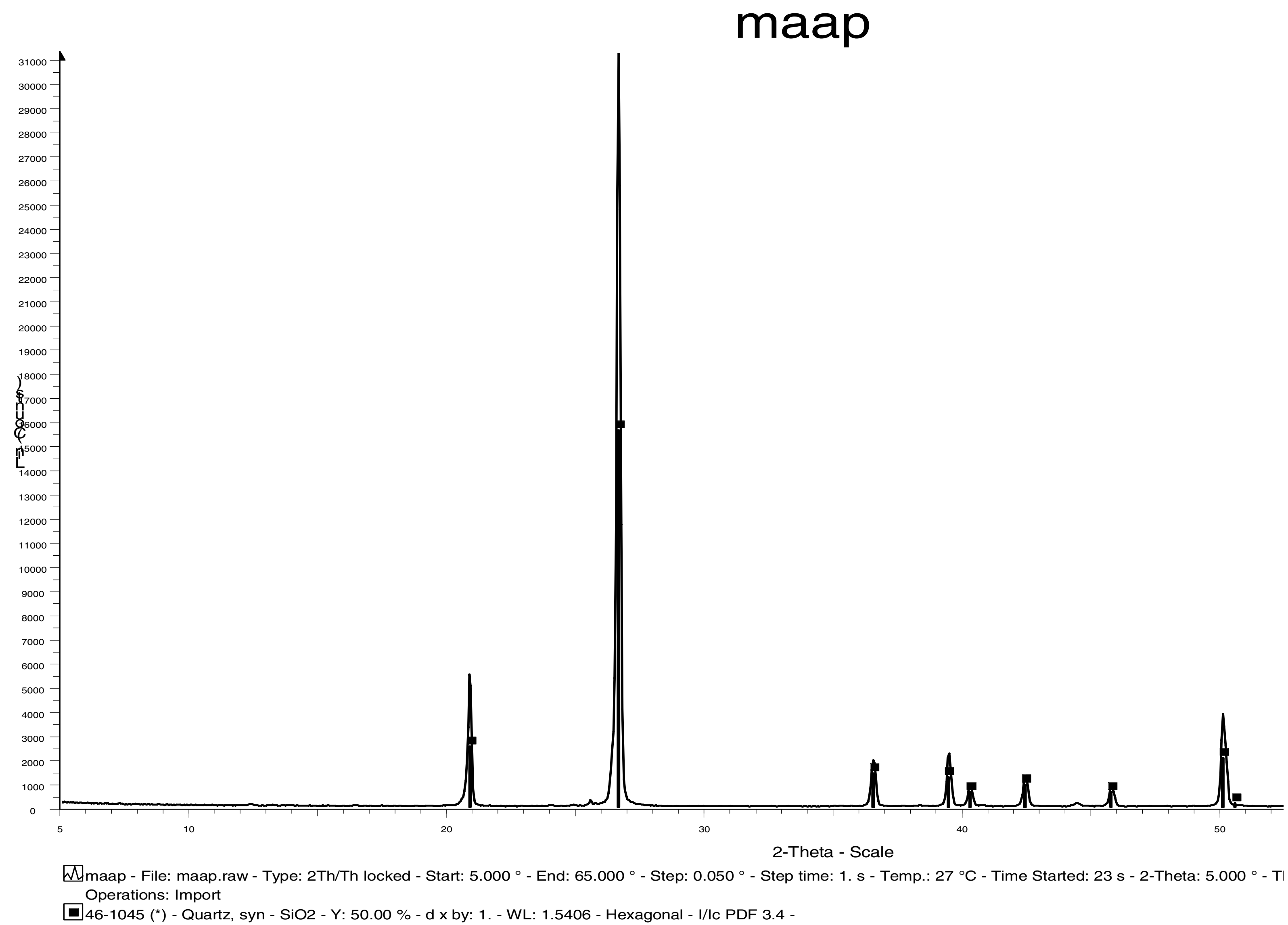

Figure B.5. XRD trace for the MAAP aquifer material.

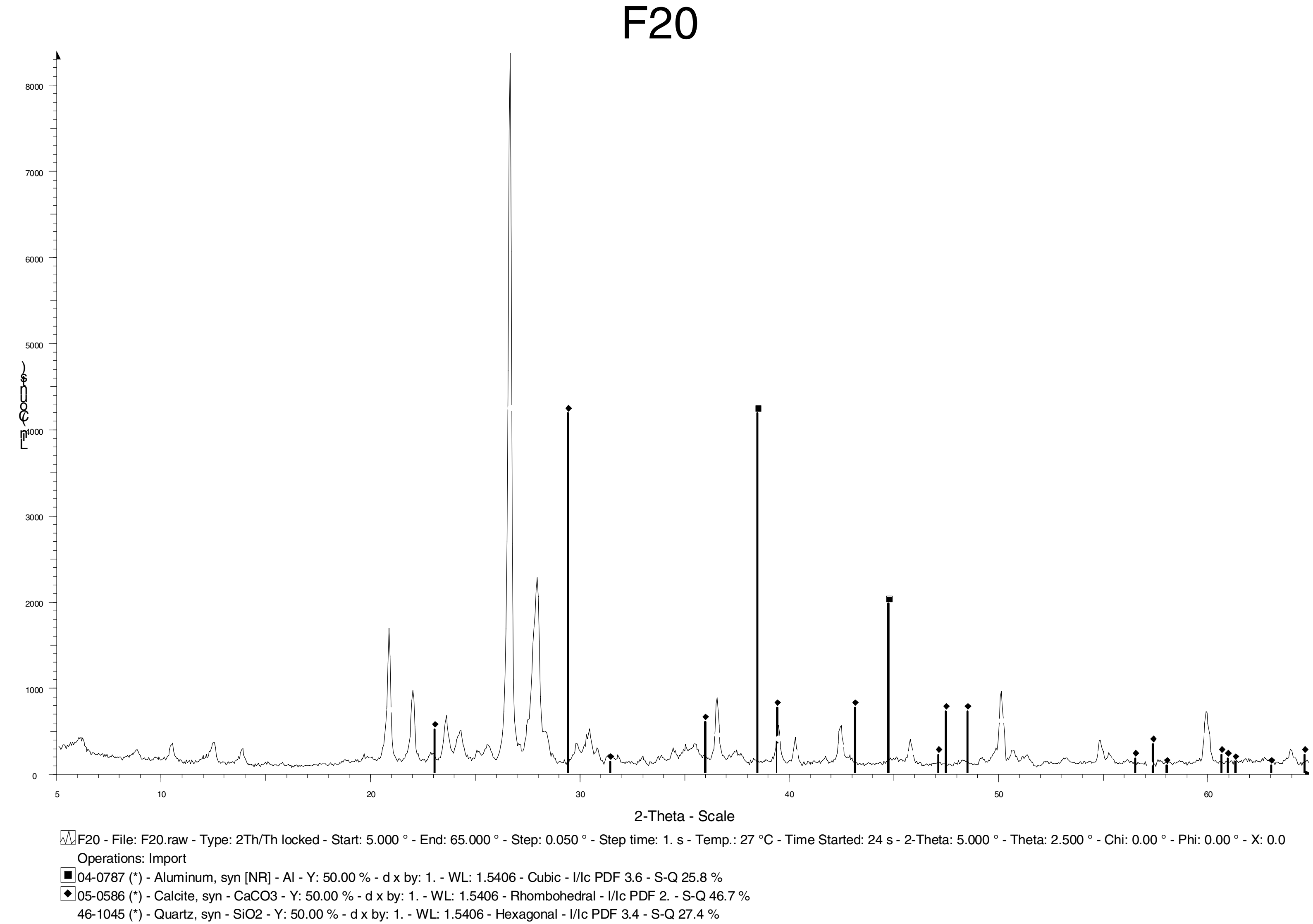

Figure B.6. XRD trace for the NFF aquifer material.

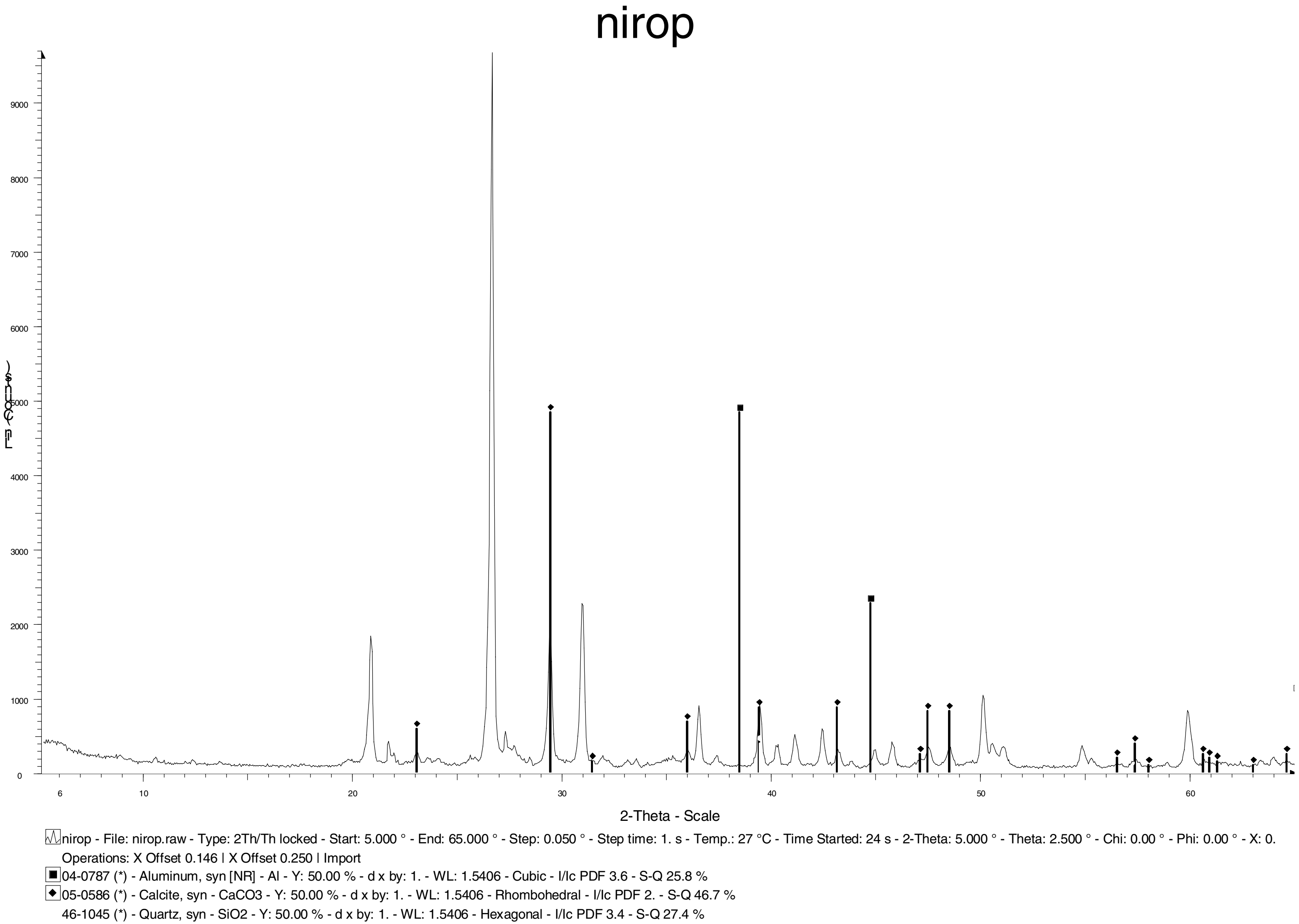

Figure B.9. XRD trace for the NIROP aquifer material.

Appendix C
Air Drying Investigation

Average reduction capacity results from the air drying investigation (all values in g $KMnO_4$/kg). Five replicates were used for each testing method. It needs to be pointed out that the dichromate COD and 7-day permanganate NOD values for each air-dried aquifer material listed in the following table might be different from those in other parts of this thesis. It is likely because the air-dried sub-samples used in other parts of this thesis were randomly taken from the homogenized bulk aquifer materials, as is not the case for the investigation conducted here.

	Method	DNTS	LAAP	MAAP	Borden	NFF	NAS-Dallas
air dried	Dichormate - COD	3.87 ± 1.32	6.20 ± 0.68	4.41 ± 2.86	13.87 ± 1.99	58.09 ± 1.33	17.55 ± 2.15
	Permanganate - COD	4.86 ± 1.21	2.10 ± 0.68	2.52 ± 1.38	2.14 ± 1.33	62.03 ± 3.99	9.17 ± 0.57
	Permanganate - NOD						
	(0.375 g/mL)	1.33 ± 0.27	0.97 ± -	0.35 ± 0.20	1.73 ± 0.28	6.38 ± 1.61	2.29 ± 0.41
	(0.750 g/mL)	1.30 ± 0.54	0.98 ± -	0.13 ± 0.06	1.77 ± 0.22	-	-
N_2 dried/air exposed	Dichormate - COD	4.97 ± 0.80	-	-	11.06 ± 1.09	61.87 - 2.98	-
	Permanganate - COD	5.34 ± 1.66	-	3.12 ± 1.22	1.18 ± 0.48	-	-
	Permanganate - NOD						
	(0.375 g/mL)	2.00 ± 0.07	-	0.65 ± 0.51	1.29 ± 0.35	-	-
	(0.750 g/mL)	1.85 ± 0.13	-	0.11 ± 0.08	1.44 ± 0.10	-	-
N_2 dried	Dichormate - COD	5.00 ± 1.22	6.36 ± 0.44	6.72 ± 5.66	11.84 ± 0.77	68.22 ± 0.86	18.27 ± 2.20
	Permanganate - COD	5.36 ± 1.18	-	4.29 ± 1.52	1.23 ± 0.49	-	8.34 ± 1.14
	Permanganate - NOD						
	(0.375 g/mL)	1.75 ± 0.24	1.16 ± -	0.22 ± 0.08	1.42 ± 0.01	14.19 ± 2.45	2.51 ± 0.24
	(0.750 g/mL)	1.67 ± 0.12	1.49 ± -	0.20 ± 0.09	1.26 ± 0.21	-	-

Appendix D

Normalization of Long-Term NOD

Normalized long-term NOD data and their best curve-fitting under different concentrations.

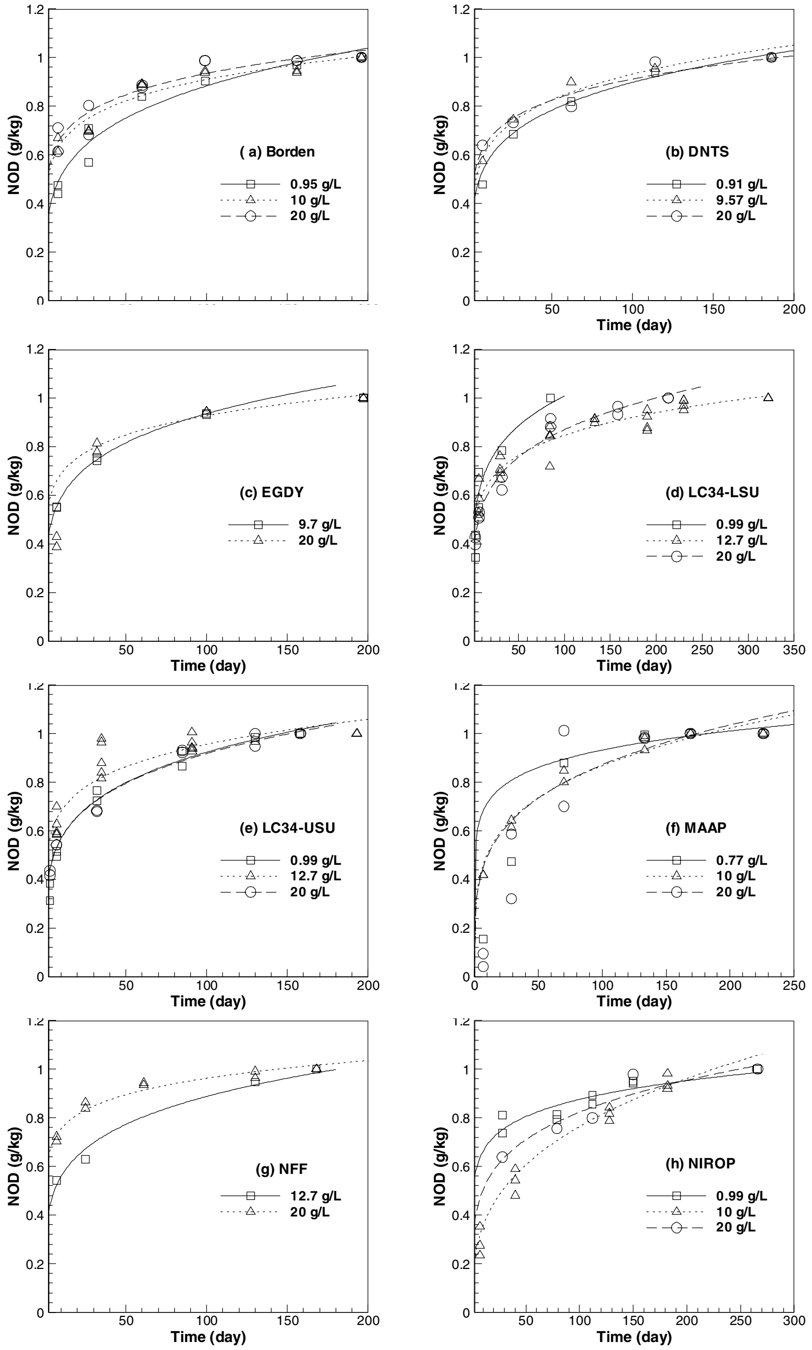

References

Adam, M. L.; Comfort, S. D.; Morley, M. C.; Snow, D. D., 2004. Remediating RDX-contaminated groundwater with permanganate: Laboratory investigations for the Pantex perched aquifer. Journal of Environmental Quality, 33, pp.2165-2173.

Almendros, G., Gonzalez-Vila, F. J., and Martin, F., 1989. Room temperature alkaline permanganate oxidation of representative humic acids. Soil Biology and Biochemistry, 21 (4), pp. 481-486.

Almendros, G. and Leal, J.A., 1990. An evaluation of some oxidative degradation methods of humic substances applied to carbohydrate-derived humic-like polymers. Journal of Soil Science, 41, pp. 51-59.

Andersen, M.S., Larsen, F., and Postma, D., Pyrite oxidation in unsaturated aquifer sediments: reaction stoichiometry and rate of oxidation. Environmental Science and Technology, 35, pp. 4074-4079.

APHA (American Public Health Association and America Water Works Association), 1946. Standard Methods for the Examination of Water and Sewage, 9th Ed., New York.

APHA (American Public Health Association and America Water Works Association), 1998. Standard Methods for the Examination of Water and Sewage, 20th Ed., New York.

Appelo, C.A.J. and Postma, D., 1996. Geochemistry, groundwater and pollution. A.A.Balkema/Rotterdam/Brookfield.

ASTM, 1990. ASTM Book of Standards on Road and Paving Materials. American Society for Testing and Materials.

Baciocchi, R., Boni, M.R., and D'Aprile, L., 2003. Hydrogen peroxide lifetime as an indicator of the efficiency of 3-chlorpphenol Fenton's and Fenton-like oxidation in soils. Journal of Hazardous Matters, B96, pp.305-329.

Bahr, J. M. and Rubin, J., 1987. Direct comparison of kinetic and local equilibrium formulations for solute transport affected by surface reactions. Water Resource Research, 23(3), pp. 438-452.

Ball, W.P., Buehler, CH., Harmon, T.C., Mackay, D.M., and Roberts, P.V., 1990. Characterization of a sandy aquifer material at the grain size scale. Journal of Contaminant Hydrology, 5, pp. 253 -295.

Banwart, S.T., 1999. Reduction of iron minerals by natural organic matter in groundwater. Geochemical et Cosmochimica Acta, 63(19/20), 2919-2928.

Barbash, A.M., Hoag, G.E., and Nadim, F., 2006. Oxidation and removal of 1,2,4,-trichilorobenzene in a sorption-desorption experiment. Water, Air, and Soil Pollution,172, pp.67–80

Barcelona, M.J. and Holm, T., 1991. Oxidation – reduction capacities of aquifer solids. Environ. Sci. Technol., 25(9), 1565-1572.

Barcelona, M.J., Holm, T., Schock, M.R., and George, G.F., 1989. Spatial and temperal gradients in aquifer oxidation-reduction conditions. Water Resource Research, 25(5), pp.991-1003.

Barnett, V. and Lewis, T., 1994. Outliers in Statistical Data. John Wiley and Sons, 1994.

Bell, M.J., Moody, P.W., Connolly, R.D., and Bridge, B.J., 1998. The role of active fractions of soil organic matter in physical and chemical fertility of Ferrosols. Australian Journal of Soil Research, 36, pp.809-819.

Blair, G.J., R.D.B. Lefroy, L. Lisle, 1995. Soil carbon fractions based on their degree of oxidation and the development of carbon management index for agricultural systems. Australian Journal of Agricultural Research, 46, 1459-1466.

Boyles, W., 1997. The Science of Chemical Oxygen Demand. Technical Information Series, Booklet No.9, Hach Company, Loveland, CO.

Brennan, E.W. and Lindsay, W.L., 1996. The role of pyrite in controlling metal ion activities in highly reduced soils. Geochimica et Cosmochimica, v. 60 (19), pp. 3609-3618.

Brownawell, B.J., Chen, H., Collier, J.M., and Westall, J.C., 1990. Adsorption of organic cations to natural materials. Environmental Science and Technology, 24, pp.1234-1241.

Burtle, J., A.M. Buswell, 1937. Oxygen Demand Studies. Sewage Works Journal, 9: 224-238.

Canfield, D.E., 1994. Factors influencing organic carbon preservation in marine sediments. Chemical Geology, 114, pp.315-329.

Carlson, K.H. and Knocke, W.R., 2000. Modeling manganese oxidation with KMnO4 for drinking water treatment. Journal of Environmental Engineering, 125(10), 892-896.

Casado, J., Lopez-Quintela, M.A., and Lorenzo-Barral, F.M., 1986. The initial rate method in chemical kinetics. Journal of Chemical Education, 63(5), pp.450-452.

Chen, G.E., Hoag, G.E., Chedda, P., Nadim, F., Woody, B.A., and Dobbs, G.M., 2001. The mechanism and applicability of in situ oxidation of trichloroethylene with Fenton's reagent. Journal of Hazardous Materials, B87, pp. 171-186.

Chen, P.H. and Watts, R.J., 2000. Determination of rates of hydroxyl radical generation in mineral-catalyzed Fenton-like oxidation, J. Chin. Inst. Environ. Eng., 10, pp. 201–208.

Christensen, T.H., Bjerg, P.L., Banwart, S.A., Jakobsen, R., Heron, G., and Albrechtsen, H.J., 2000. Characterization of redox conditions in groundwater contaminant plumes. Journal of Contaminant Hydrology, 45, 165-241.

Churcher, P.L. and Dickout, R.D., 1987. Analysis of ancient sediments for total organic carbon – some new ideas. Journal of Geochemical Exploration, 29, pp. 235-246.

Clancy, P.B., Armstrong, J., Couture, M., Lussky, R., and Wheeler, K., 1996. Treatment of chlorinated ethenes in groundwater with ozone and hydrogen peroxide. Environmental Progress, V.15 (3), pp. 187-193.

Crimi, M.L. and Siegrist, R.L., 2004. Impact of reaction conditions on MnO_2 genesis during permanganate oxidation. Journal of Environmental Engineering, 130(5), pp.562-567.

Crimi, M.L. and Siegrist, R.L., 2005. Factors affecting effectiveness and efficiency of DNAPL destruction using potassium permanganate and catalyzed hydrogen peroxide. Journal of Environmental Engineering, 131(12), pp.1724-1732.

Damm, J. H.; Hardacre, C.; Kalin, R. M.; Walsh, K. P., 2002. Kinetics of the oxidation of methyl t-butyl ether (MTBE) by potassium permanganate. Water Research, 36, pp. 3638-3646.

De-Laat, J. and Gallard, H., 1999. Catalytic decomposition of hydrogen peroxide by Fe(III) in homogeneous aqueous solution: mechanism and kinetic modeling. Environmental Science and Technology, 33, pp.2726-2732.

Domenico, P. A. and Schwartz, F.W., 1990. Physical and Chemical Hydrogeology, *First edition*. John Wiley & Sons, New York.

Domenico, P. A. and Schwartz, F.W., 1998. Physical and Chemical Hydrogeology, *Second edition*. John Wiley & Sons, New York.

Dresche, E., Gavaskar, A. R., Sass, B.M., Cumming, L.J., Drescher, M.J., and Williamson, T.K.J., 1998. Batch and column testing to evaluate chemical oxidation of DNAPL source zones. In Proceeding from the 1st International Conference on Remediation of Chlorinated and Recalcitrant Compounds, Battelle, Monterey, Calif., 1998.

Eckenfelder, W.W., J.W. Hood, 1950. A critical evaluation of routine sewage analysis. Water & Sewage Works, 97:138-141.

Eilbeck, W.J. and Mattock, G. 1987. Chemical process in wastewater treatment. John Wieley and Sons, Toronto, Ontario.

Ensing, B., Buda, F., and Baerends, E.J., 2003. Fenton-like chemistry in water: oxidation catalysis by Fe(III) and H2O2. J. Phys. Chem., 107, 5722-5731.

European Environment Agency, 1999. Requirements for Water Monitoring, Topic Report No 1/1996.

ESTCP, 1999. Technology status review in situ oxidation, November, 1999, 42 pp. http:// www.estcp.org/documents/techdocs/ISO_Report.pdf

Evanko, C.A., D.A. Dzombak, 1998. Influence of structural features on sorption on NOM-analogue organic acids to goethite, Environ. Sci. Technol., 32(19), 2846-2855.

Farmer, V.C. and Mitchell, B.D., 1963. Occurrence of oxalates in soil clays following hydrogen peroxide treatment. Soil Science, 96, pp. 221- 229.

Forsey, S. P. In Situ Chemical Oxidation of Creosote/Coal Tar Residuals: Experimental and Numerical Investigation. Ph.D. Thesis, University of Waterloo, 2004.

Fountain, J. C. 1998. Technologies for Dense Nonaqueous Phase Liquid Source Zone Remediation. Prepared for GWRTAC, http://www.gwrtac.org

Fujikawa, Y. and Fukui, M., 2001. Vertical distribution of trace metals in natural soil horizons from Japan. Part 2: effect of organic components in soil. Water, Air, and Soil Pollution, 132, pp. 305-328.

Fujimori, K., W. Ma, T. Moriuchi-Kawakami, Y. Shibutani, N. Takenaka, H. Bandow, Y. Maeda, 2001. Chemiluminescence method with potassium permanganate for the determination of organic pollutants in seawater, Analytical Sci., 16, 975-978.

Gallard, H. and De-Laat, J., 2000. Kinetic modeling of Fe(III)/H_2O_2 oxidation reactions in dilute aqueous solution using atrazine as a model organic compound. Water Research, 34(12), pp.3107-3116.

Gates, D.D. and Siegrist, R. L., 1995. In-situ chemical oxidation of trichloroethylene using hydrogen peroxide. Journal of Environmental Engineering, v. 121 (9), pp. 639-644.

Gates-Anderson, D.D., Siegrist, and Cline,S., 2001. Comparison of potassium permanganate and hydrogen peroxide as chemical oxidants for organically contaminated soils. Journal of Environmental Engineering, 1127(4), 337-347.

Grcman, H., Vodnik, D., Velikonja-Bolta, S., and Lestan, D., 2003. Heavy metals in the environment: Ethylenediaminedissuccinate as a new chelate for environmentally safe enhanced lead phytoextraction, J. Environ. Qual., 32, 500-506.

Groher, D. (2001). In situ Chemical Oxidation: An Innovative Groundwater Remediation Technology. www.environmental-center.com/articles/article1239/article1239.htm

Gu, B., Schmitt, J., Chen, Z., Liang, L., and McCarthy, J.F., 1994. Adsorption and desorption of natural organic matter on iron oxide: mechanisms and models. Environmental Science and Technology, 28, pp. 38-46.

Harada, Y. and Inoko, A., 1977. The oxidation products formed from soil organic matter by hydrogen peroxide treatment. Soil Sci. Plant Nutr., 23(4), pp. 513-521.

Hartog, N., Griffioen, J., and van der Weijden, C. H. (2002). Distribution and reactivity of O2-reducing components in sediments frm a layered aquifer. Environ. Sci. Technol., 36, pp.2338-2344.

Hartog, N. 2003. Reactivity of organic matter and other reductants in aquifer sediments. Ph.D thesis of University Utrecht, Netherland.

Hartog, N., Griffieon, J., Van Bergen, P.F., and Van-Der Weijden, C. H., 2001. Determining the reactivity of reduced components in Dutch aquifer sediments. Impact of Human Activity on Groundwater Dynamics, Proceeding of a Symposium Held during the Sixth IAHS Scientific Assessmbly at Maastricht, The Netherlands, July 2001. IAHS Publ., no.229. pp.221-227.

Haselow, J. S., Siegrist, R. L., Crimi, M., and Jarosch, T. 2003. Estimating the total oxidant demand for *in situ chemical oxidation* design. Remediation Journal, 13(4), pp.5-16.

Hatcher, P.G., Schnizer, M., Dennis, L.W., and Maciel, G.E., 1981. Aromaticity of humic substances in soil. Soil Society of America Journal, 45, pp. 1089-1094.

Hem, J. D., 1978. Redox processes at subsurface of manganese oxide and their effects on aqueous metal ions. Chemical Geology, 21, pp. 199-218.

Heron, G., Christensen, T.H. and Tjell, J.C., 1994. Oxidation capacity of aquifer sediments. Environ. Sci. Technol., 28, 153-158.

Hoffman, E.R., 1992. Instrumental Neutron Activation in Geoanalysis. Journal of Geochemical Exploration, V. 44, pp.297-319.

Hofstetter, T. B., Schwarzenbach, R.P., and Haderlein, S.B., 2003. Reactivity of Fe(II) species associated with clay minerals. Environmental Science and Technology, 37, pp.519-528.

Hood, E.D., Thomson, N.R. and Farquhar, G.J., 1997. In situ oxidation: an innovative treatment strategy to remediate trichloroethylene and perchlorroethylene DNAPLs in porous media. The 6th Symposium on Groundwater and Soil Remediation, Montreal, Qubec, Canada. March-18-21.

Hood, E.D., 2000. Permanganate flushing of DNAPL source zones: experimental and numerical investigation. PhD thesis, University of Waterloo, Waterloo, Canada.

Hood, E.D., Thomson, N.R., Grossi, D., and Farquhar, G.J., 2000. Experimental determination of the kinetic rate law for the oxidation of perchloroethylene by potassium permanganate. Chemosphere, 40, 1383-1388.

Huang, K.-C., Hoag, G. E., Chheda, P., Woody, B.A., and Dobbs, G.M., 1999. Kinetic study of oxidation of trichloroethene by potassium permanganate. Environmental Engineering Science, 16(4), 265-274.

Huang, K.-C., Hoag, G. E., Chheda, P., Woody, B.A., and Dobbs, G.M., 2002a. Chemical oxidation of trichloroethylene with potassium permanganate in a porous media. Advances in Environmental Research, 7, 217-229.

Huang, K.-C., Couttenye, R.A., and Hoag, G.E. 2002b. Kinetics of heat-assisted persulfate oxidation of methyl tert-butyl ether (MTBE). Chemosphere, 49(4), pp.413–420.

Huling, S.G., Arnold, R. G., Sierka, R.A., and Miller, M.R., 2001. Influence of peat on Fenton oxidation. Water Research, 35(7), pp. 1687-1694.

Hunter, K. S., Wang, Y., and Cappellen, P.V., 1998. Kinetic modeling of microbially-driven redox chemistry of subsurface environments: coupling transport, microbial metabolism and geochemistry. Journal of Hydrology, 209, pp. 53-80.

Hwang, I., Batchelor, B., Schlautman, M.A., and Wang, R., 2002. Effects of ferrous iron and molecular oxygen on chromium (VI) redox kinetics in the presence of aquifer solids. Journal of Hazardous Materials, B92, 143-159.

ITRC, 2000. Dense nonaqueous phase liquids (DNAPLs): review of emerging characterization and remediation technologies; DNAPLs/Chemical Oxidation Work Team; Interstate Technology and Regulatory Cooperation Work Group.June 2000; available at http://www.itrcweb.org.proxy.lib.uwaterloo.ca/DNAPL-1.pdf.

ITRC, 2001. Technical and Regulatory Guidance for In Situ Chemical Oxidation of Contaminated Soil and Groundwater, Interstate Technology and Regulatory Cooperation Work Group, In Situ Chemical Oxidation Work Team, http://www.itrcweb.org/ISCO-1.pdf

Islam, J., Singhal, N., and O'Sullivan, M., 2001. Modeling biogeochemical processes in leachate-contaminated soils: a review. Transport in Porous Media, 43, pp.407-440.

Jackson, M. L., Lim, C.H., and Zelazny, J.W., 1986. Oxides, Hydroxides, and Aluminosilicates. In *Methods of soil analysis, Part 1-Physical and Mineralogical analysis, 2nd edition, Editor by Kluter, A., American Society of Agronomy, Inc. and Soil Science Society of America, Inc.*, Madison, Wisconsin, USA.

Jones, C.W., 1999. Applications of hydrogen peroxide and derivatives. The royal Society of Chemistry, UK.

Jones, P.W. and Williams, D.R., 2001. Chemical speciation simulation used to assess [S,S']-ethylenediaminediaminedisuccinic acid (EDDS) as a readily-biodegradable replacement for EDTA in radiochemical decontamination formulations. Applied Radiation and Isotopes, 54, pp.587-593.

Jones, P.W. and Williams, D.R., 2002. Chemical speciation simulation used to assess the efficiency of environment-friendly EDTA alternative for use in pulp and paper industry, Inorganica Chimica Acta, 339, 41-50.

Kakarla, P.K., Andrews, T., Greenberg, R. S. and Zervas, D.S., 2002. Modified Fenton's processes for effective in-situ chemical oxidation-laboratory and field evaluation. Remediation, Autumn, 2002, pp.23-36.

Kakarla, P.K.C. & Watts, R.J., 1997. Depth of Fenton-like oxidation in remediation of surface soils. J. Enviro. Eng. 123, pp.11-17.

Kamei, G. and Ohmoto, H., 2000. The kinetics of reactions between pyrite and O_2-bearing water revealed from in situ monitoring of DO, Eh and pH in a closed system. Geochimica et Cosmochimica Acta, 64(15), pp.2585-2601.

Kang, N., Lee, D.S., and Yoon, J., 2002. Kinetic modeling of Fenton oxidation of phenol and monochlorphenols. Chemosphere, 47, pp. 915-924.

Kang, N., Hua, I., and Rao, P.S.C., 2004. Production and characterization of encapsulated potassium permanganate for sustained release as an in situ oxidant. Ind. Eng. Chem. Res., 43(17), pp. 5187-5193.

Kappler, A. and Harderlein, S.B., 2003. Natural organic matter as reductant for chlorinated aliphatic pollutants. Environmental Science and Technology, 37, pp.2714-2719.

Kelley, K.L., Marley, M.C., & Sperry, K.L. 2002. In-situ chemical oxidation of MTBE. CSCS/EWRI of ASCE Environmental Engineering ConfERENCE, Niagara 2002.

Khan, F.I., Husain, T., and Hejazi, R., 2004. An overview and analysis of site remediation technologies. Journal of Environmental Management, 71, pp.95–122

Kim, J., and Choi, H., 2002. Modeling in situ ozonation for the remediation of nonvolatile PAH-contaminated unsaturated soils. Journal of Contaminant Hydrology, 55, pp. 261-

285.

Knapp, E.P., Herman, J.S., Mills, A.L., and Hornberger, G.M., 2002. Changes in the sorption of coastal plain sediments due to redox alternation of mineral surfaces. Applied Geochemistry, 17, pp. 387-398.

Korom, S.F., McFarland, M. J., and Sims, R.C. 1996. Reduced sediments: a factor in the design of subsurface oxidant delivery systems. GWMR, Winter 1996, pp.100-105.

Kos, B. and Lestan, D., 2003. Influence of a biodegradable ([S,S]-EDDS) and nondegradable (EDTA) chelate and hydrogel modified soil water sorption capacity on Pb phytoextraction and leaching. Plant and Soil, 253, pp. 403-411.

Kwan, W. and Voelker, B.M., 2003. Rates of hydroxyl radical generation and organic compound oxidation in mineral-catalyzed Fenton-like systems. Environmental Science and Technology, 37,pp.1150-1158.

Lee, E.S., Seol, Y.K., Fang, Y.C., and Schwartz, F. W., 2003. Destruction Efficiencies and dynamics of reaction fronts associated with the permanganate oxidation of trichloroethylene. Environmental Science and Technology, 37, pp. 2540-2546

Lee, W. and Batchelor, B., 2003. Reductive capacity of natural reductants. Environmental Science and Technology, 37, pp.535-541.

Li, X.D., Schwartz, F.W., 2004a. DNAPL remediation with in situ chemical oxidation using potassium permanganate part I. Mineralogy of Mn oxide and its dissolution in organic acids. J. Contam. Hydrol. 68 (1–2), 39– 53.

Li, X.D., Schwartz, F.W., 2004b. DNAPL remediation with in situ chemical oxidation using potassium permanganate. II. Increasing removal efficiency by dissolving Mn oxide precipitates. J. Contam. Hydrol. 68 (3–4), 269– 287.

Lin, S.-S. and Gurol, M., 1998. Catalytic decomposition of hydrogen peroxide on iron oxide: kinetics, mechanism, and implication. Environmental Science and Technology, 32, pp.1417-1423.

Luthy, R.G., Aiken, G.R., Brusseau, M.L., Cunningham, S.D., Gschwend, P.M., Pignatello, J.J., Reinhard, M., Trainina, S.J., Weber, W.J., and Westall, J.C., 1997. Sequestration of hydrophobic organic contaminants by geosorbents. Environmental Science and Technology, 31, pp. 3341-3347.

Mackinnon, L.K. and Thomson, N.R., 2002. Laboratory-scale in situ chemical oxidation of a perchloroethylene pool using permanganate. Journal of Contaminant Hydrology, 56, 49-74.

Martin, S. T., 2003. Precipitation and dissolution of iron and manganese oxides. (unpublished paper), Harvard University.

Masschelein, W., 1977. Spectrotrophotometric determination of resudial hydrogen peroxide. Water & Sewage Works, August, pp.69-72.

Masten, S.J. and Davies, S.H.R., 1997. Efficacy of in-situ ozonation for the remediation of PAH contaminated soil. Journal of Contaminated Hydrology, v.28, pp.329-337.

Mayer, L.M., 1994. Relation ships between mineral surface and organic carbon concentrations in soil and sediments. Chemical Geology, 114, pp.347-363.

Mayer, L.M., 1999. Extent of mineral surfaces by organic matter in marine sediments. Geochimica et Cosmochimica Acta, 63(2), pp.205-275.

Meers, E., Ruttens, A., Hopgood, M.J., Samson, D., and Tack., F.M.G., 2005. Comparison of EDTA and EDDS as potential soil amendments for enhanced phytoextraction of heavy metals. Chemosphere, 58, pp.1011-1022.

Michael, A.N., Wayner, B.D., Morr, A.A., 2000. In-situ ozonation of contaminated groundwater. Environ. Prog. 19 (3), 183– 196.

Miller, C.M. and Valentine, R., 1995. Oxidation behavior of aqueous contaminants in the presence of hydrogen peroxide and filter media. Journal of Hazardous Materials, 41, pp. 105-116.

Moody, P.W., Yo, S.A., and Aitken, R.L., 1997. Soil organic carbon, permanganate fractions, and the chemical properties of acidic soils. Aust. J. Soil. Res., 35, pp.1301-1308.

Moore, W.A., R.C. Kroner and C.C. Ruchhoft, 1949. Dichromate reflux method for determination of oxygen consumed: Effectiveness in oxidation of organic compounds. Analytical Chemistry, 21(8), 953-957.

Moore, W. A., F. J. Ludzack, C. C. Ruchhoft, 1951. Determination of oxygen consumed values of organic wastes: A comparative study of methods. Analytical Chemistry, 29 (9), 1297-1300.

Morse, J.W. and Arvidson, R.S., 2002. The dissolution kinetics of major sedimentary carbonate minerals. Earth-Science Reviews, 58, pp.51-84.

Mulira, J.E., 1996. Treatment technologies for contaminated groundwater, Ministry Environment and Energy, Ontario.

Mumford, K.G., 2002. Investigation of natural oxidant demand reactions in a sandy aquifer materials. Thesis for Master of Applied Science, University of Wateloo.

Mumford, K.G., Thomson, N.R., and Allen-King, R.M., 2002. A kinetic investigation of permanganate natural oxidation demand in a sandy aquifer material. The Second International Conference on Oxidation and Reduction Technologies for In-Situ Treatment of Soil and Groundwater, Toronto, Canada, November 17-21, 2002.

Mumford, K.G., C. Lamarche, N. R. Thomson, 2004. Natural oxidant demand of aquifer materials using the push-pull technique with permanganate, ASCE J. Envir. Eng., 130(10), 1139-1146.

Mumford, K.G., Thomson, N. R., and Allen-King, R.M., 2005. Bench-Scale Investigation of Permanganate Natural Oxidant Demand Kinetics. Environ. Sci. Technol., 39(8), pp. 2835-2840.

National Research Council, 2000. Natural attenuation for groundwater remediation. National Academy Press, Washington, D.C., USA.

Nelson, M.D., Parker, B.L., Al, T.A., Cherry, J.A., and Loomer, D., 2001. Geochemical reactions resulting from in situ oxidation of PCE-DNAPL by $KMnO_4$ in a sandy aquifer. Environ. Sci. Technol., 35, 1266-1275.

Neyens, E. and Baeyens, J., 2003. A review of classic Fenteon's peroxidation as an advanced oxidation technique. Journal of Hazardous Materials, B98, 33-50.

Nyer, E. K. and Vance, D., 1999. Hydrogen peroxide treatment: the good, the bad, and the ugly. Ground Water Monitoring & Remediation. 19, pp. 54-57.

Nicholson, A., Davis, A., and Helgen, S., 2003. Elements influencing cost allocation in the Pinal Creek aquifer, Arizona, USA. Part II: Geochemical controls on groundwater quality recovery. Environmental Forensics, 4, 271-286.

Nicholson, R.V., Gillham, R.W., and Reardon, E.J. 1988. Pyrite oxidation in carbonate-buffered solution: 1. experimental kinetics. Geochim. Cosmochim. ACTA 54, 395-402.

Nyer, E.K. and Vance, D., 1999. Hydrogen Peroxide Treatment: The Good, the Bad, the Ugly, GWMR, Summer, 54-57.

Nyer, E.K., Fam, A., Kidd, D.F., Johns II, F.J., Palmer, P.L., Boettcher, G., Crossman, T.L., Suthersan, S.S., 1996. In Situ Treatment Technology. Lewis Publishers, New York, USA.

Ogram, A.N., Jessup, R.E., Ou, L.T., and Rao, P.D.C., 1985. Effects of sorption on biological degradation of 2,4-dechlorophenoxy acetic acid in soils. Applied Environmental Microbiology, 49(3), pp. 582-587.

Pankow, J.F. and Cherry, J.A., 1996. Dense chlorinated solvents and other DNAPLs in groundwater. Waterloo Press.

Pardieck, D.L., Bouwer, E.J., and Stone, A.T., 1992. Hydrogen peroxide use to increase oxidant capacity for in situ bioremediation of contaminated soils and aquifers: A review. Journal of Contaminant Hydrology, 9, pp.221-242.

Pedersen, J.K., Bjerg, P.L., and Cheristensen, T.H., 1991. Correlation of nitrate profiles with groundwater and sediment characteristics in a shallow sandy aquifer. J. Hydrol., 124. pp. 263-277.

Petigara, B. R., Blough, N.V., and Mignerey, A., 2002. Mechanisms of hydrogen peroxide decomposition in soils. Environmental Science and Technology, 36, pp.639-645.

Pignatello, J.J., 1998. Soil organic matter as a nanoporous sorbent of organic pollutants. Advances in Colloid and Interface Science, 76-77, pp. 445-467.

Pignatello, J.J., Oliveros, E., and MacKay, Allison. 2006. Advanced oxidation processes for organic contaminated destruction based on the Fenton reaction and related chemistry. Critical Reviews in Environmental Science and Technology, 36, pp.1-84.

Powell, R.M., Callaway, R.W., Michalowski, J.T., Vandegrift, S.A., and White, M.V., (1988). Comparison of methods to determine oxygen demand for bioremediation of a fuel contamination of a fuel contaminated aquifer. Intern. J. Environ. Anal. Chem., Vol. 34, pp.253-263.

Ramo, J., 2003. “Hydrogen peroxide-metals-chelating agents: interactions and analytical techniques”, Oulu university Press, Oulu.

Reardon, E. D., 2006. Personal communication.

Rhoades, J.D., 1982. Cation exchange capacity. pp. 149 –157. *In* A L. Page (ed.), *Methods of Soil Analysis, Agron., No.9, Part 2: Chemical and Mineralogical Properties.* Am. Soc. Agron., Madison, WI, USA.

Rodriguez, M.L., Timokhin, V.I., Contreras, S., Chamarro, E., and Esplugas, S., 2003. Rate equation for the degradation of nitrobenzene by ‘Fenton-like’ reagent. Advances in Environmental Research, 7, pp.583-595.

Schnarr, M., Truax, C., Farquhar, G., Hood, E., Gonullu, T., and Stickney, B., 1998. Laboratory and controlled field experiments using potassium permanganate to remediate trichloroethylene and perchloroethylene DNAPLs in porous media. Journal of Contaminant Hydrology, 29, 205-224.

Schroth, M.H., Oostrom, M., Wietsma, T.W., and Istok, J.D., 2001. In-situ oxidation of trichloroethene by permanganate: effects on porous medium hydraulic properties. Journal of Contaminant Hydrology, 50, 79-98.

Schumb, W.C., Satterfield, C.N., and Lendent, 1995. Hydrogen Peroxide, ACS Monograph 128, American Chemical Society, Washington, DC.

Scott, D.T., McKnight, D.M., Blunt-Harris, E.L., Kolesar, S.E., and Lovley, D.R., 1998. Quinone moieties act as electron acceptors in the reduction of humic substances by humic-reducing microorganisms. Environmental Science and Technology, 32, pp.2984-

2989.

Sedlak, D.L., Andren, A.W., 1994. The effect of sorption on the oxidation of polychlorinated biphenyls (PCBs) by hydroxyl radical. Water Res. 28, 1207–1215.

Seol, Y., Schwartz, F.W., 2000. Phase-transfer catalysis applied to the oxidation of non-aqueous phase trichloroethylene by potassium permanganate. J. Contam. Hydrol. 44 (2), 185–201.

Seol, Y., Zhang, H., and Schwartz, F.W., 2003. A review of in situ chemical oxidation and heterogeneity. Environmental & Engineering Geoscience, Vol. IX, No.1, pp.37-49.

Sheldon, R.A., Kochi, J.K., 1981. Metal-catalyzed reactions of organic compounds: mechanistic principles and synthetic methodology including biochemical processes. Academic Press, New York, NY.

Siegrist, R.L., Urynowicz, M.A., West, O.R., 1999. An overview of in situ chemical oxidation technology features and applications. Proceedings of the Conference on Abiotic In-Situ Technologies for Groundwater Remediation, Aug.31-Sep.2, 1999, Dallas, Texas, USA.

Siegrist, R.L., Urynowicz, M.A., West, O.R., Crimi, M.L., and Lowe, K.S., 2000. Guidance for in situ chemical oxidation at contaminated sites: technology overview with a focus on permanganate systems. U.S. EPA, Office of Science & Technology, Subsurface Contaminants Focus Area, Washington, D.C., USA.

Siegrist, R. L., Urnowica, M.L, West, O.R., Crimi, M.L., Lowe, K.S., 2001. Principles and practices of in situ chemical oxidation using permanganate. Battelle Press, Columbus, OH, USA.

Siegrist, R.L., Urynowicz, M.A., West, O.R., 2002. Genesis and effects of particles produced during in situ chemical oxidation using permanganate. Journal of Environmental Engineering, 28(11), 1068-1079.

Smith, B.A., R.J., Watts, R.J., and Atkinson, D.A. 2002. Destruction of DNAPLs by modified Fenton's reagent. In Proceeding of the Third International Conference on Remediation Chlorinated and Recalcitrant Compounds, Monterey, CA, May 20-23, 2002

Smith, B.A., Teel, A.L.,Watts, R.J., 2004. Identification of the reactive oxygen species responsible for carbon tetrachloride degradation in modified Fenton's systems. Environ. Sci. Technol. 38 (20), 5465–5469.

Smith, B.A., Teel, A.L., and Watts, R.J., 2006. Mechanism for the destruction of carbon tetrachloride and chloroform DNAPLs by modified Fenton's reagent. Journal of Contaminant Hydrology, 85, pp. 229-246.

Song, J., Peng, P., and Huang, W., 2002. Black carbon and kerogen in soils and sediments. 1. quantification and characterization. Environmental Science and Technology, 36, pp. 3960-3967.

Sparks, D.L., 1989. Kinetics of soil chemical processes. Academic Press, New York.

Stewart, R., 1964. Oxidation mechanisms: application to organic chemistry. W.A.Benjamin, Inc., New York, USA.

Stewart, R., 1965. Oxidation by permanganate. In: Wiberg, K.B. (ed.), Oxidation in Organic Chemistry, Part A. Academy Press, New York.

Stewart, C.L., 2002. Density-driven permanganate solution delivery and chemical oxidation of a thin trichloroethylene DNAPL pool in a sandy aquifer, Thesis for Master of Science, University of Waterloo.

Strukul, G. (ed.), 1992. Catalytic oxidation with hydrogen peroxide as oxidant. Kluwer Academic Publishers, Dordrecht/Boston/London.

Stumm, W. and Morgan, J.J., 1995. Aquatic chemistry: chemical equilibria and rates in natural waters (Third Edition). John Wiley & Sons Inc., New York.

Sun, Y., and Pignatello, J.J., 1992. Chemical treatment of pesticide wastes. Evaluation of Fe(III) chelates for catalytic hydrogen peroxide oxidation of 2,4-D at circumneutral pH. Journal of Agricultural Food Chemistry, 40(2), pp.332-337.

Tandy, S., Bossart, K., Mueller, R., Ritschel, J., Hauser, L., Schulin, R., and Nowack, B., 2004. Extraction of heavy metals from soils using biodegradable chelating agents. Environmental Science and Technology, 38, pp.937-944.

Tandy, S.; Ammann, A., Schulin, R., Nowack, B., 2006a. Biodegradation and speciation of residual SS-ethylenediaminedisuccinic acid (EDDS) in soil solution left after soil washing. Environmental Pollution.142(2), pp. 191-199.

Tandy, S., Schulin, R., and Nowack, B., 2006b. Uptake of metals during chelant-assisted phytoextraction with EDDS related to the solubilized metal concentration. Environmental Science and Technology, 40, pp.2753-2758.

Tebo, B.M. and He, L.M., 1998. Microbially mediated oxidative precipitation reactions. In “Mineral-Water Interfacial Reactions” (eds. By Sparks, D.L. and Grundl, T.J.), Oxiford University Press.

Teel, A.L., Warberg, C.R., Atkinson, D.A., and Watts, R.J., 2001. Comparison of mineral and soluble iron Fenton’s catalysts for the treatment of trichloroethylene. Water Research, 35(4), pp.977-984.

Tollefsrud, E.; Schreier, C. G., 2002. Effectiveness of chemical oxidation to remove organochlorine pesticides from soil. In Proceedings of the Third International Conference on Remediation of Chlorinated and RecalcitrantCompounds, Monterey,CA; Battelle Press: Columbus, OH, 2002; Paper 2C-16.

Tunnifliffe, B.S. and Thomson, N.R., 2004. Mass removal of chlorinated ethenes from rough-walled fractures using permanganate. Journal of Contaminated Hydrology., 75, pp.91-114.

Urynowicz, M.A., and Siegrist, R.L., 2005. Interphase mass transfer during chemical oxidation of TCE DNAPL in an aqueous system. Journal of Contaminant Hydrology, 80, pp. 93-106.

US DOE, 1999. Fenton’s reagent: innovative technology summary report. U.S. Department of Energy, Subsurface Contaminant Focus Area, DOE/EM-0484, Oct., 1999.

US EPA, 1996. Test methods for evaluating solid waste, Physical/Chemical Methods.

USEPA, 1998. Field application of in situ remediation technologies: chemical oxidation, EPA 542-R-98-008, 31pp., September 1998, http://www.epa.gov.swertio/download/remed/chemox.pdf

USEPA, 1999. Alternative disinfectants and oxidants guidance manual. EPA 815-R-99-014, Office of Water, United States Environmental Protection Agency.

USEPA, 2004a. How to evaluate alternative cleanup technologies for underground storage tank sites: a guide for corrective action. Plan Reviewers Office of the Underground Storage Tank, US Environmental Protection Agency. Publication # EPA 510-B-95-007.

USEPA, 2004b. Treatment Technologies for Site Cleanup: Annual Status Report (Eleventh Edition). Solid Waste and Emergency Response (5102G), EPA-542-R-03-009.

Valentine, R. L., and Wang, H. C. A., 1998. Iron oxide surface catalyzed oxidation of quinoline by hydrogen peroxide. J. Environ. Eng., 124(1), pp.31–38.

Voelker, B. M. and Sulzberger, B., 1996. Effects of fulvic acid on Fe(II) oxidation by hydrogen peroxide. Environmental Science and Technology, 30, pp. 1106-1114.

Vogt, C., Alfreider, A., Lorbeer, H., Hoffmann, D., Wuensche, L., Babel, W., 2004. Bioremediation of chlorobenzene-contaminated ground water in an in situ reactor mediated by hydrogen peroxide. Journal of Contaminant Hydrology, 68, pp. 121-141.

Waldemer, R.H. and Tratnyek, P.G., 2006. Kinetics of Contaminant Degradation by Permanganate. Environmental Science and Technology, 40(3), pp.1055 –1061.

Walling, C. (1975). Fenton's reagent revisited. Acc. Chem. Res., 8, pp. 125.

Watts , R.J. and Teel, A. L., 2006. Treatment of contaminated soils and groundwater using ISCO. Practice Periodical of Hazardous, Toxic, and Radioactive Waste Management, 10(1), pp. 2-9.

Watts, R.J., Udell, M.D., Rauch, P.A., & Leung, S.W. (1990). Treatment of pentachlorophenol-contaminated soils using Fenton's reagent. Hazardous Waste Hazardous Materials, 7(4), 335-345.

Watts, R.J., Borrenberg, B.C., Hess, T.F., Jensen, M.D., & Teel, A.L. 1999a. Role of reductants in the enhanced desorption and transformation of chloroaliphatic compounds by modified Fenton's reactions. Environmental Science and Technology, 33, pp. 3432-3437.

Watts, R.J., Foget, M.K., Kong, S.H., and Teel., A.L., 1999b. Hydrogen peroxide decomposition in model subsurface systems. Journal of Hazardous Materials, B69 pp. 229-243.

Watts, R.J., Udell, M. D., Kong, S., and Leung, S. W., 1999c. Fenton-like soil remediation catalyzed by naturally occurring iron minerals. Environmental Engineering Science, v.16 (1), pp. 93 - 102.

Watts, R. J. and Teel, A.L., 2005a. Chemistry of modified Fenton's reagent (catalyzed H2O2 propagation-CHP) for in situ soil and groundwater remediation. Journal of Environmental Engineering, 131(4), PP. 612-622.

Watts, R.J., Howsawkeng, J., Teel, A.L., 2005b. Destruction of a carbon tetrachloride DNAPL by modified Fenton's reagent. J. Environ. Eng. 131 (7), 1114–1119.

Watts, R.J., Sarasa, J., Loge, F.L., and Teel, A.L., 2005c. Oxidative and reductive pathways in manganese-catalyzed Fenton's reactions. J. Environ. Eng. 131 (1), 158–164.

Watts, R. J. and Teel., A.L., 2006. Treatment of contaminated soils and groundwater using ISCO. Practice Periodical of Hazardous, Toxic, and Radioactive Waste Management. 10(1), pp.2-9.

Water Science and Technology Board (WSTC), 2004. Contaminants in the subsurface : source zone assessment and remediation, Division on Earth and Life Studies, National Research Council of the National Academies, THE NATIONAL ACADEMIES PRESS, Washington, D.C., USA.

Weber, W.J., Huang, W., and Leboeuf, E.J., 1998. A three-domain model for sorption and desorption of organic contaminants by soils and sediments. In "Mineral-Water Interfacial Reactions, Sparks, D.L., and Grundl, T.J., Eds.; American Chemical Society: Washington DC.

Weeks, K.R., Bruell, C.J., and Mohanty, N.R., 2000. Use of Fenton's reagent for the degradation of TCE in aqueous systems and soil slurries. Soil and Sediment Contamination, 9(4), pp:331-345.

Wilson, A.D., 1955. A new method for the determination of ferrous iron in rocks and minerals. Bull. Geol. Surv. G.B., 9:56–58.

Vandevivere, P. C., Saveyn, H., Verstraete, W., Feijtel, T.C., and Schowanek, D. R., 2001. Biodegradation of metal-[S,S]-EDDS complexes. Environmental Science and Technology, 35, pp.1765-1770.

Yan, Y.E., and Schwartz, F.W., 1998. Oxidation of chlorinated solvents by potassium permanganate. Proc., Int. Conf. on Remediation of Chlorinated and Recalcitrant Compounds, Battelle, Columbus, Ohio.

Yan, Y.E. and Schwartz, F.W., 1999. Oxidative degradation and kinetics of chlorinated ethylenes by potassium permanganate. Journal of Contaminant Hydrology, 37, 343 – 365.

Yan, Y.E. and Schwartz, F.W., 2000. Kinetics and mechanisms for TCE oxidation by permanganate. Environmental Science and Technology, 34(12), 2535-2541.

Yeh, C.K.-J., Kao, Y.-A., and Cheng, C.-P., 2002. Oxidation of chlorophenols in soil at natural pH by catalyzed hydrogen peroxide: the effect of soil organic matter. Chemosphere, 46, pp. 67-73.

Yeh, C. K.-J., Wu, H.-M., & Chen, T.-C., 2003. Chemical oxidation of chlorinated non-aqueous phase liquid by hydrogen peroxide in natural sand systems. Journal of Hazardous Materials, B96, pp. 29-51.

Yin, Y. and Allen, H. E., 1999. In situ chemical treatment. www.gwrtac.org.

Zhang, H. and Schwartz, F.W., 2000. Simulating the in situ oxidative treatment of chlorinated ethylenes by potassium permanganate. Water Resources Research, 36(10), 3031-3042.

Zhou, Y., 1994. Condition control for determination of measuring permanganate index (in Chinese). China Environmental Monitoring, 10(2), 36-37.